Maria Beatriz Tomaz Ferreira
Licenciada em Química Aplicada

A rational approach towards novel modulators of necroptosis

Dissertação para obtenção do Grau de Mestre em
Química Bioorgânica

Orientador: Carlos Alberto Mateus Afonso, Professor Catedrático, Faculdade de Farmácia da Universidade de Lisboa

Co-orientador: João Manuel Janeiro Martins Ravasco, Investigador, Faculdade de Farmácia da Universidade de Lisboa

Júri:

Presidente: Professora Doutora Ana Maria Ferreira da Costa Lourenço

Arguente: Professora Doutora Paula Cristina de Sério Branco

Vogal: Professor Doutor Carlos Alberto Mateus Afonso

FACULDADE DE
CIÊNCIAS E TECNOLOGIA
UNIVERSIDADE NOVA DE LISBOA

Outubro de 2018

A rational approach towards novel modulators of necroptosis

Copyright © Maria Beatriz Tomaz Ferreira, Faculdade de Ciências e Tecnologia, Universidade Nova de Lisboa.

A Faculdade de Ciências e Tecnologia e a Universidade Nova de Lisboa têm o direito, perpétuo e sem limites geográficos, de arquivar e publicar esta dissertação através de exemplares impressos reproduzidos em papel ou de forma digital, ou por qualquer outro meio conhecido ou que venha a ser inventado, e de a divulgar através de repositórios científicos e de admitir a sua cópia e distribuição com objetivos educacionais ou de investigação, não comerciais, desde que seja dado crédito ao autor e editor.

Agradecimentos

A todas as pessoas que tornaram possível a realização desta dissertação e a minha evolução enquanto química, gostava de deixar aqui o meu mais profundo agradecimento.

Em primeiro lugar, quero agradecer ao Professor Carlos Afonso, por me ter recebido tão bem no seu laboratório e pela sua orientação científica e preocupação durante este ano.

Ao João Ravasco por toda a paciência que teve para mim durante este ano e o tempo perdido para me ajudar e ensinar tanto no laboratório como na elaboração desta dissertação

Ao grupo de investigação da Professora Cecília Rodrigues, em especial à Sara Oliveira, pela realização dos ensaios biológicos.

À Professora Maria de Jesus Perry pela disponibilidade e ajuda na realização dos ensaios de estabilidade.

Quero agradecer à Késsia, ao João e à Milene, os meus companheiros ao longo deste ano, obrigado por estarem sempre presente nas boas e nas más colunas.

A todos os colegas do laboratório, que me acompanharam durante este ano, um obrigado gigante pela ajuda, pela disponibilidade e pela partilha de conhecimento que me fizeram crescer muito como química. Quero agradecer especialmente ao Rafael, por todos os conselhos e sugestões sobre as reações que tanto me ajudaram, à Dra. Filipa Siopa, por todo o apoio e motivação, que tão importante foi durante este ano e ainda ao Dr. Carlos Monteiro que apesar de chato, ajudou-me sempre que precisei.

A todos os meus amigos, que estiveram sempre presentes e me apoiaram, em especial, à minha xuxua Gabriela, alem de uma colega, tornou-se uma amiga, umas das melhores coisas que a FCT me proporcionou e apesar de distância física durante este ano, estiveste sempre presente, obrigado por tornares estes 5 anos muito mais fáceis. Ao meu carequinha favorito, Edgar Castanheira, obrigado por estares presente desde do primeiro dia de faculdade, por me tirares duvidas quando na percebia nada da matéria, por seres o amigo que és. À Joana e à Filipa, as minhas companheiras de jantares, obrigado por me ajudarem a desanuviar e a largar o estudo.

Ao Dinis, por me acompanhar e apoiar nesta e em tantas outras etapas, por não se chatear com os meus *n* atrasos e por me ouvir mesmo quando não percebe nada do que estou a falar.

À minha família, em especial aos meus pais, pela confiança que depositam em mim, pela ajuda e pelo apoio em todas as minhas decisões e acima de tudo por estarem sempre presentes nos bons e maus momentos. Um obrigado do tamanho do mundo.

Quero agradecer ao iMED.ULisboa por ceder as suas instalações para a realização desta dissertação e à Fundação para a Ciência e Tecnologia (UID/DTP/04138/2013, COMPETE Programme (SAICTPAC/0019/2015) pelo suporte financeiro.

Resumo

A necroptose é uma forma regulada de necrose que ocorre em resposta a um dano celular ou uma infeção. Esta é independente de caspases, ocorrendo em condições nas quais a via clássica de morte celular por apoptose está inibida. A execução deste tipo de morte celular envolve o recrutamento de cinases como a RIPK1 e a RIPK3, que dão origem a um complexo denominado necrossoma e levam ao recrutamento da MLKL e consequente fosforilação, desencadeando o processo de necroptose. A RIPK1 e a RIPK3 encontram-se envolvidas numa grande variedade de patologias para as quais atualmente ainda carecem de tratamentos eficazes, como é o caso do acidente vascular cerebral, do enfarte do miocárdio ou da pancreatite aguda.

A Nec-1 foi o primeiro inibidor conhecido para a necroptose, atuando através do bloqueio da atividade da RIPK1. No entanto, esta apresenta alguns problemas tais como inespecificidade para o alvo. Como tal, novos inibidores da RIPK1 têm sido desenvolvidos, procurando apresentar melhores propriedades farmacocinéticas e farmacodinâmicas, com foco na sua estabilidade e atividade *in vivo*.

Devido à grande relevância destes novos alvos no tratamento de patologias nas quais está envolvida a necroptose, e com base num estudo preliminar de 21 derivados de Oxazol-5-(4H)-onas em linhagens de células microglia BV2 e L292, foi encontrado um composto líder, a **OXA 12**, que apresenta uma atividade inibitória semelhante à Nec-1. A partir da **OXA 12**, e utilizando a reação de Erlenmeyer-Plöch foram sintetizadas novas **OXAs** com a introdução de diversos grupos. Além destas **OXAs** ainda foram sintetizadas outras, alterando o ácido hipúrico por outros grupos como foi o caso das hidrazonas. Estes novos compostos seguiram posteriormente para avaliação biológica.

Palavras-chave: Oxazol-5-(4H)-onas; morte celular, necroptose; necrostantinas

Abstract

Necroptosis is a regulated form of necrosis that occurs in response to a cellular damage or infection. It is independent of caspases, occurring under conditions in which the classical pathway of cell death by apoptosis is inhibited. The execution of this type of cell death involves the recruitment of kinases as the RIPK1 and the RIPK3, which give rise to a complex necrosome and lead to the recruitment of the MLKL and consequent phosphorylation, triggering a necroptosis process. RIPK1 and RIPK3 are involved in a wide variety of pathologies for which they currently lack effective treatments, such as stroke, myocardial infarction or acute pancreatitis.

Nec-1 was the first known inhibitor for necroptosis, acting through the blockade of RIPK1 activity. However, this presents some problems such as non-specificity for the target. As such, new inhibitors of RIPK1 have been developed, seeking to present better pharmacokinetic and pharmacodynamic properties, focusing on their stability and activity *in vivo*.

Due to the great relevance of these new targets in the treatment of pathologies in which necroptosis is involved and based on a preliminary study of 21 Oxazol-5-(4H)-one derivatives in BV2 and L292 microglial cell lines, a lead compound, **OXA 12**, was found has an inhibitory activity similar to Nec-1. From **OXA 12** and using the Erlenmeyer-Plöch reaction new **OXAs** were synthesized with the introduction of several groups. Besides these **OXAs** were further synthesized, altering the hippuric acid by other groups such as the hydrazones. These new compounds were subsequently used for biological evaluation.

Keywords: Oxazol-5-(4H)-ones; Cell Death, Necroptosis; Necrostatin

Subject Index

1. Introduction 1

  1.1. Cell cycle 3
    1.1.1. Interphase 3
    1.1.2. Mitotic phase 4

  1.2. Cell death 6
    1.2.1. Apoptosis 6
    1.2.2. Necrosis 8

  1.3. Necroptosis as therapeutic target 11
    1.3.1. Ischemia-reperfusion injury 11
    1.3.3. Inflammatory diseases 13

  1.4. Necroptosis inhibitors 15
    1.4.1. RIPK1 15
    1.4.2. RIPK3 16
    1.4.3. MLKL 17

  1.5. Oxazol-5(4H)-ones 19

    1.5.1. Erlenmeyer-Plochl reaction 19
    1.5.2. Uses of oxazolones 21
    1.5.3. Oxazolones as necroptosis inhibitors 23

2. Objectives 25

3. Results and Discussion 29

  3.1. Synthesis of 4 or 5-substituted-2-methyl-benzimidazoles 31

  3.2. Synthesis of 1,2-dimethyl-1H-benzo[d]imidazole 32

  3.3. Synthesis of 4-(2-(4 or 5-substituted-benzimidazol-2- yl)vinyl)benzaldehyde... 33

  3.4. Synthesis of (E)-4-(2-(2H-imidazol-2-yl)vinyl)benzaldehyde 37

  3.5. Synthesis of Oxazol-5(4H)-ones 37

  3.6. Synthesis of (E)-(4-(2-(1H-benzo[d]imidazol-2-yl)vinyl)phenyl)methanol 40

  3.7. Synthesis of hydrazones or oxime 41

  3.8. Attempts hydrogenation with Pd/C 43

  3.9. Synthesis of hippuric acid derivatives 45
    3.9.1. Synthesis of N-acetylglycine 45
    3.9.2. Synthesis of (pyrazine-2-carbonyl)glycine and nicotinoylglycine s 45

  3.10. Stability assays 52
    3.10.1. UV spectra 52
    3.10.2. Development of a method for the detection of OXA 12 53
    3.10.3. Metabolic stability assays using human plasma and PBS with 20% acetonitrile 54

  3.11. Biological assays 57
    a) Substituents at C-4 position of oxazolone moiety (A) 58
    b) Benzimidazole ring moiety (B) 59
    c) Hippuric acid moiety (C) 61

4. Conclusion 65

5. Materials and methods 69
5.1. General remarks 71
5.2. Synthetic procedures[a] 73
5.2.1. General procedure for the preparation of 4 or 5-substituted-2-methyl-benzimidazoles 73
5.2.2. Procedure for the preparation of 1,2-dimethyl-1H-benzo[d]imidazole 74
5.2.3. General procedure for the preparation of 4-(2-(4 or 5-substituted-benzimidazol-2- yl)vinyl)benzaldehyde 75
5.2.4. Attempt procedure for the preparation of (E)-4-(2-(1H-imidazol-2-yl)vinyl)benzaldehyde 78
5.2.5. General procedure for the preparation of Oxazol-5(4H)-ones 79
5.2.6. Procedure for the preparation of (E)-(4-(2-(1H-benzo[d]imidazol-2-yl)vinyl)phenyl)methanol 81
5.2.7. General procedure for the preparation of hydrazones and oximes 82
5.2.8. General procedure for catalytic hydrogenation attempts 84
5.2.9. Preparation of hippuric acid derivates 85
5.2.9.1. N-acetylglycine[50] 85
5.3. Metabolic Stability Assays 90
5.3.1. UV spectra 90
5.3.2. Method for detecting OXA 12 90
5.3.3. Metabolic Stability Assays 90
5.3.3.1. PBS and 20% Acetonitrile 90
5.3.3.2. Human plasma 91
5.4. Biological assays 92

6. Bibliography 97

7. Attachments 101
7.1. Appendix 1 - 5-fluoro-2-methyl-1H-benzo[d]imidazole (1) 101
7.2. Appendix 2 – 5-(tert-butyl)-2-methyl-1H-benzo[d]imidazole (2) 103
7.3. Appendix 3 - 2,4-dimethyl-1H-benzo[d]imidazole (3) 105
7.4. Appendix 4 - 1,2-dimethyl-1H-benzo[d]imidazole (4) 107
7.5. Appendix 5 - (E)-4-(2-(1H-benzo[d]imidazol-2-yl)vinyl)benzaldehyde (5) 109
7.6. Appendix 6 - (E)-4-(2-(5-fluoro-1H-benzo[d]imidazol-2-yl)vinyl)benzaldehyde (6) 111
7.7. Appendix 7 - (E)-4-(2-(5-(tert-butyl)-1H-benzo[d]imidazol-2-yl)vinyl)benzaldehyde (7) 113
7.8. Appendix 8 - (E)-4-(2-(4-methyl-1H-benzo[d]imidazol-2-yl)vinyl)benzaldehyde (8) 115
7.9. Appendix 9 - (E)-4-(2-(1-methyl-1H-benzo[d]imidazol-2-yl)vinyl)benzaldehyde (9) 117
7.10. Appendix 10 -Attempt synthesis of (E)-4-(2-(1H-imidazol-2-yl)vinyl)benzaldehyde (10) 119
7.11. Appendix 11 - 4-((Z)-4-((E)-2-(1H-benzo[d]imidazol-2-yl)vinyl)benzylidene)-2-phenyloxazol-5(4H)-one (11) 120
7.12. Appendix 12 - 4-((E)-4-((E)-2-(4-methyl-1H-benzo[d]imidazol-2-yl)vinyl)benzylidene)-2-phenyloxazol-5(4H)-one (12) 121

7.13. Appendix 13 - 4-((Z)-4-((E)-2-(1-methyl-1H-benzo[d]imidazol-2-yl)vinyl)benzylidene)-2-phenyloxazol-5(4H)-one (13) 122

7.14. Appendix 14 - 4-((E)-4-((E)-2-(1H-benzo[d]imidazol-2-yl)vinyl)benzylidene)-2-methyloxazol-5(4H)-one (14) 123

7.15. Appendix 15 - (E)-(4-(2-(1H-benzo[d]imidazol-2-yl)vinyl)phenyl)metanol (15) 125

7.16. Appendix 16 - 2-((E)-4-((E)-(2-benzylhydrazineylidene)methyl)styryl)-1H-benzo[d]imidazole (16) 127

7.17. Appendix 17 - 2-((E)-4-((E)-(2-phenylhydrazineylidene)methyl)styryl)-1H benzo[d]imidazole (17) 129

7.18. Appendix 18 - (E)-4-((E)-2-(1H-benzo[d]imidazol-2-yl)vinyl)benzaldehyde O-benzyl oxime (18) 131

7.19. Appendix 19 – Attempt to synthetized (E)-4-(4-(2-(1H-benzo[d]imidazol-2-yl)ethyl)benzylidene)-2-phenyloxazol-5(4H)-one 133

7.20. Appendix 20 - 4-(2-(1H-benzo[d]imidazol-2-yl)ethyl)benzaldehyde 134

7.21. Appendix 21 - N-acetylglycine (21) 135

7.22. Appendix 22 - Methyl (pyrazine-2-carbonyl)glycinate (22) 137

7.23. Appendix 23 - (Pyrazine-2-carbonyl)glycine (23) 139

7.24. Appendix 24 – Nicotinoylglycine (26) 141

Figure Index

Figure 1.1. Phases of cell cycle. [Adapted from Ref. 3] 3

Figure 1.2. Extrinsic (a) and intrinsic (b) apoptotic pathway...... 7

Figure 1.3. Signalling pathway to lead cell survival (a), apoptosis (b) or necroptosis (c) 9

Figure 1.4. Necroptosis involved in injury to different organs 11

Figure 1.5. Chemical structure of identified necroptosis inhibitor targeting RIPK1...... 16

Figure 1.6. Chemical structure of identified necroptosis inhibitor targeting RIPK3...... 17

Figure 1.7. Chemical structure of identified necroptosis inhibitor targeting MLKL 18

Figure 1.8. General structure of oxazolones, with their reactive sites 19

Figure 1.9. Chemical structure of the 21 oxazolone derivatives developed in this team by Catarina Rodrigues and tested in cell lines. 23

Figure 1.10. Chemical structure of compounds developed on the basis of OXA 12 structure.... 24

Figure 2.1. Structure of OXA 12 27

Figure 3.1. ^{1}H-NMR spectrum (a) and ^{13}C-NMR spectrum (b) of compound 5 34

Figure 3.2. a) ^{1}H-NMR of the compound 11, b) ^{1}H-NMR of the reaction of hydrogenation of compound 11...... 44

Figure 3.3. a) ^{1}H-NMR of the compound 5, b) ^{1}H-NMR of the reaction of hydrogenation of compound 5...... 44

Figure 3.4. a) ^{1}H-NMR spectrum of urea resulting from an intramolecular attack of the intermediate formed with DCC, b) ^{1}H-NMR spectrum of compound 22, synthesized from the reaction between glycine methyl ester hydrochloride and pyrazine-2-carboxylic acid via a coupling using DCC and DMAP, containing DCU. 47

Figure 3.5. ^{1}H-NMR spectrum of 22 (b), synthesized from the reaction between glycine methyl ester hydrochloride and pyrazine-2-carboxylic acid via a coupling using DCC and DMAP, with formation of DCU (a) as by-product. Compound 23 (c), resulted from the hydrolysis of compound 23 using KOH. 48

Figure 3.6. UV spectra of OXA 12 in acetonitrile 52

Figure 3.7. Run in isocratic mode using as mobile phase H_2O/MeOH (0.5:9.5) and the retention time of OXA 12 was 1.82 min. 53

Figure 3.8. Run in isocratic mode using as mobile phase H_2O/MeOH (1:9) and the retention time of OXA 12 was 2.42 min. 54

Figure 3.9. Graph showing the results corresponding to human plasma assay with OXA 12, containing the area of the peak of each injection as a function of the time of the assay. 55

Figure 3.10. Graph showing the results corresponding in PBS assay, containing the area of the peak of each injection as a function of the time of the assay...... 55

Figure 3.11. Structure of OXA 12 containing five moieties. In grey, substituents at the C-4 position of the oxazolone ring (A), benzimidazole ring moiety in blue (B) and green hippuric acid moiety (C). In this moiety there is the ring of oxazolone in purple (D) and orange, the phenyl ring terminal (E). 58

Figure 7.1. ^{1}H-NMR spectra of compound **1**, in $CDCl_3$ 101

Figure 7.2. ^{13}C-NMR of compound **1**, in $CDCl_3$ 101

Figure 7.3. IR spectrum of compound 1, in ATR 102

Figure 7.4. ^{1}H-NMR spectra of compound **2**, in $CDCl_3$ 103

Figure 7.5. ^{13}C-NMR spectra of compound **2**, in $CDCl_3$ 103

Figure 7.6. IR spectrum of compound 2, in ATR 104

Figure 7.7. ^{1}H-NMR spectra of compound **3**, in $CDCl_3$ 105

Figure 7.8. ^{13}C-NMR spectra of compound **3**, in $CDCl_3$ 105

Figure 7.9. IR spectrum of compound 3, in ATR 106

Figure 7.10. ^{1}H-NMR spectra of compound **4**, in DMSO 107

Figure 7.11. ^{13}C-NMR spectra of compound **4**, in $CDCl_3$ 107

Figure 7.12. IR spectrum of compound 4, in ATR 108

Figure 7.13. ^{1}H-NMR spectra of compound **5**, in DMSO 109

Figure 7.14. ^{13}C-NMR spectra of compound **5**, in DMSO 109

Figure 7.15. IR spectrum of compound 5, in ATR 110

Figure 7.16. ^{1}H-NMR spectra of compound **6**, in DMSO 111

Figure 7.17. ^{13}C-NMR spectra of compound **6**, in DMSO 111

Figure 7.18. IR spectrum of compound 6, in ATR 112

Figure 7.19. ^{1}H-NMR spectra of compound **7**, in DMSO 113

Figure 7.20. ^{13}C-NMR spectra of compound 7, in DMSO 113

Figure 7.21. IR spectrum of compound 7, in ATR 114

Figure 7.22. ^{1}H-NMR spectra of compound **8**, in DMSO 115

Figure 7.23. ^{13}C-NMR spectra of compound 8, in DMSO 115

Figure 7.24. IR spectrum of compound 8, in ATR 116

Figure 7.25. ^{1}H-NMR spectra of compound **9**, in Acetone 117

Figure 7.26. ^{13}C-NMR spectra of compound **9**, in Acetone 117

Figure 7.27. IR spectrum of compound 9, in ATR 118

Figure 7.28. ^{1}H-NMR spectra of the attempt to synthetize compound **10**, in DMSO 119

Figure 7.29. ^{1}H-NMR spectra of the attempt to synthetize compound **10**, in DMSO 119

Figure 7.30. ^{1} H-NMR spectra of compound **11**, in DMSO 120

Figure 7.31. ^{13}C-NMR spectra of compound **11**, in DMSO 120

Figure 7.32. ^{1} H-NMR spectra of compound **12**, in Acetone 121

Figure 7.33. IR spectrum of compound 12, in ATR 121

Figure 7.34. -^{1}H-NMR spectra of compound **13**, in Acetone 122

Figure 7.35. IR spectrum of compound 13, in ATR 122

Figure 7.36. ^{1}H-NMR spectra of compound 14, in DMSO 123

Figure 7.37. ^{13}C-NMR spectra of compound 14, in DMSO 123

Figure 7.38. HSQC spectra of compound 14, in DMSO 124

Figure 7.39. IR spectrum of compound 14, in ATR 124

Figure 7.40. ^{1}H-NMR spectra of compound **15**, in DMSO 125

Figure 7.41. ^{13} C-NMR spectra of compound **15**, in DMSO 125

Figure 7.42. IR spectrum of compound 15, in ATR 126

Figure 7.43.^{1}H-NMR spectra of compound **16**, in DMSO 127

Figure 7.44. ^{13}C-NMR spectra of compound **16**, in DMSO 127

Figure 7.45. IR spectrum of compound 16, in ATR 128

Figure 7.46. ^{1}HNMR spectra of compound **17**, in DMSO 129

Figure 7.47. ^{1}H-NMR spectra of compound **17**, in DMSO 129

Figure 7.48. IR spectrum of compound 17, in ATR 130

Figure 7.49. ^{1}H-NMR spectra of compound **18**, in DMSO 131

Figure 7.50.^{1}H-NMR spectra of compound **18**, in DMSO 131

Figure 7.51. IR spectrum of compound 18, in ATR 132

Figure 7.52. ^{1}H-NMR spectra of the attempt to synthetize compound 19, in DMSO 133

Figure 7.53. ^{1}H-NMR spectra of the attempt to synthetize compound 20, in DMSO 134

Figure 7.54. ^{1}H- NMR spectra of compound **21**, in D_2O 135

Figure 7.55. ^{13} C-NMR spectra of compound **21**, in D_2O 135

Figure 7.56. IR spectrum of compound 21, in ATR 136

Figure 7.57. ^{1}H-NMR spectra of compound **22**, in $CDCl_3$ 137

Figure 7.58. ^{13}C-NMR spectra of compound **22**, in $CDCl_3$ 137

Figure 7.59. IR spectrum of compound 22, in ATR 138

Figure 7.60. ^{1}H-NMR spectra of compound **23**, in D_2O 139

Figure 7.61. ^{13}C-NMR spectra of compound **23**, in D_2O 139

Figure 7.62. IR spectrum of compound 23, in ATR 140

Figure 7.63. ^{1}H-NMR spectra of compound **26**, in D_2O 141

Figure 7.64. ^{13}C-NMR spectra of compound **26**, in D_2O 141

Scheme Index

Scheme 1.1. Conditions of the Erlenmeyer-Plöchl reaction 20

Scheme 1.2. Influence of EDGs on hippuric acid 20

Scheme 1.3. Influence of EWGs on aldehyde 20

Scheme 1.4. Reactive sites of the oxazolone skeleton [Adapted from Ref 35][35] 22

Scheme 1.5. Diversity of compounds produced from oxazolone [Adapted from Ref. 36][36] 22

Scheme 3.1. Mechanism of formation of 4 or 5-substituted-2-methylbenzimidazole 1-3........ 31

Scheme 3.2. Alkylation mechanism for the formation of 1,2-dimethylbenzimidazole 4 by reaction of 2-metilbenzimidazole with iodomethane. 32

Scheme 3.3. Mechanism for the formation of compounds 5-9 by reaction of 4 or 5-substituted-2-methyl-benzimidazoles (1-4) with the terephthalaldehyde. 33

Scheme 3.4. Attempt to synthesize the compound (E)-4-(2-(2H-imidazol-2-yl)vinyl)benzaldehyde 37

Scheme 3.5. A reaction mechanism for the formation of the oxazolone ring from hippuric acid or its derivatives 38

Scheme 3.6. A mechanism for forming OXAs (11-14) by reacting the oxazolone ring formed above with compound 5. 38

Scheme 3.7. Mechanism of reduction the aldehyde of compound 5 to alcohol 15 using $LiAlH_4$.40

Scheme 3.8. Mechanism of reduction the aldehyde of compound 5 to alcohol 15 using $NaBH_4$ 40

Scheme 3.9. Proposed mechanism for the reaction between the aldehyde 5 and a hydrazine or hydroxylamine with formation of a hydrazone (16-17) or oxime (18). 41

Scheme 3.10. Stability of the compound obtained by the displacement of electrons from the electronegative atom (N or O) to the carbon making it low susceptible to nucleophilic attacks. 42

Scheme 3.11. Attempts of the hydrogenation reaction using palladium on charcoal as catalyst. 43

Scheme 3.12. Mechanism for the formation of N-acetyl glycine 21 through the reaction of glycine with acetic anhydride. 45

Scheme 3.13. a) Formation of compound 22 from the carboxylic acid and through a coupling using DCC and DMAP as the catalyst, b) Possible mechanism of formation of a urea as a by-product resulting from an intramolecular reaction of the intermediate formed in the reaction with the DCC 47

Scheme 3.14. Hydrolysis of compound 22 using KOH as the base, for the formation of compound 23 49

Scheme 3.15. Formation of the acid chloride 24-25 from the carboxylic acid using oxalyl chloride and dimethylformamide (DMF) as catalyst, a) formation of Vilsmeier-Haack reagent through reaction between oxalyl chloride and DMF; b) reaction of Vilsmeier-Haack reagent with carboxylic acid with formation of acid chloride. 50

Scheme 3.16. Formation of acid chloride 24-25 using thionyl chloride 50

Scheme 3.17. Mechanism of formation of compound 22 and 26 through reaction between acid chloride 24 or 25 and glycine or derivative, through of S_N2 reaction com expulsion of chloride.. 51

Table Index

Table 1.1. Inhibitors reported for each target molecule 18

Table 3.1. Characterizations of compounds 1-3, synthetized through of condensation between 4 or 5-subtitutedbenzeno-1,2-diamine and triethyl orthoacetate.[a] 32

Table 3.2. Characterization of compound 4, synthetized through alkylation of 2-methylbenzimidazole 33

Table 3.3. Characterizations of compounds 5-9, synthetized by reaction between 2-methylbenzimidazole and its derivatives 1-4 with terephthalaldehyde. 36

Table 3.4. Characterization of compounds 11-14, synthetized through of reaction of compound 5-9 with hippuric acid or N-acetyl glycine (21) 39

Table 3.5. Characterization of compound 15, synthesized by reduction of aldehyde 5 41

Table 3.6. Characterization of compounds 16-18 from reaction between aldehyde 5 and hydrazine or hydroxylamine 42

Table 3.7. Characterization of compound 21, synthesized through an reaction between glycine and acetic anhydride. 45

Table 3.8. Results obtained for OXA 12 using CNS MPO 46

Table 3.9. Characterization of compound 22, synthesized from the reaction between glycine methyl ester hydrochloride and pyrazine-2-carboxylic acid via a coupling using DCC and DMAP. 48

Table 3.10. Characterization of compound 23, synthetized through hydrolysis of compound 22 using KOH 49

Table 3.11. Characterization of compound 26, synthetized through reaction between acid chloride and glycine 51

Table 3.12. Results of biological assays to OXA derivatives in BV2 murine microglia cells 57

Table 3.13. Percent protection against necroptosis for each structure synthesized with substituents at C-4 position of oxazolone moiety, using BV2 murine microglia cells for the performance of the assay 58

Table 3.14. Percent protection against necroptosis for each structure synthesized with introduction of substituents in 4 or 5-position of benzimidazole, using BV2 murine microglia cells for the performance of the assay. 60

Table 3.15. Percent protection against necroptosis for each structure synthesized with alteration in the benzimidazole heterocycle, using BV2 murine microglia cells for the performance of the assay. 61

Table 3.16. Percent protection against necroptosis for each structure synthesized with modifications in hippuric acid, using BV2 murine microglia cells for the performance of the assay. 61

Table 3.17. Percent protection against necroptosis for each structure synthesized with alterations in hippuric acid, using BV2 murine microglia cells for the performance of the assay. 62

Abbreviations

^{13}C-NMR	Nuclear Magnetic Resonance of Carbon
^{1}H-NMR	Proton Nuclear Magnetic Resonance of Proton
ACN	Acetonitrile
AcOEt	Ethyl acetate
Apaf1	Apoptotic protease activating factor 1
Bz	Benzene
CARD	Caspase recruitment domain
CNS	Central nervous system
CYLD	Cylindromatosis
d	Doublet
DCC	N,N'-Dicyclohexylcarbodiimide
DCM	Dichloromethane
DCU	Cyclohexylurea
DISC	Death-inducing signalling complex
DMAP	4-Dimethylaminopyridine
DMF	Dimethylformamide
DMSO	Dimethyl sulfoxide
DNA	Deoxyribonucleic acid
EDG	Electron donating group
EtOH	Ethanol
EWG	Electron withdrawing group
FADD	Fas-associated protein with death domain
FasL	Fas ligand
Hex	Hexane
HMBC	Heteronuclear multiple bond correlation
HMQC	Heteronuclear single quantum coherence
HPLC	High-performance liquid chromatography
IR	Infra-red spectroscopy
J	Coupling constant
m	Multiplet

M.p.	Melting point
MeOH	Methanol
MLKL	Mixed Lineage Kinase Domain Like Pseudokinase
Nec-1	Necrostatin-1
NEMO	NF-kappa-B essential modulator
NF-kB	Nuclear factor kappa-light-chain-enhancer of activated B cells
NMR	Nuclear magnetic resonance
NSA	Necrosulfonamide
Oxa	Oxazolone
Ph	Phenyl
q	Quartet
Rf	Retention factor
RIPK1	Receptor-interacting serine/threonine-protein kinase 1
RIPK3	Receptor-interacting serine/threonine-protein kinase 3
R_T	Retention time
s	Singlet
t	Triplet
THF	Tetrahydrofuran
TLC	Thin Layer Chromatography
TNF	Tumor necrosis factor
TNF-α	Tumor necrosis factor alpha
TPA	Two photons absorption
TRADD	Tumour necrosis factor receptor type 1-associated death domain protein
TRAIL	TNF-related apoptosis-inducing ligand
UV/Vis	Ultraviolet- visible spectroscopy
δ	Chemical shift

Units

µL	Microliter
Equiv.	Equivalents
g	Gram
h	Hour
Hz	Hertz
M	Molar
m/z	Mass-to-charge ratio
mg	Milligrams
MHz	Megahertz
min	Minute
mL	Millilitre
mmol	10^{-3} mole
mol	Mole
ºC	Degree Celsius
ppm	Parts per million
t	Time

1. Introduction

1.1. Cell cycle

An organism is formed through growth and cell division. At this stage, the duplication of the cellular content occurs and later the division into two daughter cells. The cycle that leads to the production of these daughter cells through division and duplication of cellular content is called the cell cycle, and can vary depending on the organism or its stage of life.[1,2]

For this cycle to be complete, it will be necessary to make the minimum number of processes for the genetic information to pass to the next generation, thus producing the two daughter cells identical to each other and to the parent cell.[1]

This cycle is composed of two main phases: the interphase, where DNA duplication occurs and the mitotic phase, longer phase of the cell cycle, where cell division occurs.[1,2]

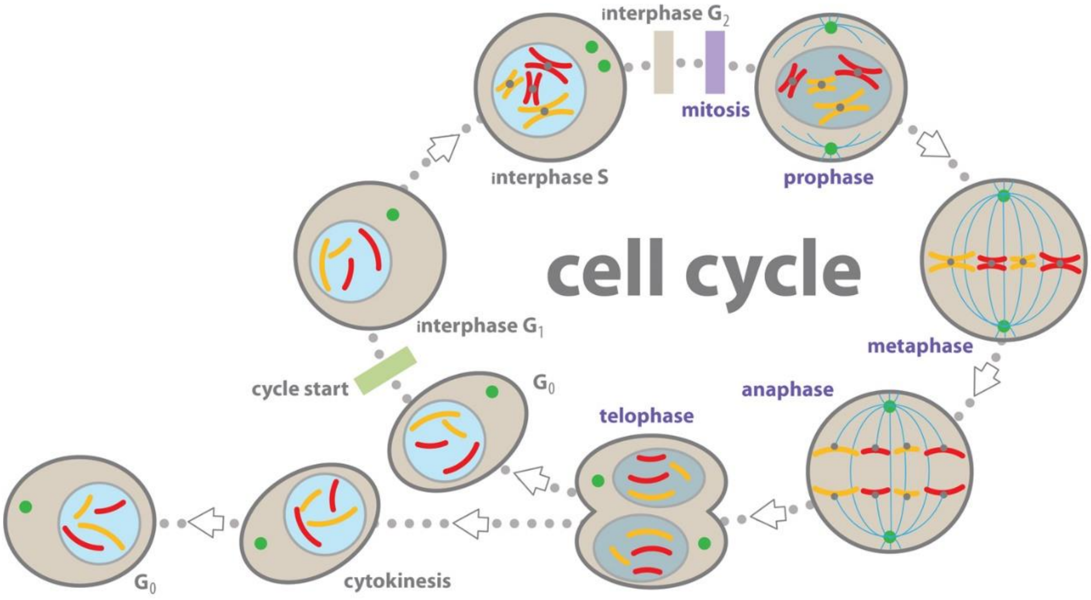
interphase G_2
mitosis
interphase S
prophase
cell cycle
interphase G_1
metaphase
cycle start
G_0
anaphase
telophase
G_0
cytokinesis

Figure 1.1. Phases of cell cycle. [Adapted from Ref. 3]

1.1.1. Interphase

a) G_1 phase

The interphase starts with the G_1 phase, which occurs after the end of the previous mitotic phase and until the beginning of the S phase (DNA synthesis). This is the first checkpoint, allows to find and repair DNA damage before the cells enters to S phase. At this stage there is still a continuous cell growth without replication.[1,2]

b) S phase

This duplication is a complex process in which it is necessary to ensure that chromosomal characteristics are inherited by the daughter cells by the creation of two exactly identical semi-conserved chromosomes.[1]

DNA replication is the main stage of this phase, beginning at the origins of replication that are scattered at various locations on the chromosome.[1]

c) G_2 phase

The G_2 phase, the last of the interphase, occurs between S phase and mitosis, and just as G_1 phase is a checkpoint, preventing the start of mitosis if aberrant genetic modifications occured.[1,2]

1.1.2. Mitotic phase

1.1.2.1. Mitosis

Mitosis is a very complex and regulated phase that occurs after the G_2 phase and where the sister chromatids are separated and distributed into a pair of identical daughter nuclei each containing a copy of the original genome. It can be divided into five different stages: prophase, prometaphase, metaphase, anaphase and telophase, each one corresponding to the completion of one specific set of activities.[1,2]

After the conclusion of mitosis, the cytokinesis begins, through which the cytoplasm divides and occurs the formation of two daughter cells each containing a nucleus.[1,2]

a) Prophase

In the prophase occurs the condensation of the replicated chromosomes and these are long, thin and thread-like. Each chromosome has two chromatids. The two chromatids are joined at the centromere. There is the formation of the mitotic spindle outside the nucleus and between the two centrosomes.[1,2]

b) Prometaphase

After the conclusion of the prophase there is a transition period until the beginning of the metaphase which is called the prometaphase. This phase begins with the disintegration of the nuclear envelope and cellular microtubules attach to chromosomal kinetochores in the centromere.[1,2]

c) Metaphase

After prometaphase, the chromosomes are drawn to the opposite ends of the cell by the centrosomes and the metaphase is reached when the alignment of the chromosomes occurs in the equatorial plane, in the middle of the poles.[1,2]

d) Anaphase

The transition from metaphase to anaphase occurs by breaking the connection between the sister chromatids and the formation of the daughter chromosomes. These newly formed daughter chromosomes are separated and pulled to opposite ends of the cell by shortening the kinetochore microtubules.[1,2]

e) Telophase

In the last phase of mitosis, the daughter chromosomes reach the poles and decondense. There is also the formation of a new nuclear envelope thus completing the formation of two new nuclei.[1,2]

1.1.2.2. Cytokinesis

At the end of mitosis, cytokinesis begins. This process occurs by dividing the cytoplasm into two, leading to the formation of two daughter cells each containing its own nucleus.[1,2]

1.2. Cell death

Cell death plays a very important role in the development of the human, animals and plants, staying throughout life. In a tissue, cell division and cell death are regulated in order to achieve an equilibrium.[1]

Cell death can occurs in different ways, such as apoptosis, when a cell activates an intracellular death program which occurs in a programmed manner or by necrosis, in the case of an inflammatory response that occurs in a disorganized way.[1,4]

1.2.1. Apoptosis

Apoptosis is a type of programmed cell death in which cells activate an intracellular death, in a controlled manner. However, this is not the only form of programmed cell death.

In this type of cell death, characteristic morphological changes occur in cells. Apoptotic cells shrink and condense, the cytoskeleton collapses, the nuclear envelope disassembles and the nuclear chromatin condenses and breaks up into fragments.[1]

These fragments, the surface of the cell and apoptotic bodies, are chemically altered and thus easier to identify by macrophages or neighboring cells. Such features enhance these apoptotic cells to be phagocytosed by the macrophages before their contents are released. Through this process, the cell dies and is rapidly eliminated without causing a harmful inflammatory response, contrary to necrosis.[1]

As apoptosis is a highly regulated and controlled process that confers advantages during an organism's lifecycle, this programmed cell death is highly important in the development and homeostatic maintenance animals and plants, through the elimination of abnormal, misplaced, non-functional or potentially dangerous cells.[1]

At this stage, there is a change in the plasma membrane of the apoptotic cells through the displacement of the phospholipid phosphatidylserine to the outer layer of the lipid bilayer of the plasma membrane, serving as a marker for phagocytosis by neighboring cells or macrophages.[1]

Apoptosis is performed by a similar intracellular machinery in all animals. Importantly, by definition it is dependent on caspases, a family of proteases containing cysteine residues, capable of cleaving proteins specific in the residue of aspartic acid.[1]

Caspases are synthesized in the cell and remain as inactive precursors or procaspases. The cascade is initiated by the initiator-procaspases, which contain a caspase recruitment domain (CARD) within a long pro-domain, which allows binding to adapter proteins in activation complexes, when a signal for the cell to enter into apoptosis occurs.[1]

In these complexes, the initiator procaspases cleave and activate to each other irreversibly. And once activated, these caspases cleave and activate the executioner procaspases and, thus, the caspase proteolytic cascade is initiated.[1]

The caspase required for apoptosis depends on the type of cell and the stimulus.[1]

There are two known pathways for activation of the caspase cascade leading to apoptosis, the extrinsic pathway and the intrinsic pathway (Figure 1.2). Each of these pathways uses its own initiator procaspase and its activation complex.[1,5]

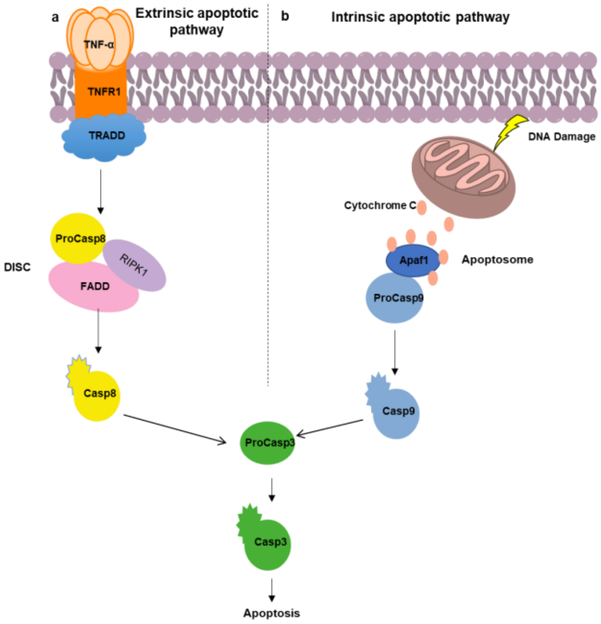
a
Extrinsic apoptotic pathway
b
Intrinsic apoptotic pathway
TNF-α
TNFR1
TRADD
DNA Damage
Cytochrome C
ProCasp8
RIPK1
DISC
FADD
Apaf1
Apoptosome
ProCasp9
Casp8
Casp9
ProCasp3
Casp3
Apoptosis

Figure 1.2. Extrinsic (**a**) and intrinsic (**b**) apoptotic pathway

1.2.1.1. Extrinsic pathway of apoptosis

The binding of extracellular signalling proteins to death receptors, belonging to the tumor necrosis factor (TNF) family, leads to the activation of the extrinsic apoptosis pathway (Figure 1.2a).[1,5]

Activation of this pathway may occur by either binding of the Fas ligand (FasL) to the Fas receptor resulting in the binding of the Fas-associated protein with death domain (FADD), or via TNF receptor activation, resulting in the binding of the adapter protein TRADD, and consequent recruitment of FADD and receptor-interacting serine/threonine-protein kinase 1 (RIPK1).[1,5]

FADD, recruits initiator procaspase (*procaspase-8* or *procaspase-10*) forming a death-inducing signalling complex (DISC). Once activated in the DISC, the initiator procaspases activate executioner procaspases, thereby inducing apoptosis.[1,5]

The extrinsic pathway of apoptosis may be inhibited by the production of *decoy receptors* by the cells, these having a ligand-binding domain, but not a death domain, inhibiting apoptosis by inhibiting the death receptor. However, they can also produce blocking proteins, such as FLIP, that compete with the initiating procaspases for binding to the DISC complex, inhibiting them. These inhibitory mechanisms serve to prevent unnecessary pathway activation.[1,5]

1.2.1.2. Intrinsic pathway of apoptosis

Apoptosis can also be activated within the cell in response to certain stimuli. This pathway (Figure 1.2b) depends on the release into the cytosol of mitochondrial proteins that can activate the caspase proteolytic cascade in the cytoplasm.[1]

One of the crucial proteins of this pathway is cytochrome c, which binds to the procaspase-activating adapter protein, apoptotic protease activating factor-1 (Apaf1), leading to apoptosome formation (equivalent to DISC). Apaf1 proteins recruit the initiator procaspases proteins (*procaspase-9*) in the apoptosome. Once activated, they activate the executioner procaspases resulting in apoptosis.[1,5]

The regulation of this pathway by the Bcl2 proteins occurs by controlling the release of cytochrome c and other proteins into the cytosol. Pro-apoptotic Bcl2 proteins induce apoptosis by increasing the release of proteins, in the case of the anti-apoptotic Bcl2 proteins, they inhibit apoptosis by blocking the release of these proteins.[1,5]

Besides the Bcl2 proteins, there are inhibitor of apoptosis (IAP) proteins that are also intracellular regulators of apoptosis. These binds and inhibit the active caspases.[1]

1.2.2. Necrosis

In contrast to apoptosis, necrosis is an unregulated cell death type that occurs through autolysis caused by external factors such as infection or trauma.[6] As it follows a different transduction pathway than apoptosis this type of cell death originates a swelling of the organelles, an early increased permeability of the plasma membrane[7,8] and consequently to a loss of intracellular content to the extracellular space, thus causing an inflammatory response.[7]

Until a few years ago, necrosis was considered an unregulated process unlike apoptosis.[9] However, recent studies reveal that there is a type of necrosis that can be regulated but exhibits similar characteristics as necrotic cell death, the necroptosis or necrosis programmed.[6]

1.2.2.1. Necroptosis

The necroptosis is a term used a few years and refers to a type of programmed necrosis.[9] This is caspase-independent and occurs when apoptosis is inhibited.[7,8]

This type of cell death occurs through a variety of intracellular and extracellular stimuli that activate ligands of death receptor family[10,11], being involved in a variety of pathologies such as myocardial infraction[12], stroke[13], atherosclerosis[14] or Crohn's disease[15].

1.2.2.1.1. Necroptosis signalling pathway

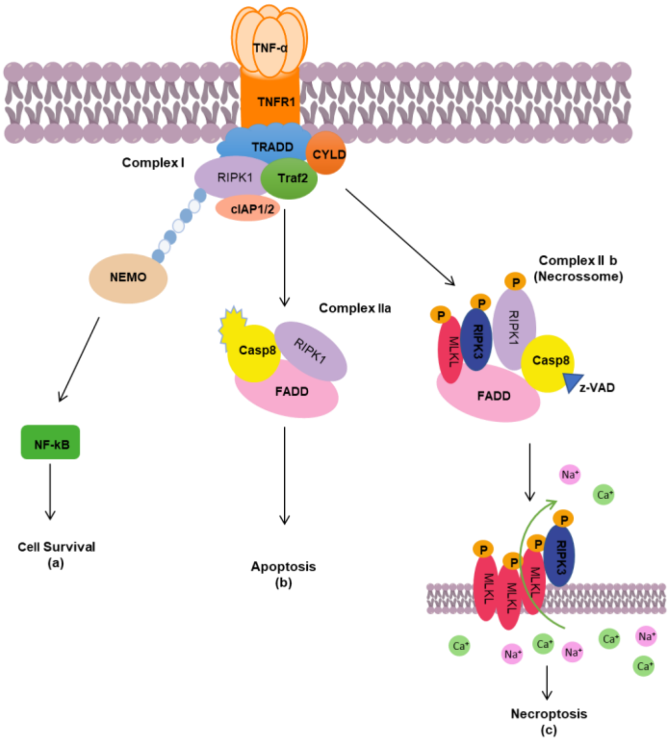
TNF-α
TNFR1
TRADD
CYLD
Complex I
RIPK1
Traf2
cIAP1/2
NEMO
NF-κB
Cell Survival
(a)
Complex IIa
Casp8
RIPK1
FADD
Apoptosis
(b)
Complex II b
(Necrossome)
P
MLKL
RIPK3
RIPK1
Casp8
FADD
z-VAD
Na+
Ca+
Necroptosis
(c)

Figure 1.3. Signalling pathway to lead cell survival (**a**), apoptosis (**b**) or necroptosis (**c**)

Activation of this signaling pathway occurs by the binding of the ligands of the death receptor family (such as TNF-α, FasL and TRAIL) to their receptors on the plasma membrane, triggering the formation of complex I. This complex depending on modifications such as ubiquitination and phosphorylation can determine the life or death of the cell.[7,16]

Upon ubiquitination RIPK1, recruits the TNF mediators, NEMO and TAK1, activating downstream pathways of NF-κB and MAP (Figure 1.3a).[7]

However, the inhibition of the NF-kB pathway by the protein synthesis inhibitor, cyclohexamine, and the deubiquitination of RIPK1 by CYLD leads to cell death, inducing the formation of complex IIa (Figure 1.3b). [7,16]

Complex IIa is composed of RIPK1 and TRADD, which recruits FADD, and this in turn recruits procaspase-8. This initiates the apoptotic pathway by inhibition of necroptosis through the cleavage of RIPK1 and receptor-interacting serine/threonine-protein kinase 3 (RIPK3).

If apoptosis is inhibited, RIPK1 recruits RIPK3 by binding to RIP-homotypic interacting motif (RHIM) domains to form an amyloid complex, necrossome.[4,7,8,16] In this complex, the autophosphorylation of RIPK3, leads to recruitment of its substrate, mixed lineage kinase domain like pseudoquinase (MLKL) (Figure 1.3c).[7,8]

The MLKL acts as a necroptosis executioner and is found in the cytosol as a monomer when inactive.[8] Upon RIPK3 activation, its kinase domain binds to the C-terminal domain of MLKL leading to phosphorylation of MLKL.[7,8]

Consequently, oligomerization of the *N*-terminal domain of MLKL occurs through destabilization of the MLKL structure followed by translocation to the plasma membrane, where permeabilization of the membrane.[7,8]

1.3. Necroptosis as therapeutic target

Necroptosis, a regulated form of necrosis, is associated with many pathologies such as myocardial infarction[12] or atherosclerosis[14].

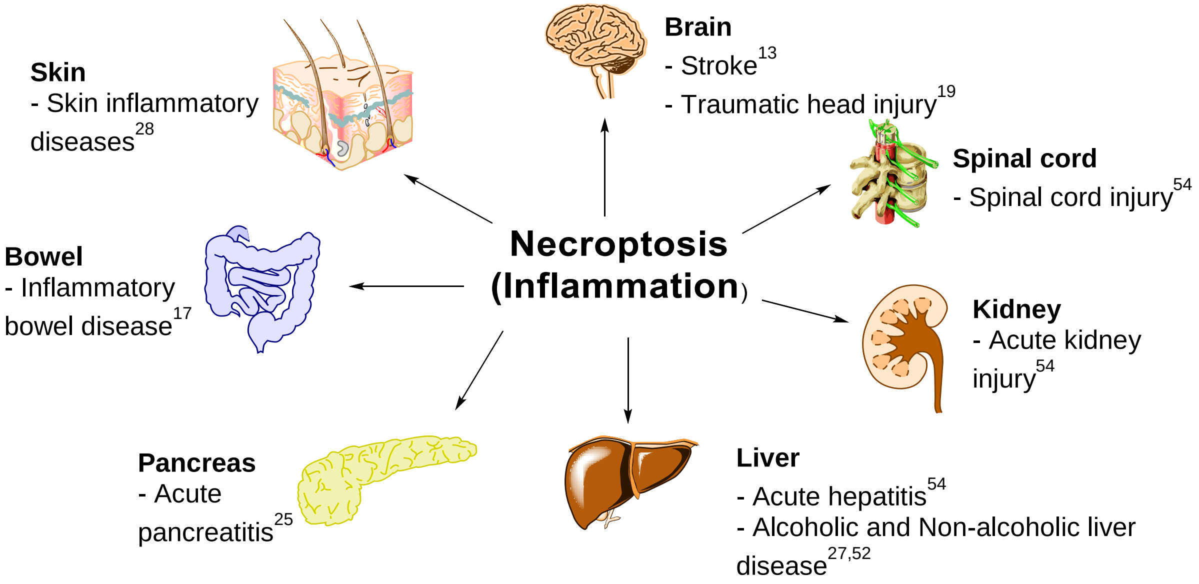
Necroptosis (Inflammation)
Skin
- Skin inflammatory diseases[28]
Brain
- Stroke[13]
- Traumatic head injury[19]
Spinal cord
- Spinal cord injury[54]
Bowel
- Inflammatory bowel disease[17]
Kidney
- Acute kidney injury[54]
Pancreas
- Acute pancreatitis[25]
Liver
- Acute hepatitis[54]
- Alcoholic and Non-alcoholic liver disease[27,52]

Figure 1.4. Necroptosis involved in injury to different organs

1.3.1. Ischemia-reperfusion injury

Ischemia-reperfusion injury is a common type of cell damage. Ischemia occurs when there is a lack of blood supply through the obstruction of a tissue, resulting in the lack of oxygen and nutrients that in the case of being prolonged leads to cell death. Reperfusion occurs following ischemia, through the reintroduction of blood flow to tissues where it has been missing for some time and can lead to inflammation.[7,10]

This type of injury can be reversible, when it is possible to restore the bloodstream or irreversible, when the deprivation is persistent and leads to cell death.[7,10] During restoration of blood flow resulting in the reintroduction of oxygen, the formation of reactive oxygen species (ROS) and pore opening occur, leading to inflammation and death by necrosis.[17]

In vivo studies administering Necrostatin-1 (Nec-1) before reperfusion in animal models, revealed the inhibition of RIPK1-dependent necrosis, leading to the reduction of infarct size.[12]

1.3.1.1. Stroke

Stroke occurs due to obstruction of the blood vessels in the brain by thrombosis or embolism or through an intracerebral hemorrhage.[10]

Blood vessels obstruction can be prolonged, leading to death of brains cells due to lack of oxygen. In the case of hemorrhage, this occurs through the rupture and leakage of a blood vessel leading to damage in the cells.[13]

Degterev *co-workers* demonstrated that necroptosis may play a role in stroke, since that with using Nec-1 has occurred a delay of ischemic neuronal injury.[9] Another study, performed by Xingshun Xu *co-workers* in mices using two protective agents, HMG (anti-apoptotic) and Nec-1 (anti-necrotic), also demonstrated a decrease in infarct size, and combined treatment may be a clinically useful.[13]

1.3.1.2. Traumatic brain injury

Traumatic brain injury occurs when an external mechanical force is applied to the brain, causing secondary injuries such as ischemia-reperfusion, hemorrhage or edema, leading to difficulties in the functioning or even death of neuronal cells.[10]

Data obtained in one study revealed that necroptosis may play a role in traumatic brain injury, since the administration of Nec-1 in a mouse model after controlled cortical impact revealed a decrease in tissue injury in the brain and inflammation, increasing motor function and memory space.[18]

1.3.2. Neurodegenerative diseases

1.3.2.1. Huntington's Disease

Huntington's disease is an autosomal dominant progressive neurodegenerative disease occurring in a single gene called Huntingtin, through of the formation of the mutant protein, result of triple repeats of CAG in the gene encoding Huntingtin protein. This disease is often the result of genetic inheritance and it is characterized by motor, cognitive and psychiatric deficits and may occur at any time in life, however it is more frequent that the symptoms begin in middle age.[7,10,19]

Assays using Nec-1 in immortalized striatal neuronal line expressing mutant HTT reduces cell death and using in mutant HTT-expressing R6/2 transgenic mouse model delays the onset and progression of disease.[20]

1.3.2.2. Alzheimer's disease

Alzheimer's disease is a multifactorial chronic neurodegenerative disorder characterized by progressive loss of memory and motor functions and the leading cause of dementia. Although its etiology is still not fully understood, it characterized by the formation of intracellular neurofibrillary tangles and extracellular β-amyloid protein deposits, leading to neuronal cell death in the cerebral cortex and other regions.[10]

In vivo model, administration of Nec-1, in previously treated aluminum mouse resulted in a decrease in neuronal cell death, improved learning and memory, and still decrement expression of Aβ and Tau protein levels.[21]

1.3.3. Inflammatory diseases

1.3.3.1. Acute pancreatitis

Pancreatitis is an inflammation in the pancreas, which may be acute or chronic.[22]

Studies in experimental models reported that in acute pancreatitis, acinar cells can die both by apoptosis and by necrosis, varying the severity of pancreatitis proportionally with necrosis and inversely proportional to apoptosis.[22]

RIPK3 plays an important role in necroptosis. Studies where pancreatitis is induced by cerulein have shown an increase in RIPK3 expression only in pancreatic tissues, or a few hours later there were several areas with acylar cell loss and necrosis. This effect was prevented by using deficient RIPK3 lines and a decrease in serum amylase was still observed in comparison with normal cells. Through this observation and taking into account of pancreatitis induced by cerulein can confirm the involvement of necroptosis in this pathology.[23]

However, it is recently been reported that administration of Nec-1 has no protective effect on cerulein induced pancreatitis. This even has a contrary effect, accelerating the death of cells. [24]

1.3.3.2. Chronic liver diseases

Chronic liver disease can occur through several factors, such as alcohol consumption or fat accumulation. Over time, the disease progresses through several stages between tissue damage and liver dysfunction.

1.3.3.2.1. Alcoholic liver disease

Alcoholic liver disease occurs after a chronic ingestion of alcohol.[10]

Evidence shows that apoptosis is linked to alcoholic liver disease, however, treatment with a pan-caspase inhibitor is not sufficient to prevent liver damage. Other studies show that RIPK3 expression increases with or without pan-caspase inhibitor after chronic administration of ethanol, the expression of this kinase being evidence of necropsosis.[10,25] It has also been reported that mice with RIPK3-deficient show protection against liver damage induced by ethanol. However, when administered Nec-1, it did not modify the expression of RIPK1, not attenuating the liver injury. This may occur if the pathology is independent of RIPK1 or due to pharmacokinetic problems with Nec-1.[10,26]

1.3.3.3. Skin inflammatory diseases

Epidermal keratinocytes are the first line of defense against potentially pathogenic microorganisms since they provide a structural and immunological barrier. When exposed to lesions, they send signals triggering immune responses. Since of responses sent by epidermal keratinocytes is implicated in inflammatory skin disease.[10,27]

One study found that specific epidermal ablation of FADD leads to spontaneous necrosis of keratinocytes and to the development of severe skin injury. This necrosis was prevented by RIP3 deficiency, thus showing that RIP3-dependent necrosis of FADD-deficient keratinocytes triggers severe inflammation of the skin of mice.[10,27] Inflammations can also be triggered in mice by deficient caspase-8 in studies.[10,28]

It can then be concluded that both FADD and caspase-8 play an important role in preventing skin inflammation.

1.4. Necroptosis inhibitors

Necroptosis is a very complex process, and in order for it to be viably “druggable”, a careful evaluation of the pathway and its intricate interconnexions with other biochemical paths have to be considered. Nowadays, to pharmacologically interfere with RIPK1, RIPK3 and MLKL have been targeted, as they form the necrosome and from there occurs transduction of many other downstream signaling (e.g the translocation of the phosphorylated MLKL to the plasma membrane where it can lead to the swelling of organelles and to membrane rupture).[29]

Based on these targets, studies have been initiated to discover necroptosis inhibitors. However, so far, no drug has reached the marked, is still in clinical trials.

1.4.1. RIPK1

Necroptosis can be induced by ligands of the death receptor, with RIPK1 being the first site where this pathway can be inhibited.

Necrostatins, small molecules inhibitors of necroptosis, were reported for the first time in 2005 by Degterev *et al*.[9] These compounds were identified through of a screening using TNF-α as pathway inducer and the caspase inhibitor zVAD-fmk to inhibitor apoptosis, leading to necroptosis.

Necrostatins (Figure 1.5a) are selective for RIPK1 receptor, inhibiting their catalytic activity and thus inhibiting necroptosis.[14,30] Nec-1, the first known inhibitor of necroptosis, it has been the most studied although there are other necrostatins with inhibitory activity such as Nec-3 and Nec-4.[30]

Necrostatins were optimized in order to increase activity and metabolic stability. From the optimization of Nec-1, 7-Cl-O-Nec-1 (Nec-1s) was synthesized by addition of a Cl at the 7-position of the indole ring which provided an increase in activity and substitution of thio-hydantoin by hydantoin which increased stability and eliminated toxicity. Furthermore, this molecule presented no off-target activity against indoleamine-2,3-dioxygenase, as happened with the Nec-1 [14,30]

In order to further improve necrostatin activity, PN10 (Figure 1.5c), a hybrid compound (a combination of Nec-1s and a fragment of Ponatibib), was developed. This compound proved to be highly potent and selective for RIPK1, taking advantage of the best properties of each of the other two inhibitors and increased interactions with the active site.[31]

Harris *et. al.* described three novel classes of compounds with inhibitory activity against necroptosis (aminoisoquinolines, pyrrolo[2,3-b]pyridines e furo[2,3-d]pyrimidines) following the screening of GSK kinase inhibitor libraries.[30,32] From the crystalline structure of a compound of the first series with RIPK1 it was possible to identify the zones of the interaction of the compound with RIPK1. The X-ray structure showed that 1-aminoisoquinoline forms hydrogen bonds with the

Met95 hinge residue of RIPK1. Central urea forms hydrogen bonds with DL15 ASP156 and the Glu63 side chain.[32]

Of these three series, Cpd 27 (Figure 1.5b), belonging to the last series, was selected for *in vivo* assays where necroptosis is induced by TNF-α.[32]

Pazopanib (Figure 1.5d), a selective tyrosine kinase receptor inhibitor, has been more recently identified to decrease necroptosis. This selectively inhibits RIPK1, without decreasing the *in vitro* activity of RIPK3.[33]

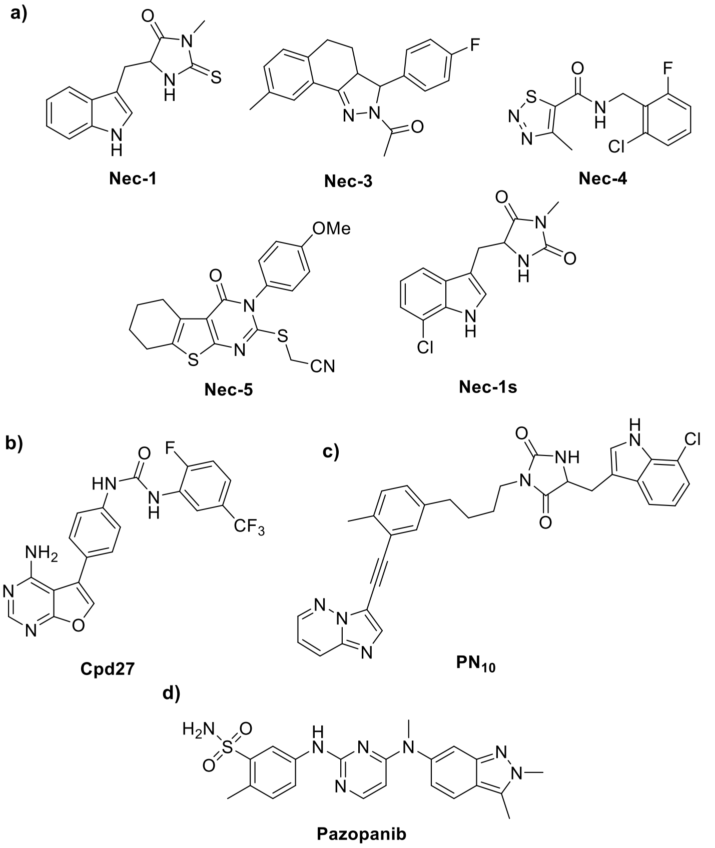

Figure 1.5. Chemical structure of identified necroptosis inhibitor targeting RIPK1

1.4.2. RIPK3

RIPK3, the second protein required for necroptosis execution, was discovered after RIPK1, its binding partner through the RHIM, that leads to the formation of the necrosome.[30]

Once the catalytic activity of this kinase or RIPK1 is inhibited, the activation of necroptosis will also be inhibited or canceled, since this protein plays two distinct roles, on one hand it activates the necrotic activity and on the other recruits the MLKL. Phosphorylation of this by RIPK3 is the key step in the execution of necroptosis.[30]

Once the importance of this protein in the activation of necroptosis has been developed, small inhibitory molecules of this kinase (Figure 1.6).

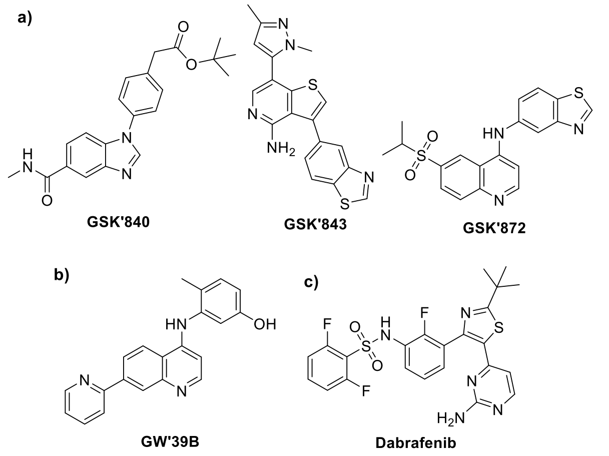

Figure 1.6. Chemical structure of identified necroptosis inhibitor targeting RIPK3

The first three inhibitors to be identified were GSK'840, GSK'843 and GSK'872 (Figure 1.6a) by Kaiser *co-workers*.[34]

Of the three compounds identified, GSK'840 was the one that presented a better profile, however this is active in human cells but not in mouse cells, unlike the other two that have inhibitory activity in mouse cells. These results demonstrate that the binding ability of RIPK3 to the compound depends on the cell type and also show the contribution of the activity of this kinase to necroptosis.[34]

GW'39B (Figure 1.6b), was identified as an inhibitor of RIPK3, exhibiting a structure similar to GSK'872, another inhibitor of RIPK3. This compound blocks the phosphorylation of MLKL and translocation to the plasma membrane by inhibiting RIPK3 in both murine and human cells.[34]

Dabrafenib (Figure 1.6c), a BRAF inhibitor was also shown to inhibit of RIPK3, by disrupting binding of RIPK3 to MLKL. This is the only inhibitor of RIPK3 that has been tested in vivo.

Another indirect approach for the inhibition of RIPK3 is found in the complex of Hsp90 with co-chaperone Cdc37 that is associated with RIPK3, so its inhibitors prevent the activation of RIPK3 in the necrosome.[30]

1.4.3. MLKL

The third hypothesis for the inhibition of necroptosis lies in the necroptosis executioner, the pseudokinase MLKL.[14]

The discovery of necrosulfonamide (NSA) (Figure 1.7a) as an inhibitor of necroptosis was important for the identification of MLKL since present activity only after necrosome formation. This molecule acts as a Michael acceptor, by coupling α, β-unsaturated enone with the Cys86 residue of MLKL.[14] For this reason, it is not possible to use this compound in non-murine cells lacking the cysteine residue.[14,30]

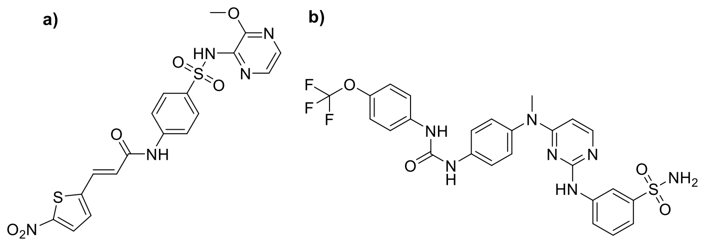

Necrosulphonamide (NSA)

Compound 1

Figure 1.7. Chemical structure of identified necroptosis inhibitor targeting MLKL

More recently, "Compound 1" (Figure 1.7b) has also been reported to target MLKL, preventing the pseudokinase from altering its conformation being phosphorylated by RIPK3. However, this compound is toxic to cells and is not selective for MLKL, having its application limited.[14]

Table 1.1. Inhibitors reported for each target molecule

Target molecule	Necroptosis inhibitors
RIPK1	Nec-1, Nec-3, Nec-4, Nec-5, Nec-1s Cpd27 PN10 Pazopanib GSK’481, GSK2982772 Compound 56 (HIPA-56) Tozasertib GSK2606414, GSK2656157
RIPK3	GSK’840, GSK’843, GSK’872 GW’39B Dabrafenib
MLKL	NSA Compound 1

1.5. Oxazol-5(4H)-ones

Oxazol-5(4H)-one (hereinafter only referred to as Oxazolones) are small and simple molecules, very valuable and versatile. They have applications in several areas of research, such as organocatalysis or photochemistry, due to the presence of several reactive sites, represented in Figure 1.8 as N-3, C-4 and C-5, where a varied set of modifications can occurs.[35,36]

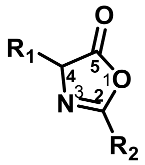

Figure 1.8. General structure of oxazolones, with their reactive sites

Plochl *et al*, synthesized the first oxazolone in 1883, through by the condensation of a benzaldehyde with hippuric acid in the presence of acetic anhydride. It was only in 1900, that Erlenmeyer established the first correct structure of oxazolone (Figure 1.8), containing a 5-membered ring with O and N as the heteroatom, which he called "azolactone".[36–38]

From this oxazolone, it is possible to easily generate an oxazole enolate through abstraction of the acidic proton at C-4, the formation of a reactive ketene or 1,3-dipolar through the use of a Lewis acid. The ring may also be opened by a nucleophile to the carbonyl.[36]

1.5.1. Erlenmeyer-Plochl reaction

The Erlenmeyer-Plöchl reaction was first described in 1883 by Plöchl as the condensation of benzaldehyde with hippuric acid in the presence of acetic anhydride and sodium acetate (Scheme 1.1),[38] occurring in the absence of any solvent, it can be said that this reaction follows the principles of green chemistry because it minimizes the use and production of hazardous substances.[35]

The reaction takes place in two steps, beginning with a cyclization of hippuric acid and its derivatives, followed by a Perkin condensation, thus producing Erlenmeyer azolactone.[38]

In this reaction competition occurs for the product resulting from the transacylation and condensation of the hippuric acid.[39]

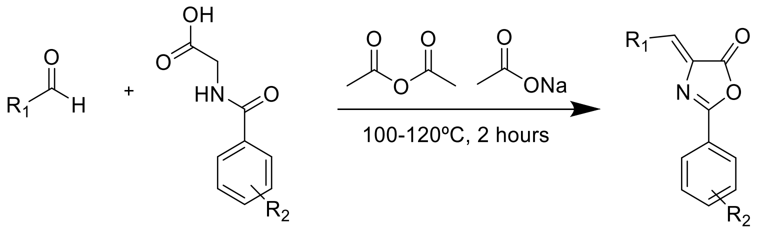
OH
O
R1
H
+
HN
O
O
O
O
O
ONa
100-120ºC, 2 hours
R2
R1
O
N
O
R2

Scheme 1.1. Conditions of the Erlenmeyer-Plöchl reaction

This type of reaction is influenced by the electronic characteristics of the compounds, which are sensitive to the nature of the substituents, with a decrease in the reaction time in the presence of electron donating groups (EDG) in the hippuric acid that increase the reactivity due to high nucleophilicity of the oxygen atom on the amide carbonyl group (Scheme 1.2).[39,40]

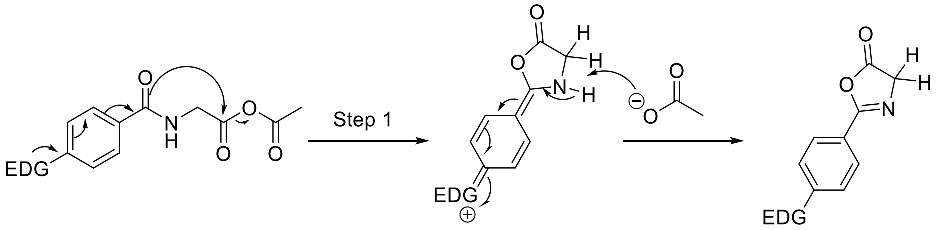
EDG
N
H
O
O
O
Step 1
EDG
N
H
H
H
O
O
EDG
N
H
H
O
O

Scheme 1.2. Influence of EDGs on hippuric acid

However, electron withdrawing groups (EWG) in the aldehyde also decrease the reaction time, by increasing the electrophilicity of the carbonyl group (Scheme 1.3).[39,40]

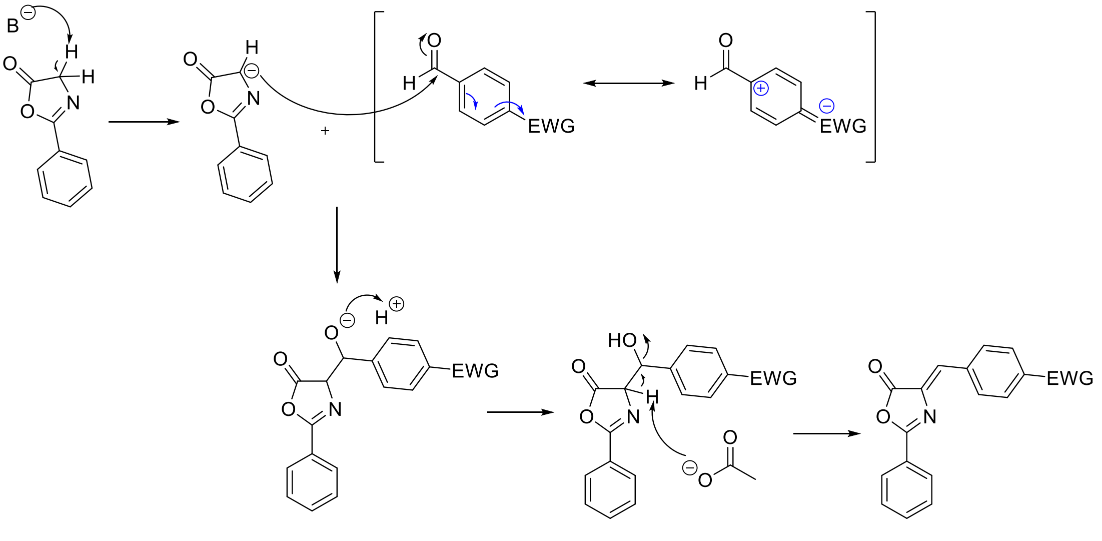
B
H
H
N
O
O
H
N
+
H
O
EWG
H
O
EWG
H
O
EWG
HO
H
EWG
O
EWG

Scheme 1.3. Influence of EWGs on aldehyde

To better understand the influence of the various substituents in this reaction the Hammett equation can be applied.

1.5.1.1. The Hammett equation

The Hammett equation (1) described in 1937 relates the structure and reactivity of benzoic acid and its derivatives with substituents in *-meta* and *-para* positions with the rate of reaction.[39,41]

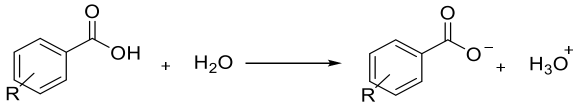

This equation can be expressed as follows:

$$\rho\sigma_x = \log\frac{k_x}{k_H} \qquad (1)$$

where ρ is the reaction constant, σ_x is the constant of the substituent and quantifies the electronic contribution of that substituent, k_x e k_H are respectively the velocity constants for the reaction with the ring substituted X and for the unsubstituted ring.[39,41]

The σ_x quantifies the electronic contribution of this substituent and the values for each substituent in the *-meta* and *-para* position of the aromatic ring have been tabulated since 1937 by Hammett. The EWGs present positive σ_x values, stabilizing the increase of the negative charge in the reaction center, while EDGs present negative values of σ_x, stabilizing the positive charge in the reaction center.[39,41]

In relation to ρ, this one informs on the speed of the step determinant of the reaction and presents positive values of ρ when the reaction speed given by the presence of EWGs, while the negative values of ρ means speed of the reaction by the EDGs.[39,41]

When the value of ρ is much greater than +1.00 and much less than -1.00 then the reaction under study is sensitive to variations of the substituent, whereas a value of ρ close to 0 means that the reaction is insensitive to variation of the substituent on the aromatic ring.[39,41]

1.5.2. Uses of oxazolones

Oxazolones are compounds which are of considerable interest, since their structure has several reactive sites and from them it is possible to produce a wide variety of compounds that can be applied in both chemistry and biology.[36]

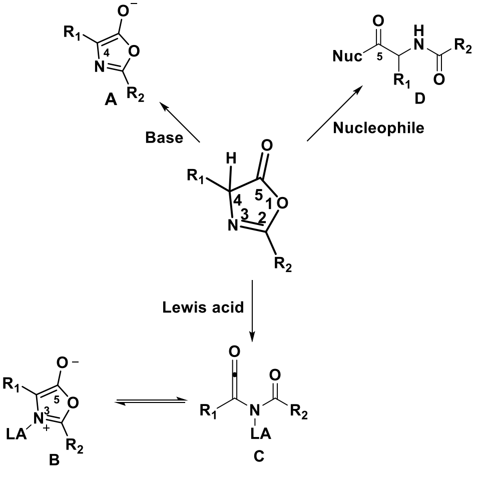
A
Base
Nucleophile
D
Nuc
Lewis acid
B
C
LA
R1
R2
O

Scheme 1.4. Reactive sites of the oxazolone skeleton [Adapted from Ref 35]

The oxazolones contain a proton of acidic nature at C-4, adjacent to the carbonyl, which can easily form an enolate A in a basic medium and it has the possibility to react with several electrophiles. Another possible reaction may occur by the reaction of a Lewis acid with oxazolone and formation of the reactive ketene C or 1,3-dipole B, with the possibility of both reacting by cycloaddition with the formation of several heterocyclic compounds. Finally, the oxazolone further contains a site of electrophilic nature, C-5, where attack by a variety of nucleophiles on the carbonyl can occur and formation of a variety of protected amino acids after ring opening (Scheme 1.4).[35,36]

Due to reactivity of its structure, oxazolone was considered a good substrate for the production of other heterocycles (Scheme 1.5).[36]

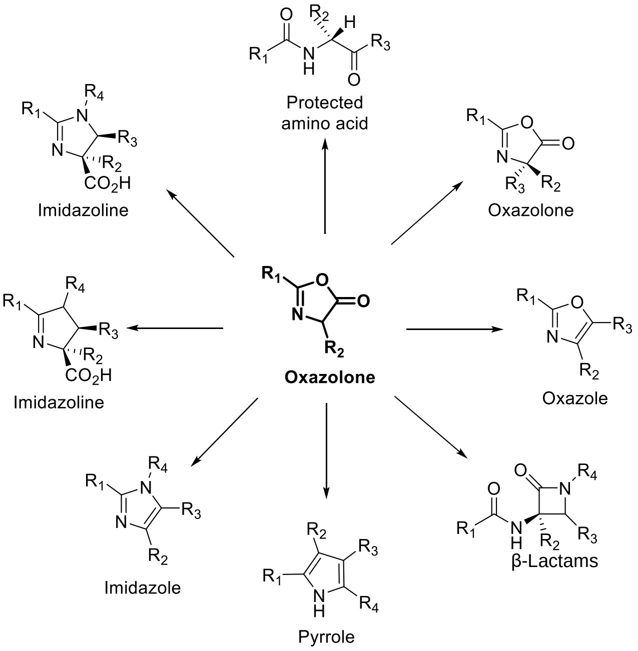
Protected amino acid
Imidazoline
Oxazolone
Imidazoline
Oxazolone
Oxazole
Imidazole
Pyrrole
β-Lactams

Scheme 1.5. Diversity of compounds produced from oxazolone [Adapted from Ref. 36]

Due to its reactivity, the oxazolone ring can be used as a substrate for the synthesis of enantiomerically pure amino acids using organocatalysts, or others moiety of biological interest may be formed from this ring (Scheme 1.5).[36]

The oxazolone ring may also contain an exocyclic double bond at C-4, which induces a new reactive site and allows the synthesis of new structures. With the appearance of this double bond a highly conjugated system was formed allowing higher light absorption and thus the possibility of applications in the field of photochemistry.[35,42–44]

Oxazolone derivatives have been described as pH[45], Fe^{3+} [46] or glucose[47] sensors in solid matrices. More recent studies also point out the possibility of these oxazolones being used as photoswitches[42]. In this research group studies were realized using oxazolone derivatives, concluding that they can be used in the construction of new TPA (Two Photon Absorption) sensors.[39,43,44]

1.5.3. Oxazolones as necroptosis inhibitors

A preliminary screening using a small family of 21 oxazolones (Figure 1.9), developed by Dr. Catarina Rodrigues in the Bioorganic Chemistry Group at iMed.ULisboa, was tested in cell lines (BV2 murine microglia cells and L929 cells).

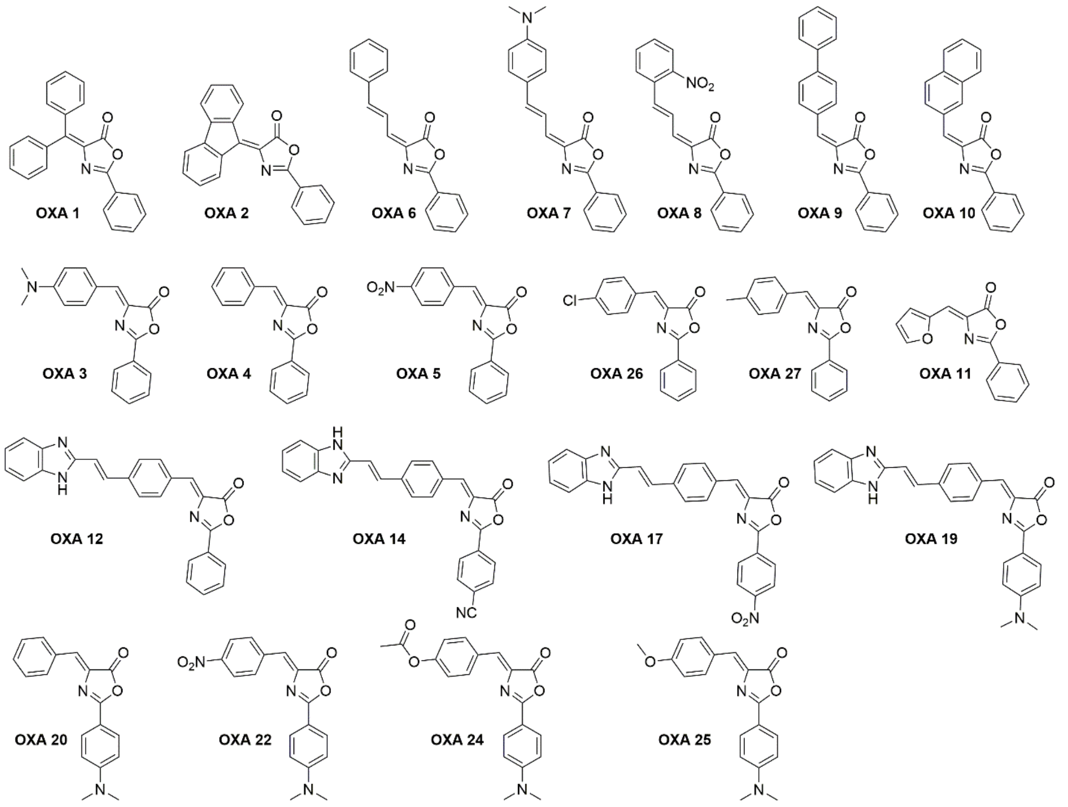

Figure 1.9. Chemical structure of the 21 oxazolone derivatives developed in this team by Catarina Rodrigues and tested in cell lines.

From this screening it was possible to identify a compound, **OXA 12**, which has inhibitory activity similar to the known necroptosis inhibitor, Nec-1, which as described before presents some disadvantages.

The result of these assays was the starting point for the development of new possible inhibitors of necroptosis based on **OXA 12** and to increase its inhibitory activity. From this, were developed in our laboratory by Dr. Mónica Estevão more compounds based on the structure of **OXA 12** (Figure 1.10), not yet being possible to obtain any compound with a superior activity. However, the results obtained will be useful for the study structure-activity relationship, giving information about the influence of each group.

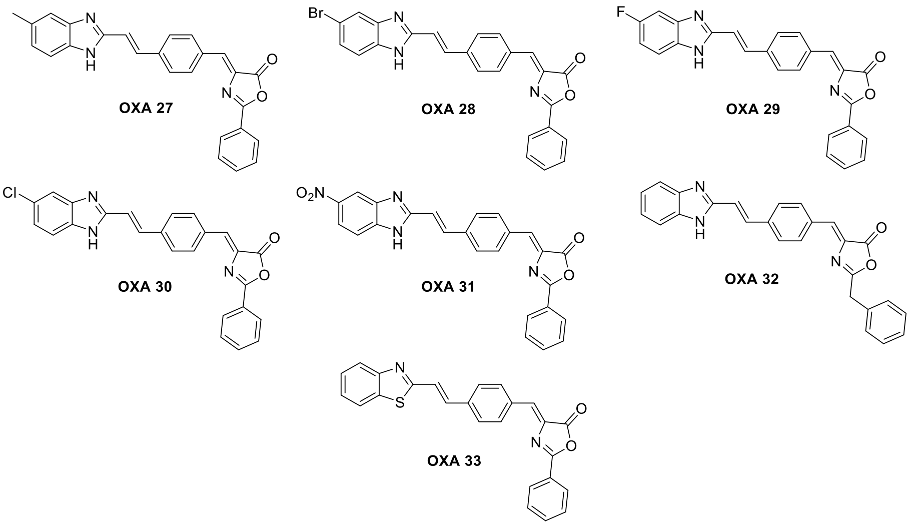

OXA 27

OXA 28

OXA 29

OXA 30

OXA 31

OXA 32

OXA 33

Figure 1.10. Chemical structure of compounds developed on the basis of **OXA 12** structure

In the first screening only **OXA 12** and compounds derived from it, **OXA 14**, **OXA 17** and **OXA 19**, exhibited inhibitory activity so it can be understood that benzimidazole will be an important group for inhibition, from this fact, the compounds of Figure 1.10. were synthesized.

2. Objectives

Considering the previous studies performed by this Team, the main purpose of this project Master Thesis is the development of new potential modulators of necroptosis based on the **OXA 12** moiety. Through the synthesis of different compounds, containing different substitution patterns based on **OXA 12**,

The synthesized compounds were further evaluated using BV2 murine microglia cells and the methodology used for the above compounds. In order to establish a structure-activity relationship (SAR) and to find or propose new or optimized modifications or structures, which have an optimized activity, are more potent and/or have better pharmacokinetic/pharmacodynamic properties.

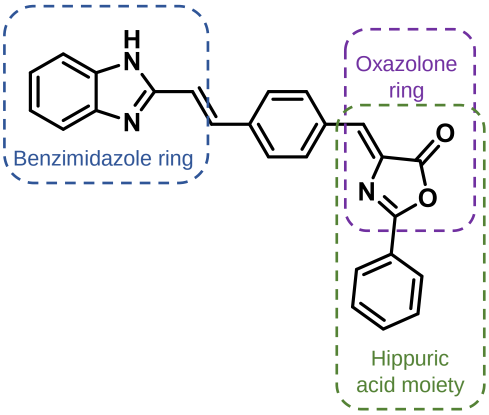

Figure 2.1. Structure of **OXA 12**

3. Results and Discussion

3.1. Synthesis of 4 or 5-substituted-2-methyl-benzimidazoles

The synthesis of **OXA 12** and its derivatives is initiated by the condensation of a diamine with triethyl orthoacetate at reflux to form 2-methylbenzimidazoles (Scheme 3.1)

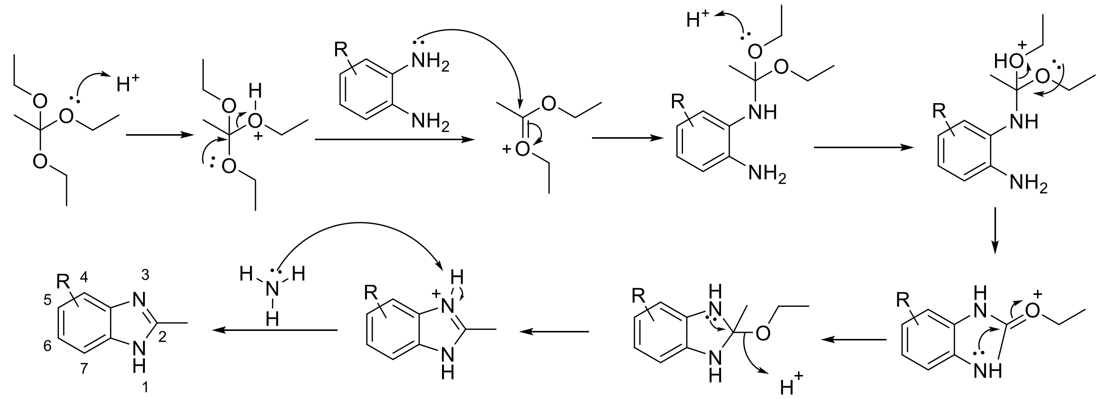

1 R = *5*-Fluor
2 R = *5*-*Tert*-butyl
3 R = *4*-Me

Scheme 3.1. Mechanism of formation of 4 or 5-substituted-2-methylbenzimidazole **1-3**

Mechanistically, the amine acts as nucleophile, attacking the carbon of the activated triethyl orthoacetate derived from acid catalyzed ethanol elimination as a good leaving group. Next, another nucleophilic attack occurs, this time from the other amine resulting in the expulsion of another ethanol molecule. Finally, the amine donates its protons to the formation of double bond and expulsion of the last ethanol molecule, resulting in a more stable compound due to its extension of aromaticity. (Scheme 3.1)

The reaction can be monitored by TLC, through the disappearance of the diamine spot and formation of a more polar new specie (with lower retention factor (Rf)) corresponding to the 2-methylbenzimidazole products (**1-3**).

The formation of these derivatives was confirmed by NMR spectroscopy (Appendix 1-3), through the appearance of a signal at approximately 2.6 ppm in the ^{1}H-NMR spectrum, attributed to the C10 protons. The ^{13}C-NMR spectrum analysis also shows the appearance of two characteristic signals, one at approximately 15 ppm corresponding to C10 and the other at approximately 150 ppm corresponding to C8 sp^{2} carbon. In addition to these characteristic signals, in each of the compounds appear the signals corresponding to the substituent introduced and also disappearance of the signal corresponding to the proton bounded to carbon in the ^{1}H-NMR (Table 3.1).

Table 3.1. Characterizations of compounds **1-3**, synthetized through of condensation between 4 or 5-subtitutedbenzeno-1,2-diamine and triethyl orthoacetate.[a]

.	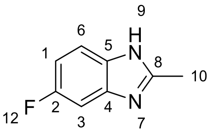 **1**	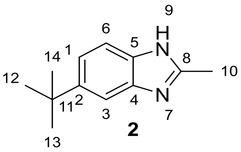 **2**	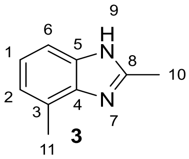 **3**
Yield (%)	66%	93%	51%
^{1}H-NMR	7.44 (dd, J = 8.8, 4.7 Hz, 1H, H6) 7.21 (dd, J = 9.0, 2.5 Hz, 1H, H3) 6.97 (td, *J* = 9.2, 2.4 Hz, 2H, H1) 2.63 (s, 3H, H10).)	7.56 (d, *J* = 1.5 Hz, 1H, H3) 7.49 (d, *J* = 8.5 Hz, 1H H1) 7.31 (dd, J = 8.5, 1.8 Hz, 1H, H6) 2.66 (s, 3H, H10) 1.35 (s, 9H, H12,13,14)	7.38 (d, J = 7.9 Hz, 1H, H6) 7.13 (t, J = 7.6 Hz, 1H, H1) 7.04 (d, J = 7.3 Hz, 1H, H2) 2.63 (s, 3H, H10) 2.57 (s, 3H, H11).
^{13}C-NMR	160.91 (C2) 157.76 (C8) 152.36,152.33 (C1) 135.14 (C4) 131.71 (C5) 114.90 (C6) 110.50, 110.16 (C3) 15.04 (C10)	150.95 (C8) 145.84 (C2) 137.08 (C4) 135.53 (C5) 120.25 (C1) 113.55 (C3) 110.04 (C6) 34.50 (C11) 31.48 (C12,13,14) 14.14 (C10)	151.07 (C8) 138.65 (C5) 137.99 (C4) 124.98 (C3) 122.75 (C1) 122.23 (C2) 111.72 (C6) 17.32 (C11) 14.95 (C10)

[a] Atoms numeration according to ChemDraw assignment

3.2. Synthesis of 1,2-dimethyl-1H-benzo[d]imidazole

This reaction occurs according to procedure described in the literature.[48]

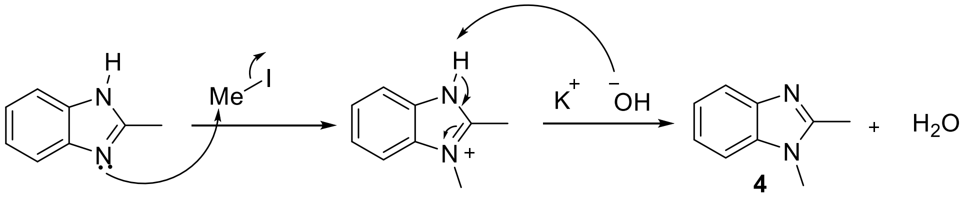

Scheme 3.2. Alkylation mechanism for the formation of 1,2-dimethylbenzimidazole **4** by reaction of 2-metilbenzimidazole with iodomethane.

The mechanism of this reaction can be described by a S_N2 type nucleophilic substitution reaction, where the tertiary amine of the benzimidazole ring acts as a nucleophile, favoring the attack on the adjacent carbon to the halogen, transiently resulting in the protonated amine. This was then treated with potassium hydroxide leading to the formation of 1,2-dimethylbenzimidazole **4** (Scheme 3.2).

The reaction was monitored by TLC, verifying the disappearance of the spot corresponding to the starting material and the formation of a less polar compound, with higher Rf than the starting material, which correspond to the product. There is also a spot at the application point corresponding to the salts formed during the reaction.

The compound was obtained after extractions using DCM, with a yield of 89%, and the presence was confirmed by the use of NMR spectroscopy (Appendix 4), with the appearance of a new singlet at 3.7 ppm in the ^{1}H-NMR spectrum corresponding to the protons of the introduced methyl group (C11). In the ^{13}C-NMR spectrum, a 29.8 ppm signal corresponding to this same signal also appears. (Table 3.2)

Table 3.2. Characterization of compound **4**, synthetized through alkylation of 2-methylbenzimidazole[a]

Compound	^{1}H-NMR	^{13}C-NMR
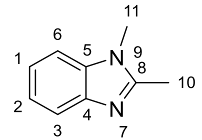 11 6 5 N 9 8 1 10 2 4 N 3 7 **4**	7.51 – 7.42 (m, 2H, H3,6) 7.21 – 7.03 (m, 2H, H1,2) 3.70 (s, 3H, H11) 1.13 (s, 3H, H10).	151.83 (C8) 142.47 (C4) 135.78 (C5) 122.00 (C1) 121.83 (C2) 118.92 (C3) 108.89 (C6) 29.81 (C11) 13.76 (C10)

[a] Atoms numeration according to ChemDraw assignment

3.3. Synthesis of 4-(2-(4 or 5-substituted-benzimidazol-2- yl)vinyl)benzaldehyde

The second step for the synthesis of this **OXA** family was condensation, reactions between the 4 or 5-substituted-2-methylbenzimidazole and the terephthalaldehyde at 120ºC in the presence of acetic anhydride and acetic acid.

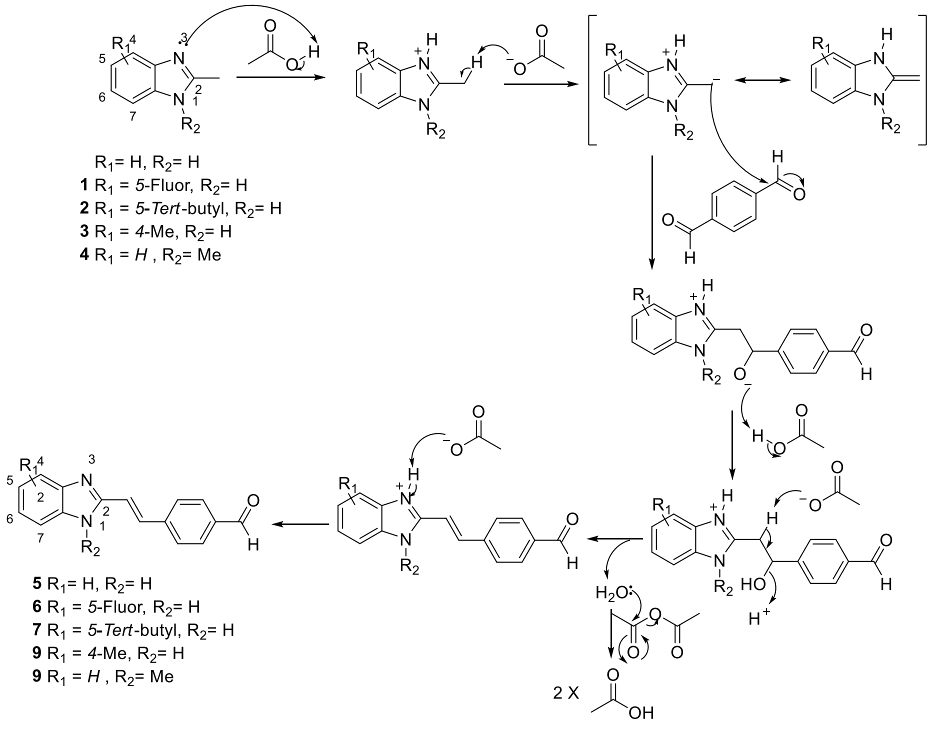
R1= H, R2= H
1 R1 = 5-Fluor, R2= H
2 R1 = 5-Tert-butyl, R2= H
3 R1 = 4-Me, R2= H
4 R1 = H , R2= Me
5 R1= H, R2= H
6 R1 = 5-Fluor, R2= H
7 R1 = 5-Tert-butyl, R2= H
9 R1 = 4-Me, R2= H
9 R1 = H , R2= Me
R1
R2
N
H
O
OH
H2O
H+
2 X

Scheme 3.3. Mechanism for the formation of compounds **5-9** by reaction of 4 or 5-substituted-2-methyl-benzimidazoles (**1-4**) with the terephthalaldehyde.

The protonated benzimidazole was deprotonated on the methyl group forming an ylide that will attack one of the aldehydes of the terephthalaldehyde, generating a new C-C a single bond between the two reagents. Subsequent dehydration results in the desired product. (Scheme 3.3)

Although used stoichiometrically reagents, monitorization by TLC shows consumption of the aldehyde was not complete, despite total consumption of benzimidazole was observed, and it verified the appearance of several spots. This event may occur due to benzimidazole availability to react again with formed product resulting in a compound containing benzimidazole as a substituent on both sides. However, double modification of the aldehyde was reduced by the reduced reactivity of the generated product towards a second condensation compared to the initial dialdehyde, combined with the use of the reactants in a 1:1 stoichiometry**.**

Despite the appearance of various spots on the TLC, after precipitation of the compound during the work-up, a crude containing only the desired compound and the unreacted dialdehyde was obtained. This was further purified by column chromatography using a solvent gradient (AcOEt:Hex (4:1) to AcOEt). The product was obtained in a low yield, the explanation to go through the formation of by-products during the reaction, loss of compound in the precipitation or still retention of the compound during the performance of the chromatographic column.

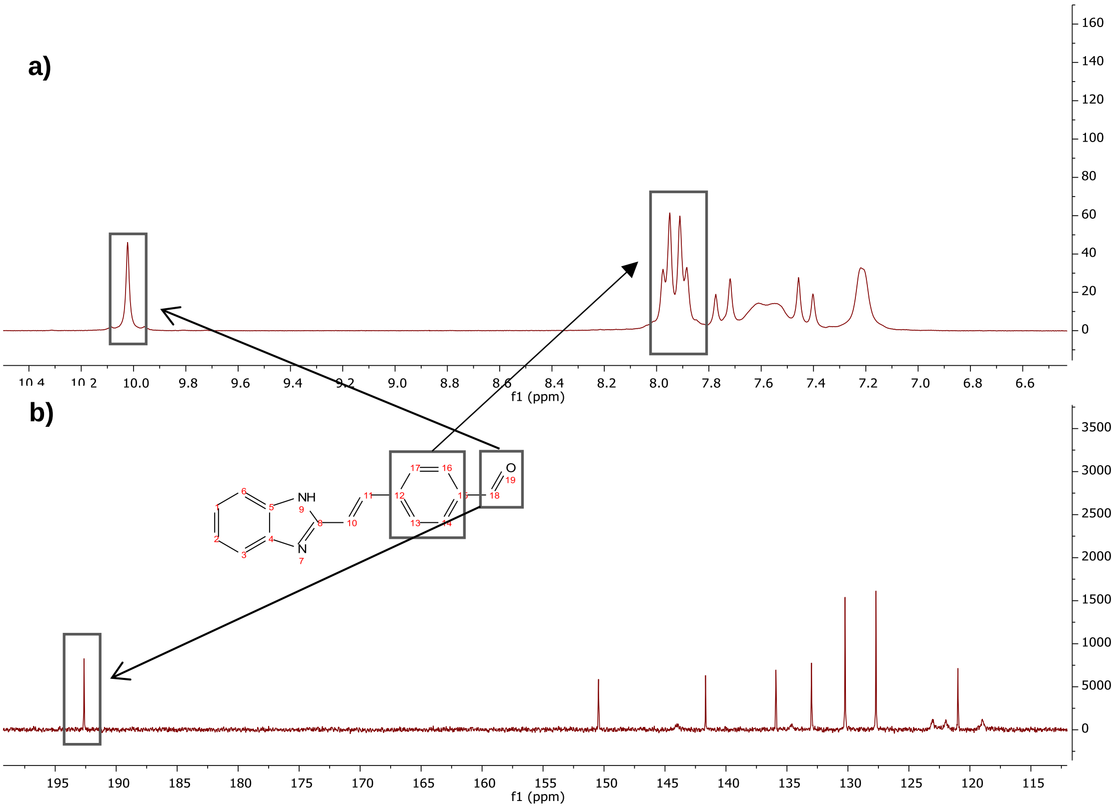

Figure 3.1. ^{1}H-NMR spectrum (**a**) and ^{13}C-NMR spectrum (**b**) of compound **5**

Confirmation of the presence of the desired compound and its purity was obtained by NMR spectroscopy (Appendix 5-9), with the appearance in the ^{1}H-NMR spectrum (Figure 3.1a) of a 10 ppm singlet characteristic of the aldehyde (C18) and disappearance of the singlet at 2.6 ppm corresponding to the protons of C10, in addition, there was an increase in the number of protons in the aromatic zone, corresponding to the protons of the new ring (Figure 3.1a). In the ^{13}C-NMR spectrum (Figure 3.1b), typical aldehyde signal also appears at approximately 190 ppm (Table 3.3).

Table 3.3. Characterizations of compounds **5-9**, synthetized by reaction between 2-methylbenzimidazole and its derivatives **1-4** with terephthalaldehyde.[a]

	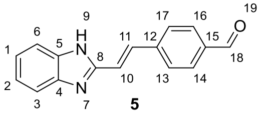 **5**	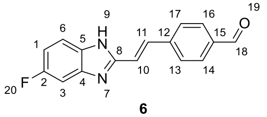 **6**	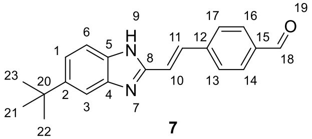 **7**	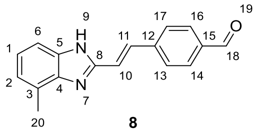 **8**	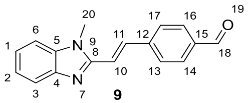 **9**
Yield (%)	40%	53%	5%	8%	55%
^{1}H-NMR	10.02 (s, 1H, H18) 7.96 (d, J = 8.1 Hz, 2H, H14,16) 7.90 (d, J = 8.2 Hz, 2H, H13,17) 7.74 (d, J = 16.5 Hz, 1H, H11) 7.57 (t, *J* = 4.5 Hz, 2H, H3,6) 7.42 (d, J = 16.6 Hz, 1H, H10) 7.20 (dd, J = 6.1, 3.2 Hz, 2H, H1,2)	10.01 (s, 1H, H18) 7.94 (d, J = 7.7 Hz, 2H, H14,16) 7.87 (d, J = 8.1 Hz, 2H, H13,17) 7.77 (d, J = 17.2 Hz, 1H, H6) 7.60 – 7.50 (m, 1H, H11) 7.49 – 7.22 (m, 2H, H1,3) 7.05 (t, J = 9.5 Hz, 1H, H10)	10.07 (s, 1H, H18) 8.07 (d, *J* = 15.9 Hz, 1H, H11) 8.03 – 7.95 (m, 2H, H14,16) 7.68 – 7.54 (m, 2H, H13,17) 7.47 (dd, J = 8.5, 0.7 Hz, 1H, H3) 7.25 (dd, J = 8.5, 1.8 Hz, 1H, H1) 7.22 – 7.11 (m, 1H, H6) 7.03 (dd, J = 8.6, 0.7 Hz, 1H, H10) 1.33 (s, 9H, H21,22,23).	10.04 (s, 1H, H18) 7.95 (d, J = 7.9 Hz, 2H, H14,16) 7.85 (d, J = 8.1 Hz, 2H, H13,17) 7.78 (d, J = 16.6 Hz, 1H, H11) 7.46 (d, J = 16.5 Hz, 1H, H6) 7.39 (d, J = 8.2 Hz, 1H, H2) 7.11 (t, J = 7.6 Hz, 1H, H1) 7.01 (d, J = 7.2 Hz, 1H, H10) 2.57 (s, 3H, H20).	10.06 (s, 1H, H18) 8.07 – 7.90 (m, 5H, H11,13,14,15,16) 7.70 (d, J = 15.7 Hz, 1H, H10) 7.66 – 7.61 (m, 1H, H3) 7.54 – 7.47 (m, 1H, 6) 7.34 – 7.10 (m, 2H, H1,2) 4.02 (s, 3H, H20)
^{13}C-NMR	192.64 (C18) 150.45 (C8) 143.99 (C4) 141.68 (C12) 135.91 (C15) 134.55 (C5) 132.98 (C11) 130.23 (C14,16) 127.70 (C13,17) 123.05 (C1) 121.98 (C2) 120.98 (C10) 118.97 (C3) 111.37 (C6)	192.67 (C18) 152.04 (C2) 141.66 (C12) 135.94 (C15) 133.29 (C6) 130.23 (C14,16) 127.74 (C13,17) 120.82 (C1) 115.92 (C11) 110.71 (C3) 110.37 (C10	192.49 (C18) 153.12 (C8) 145.63 (C12) 144.19 (C15) 142.20 (C4) 141.22 (C5) 137.69 (C11) 130.66 (C14,16) 128.11 (C13,17) 120.36 (C2) 116.20 (C3) 111.65 (C10) 108.99 (C6) 32.17 (C20) 29.89 (C21,22,23)	191.41 (C18) 149.76 (C8) 142.02 (C12) 136.38 (C15) 132.59 (C11) 129.98 (C14,16) 127.45 (C13,17) 122.80 (C1) 122.69 (C2) 120.83 (C10) 119.03 (C3) 117.75 (C6) 16.16 (C20)	192.28 (C18) 151.34 (C8) 144.37 (C5) 143.05, 137.31 (C4) 135.34 (C11) 130.76 (C14,16) 128.68 (C13,17) 123.27 (C1) 123.07 (C2) 119.92 (C10) 118.27 (C15) 110.70 (C3,6)

[a] Atoms numeration according to ChemDraw assignment

3.4. Synthesis of (E)-4-(2-(2H-imidazol-2-yl)vinyl)benzaldehyde

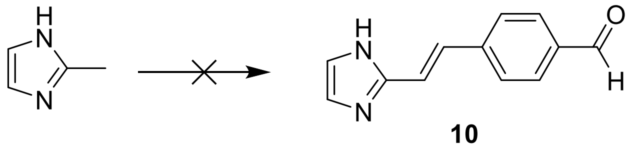

10

Scheme 3.4. Attempt to synthesize the compound (*E*)-4-(2-(2H-imidazol-2-yl)vinyl)benzaldehyde

The attempt to synthesize this compound occurred through the use of two different methods.

Initially, the same reaction conditions of the formation of compound **5** were used, however after analysis of the compound obtained by the use of NMR spectroscopy, it was found to exist only the starting materials (Appendix 10).

Since under these conditions the desired compound was not obtained, a second attempt was made, following a literature procedure for the condensation of 2-methylimidazole with a di-substituted benzaldehyde.[49] In this case, a reaction occurred, not verifying the presence of the starting materials. However, it was not possible to identify the compound, being a mixture of signals.

Synthesis of compound **10** was abandoned after the previous attempts.

In the first attempt, 2-methylimidazole was used, in the same conditions for the compound **5,** replacing the 2-methybenzimidazole. This compound has a less acidic proton than 2-methylbenzimidazole, since it lacks the stabilization by resonance of the respective conjugated base, observed for the 2-methylbenzimidazole. Since the nucleophilicity of the conjugated base is reduced, the reaction did not occur.

In the second attempt, a literature procedure was used in which 2-methylimidazole acted as a nucleophile by attacking an aldehyde, in this case containing two -Cl groups, in the -*ortho* and -*para* position, making this aldehyde more electrophilic compared to terephthalaldehyde and the reaction the formation of compound **10** did not occur again.

3.5. Synthesis of Oxazol-5(4H)-ones

The last step for the synthesis of **OXA 12** and its derivatives was performed according to the procedure described by Plöch-Erlenmeyer[50], in two steps. The first being the formation of the oxazolone ring through a cyclization of the hippuric acid activated by acetic anhydride (Scheme 3.5.) and the second, the reaction of this ring with the previously formed aldehydes **5-9.** (Scheme 3.6)

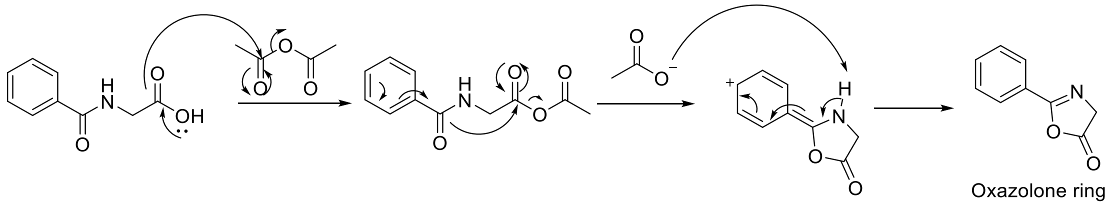

Scheme 3.5. A reaction mechanism for the formation of the oxazolone ring from hippuric acid or its derivatives

The first step, starts by the activation the carboxylic acid functional group present in the hippuric acid by creating a better leaving group. The free electron pair present in amide reacts as nucleophile, attacking the anhydride to form the 5-membered oxazolone ring (Scheme 3.5).

The second step, is initiated by keto-enol equilibrium, making this molecule capable of attacking the electrophilic aldehyde **5** and its derivatives (**6-9)**. Finally, the other acidic proton is removed by forming the double bond, through dehydration, with expulsion of H_2O (Scheme 3.6.).

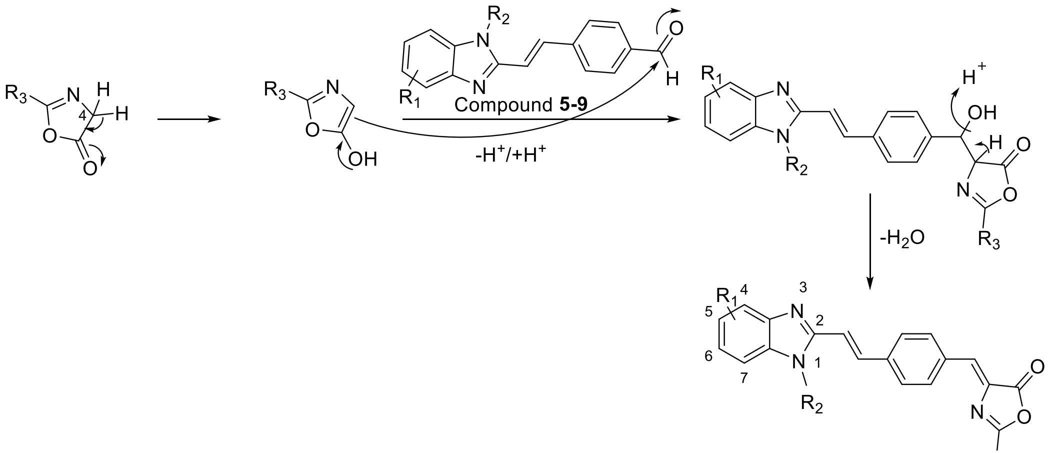

11 R_1 = H; R_2 = H; R_3 = -Ph
12 R_1 = 4-Me; R_2 = H; R_3 = -Ph
13 R_1 = H; R_2 = Me; R_3 = -Ph
14 R_1 = H; R_2 = H; R_3 = -Me

Scheme 3.6. A mechanism for forming **OXAs** (**11-14**) by reacting the oxazolone ring formed above with compound **5**.

During the course of the reaction, it was monitored by TLC for the disappearance of the starting material (**5-9**) and the appearance of a new compound with a higher Rf than the starting material (compound less polar).

After washing with water and methanol to remove the traces of hippuric acid and other starting materials, it was possible to isolate compound **11-14** (**OXAs**). These compounds were characterized using NMR spectroscopy (Appendix 11-14), however, it was not possible to obtain ^{13}C-NMR spectra of all compounds and the spectra obtained did not show a good peak resolution due to the low solubility in DMSO. With the obtained spectra and by comparison with the literature[43], it was possible to verify the formation of the desired product through the changes observed in the spectrum. The characteristic singlet of the aldehyde at 10 ppm disappeared in the ^{1}H-NMR spectrum and the increase in the number of protons in the aromatic zone. In the case of ^{13}C-NMR spectrum, there is also the disappearance of the carbon at 190 ppm, characteristic of the aldehyde, however, the appearance of another signal in the same zone, approximately 200 ppm, corresponding to the C23 (ester carbonyl). (Table 3.4)

In the case of compound **14**, which was synthesized by the same method, *N*-acetyl glycine **21** was used instead of hippuric acid to form the oxazolone ring, resulting in a compound having a methyl terminal instead of phenyl. Regarding the NMR analysis of this compound (Appendix 14), in addition to the disappearance of the characteristic aldehyde signal, it was verified the appearance of a singlet at 2.40 ppm in the ^{1}H-NMR spectrum corresponding to the methyl protons (C25). The presence of a signal at 15.53 ppm in the ^{13}C-NMR spectrum was also observed (Table 3.4).

Table 3.4. Characterization of compounds **11-14**, synthetized through of reaction of compound **5-9** with hippuric acid or *N*-acetyl glycine **(21)** [a]

	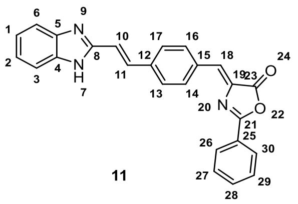 **11**	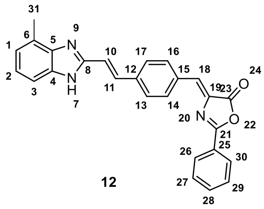 **12**	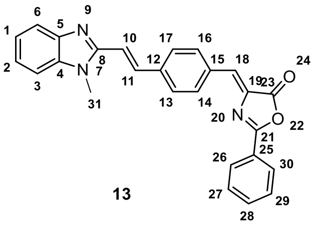 **13**	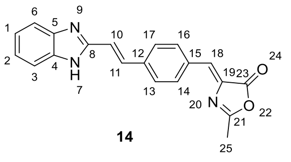 **14**
Yield (%)	40%	26%	10%	22%
^{1}H-NMR	8.38 (d, J = 8.1 Hz, 2H, H26,30) 8.16 (d, J = 7.4 Hz, 2H, H27,29) 7.84 (d, J = 8.1 Hz, 2H, H11,28) 7.79 – 7.62 (m, 4H, H13,14,16,17) 7.57 (dd, J = 6.0, 3.3 Hz, 2H, H3,6) 7.44 – 7.33 (m, 2H, H10,18) 7.21 (dd, J = 6.0, 3.1 Hz, 2H, H1,2).	8.41 (d, J = 8.3 Hz, 2H, H26,30) 8.26 – 8.19 (m, 2H, H27,29) 7.83 (d, J = 8.3 Hz, 1H, H11) 7.79 – 7.59 (m, 6H, H3,13,14,16,17,28) 7.44 (d, J = 16.6 Hz, 1H, H1) 7.31 (s, 1H, H18) 7.12 (t, J = 7.6 Hz, 1H, H2) 7.04 (t, J = 7.7 Hz, 1H, H10) 3.31 (s, 3H, H31).	8.43 (d, J = 8.2 Hz, 2H, H26,30) 8.22 (d, J = 8.8 Hz, 2H, H27,29) 8.04 – 7.45 (m, 10H, H3,6,10,11,13,14,16,17,18,28) 7.29 – 7.19 (m, 2H, H1,2) 4.03 (s, 3H, H31)	8.23 (d, J = 8.2 Hz, 2H, H14,16) 7.83 (d, J = 3.6 Hz, 1H, H11) 7.78 (d, J = 8.4 Hz, 2H, H13,17) 7.74 – 7.68 (m, 1H, H18) 7.61 – 7.47 (m, 2H, H3,6) 7.43 – 7.35 (m, 1H, H10) 7.26 – 7.13 (m, 2H, H1,2) 2.40 (s, 3H, H25)
^{13}C-NMR	207.27 (C23) 166.85 (C21) 163.06 (C8) 138.39 (C5) 136.88 (C4) 133.73 (C11) 133.69 (C15) 133.38 (C12) 133.17 (C18) 132.85 (C14,16) 130.71 (C19) 129.96 (C13,17) 129.37 (C27,29)			167.48 (C23) 166.94 (C21) 150.70 (C8) 139.72 (C5) 133.48 (C4) 132.79 132.64 (C14,16) 130.46 129.13 127.56 (C13,17) 122.48 (C1,2) 119.67 15.53 (C25)

128.02 (C28)
127.53 (C25,26,30)
125.12 (C2)
122.33 (C1)
119.67 (C6)
114.18 (C10)
110.20 (C3)

[a] Atoms numeration according to ChemDraw assignment

3.6. Synthesis of *(E)*-(4-(2-(1H-benzo[d]imidazol-2-yl)vinyl)phenyl)methanol

Reduction of aldehydes and ketones to alcohols can be performed using various reducing agents such as $LiAlH_4$ and $NaBH_4$.

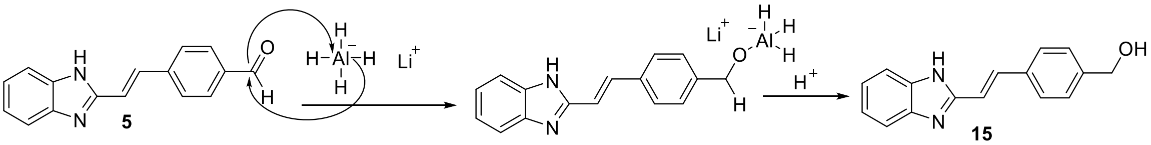

Scheme 3.7. Mechanism of reduction the aldehyde of compound **5** to alcohol **15** using $LiAlH_4$.

The reduction mechanism using $LiAlH_4$ occurs through the attack of the nucleophilic hydride to the electrophilic carbonyl carbon, leading to the alkoxide which is stabilized by complexation with the metal. Then, through an acid-base reaction occurs the oxygen protonation of the alkoxide thus forms the alcohol.[51] (Scheme 3.7)

This reaction can also occur using $NaBH_4$, the mechanism of the reaction occurs similarly, however, $LiAlH_4$ is a stronger reducing agent because the Al-H bond is weaker than the B-H bond.

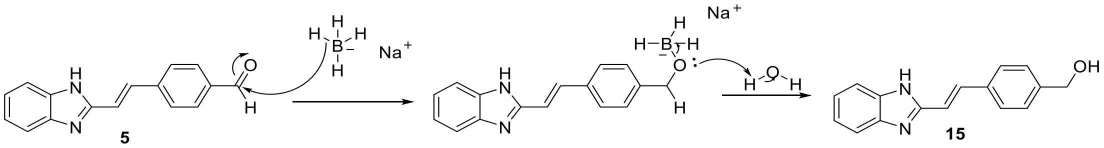

Scheme 3.8. Mechanism of reduction the aldehyde of compound **5** to alcohol **15** using $NaBH_4$

The reduction mechanism using $NaBH_4$ as a reducing agent occurs through the nucleophilic attack of the H bond of BH_4 to the electrophilic carbonyl carbon resulting from the formation of a C-H bond and breaking the carbonyl double bond with formation of an alkoxide, a negatively charged oxygen atom, which is stabilized by boron through the formation of boronate. During the work-up occurs the formation of alcohol through an acid-base reaction with water.[51] (Scheme 3.8)

Both reactions, were monitored by TLC, with the total disappearance of the spot corresponding to compound **5** in a few minutes and the appearance of a compound with a lower Rf, being able to correspond to the complex from which the product. After addition of water, the conversion of the intermediate into the desired alcohol takes place through a reaction of acid-base.

In both methods it was possible to obtain the desired compound, with yield approximately 95%, verified by the use of NMR spectroscopy (Appendix 15). In the ^{1}H-NMR spectrum, the aldehyde **5** signal disappeared at 10 ppm and the appearance of a singlet at 4.53 ppm occurred which was attributed to the C18-linked protons. Regarding the ^{13}C-NMR spectrum, the aldehyde **5** signal disappeared at 192.64 ppm and appeared at 62.71 ppm the C18 (carbon bonded to the hydroxyl group). (Table 3.5)

Table 3.5. Characterization of compound **15**, synthesized by reduction of aldehyde **5**[a]

Compound	^{1}H-NMR	^{13}C-NMR
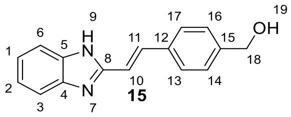 **15**	7.70 (d, J = 14.0 Hz, 1H, H11) 7.66 – 7.59 (m, 2H, H14,16) 7.53 (dd, J = 6.0, 3.2 Hz, 2H, H3,6) 7.38 (d, J = 7.9 Hz, 2H, H13,17) 7.24 (d, J = 12.8 Hz, 1H, H10) 7.17 (dd, J = 6.2, 3.0 Hz, 2H, H1,2) 4.53 (s, 2H, H18)	151.20 (C8) 143.55 (C4,5) 134.34 (C11,12) 134.31 (C15) 127.04 (C14,16) 126.92 (C13,17) 122.10 (C1,2) 121.14 (C3) 117.17 (C10) 114.94 (C6) 62.71 (C18)

[a] Atoms numeration according to ChemDraw assignment

3.7. Synthesis of hydrazones or oxime

The hydrazones or oximes are formed by the reactions between hydrazines or hydroxylamines and aldehydes or ketones.

The hydrazine or hydroxylamine nitrogen acts as a strong nucleophile, capable of promoting carbonyl attacks, since it contains free electrons that can be donated to an electron-deficient species, in this case carbonyl carbon.[51] (Scheme 3.9)

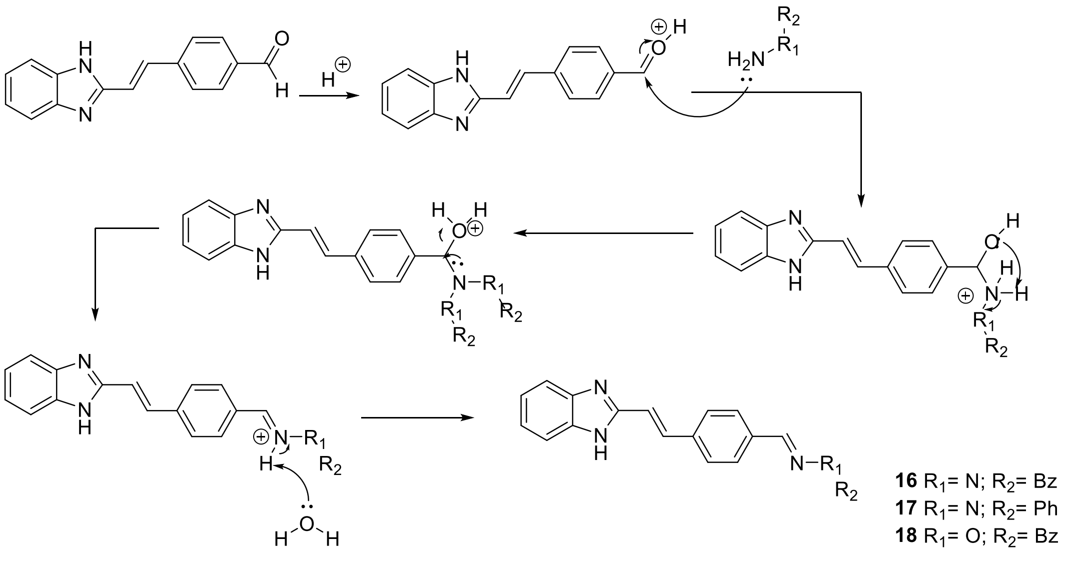

16 R_1= N; R_2= Bz
17 R_1= N; R_2= Ph
18 R_1= O; R_2= Bz

Scheme 3.9. Proposed mechanism for the reaction between the aldehyde **5** and a hydrazine or hydroxylamine with formation of a hydrazone (**16-17**) or oxime (**18**).

The reaction occurs in two steps, the first of addition of the hydrazine or hydroxylamine to the aldehyde with formation of a tetrahedral intermediate, characteristic of nucleophilic additions. Then, the proteolytic rearrangement followed by a dehydration occurs, with the driving force being the double bond, thus obtaining the desired compounds (Scheme 3.9). These structures have higher stability since the heteroatom adjacent to the nitrogen, another nitrogen in the case of the hydrazone and an oxygen in the case of the oxime, presents a free pair of electrons that can participate in the delocalization of the double bond of the imine decreasing the positive charge of adjacent carbon. This causes an increase in the LUMO energy of the compound, making it less susceptible to nucleophilic attacks[51] (Scheme 3.10).

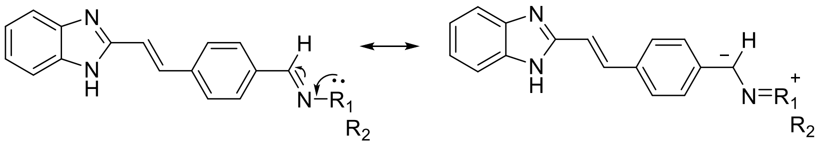

16 R$_1$= N; R$_2$= Bz
17 R$_1$= N; R$_2$= Ph
18 R$_1$= O; R$_2$= Bz

Scheme 3.10. Stability of the compound obtained by the displacement of electrons from the electronegative atom (N or O) to the carbon making it low susceptible to nucleophilic attacks.

These compounds precipitated during the reaction and were then filtered and washed with acetonitrile.

The confirmation of the formation of the compound occurred by NMR spectroscopy (Appendix 16-18), however, as in previous compounds the resolution of the signals was poor due to reduced solubility of the compounds in DMSO, with the appearance of a singlet at approximately 8.3 ppm in ^{1}H-NMR spectrum corresponding to the C18 proton, the increase of the protons in the aromatic zone, and the disappearance of the singlet at 10 ppm characteristic of the aldehyde. In the ^{13}C-NMR spectrum, the appearance of C18 at about 145 ppm and disappearance of the signal at 190 ppm of aldehyde **5** (Table 3.6).

Table 3.6. Characterization of compounds **16-18** from reaction between aldehyde **5** and hydrazine or hydroxylamine [a]

	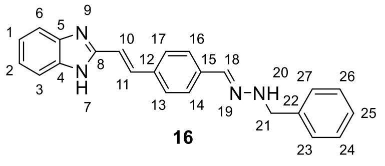 **16**	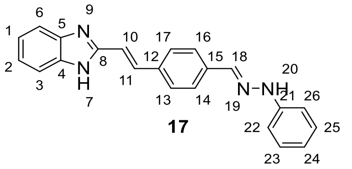 **17**	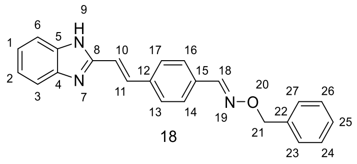 18
Yield (%)	70%	40%	72%
^{1}H-NMR	8.30 (s, 1H, H18) 8.06 (d, J = 16.5 Hz, 1H, H11) 7.81 – 7.74 (m, 2H, H3,6) 7.68 (d, J = 8.2 Hz, 2H, H14,16) 7.58 (d, J = 9.6 Hz, 2H, H13,17) 7.57 – 7.46 (m, 2H, H23,27)	7.88 (s, 1H, H18) 7.69 (s, 5H, H3,13,14,16,17) 7.58 – 7.48 (m, 2H, H6,11) 7.34 – 7.14 (m, 5H, H22,23,24,25,26) 7.10 (d, J = 8.0 Hz, 2H, H1,2)	8.33 (s, 1H, H18) 7.69 (d, J = 7.2 Hz, 4H, H13,14,16,17) 7.55 (dd, J = 6.0, 3.3 Hz, 2H, H3,6) 7.50 – 7.31 (m, 5H, H23,24,25,26,27)

	7.39 – 7.31 (m, 3H, H24,25,26)	6.77 (t, J = 7.3 Hz, 1H, H10)	7.27 (d, J = 16.5 Hz, 1H, H10)
	7.30 – 7.13 (m, 3H, 1,2,10)		7.19 (dd, *J* = 6.1, 3.0 Hz, 2H, H1,2)
	4.40 (s, 2H, H21).		5.19 (s, 2H, H21).
^{13}C-NMR		150.98 (C8)	
	139.88	145.09 (C18)	150.70 (C8)
	139.17	136.30 (C4)	148.82 (C18)
	137.23	135.84 (C21)	137.57 (C22)
	132.79	135.19 (C5)	137.30
	131.96	133.91 (C12)	133.46 (C11)
	129.08	132.26 (C15)	132.05
	128.83	131.63 (C11)	128.35 (C24,26)
	128.36	129.14 (C23,25)	128.26 (C23,27)
	126.35	127.38 (C14,16)	127.85 (C25)
	126.03	126.06 (C13,17)	127.42 (C13,17)
	114.14	122.07 (C24)	127.41 (C14,16)
	114.13	118.97 (C3)	122.18 (C1,2)
	112.34	117.36 (C10)	118.66 (C10)
	109.15	112.10 (C22,26)	75.58 (C21)
		99.03 (C6)	

[a] Atoms numeration according to ChemDraw assignment

3.8. Attempts hydrogenation with Pd/C

The hydrogenation of alkenes originated saturated alkanes, through the coordination of the double bond with the surface of the catalyst where the hydrogen is also adsorbed. Next, two hydrogen atoms are transferred to the alkene forming a chemical bond C-H. The addition of these hydrogens often occurs on the same face.[51]

In order to realize the importance of the double bond between the C10-C11 carbon and even if the rotation of the single bond in the case of hydrogenation influenced the bonding, the hydrogenation of compound **11** (**OXA 12**), was initiated. (Scheme 3.11))

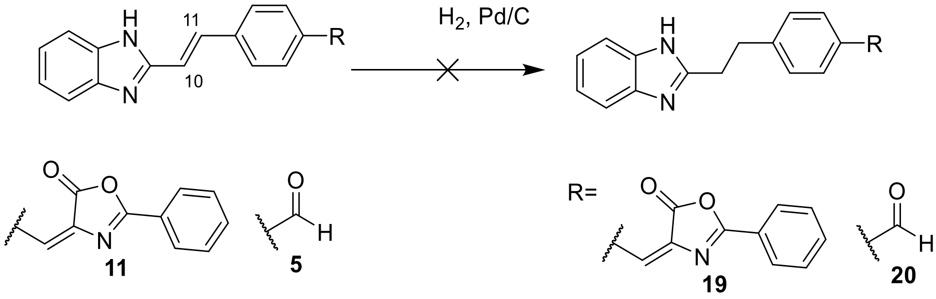

Scheme 3.11. Attempts of the hydrogenation reaction using palladium on charcoal as catalyst.

Initially, the hydrogenation was performed using Pd/C and hydrogen at atmospheric pressure. However, after ^{1}H-NMR analysis, it was found that the obtained compound was not expected nor the starting material, it being verified that a reaction occurred. However, it is not possible to characterize the present compounds, with the possibility of hydrogenation taking place at various positions of the compound. (Figure 3.2)

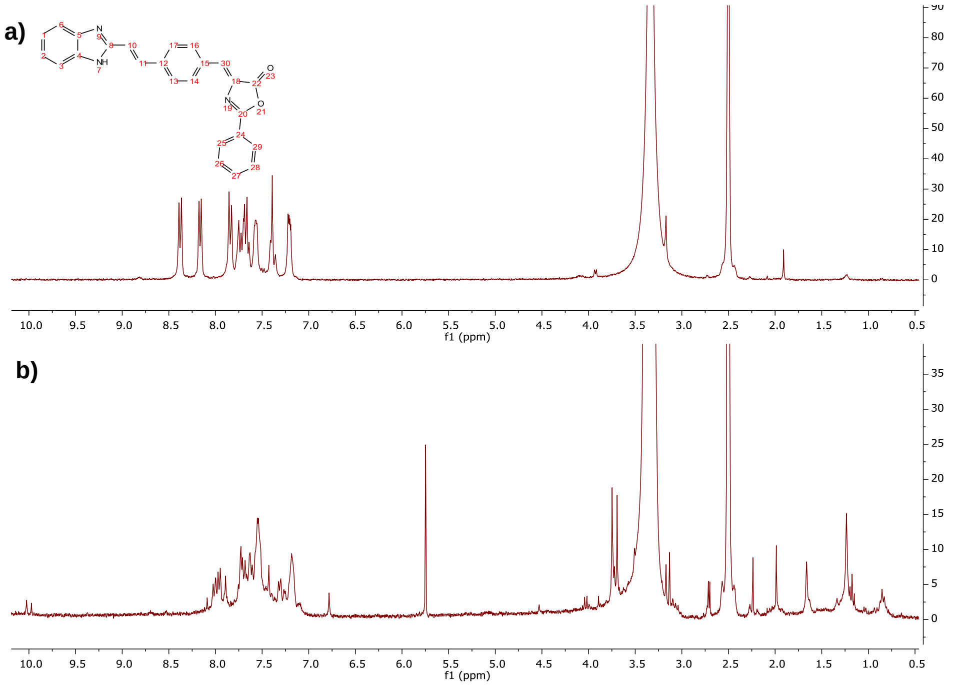

Figure 3.2. a) ^{1}H-NMR of the compound **11**, **b)** ^{1}H-NMR of the reaction of hydrogenation of compound **11**

Since it was not possible to obtain the desired compound from compound **11**, the attempt to hydrogenate compound **5** under the same reaction conditions was initiated.

This compound, besides being smaller, still contains less sites in which hydrogenation can occur, being able to facilitate the reaction. However, after the completion of the reaction and by analysis of the ^{1}H-RMN spectrum obtained, it was found that no reaction occurred, the spectrum corresponding only to the starting material. (Figure 3.3)

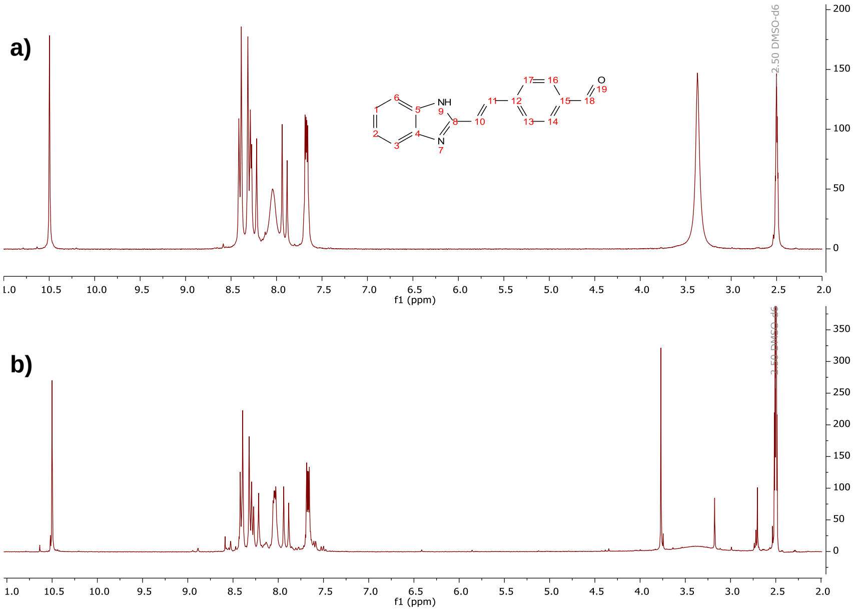

Figure 3.3. a) ^{1}H-NMR of the compound **5**, **b)** ^{1}H-NMR of the reaction of hydrogenation of compound **5**

Since hydrogenation using hydrogen atmosphere did not result in obtaining any of the desired compounds, hydrogenation was realized in a reactor under pressure (9.87 atm).

However, as in the previous reaction, by analysis of the ^{1}H-NMR spectrum, it was found that no reaction occurred.

3.9. Synthesis of hippuric acid derivatives

3.9.1. Synthesis of *N*-acetylglycine

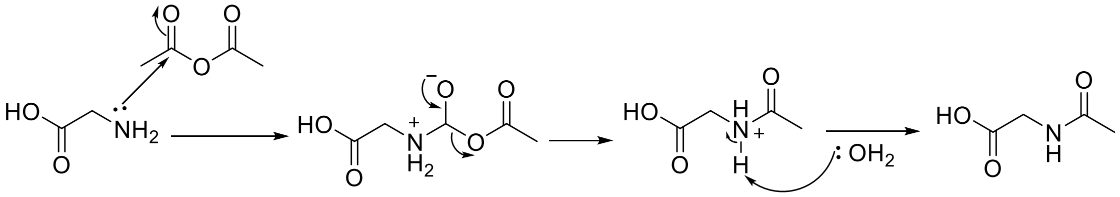

21

Scheme 3.12. Mechanism for the formation of *N*-acetyl glycine **21** through the reaction of glycine with acetic anhydride.

N-acetyl glycine **21** was synthesized through the reaction of glycine with acetic anhydride, via an addition-elimination reaction. The free electrons of the amine group of glycine acts as a nucleophile and attacks a carbonyl carbon of acetic anhydride, a reaction that is facilitated by the acetate presence, a good leaving group (Scheme 3.12).

After isolation of compound **21** in 49% yield, through filtration and without needing purification, it was characterized by NMR (Appendix 21, Table 3.7).

Table 3.7. Characterization of compound **21**, synthesized through an reaction between glycine and acetic anhydride.[a]

Compound	^{1}H-NMR	^{13}C-NMR
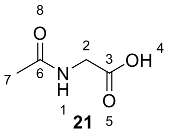 **21**	3.90 (s, 2H, H2) 1.97 (s, 3H, H7)	174.64 (C3) 173.47(C6) 41.01 (C2) 21.46 (C7)

[a] Atoms numeration according to ChemDraw assignment

3.9.2. Synthesis of (pyrazine-2-carbonyl)glycine and nicotinoylglycine s

The synthesis of these derivatives of hippuric acid was performed with the objective of improving the solubility of **OXA 12**, the great problem of this compound, without a great variation of its structure, since it was verified that the activity of this compound is sensitive to the substitutions carried out in several positions, as will be discussed later**.**

From these observations and also from the results obtained by Professor Rui Moreira for this compound, through the use of a multiparametric algorithm, CNS MPO (central nervous system multiparameter optimization), for calculation of a score value for compounds directed to the CNS, since the compound will be administered intrathecally, the development of these new compounds began.

This algorithm uses a set of 6 physico-chemical parameters (lipophilicity, distribution coefficient, molecular weight, polar surface area, number of H and pKa binding donors) to obtain a total score value (ranges from 0 to 6).

According to the reference[52], the MPO score value is intended to be greater than 4, since a higher value means that this compound has desirable ADME and safety conditions for CNS targeted compounds. However, there are drugs targeted to the CNS with values below 4.

On basis of those studies, we selected the insertion of nitrogen atoms on the phenyl ring as an appropriate alternative in order to increase the water solubility of the target compound.

For **OXA 12**, the results presented in the Table 3.8.

Table 3.8. Results obtained for **OXA 12** using CNS MPO

Physico-chemical parameters		**Individual Score**	**Total Score**
MW	391.43	0.77	3.57
clogP	5.29	0	
clogD$_{7.4}$	5.69	0	
TPSA	67.34	1	
HBD	1	0.8	
pK_a	5.34	1	

The formation of this derivatives can occur through the reaction of an acid chloride with glycine. However, this acyl chloride may also be formed from a carboxylic acid, using oxalyl chloride or thionyl chloride. Another hypothesis for the formation of these derivatives occurs through a coupling reaction based on Steglish esterification followed by hydrolysis.

a) Formation of hippuric acid derivatives using Steglich esterification as a base

The formation of hippuric acid derivatives occur with a carboxylic acid and *N,N'*-dicyclohexylcarbodiimide (DCC) coupling, catalysed by 4-dimethylaminopyridine (DMAP).

Initially, occurs the reaction between DCC and the carboxylic acid forming an O-acylurea intermediate. Then, the DMAP, a nucleophile stronger than the amine, reacts with O-acylurea leading to the formation of a reactive amide and dicyclohexylurea (DCU), hard to eliminate. This formed species promotes the rapid reaction of the amine with the carbonyl group leading to the formation of compound **22** and the regeneration of DMAP. (Scheme 3.13a).

The reaction was monitored by TLC, with the appearance of two spots with higher Rf than the starting material (application point). The crude was purified by column chromatography, the two spots being isolated, which were analyzed using NMR spectroscopy (Figure 3.4).

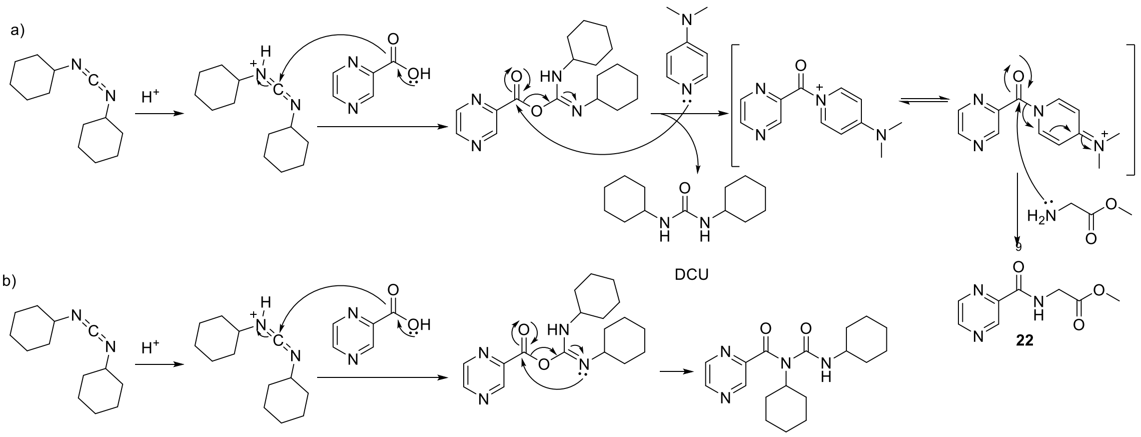

Scheme 3.13. a) Formation of compound **22** from the carboxylic acid and through a coupling using DCC and DMAP as the catalyst, **b)** Possible mechanism of formation of a urea as a by-product resulting from an intramolecular reaction of the intermediate formed in the reaction with the DCC

The spot with lower Rf has been found to correspond to the desired product (Figure 3.4b) while the other may correspond to a urea resulting from an intramolecular attack of the intermediate formed with DCC (Scheme 3.13b, Figure 3.4a).

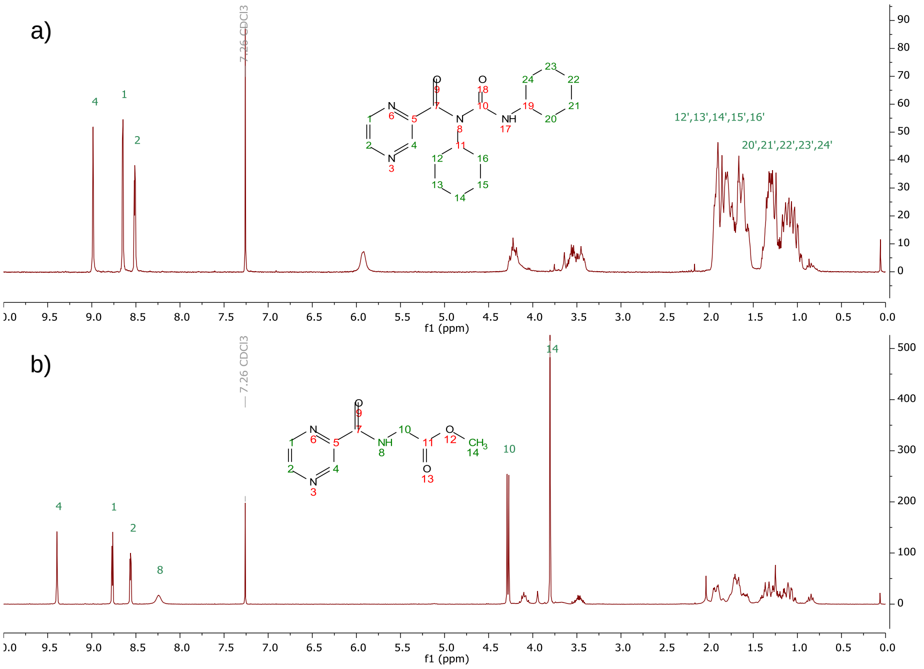

Figure 3.4. a) ^{1}H-NMR spectrum of urea resulting from an intramolecular attack of the intermediate formed with DCC, **b)** ^{1}H-NMR spectrum of compound **22**, synthesized from the reaction between glycine methyl ester hydrochloride and pyrazine-2-carboxylic acid via a coupling using DCC and DMAP, containing DCU.

Nevertheless, after purification the ^{1}H-NMR spectrum still showed the presence of the characteristic signals of DCU (Figure 3.5a). In order to eliminate this, the compound **22** was dissolved in DCM, solvent in which the DCU is poorly soluble, followed by filtration and evaporation. This process was repeated several times until the DCU was completely eliminated allowing the isolation of **22** in 55 %.

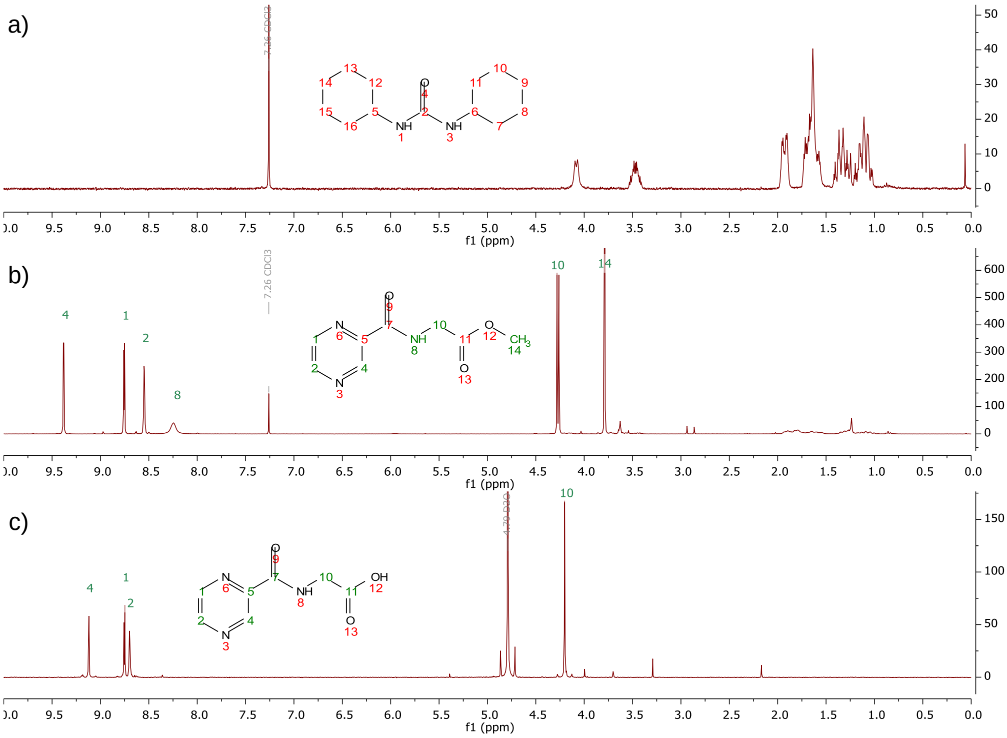

Figure 3.5. ^{1}H-NMR spectrum of **22** (**b**), synthesized from the reaction between glycine methyl ester hydrochloride and pyrazine-2-carboxylic acid via a coupling using DCC and DMAP, with formation of DCU (**a**) as by-product. Compound **23** (**c**), resulted from the hydrolysis of compound **23** using KOH.

The presence of the compound, as already mentioned, was confirmed by NMR spectroscopy (Appendix 22), verifying for the presence of the corresponding signals to the compound **22** (Figure 3.5b) without the presence of DCU (Table 3.9).

Table 3.9. Characterization of compound **22,** synthesized from the reaction between glycine methyl ester hydrochloride and pyrazine-2-carboxylic acid via a coupling using DCC and DMAP.[a]

Compound	^{1}H-NMR	^{13}C-NMR
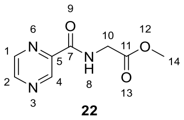 **22**	9.38 (d, *J* = 1.5 Hz, 1H, H4) 8.76 (d, *J* = 2.4 Hz, 1H, H1) 8.55 (dd, *J* = 2.5, 1.5 Hz, 1H, H2) 8.25 (s, 1H, H8) 4.27 (d, *J* = 5.6 Hz, 2H, H10) 3.79 (s, 3H, H14).	169.92 (C11) 163.32 (C7) 147.61 (C1) 144.40 (C4) 143.92 (C2) 52.55 (C10) 41.17 (C14)

[a] Atoms numeration according to ChemDraw assignment

The pure compound **22** was then hydrolyzed to carboxylic acid **23** (Scheme 3.15).

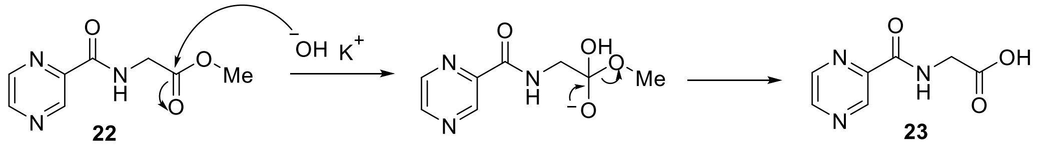

Scheme 3.14. Hydrolysis of compound **22** using KOH as the base, for the formation of compound **23**

This reaction occurs by the nucleophilic attack of -OH to carbonyl carbon of ester with expulsion of methoxy group, a good leaving group, leading a formation of the derivate of hippuric acid, the compound **23** (Scheme 3.14).

The reaction was monitoring by TLC, verified the disappearance of compound **22** and the appearance of a spot on the application point, corresponding to carboxylate.

Since it is at the application point, such as the salt is formed, it is not possible to purify it through a chromatographic column, it being only possible to obtain the pure compound through precipitation. In this case, the precipitation occurs by varying the pH of the solution through the slow addition of HCl 1 M. However, this process was difficult to perform since the compound is sensitive to pH variation, the structure has several basic sites and as the reaction was realized on a small scale, the addition of a small amount of aqueous solution of HCl 1 M leads to a wide pH variation.

After precipitation and filtration of a compound, this was characterized by NMR spectroscopy (Appendix 23), confirming the formation of compound **23** in 69% (Figure 3.5c) by the disappearance of the singlet at 3.77 ppm attributed to the C14 of compound **22**, removed during the hydrolysis. In the ^{13}C-NMR spectrum also the disappearance of the signal corresponding to this C14, at 41.17 ppm (Table 3.10).

Table 3.10. Characterization of compound **23**, synthetized through hydrolysis of compound **22** using KOH[a]

Compound	^{1}H-NMR	^{13}C-NMR
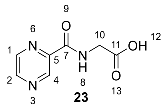	9.13 (d, J = 1.4 Hz, 1H, H4) 8.76 (d, *J* = 2.5 Hz, 1H, H1) 8.71 (dd, J = 2.6, 1.4 Hz, 1H, H2) 4.20 (s, 2H, H10)	173.28 (C11) 165.74 (C7) 147.23 (C2) 147.18 (C5) 144.19 (C4) 142.87 (C1) 41.18 (C10)

[a] Atoms numeration according to ChemDraw assignment

b) Formation of hippuric acid derivatives through acid chloride

In the reaction of forming an acid chloride from a carboxylic acid, it is first necessary to activate the acid by making the hydroxyl a good leaving group.

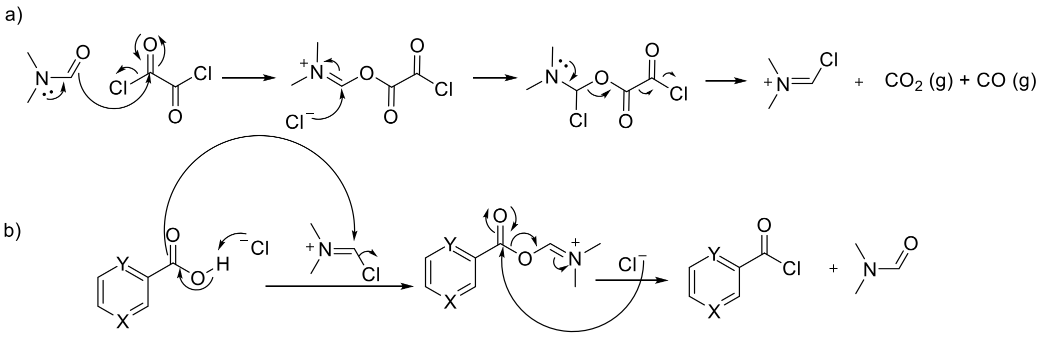

24 X = N; Y = H
25 X = N; Y = N

Scheme 3.15. Formation of the acid chloride **24-25** from the carboxylic acid using oxalyl chloride and dimethylformamide (DMF) as catalyst, **a)** formation of Vilsmeier-Haack reagent through reaction between oxalyl chloride and DMF; **b)** reaction of Vilsmeier-Haack reagent with carboxylic acid with formation of acid chloride.

The formation of the acid chloride using oxalyl chloride is initiated by the reaction of this chloride with DMF and the formation of a highly electrophilic intermediate, Vilsmeier -Haack reagent, by replacing the hydroxyl group with chlorine via a tetrahedral intermediate. (Scheme 3.15a).

Next, the acid attack on the highly electrophilic Vilsmeier-Haack reagent occurs at the double bond C-N forming an intermediate which undergoes a chlorine ion attack with formation of the acid chloride and regeneration of the DMF (Scheme 3.15b).

Another way of forming the acid chloride is by the use of thionyl chloride (Scheme 3.16)

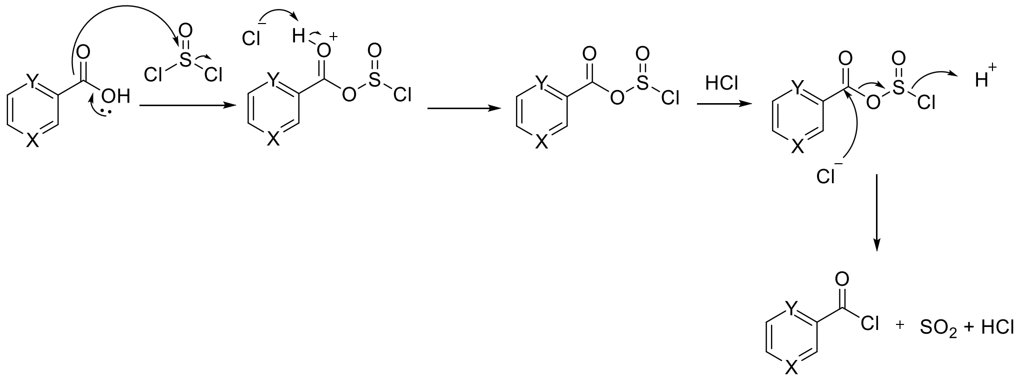

24 X = N; Y = H
25 X = N; Y = N

Scheme 3.16. Formation of acid chloride **24-25** using thionyl chloride

Thionyl chloride contains an electrophilic centre on the sulphur atom and the attack of the carboxylic acid (nucleophile) occurs at this centre with the formation of an unstable and highly electrophilic intermediate. The electrophilicity of this intermediate facilitates the attack of the chloride ion (weak nucleophile) and the formation of the acid chloride through the collapse of the tetrahedral structure and release of HCl and SO_2. After this step, the reaction is irreversible since the formed gases can be lost. (Scheme 3.16)

Upon formation of the acid chloride (using oxalyl chloride or thionyl chloride) it is used directly in the next step without further purification.

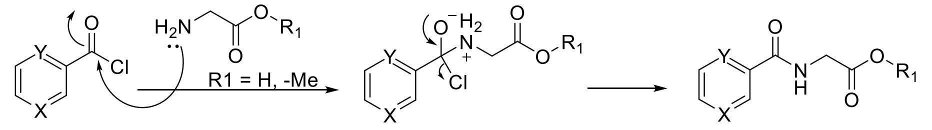

24 X = N, Y = H
25 X = Y = N

22 X = N, Y = N, R1 = -Me
26 X = Y = N, R1 = H

Scheme 3.17. Mechanism of formation of compound **22** and **26** through reaction between acid chloride **24** or **25** and glycine or derivative, through of S_N2 reaction com expulsion of chloride.

The acid chloride formed may react with glycine to form compound **26** via an addition-elimination reaction. Initially it was possible to obtain compound **26** using this method. However, when the same reaction was attempted on a larger scale did not work. Thus, in order to understand whether the problem would be the formation of the acid chloride or the reaction with the glycine, the reaction was realized using the same conditions, but exchanging the glycine for the glycine methyl ester hydrochloride, leading to the formation of compound **22**, already synthesized by another method.

In this reaction, the electrophilic carbonyl carbon of the acid chloride (**24** or **25**) is attacked by the nucleophilic amine of the glycine or derivative, with expulsion of the chloride, a good leaving group. This results in the formation of the hippuric acid derivative (**22** or **26**) with additional release of HCl formed during the reaction (Scheme 3.17). The absence of reaction for glycine is probably due to the preferential formation of the corresponding mixed anhydride derived from non-reactivity of the amino group due to being protonated.

In the case of the reaction in which R_1 = Me it was still necessary to carry out an additional step of hydrolysis to obtain the acid, shown to be carried out as shown in Scheme 3.14.

The formation of compound **26** was verified by the use of NMR spectroscopy (Appendix 24), observing the presence of the signals corresponding to those expected for the compound (Table 3.11).

Table 3.11. Characterization of compound **26**, synthetized through reaction between acid chloride and glycine[a]

Compound	^{1}H-NMR	^{13}C-NMR
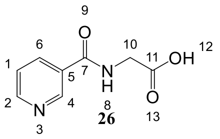 **26**	9.14 (s, 1H, H4) 9.05 – 8.79 (m, 2H, H2,6) 8.07 (dd, J = 8.1, 5.8 Hz, 1H, H1) 3.60 (s, 3H, H10)	172.37 (C11) 168.90 (C7) 145.19 (C2) 143.75 (C4) 143.15 (C6) 135.46 (C5) 126.73 (C1) 41.48 (C10)

[a] Atoms numeration according to ChemDraw assignment

3.10. Stability assays

OXA 12, the compound synthesized in this laboratory showed the highest inhibitory activity against necroptosis, was submitted to stability assays in human plasma and phosphate-buffered saline (PBS) with 20% ACN. No microsomal assay was performed because of previously obtained results.

Before the start of the assays it was necessary to develop a method for the detection of compound.

3.10.1. UV spectra

UV spectra of the compound were initially performed in order to determine the wavelength of maximum absorption of the compound, in this case at about 414 nm, wavelength at which the HPLC detector should detect the compound.

However, the lack of solubility of the compound was soon found to be a problem which could affect the results of the stability assays, since complete dissolution of the compound did not occur in any organic or aqueous solvent, making it difficult to prepare solutions with the desired concentration, as the stock solution is a suspension and not a solution.

Due to this problem spectra were draw using various solvents (acetonitrile, methanol and phosphate buffer), obtaining the best dissolution for ACN, exhibiting the best absorption spectrum (Figure 3.6). It was also the solvent used to prepare the stock solution.

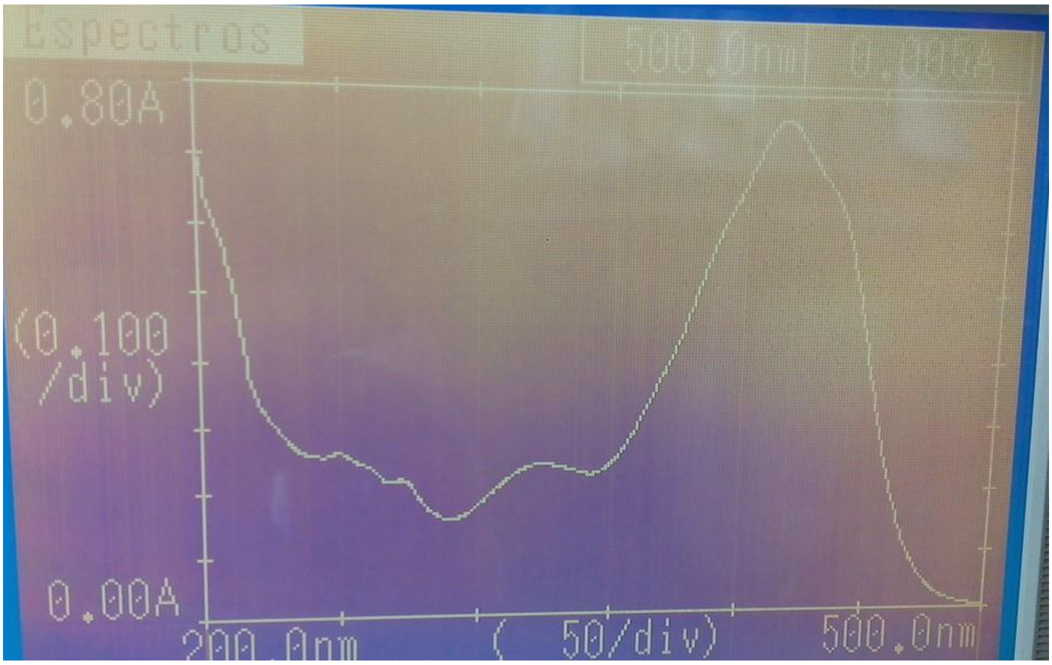

Figure 3.6. UV spectra of **OXA 12** in acetonitrile

3.10.2. Development of a method for the detection of OXA 12

A method for detection of **OXA 12** was developed using Elite LaChrom (VWR Hitachi) system comprised of an L-2130 pump, an L-2400 UV detector and a Rheodyne® manual sample injector with a 20 µL sample loop. Chromatography separation was achieved on a LichroCART® 125-4 - Lichrospher® 100 RP-18 (5 µm) and the compound was detected at 400 nm, value taken from the UV-vis spectrum.

The first run was in gradient mode, using as the mobile phase an increasing gradient of the H_2O/MeOH mixture (8:2 to 0.5:9.5) for 30 minutes. Detection of **OXA 12** occurred at R_T = 26 min (6 minutes after the onset of elution with H_2O/MeOH (0.5:9.5)).

The run was repeated three times in order to validate the results obtained.

Then, after realizing the behaviour of compound, an isocratic run for 30 minutes was performed, using as mobile phase H_2O/MeOH (0.5:9.5), solvent mixture in which the compound was detected in the gradient run. (Figure 3.7)

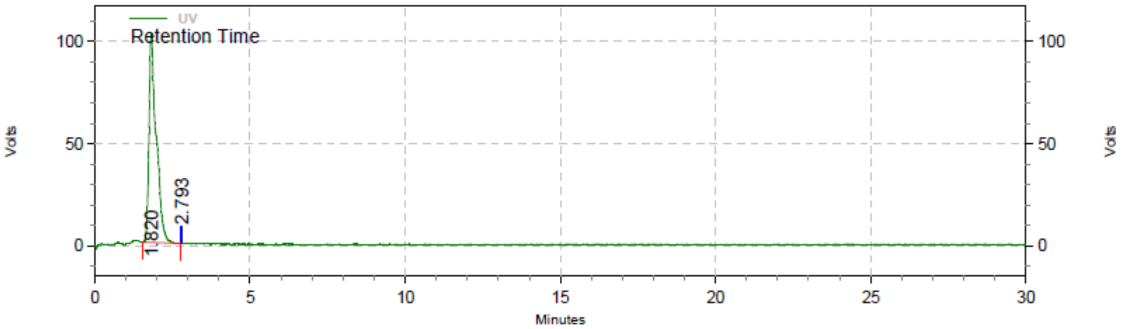

UV Results

Retention Time	Area	Area %	Height	Height %
1.820	6662135	99.99	410022	99.96
2.793	336	0.01	160	0.04
Totals	6662471	100.00	410182	100.00

Figure 3.7. Run in isocratic mode using as mobile phase H_2O/MeOH (0.5:9.5) and the retention time of **OXA 12** was 1.82 min.

However, as verified that the compound has a low R_T and there may be an interference from the peaks of the solvents being close to the injection peak, a second run was conducted by changing the mobile phase to a solvent mixture of H_2O/MeOH (1:9), obtained a slightly higher retention time, R_T = 2.42 min, and this method can be used for detection of **OXA 12** (Figure 3.8).

The result obtained in this isocratic mode run was repeated three times under the same conditions and the results obtained in this run were validated.

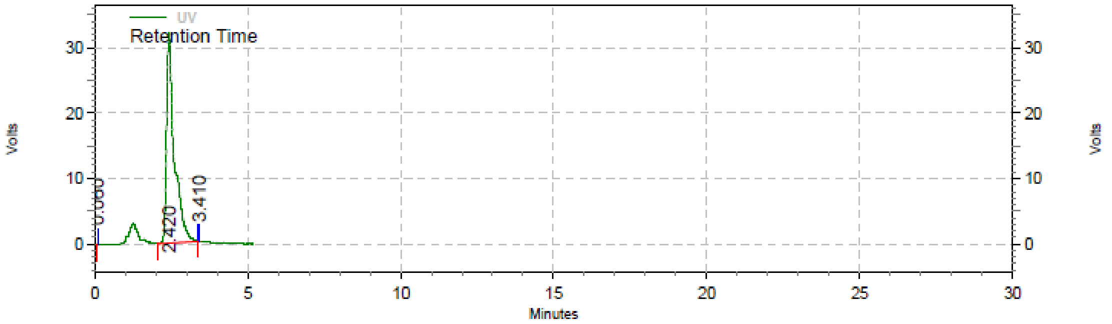

UV Results

Retention Time	Area	Area %	Height	Height %
0.060	955	0.04	429	0.33
2.420	2270480	99.94	128706	99.45
3.410	405	0.02	285	0.22
Totals	2271840	100.00	129420	100.00

Figure 3.8. Run in isocratic mode using as mobile phase H_2O/MeOH (1:9) and the retention time of **OXA 12** was 2.42 min.

3.10.3. Metabolic stability assays using human plasma and PBS with 20% acetonitrile

After obtaining this method for detection of **OXA 12**, the stability assays of the compound were conducted in human plasma and PBS with 20% acetonitrile (phosphate buffer is at pH 7.4) to simulate *in vivo* condition

a) Human plasma

The solution containing **OXA 12** in 2 mL of human plasma and 0.5 mL of PBS, was prepared and maintained during the assay at 37 ° C.

The first injection was made shortly after the preparation of the solution, considering t = 0 min. Injections were repeated over 26 h. For each injection, 200 µL of the plasma solution were withdrawn, 400 µL of acetonitrile were added to induce precipitation of the plasma proteins. The solution was centrifuged to 10000 rpm and 20 µL of supernatant was withdrawn for injection in HPL, thus quantifying the quantity of compound remaining through time. After the runs, the values of the peak area were plotted against the times of injection to draw the graph of Figure 3.9.

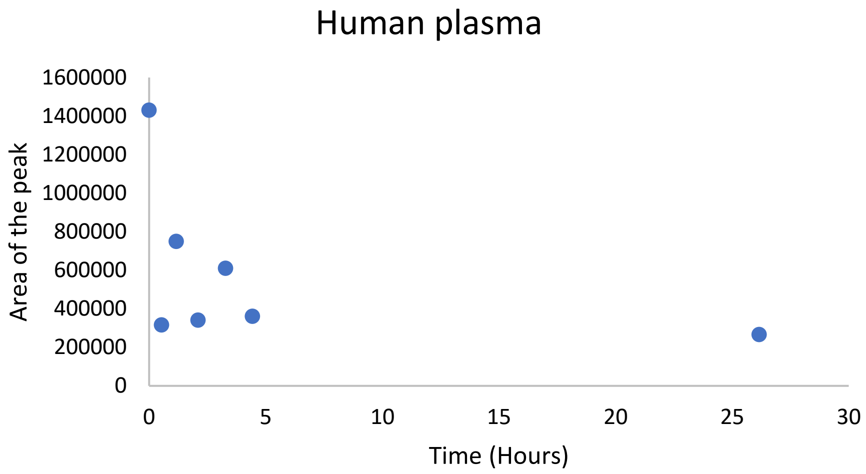

Figure 3.9. Graph showing the results corresponding to human plasma assay with **OXA 12**, containing the area of the peak of each injection as a function of the time of the assay.

During the course of the assay, there was a slight turbidity in the solution which may be an indicator that precipitation of the compound was occurring.

b) PBS with 20% acetonitrile

A solution of PBS with 20% ACN and **OXA 12** was prepared, and a sample was withdrawn after the addition of **OXA 12** for the first injection. At each injection, 20 µL were withdrawn directly from the solution and injected without any treatment in HPLC, occurring the quantification of the present compound.

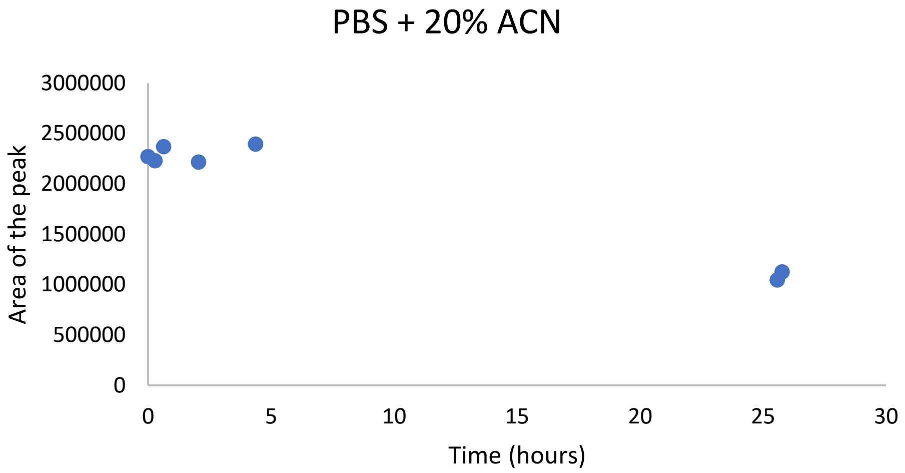

.

Figure 3.10. Graph showing the results corresponding in PBS assay, containing the area of the peak of each injection as a function of the time of the assay.

As in the previous assay, after the runs, the values of the peak area were plotted against the times of injection to draw the graph of Figure 3.10. There was also a slight turbidity solution, as had happened in the previous assay.

After performing these assays, the results obtained were inconclusive, since there was no gradual decrease in peak area of the compound over time which would result in a value of half-life of the compound under those conditions. Instead, oscillations of the area have always been observed in the same range of values, which may mean that precipitation of the compound was occurring due to poor solubility, and thus the decrease of the peak area, however, the precipitated compound may dissolve again and then again increase the area. Therefore, it was not possible to obtain conclusions of the stability.

3.11. Biological assays

Throughout this dissertation the compounds present in Table 3.12. were synthesized and subsequently the ability of each to inhibit necroptosis was assessed by performing biological assays on BV2 murine microglia cells using zVAD-fmk as an inhibitor of apoptosis. Those tests were performed by Sara Oliveira from Cellular Function and Therapeutic Targeting Laboratory at iMed.ULisboa (FF-UL) headed by Professor Cecilia Rodrigues. However, it was not possible to synthesize any compound having the same, or higher, inhibitory than **OXA 12**, which was also synthesized again.

Table 3.12. Results of biological assays to **OXA** derivatives in BV2 murine microglia cells

Entry	Compound	% Protection	Entry	Compound	% Protection
1	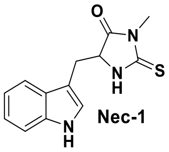 **Nec-1**	93.9	**6**	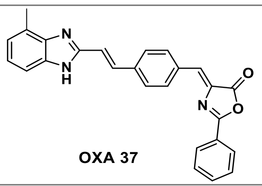 **OXA 37**	9.0
2	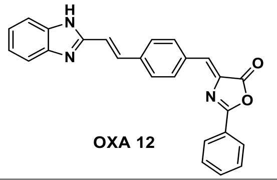 **OXA 12**	64.5	**7**	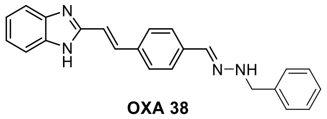 **OXA 38**	23.3
3	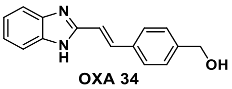 **OXA 34**	5.2	**8**	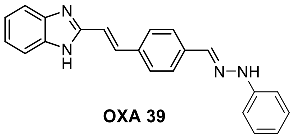 **OXA 39**	36.5
4	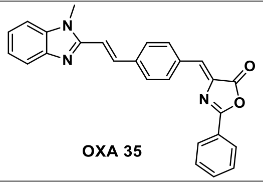 **OXA 35**	43.0	**9**	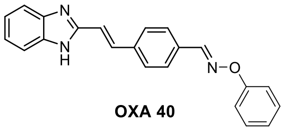 **OXA 40**	23.7
5	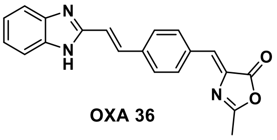 **OXA 36**	1.2			

Based on the results of the above table and taking into account all compounds evaluated with the aim of inhibiting necroptosis, the influence of the modifications to the structure of **OXA 12** are discussed below by considering the **A-E** moiety (Figure 3.11).

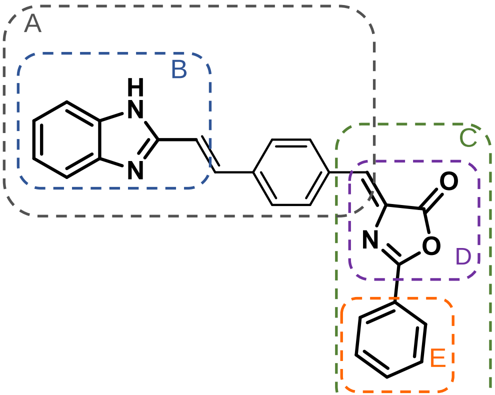

Figure 3.11. Structure of **OXA 12** containing five moieties. In grey, substituents at the C-4 position of the oxazolone ring (**A**), benzimidazole ring moiety in blue (**B**) and green hippuric acid moiety (**C**). In this moiety there is the ring of oxazolone in purple (**D**) and orange, the phenyl ring terminal (**E**).

a) Substituents at C-4 position of oxazolone moiety (A)

Synthesis of a small family of compounds containing different substituents at the C-4 position of the oxazolone ring (**A**). The results of the biological assays on these compounds are given in Table 3.13.

Table 3.13. Percent protection against necroptosis for each structure synthesized with substituents at C-4 position of oxazolone moiety, using BV2 murine microglia cells for the performance of the assay

Entry	Compound	% Protection	Entry	Compound	% Protection
1	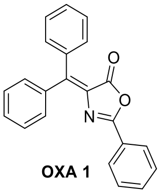 **OXA 1**	-10,6	**10**	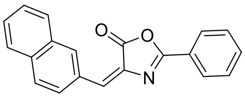 **OXA 10**	0.3
2	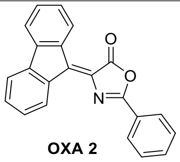 **OXA 2**	-0.4	**11**	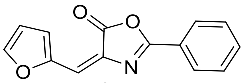 **OXA 11**	-2.0
3	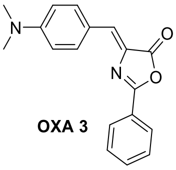 **OXA 3**	-16.1	**12**	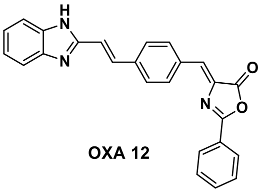 **OXA 12**	71,397
4	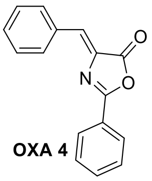 **OXA 4**	-5.4	**13**	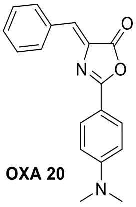 **OXA 20**	-3.5

5	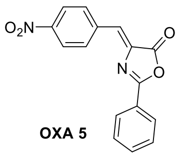 **OXA 5**	-0.5	**14**	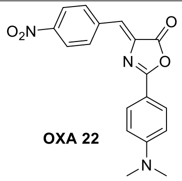 **OXA 22**	-4.8
6	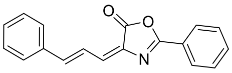 **OXA 6**	5.2	**15**	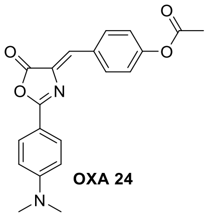 **OXA 24**	2.0
7	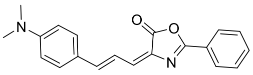 **OXA 7**	0.4	**16**	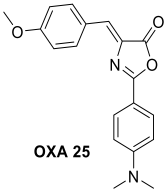 **OXA 25**	-3.8
8	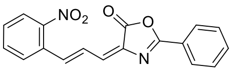 **OXA 8**	-1.8	**17**	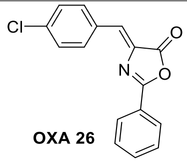 **OXA 26**	6.7
9	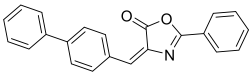 **OXA 9**	-1.3	**18**	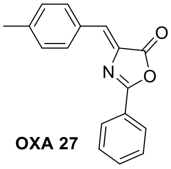 **OXA 27**	-7.6
	Nec-1*	94.9		**OXA 12***	73.0

* Mean value of the assays performed

Using the results of the biological assays performed on these compounds, we have found that **OXA 12** (entry 12, Table 3.13) was the compound that has the highest percentage of protection against necroptosis, when induced by z-VAD fmk. By analyzing the structures of all the compounds, it can be seen that the benzimidazole ring may be responsible for increasing the protection percentage, since this moiety does not exist in the other compounds.

b) Benzimidazole ring moiety (B)

1) Substituents in 4 or 5-position

Synthesis of different 4 or 5-substituted benzimidazole (**B**) moiety of **OXA 12** was performed. The results of the biological assays being shown in Table 3.14.

Table 3.14. Percent protection against necroptosis for each structure synthesized with introduction of substituents in 4 or 5-position of benzimidazole, using BV2 murine microglia cells for the performance of the assay.

Entry	Compound	% Protection	Entry	Compound	% Protection
1	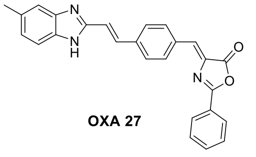 **OXA 27**	-12.6	**4**	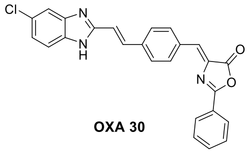 **OXA 30**	-4,4
2	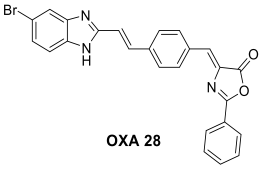 **OXA 28**	7.1	**5**	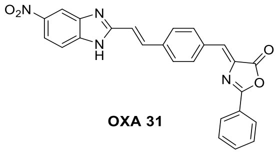 **OXA 31**	4.0
3	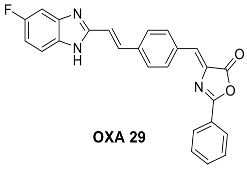 **OXA 29**	43.0	**6**	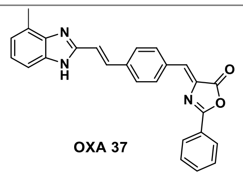 **OXA 37**	9,0
	Nec-1*	94.9		**OXA 12***	73.0

* Mean value of the assays performed

The introduction of a methyl group, electron donating group, at the 4-position (Entry 6, Table 3.14) or 5-position (Entry 1, Table 3.14) on the benzimidazole **B**, was one of the changes made to the base skeleton of **OXA 12**, resulting in a total loss of the inhibitory activity presented in **OXA 12**.

OXA 37 (Entry 4, Table 3.14) has been synthesized based on Nec-1s, a chlorine-containing compound in the 7-position of indole ring and increases the activity of Nec-1s compared to Nec-1. However, **OXA 37** (Entry 4, Table 3.14) contains a methyl group which can not be compared to chlorine. There is no data on the presence of chlorine or other halogen in that position.

The other derivatives synthesized on the basis of the alteration of this block **B** resulted in the introduction of several electron withdrawing group on the 5-position in the benzimidazole. A loss of activity has been found in almost all of the compounds of this group except for the compound containing the fluorine (Entry 3, Table 3.14), in which case decrease in the activity was also observed, despite lower. A possible explanation is the fact that the fluorine is bioisostere of hydrogen, thus having a size similar to the hydrogen atom, and this type of compounds may have similar biological properties.

2) Heterocycle modifications (B)

One of the modifications in this moiety was the methylation of the -NH in the benzimidazole **B** (Entry 2, Table 3.15) which resulted in a loss of activity compared to **OXA 12**. Importantly, this indicates the possibility of this hydrogen having a key role in the binding to the active site. There was also loss of activity when benzimidazole was replaced by benzothiazole (Entry 1, Table 3.15), and the same conclusion was also drawn.

Table 3.15. Percent protection against necroptosis for each structure synthesized with alteration in the benzimidazole heterocycle, using BV2 murine microglia cells for the performance of the assay.

Entry	Compound	% Protection	Entry	Compound	% Protection
1	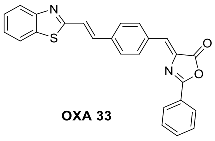 OXA 33	-18.9	**2**	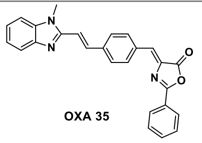 OXA 35	3.0
	Nec-1*	94.9		**OXA 12***	73.0

* Mean value of the assays performed

c) Hippuric acid moiety (C)

To highlight the importance of the moiety **C** in the inhibitory activity of **OXA 12** on necroptosis, a series of compounds were also developed.

1) Hippuric acid moiety modifications

OXA 36 (Entry 5, Table 3.16) was synthesized using the *N*-acetyl glycine instead of the hippuric acid resulting in a compound without the phenyl ring **E**. This compound, such as in the previous case, lost the inhibitory activity, thus realizing that this ring has a function in the interaction with the target.

In addition to the synthesis of this compound, other compounds with different substituents in *-para* position of the ring **E** were synthesized. It was found that with the EWG groups, -CN (Entry 1, Table 3.16) and -NO_2 (Entry 2, Table 3.16), the scaffold lost total inhibitory activity, however, with -NMe_2 (Entry 3, Table 3.16), EDG, it obtained an inhibitory activity similar to **OXA 12**.

OXA 32 (Entry 4, Table 3.16), compound synthesized by increasing the chain between the oxazolone **D** and the phenyl ring **E**, maintained inhibitory activity against necroptosis, although lower than **OXA 12**.

Table 3.16. Percent protection against necroptosis for each structure synthesized with modifications in hippuric acid, using BV2 murine microglia cells for the performance of the assay.

Entry	Compound	% Protection	Entry	Compound	% Protection
1	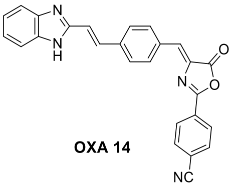 OXA 14	9.8	**4**	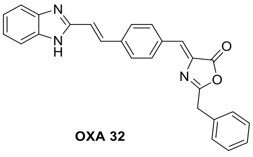 OXA 32	40.1

2	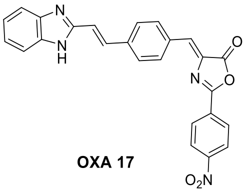 OXA 17	13.7	**5**	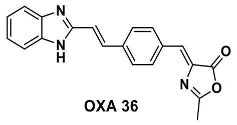 OXA 36	1.2
3	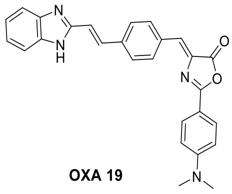 OXA 19	56.6			
	Nec-1*	94.9		**OXA 12***	73.0

* Mean value of the assays performed

2) Hippuric acid moiety alterations

To verify the importance of moiety **C** for the inhibitory activity of the compound, the **OXAs 34**, **38**, **39** and **40** (Entry 1, 2, 3 and 4, respectively) were synthesized, the results of the biological assays being in Table 3.17.

OXA 34 (Entry 1, Table 3.17), a compound that instead of this moiety contains only one -OH group, was found to lose total inhibitory activity which suggests that moiety is important for the interaction of **OXA 12** to the active site.

Then, a batch of two hydrazones (Entry 2 and 3, Table 3.17) and one oxime (Entry 4, Table 3.17), all containing the ring **E**, has synthesized, with one of the hydrazones containing a benzyl group, while the other two compounds contain a terminal phenyl ring. After the assays, the three compounds showed a decreased inhibitory activity when compared to **OXA 12**, despite still having an activity in the order of 30%. These results suggest the exchange of the oxazolone ring by the hydrazone or the oxime leads to a major, but not total loss of activity, which proves the importance of this group and also shows that possibly the little maintained activity comes from the ring **E**, showing once again the importance of this ring in accordance to our previous results.

Table 3.17. Percent protection against necroptosis for each structure synthesized with alterations in hippuric acid, using BV2 murine microglia cells for the performance of the assay.

Entry	Compound	% Protection	Entry	Compound	% Protection
1	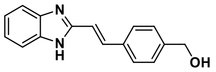 OXA 34	5.2	**3**	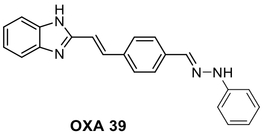 OXA 39	36.5
2	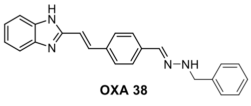 OXA 38	23.3	**4**	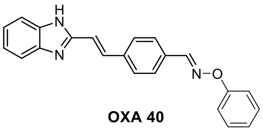 OXA 40	23.7
	Nec-1*	94.9		**OXA 12***	73.0

* Mean value of the assays performed

After analysing the results obtained from the assays of these compounds, it was concluded that the moiety **C,** synthesized through an intramolecular reaction of the hippuric acid, is important for the interaction with the active site.

4. Conclusion

New Oxazolones were synthesized using the Erlenmeyer-Plöch reaction, affording the compounds in low to moderate yield (10-40%), which were further characterized by ^{1}H-NMR and ^{13}C-NMR.

In addition to these compounds, others based on the skeleton of **OXA 12** have also been developed, e.g. by altering the ring of hippuric acid by other groups such as hydrazone, oxime or only by reduction of the intermediate compound to an alcohol. These compounds were synthesized in moderate to high yields (40-96%) and were characterized by ^{1}H-NMR and ^{13}C-NMR.

All synthesized compounds, based on **OXA 12**, were evaluated for their ability to inhibit necroptosis by performing assays using BV2 murine microglia cells. However, **OXA 12** remains the compound that has the highest capacity to inhibit necroptosis.

OXA 12 has a value of cLogP = 5.29, this value being considered high and results from the low hydrophobicity of the compound. The compounds synthesized on the basis of this also have low solubility in organic and aqueous solvents, this being a problem presented by these compounds.

From the presented problem, the development of new compounds was initiated, in an attempt to increase the solubility, without making deep alterations in the **OXA 12** skeleton.

In the future, it is intended to conclude the synthesis of these new compounds for later biological evaluation. Another objective is the in vivo assays using **OXA 12** or if found the new compound with greater solubility.

5. Materials and methods

5.1. General remarks

Reagents and solvents: All commercial solvents were distilled. The anhydrous solvents used were prepared according to general procedures.[53] The reagents used were purchased from Aldrich, Alfa Aesar, Fluorochem or TCI and were used without further purification.

Stationary phases: The evolution of the reactions was monitored by TLC using silica Merck Kieselgel 60 F_{254} plates, on aluminium support. Purifications by chromatographic column were performance using silica gel Merck 60A (0.04-0.063 nm), using as solvent mixtures indicated in each procedure.

Nuclear magnetic resonance (NMR): Spectra were obtained using Bruker Avence II 300. ^{1}H-NMR spectra were acquired at 300 MHz and ^{13}C-NMR spectra at 75 MHz. This spectrum was performed using deuterated solvents which served as reference for spectrum analysis. The analysis of ^{1}H-NMR was always performed with the same format: deuterated solvent; chemical shift of the signal (δ, in ppm); multiplicity of signal, coupling constant (J, Hz), signal strength (nH, n number of protons), assignment in the molecule.

Infrared spectroscopy (IR): Performed on a spectrophotometer of Bruker, Alpha II. In the description will be presented the frequencies of the characteristic bands. In each case, the data will be presented as follows: maximum absorption rate (υ_{max} in cm^{-1}); attribution of the functional group present in the compound, whenever possible.

Melting points: measured using Bibby Scientific SMP10 Melting Point Apparatus, Stuart.

High-performance liquid chromatography (HPLC): HPLC analysis were performed on an Elite LaChrom (VWR Hitachi) system comprised of an L-2130 pump, an L-2400 UV detector and a Rheodyne® manual sample injector with a 20 µL sample loop. Chromatography separation was achieved on a LichroCART® 125-4 - Lichrospher® 100 RP-18 (5 µm). Software program used for the chromatograms was EZChrom Elite.

Ultraviolet-visible spectroscopy (UV): UV-vis was performed on a Shimadzu, UV-1601 spectrophotometer & CPS-240A cps cell spectrophotometer, in quartz cell support. Measurements of the absorption spectrum were made in a range of 200-500 nm.

MS (ESI+): High resolution ESI positive mode mass spectra were obtained on a QqTOF Impact IITM mass spectrometer (Bruker Daltonics) operating in the high resolution mode at Instituto Superior Técnico. Samples were analyzed by flow injection analysis (FIA) using a isocratic gradient 50 A:50 B of 0.1% formic acid in water (A) and 0.1% of formic acid in acetonitrile (B), at a flow rate of 5 µLmin-1 over 15 min. Calibration of the TOF analyzer was performed with a calibrant solution of sodium formate 10 mM. The full scan mass spectra were acquired over a mass range of 50-1500 m/z at a spectra rate of 0.2 Hz, Data was processed using Data Analysis 4.2 software.

Acetate buffer pH 5.4: 8.8 mL of 0.2 M solution of AcOH plus 41.2 mL of 0.2 M solution of AcONa, dilute to a total of 100 mL with distilled water

5.2. Synthetic procedures[a]

5.2.1. General procedure for the preparation of 4 or 5-substituted-2-methyl-benzimidazoles

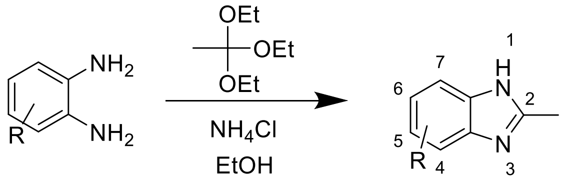

1 - R = 5-Fluor
2 - R = 5-Tercbutoxi
3 - R = 4-Me

Following the literature procedure[54].To a solution of 3 or 4-substituted-1,2-diamine (2 mmol scale) in EtOH (0.53 M) was added ammonium chloride (15 mol%) and triethyl orthoacetate (1.05 equiv.). The solution was reflux for three hours. The solvent was removed under reduced pressure and the crude reaction was purified by column chromatography using AcOEt as eluent.

5-fluoro-2-methyl-1H-benzo[d]imidazole

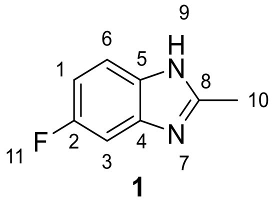

1

Isolated as a beige solid (238 mg, 66% yield, starting from 4-fluorobenzene-1,2-diamine (303 mg, 2.40 mmol)).

M.p. 170-173ºC

^{1}H NMR (300 MHz, Chloroform-*d*) δ (ppm) 7.44 (dd, *J* = 8.8, 4.7 Hz, 1H, H6), 7.21 (dd, *J* = 9.0, 2.5 Hz, 1H, H3), 6.97 (td, *J* = 9.2, 2.4 Hz, 2H, H1), 2.63 (s, 3H, H10).

^{13}C NMR (75 MHz, CDCl$_3$) δ (ppm) 160.91 (C2), 157.76 (C8), 152.36, 152.33 (C1), 135.14 (C4), 131.71 (C5), 114.90 (C6), 110.50, 110.16 (C3), 15.04 (C10).

IR (ATR) ν (cm^{-1}): 3118.49, 3009.20, 2918.84, 2790.17, 2689.94, 1596.34, 1549.70, 1483.93, 1434.72, 1411.52, 1382.23, 1130.02, 1108.37, 952.51, 850.23, 790.98, 775.92, 656.45, 591.29

[a] Atoms numeration according to ChemDraw assignment

5-(*tert*-butyl)-2-methyl-1H-benzo[d]imidazole

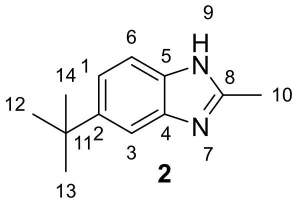

2

Isolated as a black solid (215 mg, 93% yield, starting from 4-(*tert*-butyl)benzene-1,2-diamine (199 mg, 2.30 mmol)).

M.p. 138-140 ºC

^{1}H NMR (300 MHz, Chloroform-*d*) δ (ppm) 7.56 (d, *J* = 1.5 Hz, 1H, H3), 7.49 (d, *J* = 8.5 Hz, 1H, H1), 7.31 (dd, *J* = 8.5, 1.8 Hz, 1H, H6), 2.66 (s, 3H, H10), 1.35 (s, 9H, H12,13,14).

^{13}C NMR (75 MHz, $CDCl_3$) δ (ppm) 150.95 (C8), 145.84 (C2), 137.08 (C4), 135.53 (C5), 120.25 (C1), 113.55 (C3), 110.04 (C6), 34.50 (C11), 31.48 (C12,13,14), 14.14 (C10).

IR (ATR) ν (cm^{-1}): 3063.71, 2950.54, 2904.90, 2861.96, 2800.94, 1461.17, 1403.04, 1357.73, 1284.57, 1018.57, 1018.82, 811.55, 799.74, 674.26, 654.98

2,4-dimethyl-1H-benzo[d]imidazole

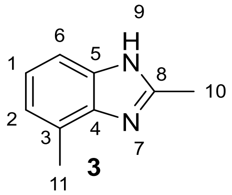

3

Isolated as a brown light solid (123 mg, 51% yield, starting from 3-methylbenzene-1,2-diamine (200 mg, 1.64 mmol)).

M.P. 169-172 ºC

^{1}H NMR (300 MHz, Chloroform-*d*) δ (ppm) 7.38 (d, *J* = 7.9 Hz, 1H, H6), 7.13 (t, *J* = 7.6 Hz, 1H, H1), 7.04 (d, *J* = 7.3 Hz, 1H, H2), 2.63 (s, 3H, H10), 2.57 (s, 3H, H11).

^{13}C NMR (75 MHz, $CDCl_3$) δ (ppm) 151.07 (C8), 138.65 (C5), 137.99 (C4), 124.98 (C3), 122.75 (C1), 122.23 (C2), 111.72 (C6), 17.32 (C11), 14.95 (C10).

IR (ATR) ν (cm^{-1}): 3106.07, 3057.00, 2917.09, 2853.85, 2726.58, 1621.05, 1543.60, 1451.57, 1451.57, 1422.49, 1409.39, 1357.30, 1279.39,1232.41, 1079.47, 1021.23, 784.92, 747.75.

5.2.2. Procedure for the preparation of 1,2-dimethyl-1H-benzo[d]imidazole

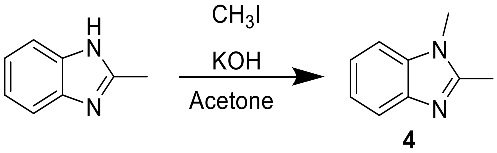

4

Following the literature procedure[48], to a mixture of 2-methyl-benzoimidazole (1 g, 7.57 mmol, 1equiv.) and potassium hydroxide (2.55 g, 6 equiv.) in acetone (30.4 mL, 0.25 M) was added iodomethane (0.660 mL, 10.59 mmol, 1.4 equiv.). The mixture was stirred at room temperature for 30 minutes. Then, was added H_2O (50 mL) and the organic phase was extracted with DCM (3x50 mL), dried with Na_2SO_4, filtered and the solvent was removed under vacuum.

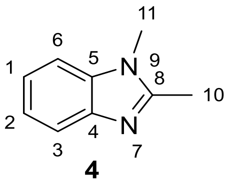

4

Isolated as a white solid (1.07 g, 89% yield).

M.p. 112-115 ºC

^{1}H NMR (300 MHz, DMSO-*d*$_6$) δ (ppm) 7.51 – 7.42 (m, 2H, H3,6), 7.21 – 7.03 (m, 2H, H1,2), 3.70 (s, 1H, H11), 1.13 (s, 3H, H10).

^{1}H NMR (300 MHz, Chloroform-*d*) δ (ppm) 7.78 – 7.58 (m, 1H, H3), 7.21 – 7.03 (m, 1H) 7.37 – 7.11 (m, 3H, H1,2,6), 3.68 (s, 3H, H11), 2.59 (s, 3H, H10).

^{13}C NMR (75 MHz, CDCl$_3$) δ (ppm) 151.83 (C8), 142.47 (C4), 135.78 (C5), 122.00 (C1), 121.83 (C2), 118.92 (C3), 108.89 (C6), 29.81 (C11), 13.76 (C10).

IR (ATR) ν (cm^{-1}): 3221.14, 3057.63, 3027.03, 2945.10, 1512.60, 1480.08, 1447.01, 1427.00, 1401.35, 1329.50, 1286.85, 1240.06, 1125.67, 1002.77, 859.76, 735.24

The analytical data were consistent with literature values.[48]

5.2.3. General procedure for the preparation of 4-(2-(4 or 5-substituted-benzimidazol-2- yl)vinyl)benzaldehyde

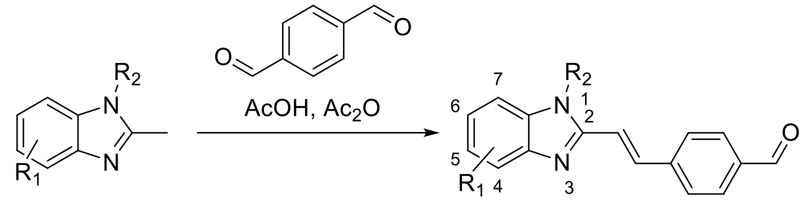

R_1 = H, R_2 = H
1 - R_1 = 5-Fluor, R_2 = H
2 - R_1 = 5-*Terc*-butyl, R_2 = H
3 - R_1 = 4-Me, R_2 = H
4 - R_1 = H, R_2 = Me

5 - R_1 = H, R_2 = H
6 - R_1 = 5-Fluor, R_2 = H
7 - R_1 = 5-*Terc*-butyl, R_2 = H
8 - R_1 = 4-Me, R_2 = H
9 - R_1 = H, R_2 = Me

The compounds were synthesized following the general method described in literature[55]. A mixture of 4,5-substituted-2-methylbenzimidazole (417.27 µmol - 3.78 mmol scale, 1 equiv.), terephtalaldehyde (1 equiv.), acetic anhydride (3.2 equiv.) and acetic acid (2.6 equiv.) was stirred at 120ºC overnight and the cooled to room temperature. Then, HCl was added and the mixture stirred for 1 hour. The mixture was filtered, washed with water. An aqueous solution of NaOH 30% was added to the filtrate until precipitate. This was filtered and washed with water. The crude reaction was purified by column chromatography using as eluent a gradient hexane and ethyl acetate (AcOEt/ Hex (4:1) to AcOEt).

(E)-4-(2-(1H-benzo[d]imidazol-2-yl)vinyl)benzaldehyde

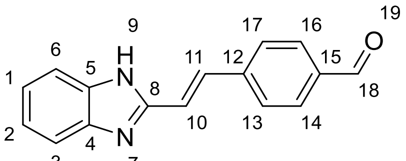

5

Isolated as a yellow solid (0.337 mg, 40% yield, starting from compound **5** (500 mg, 3.78 mmol)). M.p. 195-198 ºC

^{1}H NMR (300 MHz, DMSO) δ (ppm) 10.02 (s, 1H, H18), 7.96 (d, *J* = 8.1 Hz, 2H, H14,16), 7.90 (d, *J* = 8.2 Hz, 2H, H13,17), 7.74 (d, *J* = 16.5 Hz, 1H, H11), 7.57 (t, *J* = 4.5 Hz, 2H, H3,6), 7.42 (d, *J* = 16.6 Hz, 1H, H10), 7.20 (dd, *J* = 6.1, 3.2 Hz, 2H, H1,2).

^{13}C NMR (75 MHz, DMSO) δ (ppm) 192.64 (C18), 150.45 (C8), 143.99 (C4), 141.68 (C12), 135.91 (C15), 134.55 (C5), 132.98 (C11), 130.23 (C14,16), 127.70 (C13,17), 123.05 (C1), 121.98 (C2), 120.98 (C10), 118.97 (C3), 111.37 (C6).

IR (ATR) ѵ (cm^{-1}): 3306.67, 3046.44, 2831.64, 2745.45, 1661.53 (C=O), 1597.13, 1267.01, 1416.67, 1305.67, 1165.47, 805.09, 763.83, 743.82

The analytical data were consistent with literature values.[55]

(E)-4-(2-(5-fluoro-1H-benzo[d]imidazol-2-yl)vinyl)benzaldehyde

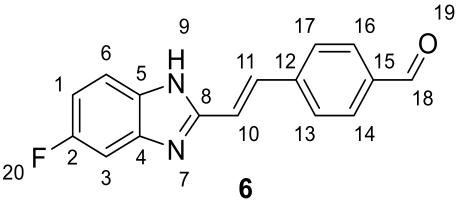

6

Isolated as a yellow solid (217 mg, 59% yield, starting from compound **1** (207 mg, 1.38 mmol). M.p. 217-219 ºC

^{1}H NMR (300 MHz, DMSO-*d*$_6$) δ (ppm) 10.01 (s, 1H, H18), 7.94 (d, *J* = 7.7 Hz, 2H, H14,16), 7.87 (d, *J* = 8.1 Hz, 2H, H13,17), 7.77 (d, *J* = 17.2 Hz, 1H, H6), 7.60 – 7.50 (m, 1H, H11), 7.49 – 7.22 (m, 2H, H1,3), 7.05 (t, *J* = 9.5 Hz, 1H, H10).

^{13}C NMR (75 MHz, DMSO) δ (ppm) 192.67 (C18), 152.04 (C2), 141.66 (C12), 135.94 (C15), 133.29 (C6), 130.23 (C14,16), 127.74 (C13,17), 120.82 (C1), 115.92 (C11), 110.71 (C3), 110.37 (C10).

IR (ATR) ѵ (cm^{-1}): 3354.64, 1693.56 (C=O), 1682. 91, 1599.86, 1567.16, 1567.16, 1438.42, 1218.58, 1138.67, 962.59, 812.66, 607.37

MS (ESI+) m/z calc for $[C_{16}H_{11}N_2O+1]$ 267.0855, found 267.0936 $[M+H]^+$

(E)-4-(2-(5-(*tert*-butyl)-1H-benzo[d]imidazol-2-yl)vinyl)benzaldehyde

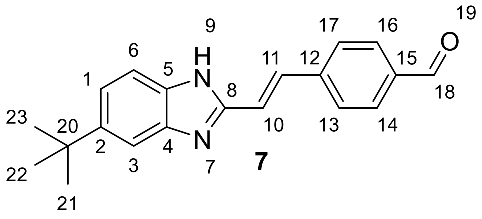

7

Isolated as a brow oil (9.7 mg, 5% yield, starting from compound **2** (124 mg, 658,61µmol))

^{1}H NMR (300 MHz, Acetone-*d*$_6$) δ (ppm) 10.07 (s, 1H, H18), 8.07 (d, *J* = 15.9 Hz, 1H, H11), 8.03 – 7.95 (m, 2H, H14,16), 7.68 – 7.54 (m, 2H, H13,17), 7.47 (dd, J = 8.5, 0.7 Hz, 1H, H3), 7.25 (dd, J = 8.5, 1.8 Hz, 1H, H1), 7.22 – 7.11 (m, 1H, H6), 7.03 (dd, J = 8.6, 0.7 Hz, 1H, H10), 1.33 (s, 9H, H21,22,23).

^{13}C NMR (75 MHz, Acetone) δ ppm 192.49 (C18), 153.12 (C8), 145.63 (C12) 144.19 (C15), 142.20 (C4), 141.22 (C5), 137.69 (C11), 130.66 (C14,16), 128.11 (C13,17), 120.36 (C2), 116.20 (C3), 111.65 (C10), 108.99 (C6), 32.17 (C20), 29.89 (C21,22,23).

IR (ATR) ν (cm^{-1}): 2955.56, 2923.34, 2853.23, 1737.90 (C=O), 1699.48, 1599.83, 1459.83, 1459.01, 1363.20, 1202.49, 1014.75, 808.75

(E)-4-(2-(4-methyl-1H-benzo[d]imidazol-2-yl)vinyl)benzaldehyde

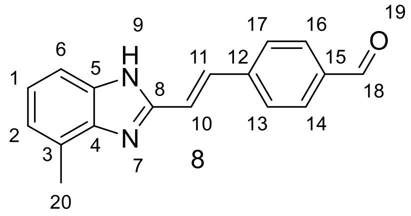

8

Isolated as brown light solid (8 mg, 8% yield, starting from compound **3** (61 mg, 417.27 mmol)). M.p. 89-90ºC

^{1}H NMR (300 MHz, Acetone-*d*$_6$) δ (ppm) 10.04 (s, 1H, H18), 7.95 (d, *J* = 7.9 Hz, 2H, H14,16), 7.85 (d, *J* = 8.1 Hz, 2H, H13,17), 7.78 (d, *J* = 16.6 Hz, 1H, H11), 7.46 (d, *J* = 16.5 Hz, 1H, H6), 7.39 (d, *J* = 8.2 Hz, 1H, H2), 7.11 (t, *J* = 7.6 Hz, 1H, H1), 7.01 (d, *J* = 7.2 Hz, 1H, H10), 2.57 (s, 3H, H20).

^{13}C NMR (75 MHz, Acetone) δ ppm 191.41 (C18), 149.76 (C8), 142.02 (C12), 136.38 (C15), 132.59 (C11), 129.98 (C14,16), 127.45 (C13,17), 122.80 (C1), 122.69 (C2), 120.83 (C10), 119.03 (C3), 117.75 (C6), 16.16 (C20).

IR (ATR) ν (cm^{-1}): 2922.08, 2851.62, 1735.21(C=O), 1684.27, 1598.25, 1557.39, 1375.42, 1207.61, 1166.05, 964.18, 812.12, 780.61, 747.42

MS (ESI+) m/z calc for [$C_{17}H_{14}N_2O$+1] 263.1106, found 263.1179 [M+H]$^+$

***(E)*-4-(2-(1-methyl-1H-benzo[d]imidazol-2-yl)vinyl)benzaldehyde**

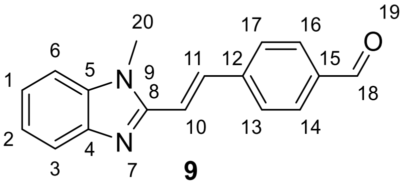

9

Isolated as a dark brown oil (42.5 mg, 12% yield, starting from compound **4** (199.5 mg, 1.37 mmol)).

^{1}H NMR (300 MHz, Acetone-*d*$_6$) δ (ppm) 10.06 (s, 1H, H18), 8.07 – 7.90 (m, 5H, H11,13,14,15,16), 7.70 (d, *J* = 15.7 Hz, 1H, H10), 7.66 – 7.61 (m, 1H, H3), 7.54 – 7.47 (m, 1H, 6), 7.34 – 7.10 (m, 2H, H1,2), 4.02 (s, 3H, H20).

^{13}C NMR (75 MHz, Acetone) δ (ppm) 192.28 (C18), 165.93 (C8) 151.34 (C8), 144.37 (C5), 143.05, 137.31 (C4), 135.34 (C11), 130.76 (C14,16), 128.68 (C13,17), 123.27 (C1), 123.07 (C2), 119.92 (C10), 118.27 (C15), 110.70 (C3,6).

IR (ATR) v (cm^{-1}): 1691.21 (C=O), 1595.64, 1462.23, 1333.88, 1213.01, 1166.33, 970.80, 816.89, 804.30, 747.38

MS (ESI+) m/z calc for [$C_{17}H_{14}N_2O$+1] 263.1106, found 263.1171 [M+H]$^+$

5.2.4. Attempt procedure for the preparation of *(E)*-4-(2-(1H-imidazol-2-yl)vinyl)benzaldehyde

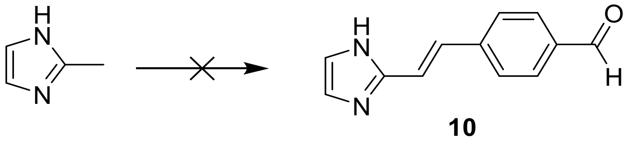

10

Method A

A mixture of 2-methyl-1H-imidazole (200 mg, 2.4 mmol, 1 equiv.), terephtalaldehyde (1 equiv.), acetic anhydride (3.2 equiv.) and acetic acid (2.6 equiv.) was stirred at 120ºC overnight and the cooled to room temperature. Then, HCl was added and the mixture stirred for 1 hour. The mixture was filtered, washed with water. An aqueous solution of NaOH 30% was added to the filtrate until precipitate. This was filtered and washed with water.

Method B

Following a literature procedure[49], a mixture of 2-methyl-1H-imidazole (200 mg, 2.4 mmol, 1.5 equiv.), terephtalaldehyde (1 equiv.), acetic anhydride (0.5 equiv.) was stirred at 140ºC overnight. The mixture was cooled to room temperature and H_2O was added. Then, the mixture was acidified and wash with diethyl ether. The aqueous phase was basified and the compound precipitated, was filtered and dry under vacuum.

5.2.5. General procedure for the preparation of Oxazol-5(4H)-ones

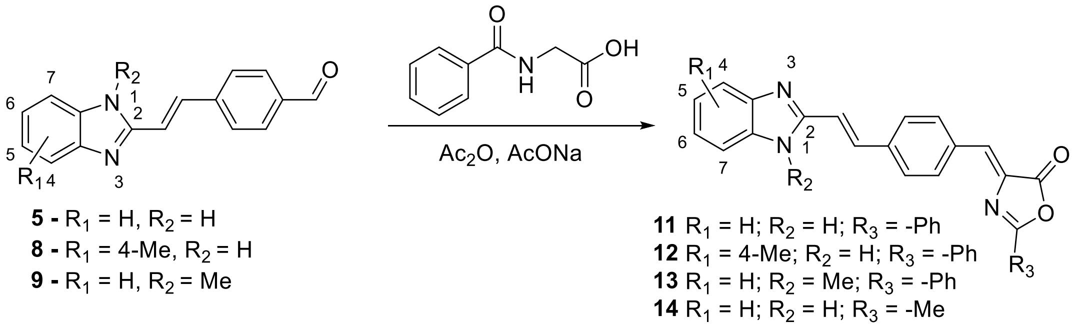

5 - R_1 = H, R_2 = H
8 - R_1 = 4-Me, R_2 = H
9 - R_1 = H, R_2 = Me

11 R_1 = H; R_2 = H; R_3 = -Ph
12 R_1 = 4-Me; R_2 = H; R_3 = -Ph
13 R_1 = H; R_2 = Me; R_3 = -Ph
14 R_1 = H; R_2 = H; R_3 = -Me

The compounds were obtained, based on a synthesis described in literature.[43,44] A mixture of 4-(2-(5,6-substituted-benzimidazol-2-yl)vinyl)benzaldehyde (30 – 600 µmol scale, 1 equiv.) , hippuric acid (1 equiv.), sodium acetate (1 equiv.) and acetic anhydride (3 equiv.) was heated at 110ºC for 2 hours. Then, cooled to room temperature and the solid obtained was washed with distilled water (2x) and MeOH (4x).

4-((Z)-4-((E)-2-(1H-benzo[d]imidazol-2-yl)vinyl)benzylidene)-2-phenyloxazol-5(4H)-one

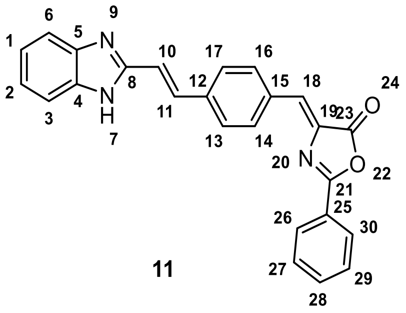

11

Isolated as orange solid (96.9 mg, 40% yield, starting from compound **5** (150 mg, 604.16 µmol))
M.p. 233-237ºC (decomposition).
^{1}H NMR (300 MHz, DMSO-d_6) δ (ppm) 8.38 (d, J = 8.1 Hz, 2H, H26,30), 8.16 (d, J = 7.4 Hz, 2H, H27,29), 7.84 (d, J = 8.1 Hz, 2H, H11,28), 7.79 – 7.62 (m, 4H, H13,14,16,17), 7.57 (dd, J = 6.0, 3.3 Hz, 2H, H3,6), 7.44 – 7.33 (m, 2H, H10,18), 7.21 (dd, J = 6.0, 3.1 Hz, 2H, H1,2).
^{13}C NMR (75 MHz, DMSO) δ (ppm) 207.27 (C23), 166.85 (C21), 163.06 (C8), 138.39 (C4), 136.88 (C4), 133.73 (C11), 133.69 (C15), 133.38 (C12), 133.17 (C18), 132.85 (C14,16), 130.71 (C19), 129.96 (C13,17), 129.37 (C27,29), 128.02 (C28), 127.53 (C25,26,30), 125.12 (C2), 122.33 (C1), 119.67 (C6), 114.18 (C10), 110.20 (C3)
MS (ESI+) m/z calc for [$C_{25}H_{17}N_3O_2$+1]: 392.42, found: 424.3 [M+MeOH]$^+$, 392.2 [M+H]$^+$
The analytical data were identical with literature values.[43,44]

4-(*(E)*-4-(*(E)*-2-(4-methyl-1H-benzo[d]imidazol-2-yl)vinyl)benzylidene)-2-phenyloxazol-5(4H)-one

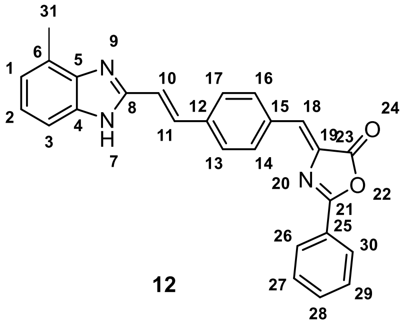
31
6
9
1
5
N
10
17
16
8
12
15
18
24
2
4
N
H
11
19
23
O
3
7
13
14
20
N
O
22
21
25
26
30
27
29
28

12

Isolated as orange solid (3.2 mg, 26% yield, starting from compound **8** (8 mg, 30.5 µmol))

M.p. 138-140ºC

^{1}H NMR (300 MHz, Acetone-*d*$_6$) δ (ppm) 8.41 (d, *J* = 8.3 Hz, 2H, H26,30), 8.26 – 8.19 (m, 2H, H27,29), 7.83 (d, *J* = 8.3 Hz, 1H, H11), 7.79 – 7.59 (m, 6H, H3,13,14,16,17,28), 7.44 (d, *J* = 16.6 Hz, 1H, H1), 7.31 (s, 1H, H18), 7.12 (t, *J* = 7.6 Hz, 1H, H2), 7.04 (t, *J* = 7.7 Hz, 1H, H10), 3.31 (s, 3H, H31).

IR (ATR) ν (cm^{-1}): 3566.68, 3344.26, 2970.09, 2870.35, 2360.23, 2342.33, 1793.84 (C=O,), 1646.79, 1646.79,1558.54, 1542.23, 1375.33, 1324.70, 1296.11, 1162.06, 1107.46, 963.61, 954.04, 857.67, 861.52, 816.52, 776.46, 746.15, 697.56

4-((Z)-4-((E)-2-(1-methyl-1H-benzo[d]imidazol-2-yl)vinyl)benzylidene)-2-phenyloxazol-5(4H)-one

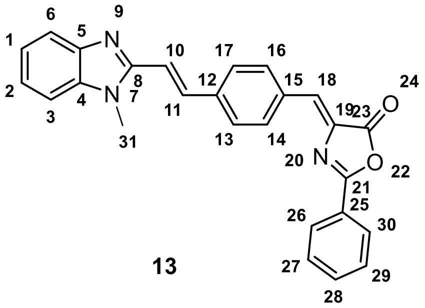
6
9
1
5
N
10
17
16
8
12
15
18
24
2
4
N
7
11
19
23
O
3
31
13
14
20
N
O
22
21
25
26
30
27
29
28

13

Isolated as dark orange solid (5 mg, 10% yield, started from compound **9** (32 mg, 121.62 µmol))

M.p. 156-159ºC (decomposition).

^{1}H NMR (300 MHz, Acetone-*d*$_6$) δ (ppm) 8.43 (d, *J* = 8.2 Hz, 2H, H26,30), 8.22 (d, *J* = 8.8 Hz, 2H, H27,29), 8.04 – 7.45 (m, 10H, H3,6,10,11,13,14,16,17,18,28), 7.29 – 7.19 (m, 2H, H1,2), 4.03 (s, 3H, H31).

IR (ATR) ν (cm^{-1}): 1791.42 (C=O), 1650.83, 1602.49, 1326.18, 1241.02, 1160.93, 1071.18, 980.20, 695.64

4-(*(E)*-4-(*(E)*-2-(1H-benzo[d]imidazol-2-yl)vinyl)benzylidene)-2-methyloxazol-5(4H)-one

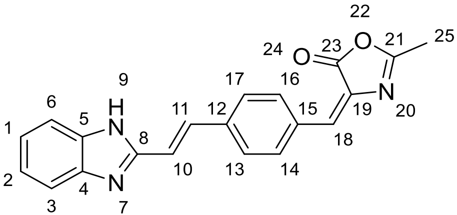

14

Isolated as a light brown (14.3 mg, 22% yield, starting from compound **5** (50 mg, 190.62 µmol)

M.p.: 163-168 °C

^{1}H NMR (300 MHz, Acetone-*d*$_6$) δ (ppm) 8.23 (d, J = 8.2 Hz, 2H, H14,16), 7.83 (d, J = 3.6 Hz, 1H, H11), 7.78 (d, J = 8.4 Hz, 2H, H13,17), 7.74 – 7.68 (m, 1H, H18), 7.61 – 7.47 (m, 2H, H3,6), 7.43 – 7.35 (m, 1H, H10), 7.26 – 7.13 (m, 2H, H1,2), 2.40 (s, 3H, H25).

^{13}C NMR (75 MHz, DMSO) δ (ppm) 167.48 (C23), 166.94 (C21), 150.70 (C8), 139.72 (C5), 133.48 (C4), 132.79, 132.64 (C14,16), 130.46, 129.13, 127.56 (C13,17), 122.48 (C1,2), 119.67, 15.53 (C25

IR (ATR) ν (cm^{-1}): 3415.50, 3197.20, 1641.58 (C=O), 1630.62, 1597.89, 1379.80, 1221.72, 970.86, 815.45, 746.34

MS (ESI+) m/z calc for [$C_{20}H_{15}N_3O_2$+1] 330.1164, found 330.1236 $[M+H]^+$

5.2.6. Procedure for the preparation of *(E)*-(4-(2-(1H-benzo[d]imidazol-2-yl)vinyl)phenyl)methanol

Method A

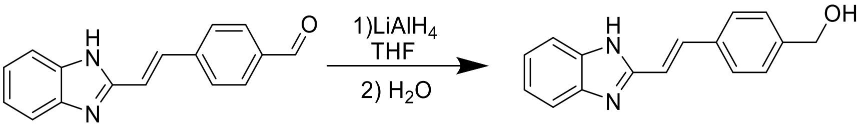

15

To a solution of the *(E)*-4-(2-(1H-benzo[d]imidazol-2-yl)vinyl)benzaldehyde (200 mg, 805 µmol, 1 equiv.) in THF anhydrous (8.1 mL, 0.1 M) was added $LiAlH_4$ (30.57 mg, 1 equiv.) in ice bath and inert atmosphere. The mixture was stirred at room temperature for 1hour. Then, after the consumption of the starting material by TLC, was added H_2O (60 µL, 4 equiv.) and was left under stirring for 20 minutes. The solution was filtered and washed with THF. The solvent was evaporated under vacuum.

Method B

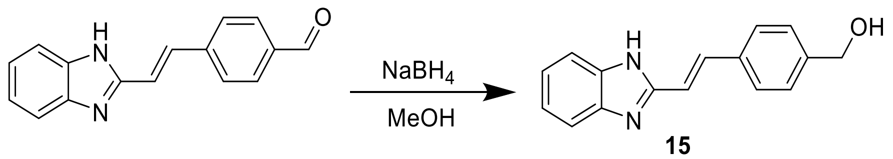

15

To a solution of E)-4-(2-(1H-benzo[d]imidazol-2-yl)vinyl)benzaldehyde (50 mg, 201.39 µmol, 1 equiv.) in methanol (2.1 mL, 0.1 M) was added NaBH$_4$ (15 mg, 2 equiv.) in ice bath. The reaction was monitoring by TLC and when the starting material was consumed, water (30 µL, 8 equiv.) was added. Then, the methanol was evaporated and the organic was extracted with DCM, dried with Na$_2$SO$_4$, filtered and the solvent was removed under vacuum.

(E)-(4-(2-(1H-benzo[d]imidazol-2-yl)vinyl)phenyl)methanol

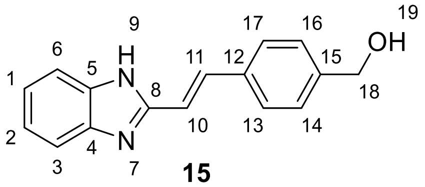

15

Isolated as orange solid (194 mg, 96% yield, starting from compound **5** (200 mg, 805 µmol)).

M.p.: 241-243 ºC

^{1}H NMR (300 MHz, DMSO-d_6) δ (ppm) 7.70 (d, J = 14.0 Hz, 1H, H11), 7.66 – 7.59 (m, 2H, H14,16), 7.53 (dd, J = 6.0, 3.2 Hz, 2H, H3,6), 7.38 (d, J = 7.9 Hz, 2H, H13,17), 7.24 (d, J = 12.8 Hz, 1H, H10), 7.17 (dd, J = 6.2, 3.0 Hz, 2H, H1,2), 4.53 (s, 2H, H18).

^{13}C NMR (75 MHz, DMSO) δ (ppm) 151.20 (C8), 143.55 (C4,5), 134.34 (C11,12), 134.31 (C15), 127.04 (C14,16), 126.92 (C13,17), 122.10 (C1,2), 121.14 (C3), 117.17 (C10), 114.94 (C6), 62.71 (C18).

IR (ATR) ν (cm^{-1}): 175.07, 3066.02, 3017.73, 2939.31, 2922.41, 2862.01, 2807.99, 1519.56, 1426.92, 1276.28, 1208.47, 1004.45, 966.42, 826.22, 788.12, 734.03

MS (ESI+) m/z calc for [$C_{16}H_{14}N_2O$+1] 251.1106, found 251.1173 [M+H]$^+$

5.2.7. General procedure for the preparation of hydrazones and oximes

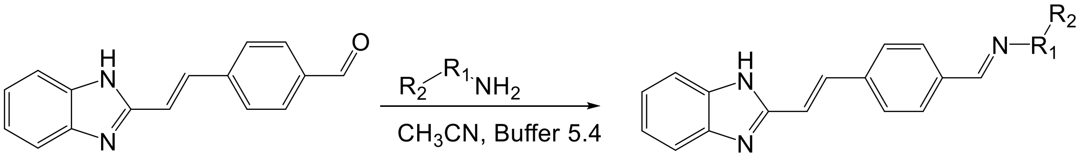

16 R_1= N; R_2= Bz
17 R_1= N; R_2= Ph
18 R_1= O; R_2= Bz

To a solution of *(E)*-4-(2-(1H-benzo[d]imidazol-2-yl)vinyl)benzaldehyde (100.69 µmol scale, 1 equiv.) in acetonitrile (0.1 M) was added hydrazine (1.3 equiv.) followed by buffer of pH 5.4 (0.1

M). The mixture was stirred at room temperature overnight. Then, the precipitate was formed and filtered by collecting the crystals.

2-((E)-4-((E)-(2-benzylhydrazineylidene)methyl)styryl)-1H-benzo[d]imidazole

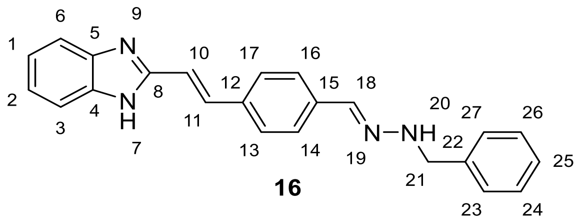

16

Isolated as yellow solid (24.8 mg, 70% yield, starting from compound **5** (25 mg, 100.69 µmol)

M.p. 293-294ºC

^{1}H NMR (300 MHz, DMSO-*d_6*) δ (ppm) 8.30 (s, 1H, H18), 8.06 (d, *J* = 16.5 Hz, 1H, H11), 7.81 – 7.74 (m, 2H, H3,6), 7.68 (d, *J* = 8.2 Hz, 2H, H14,16), 7.58 (d, *J* = 9.6 Hz, 2H, H13,17), 7.57 – 7.46 (m, 2H, H23,27), 7.39 – 7.31 (m, 3H, H24,25,26), 7.30 – 7.13 (m, 3H, 1,2,10), 4.40 (s, 2H, H21).

^{13}C NMR (75 MHz, DMSO) δ (ppm) 139.88, 139.17, 137.23, 132.79, 131.96, 129.08, 128.83, 128.36, 126.35, 126.03, 114.14, 114.13, 112.34, 109.15.

IR (ATR) ν (cm^{-1}): 3326.62, 2735.10, 2604.27, 1642.37, 1624.77, 1566.00, 1459.72, 1299.78, 1213.06, 976.88, 818.25, 751.22

2-(*(E)*-4-(*(E)*-(2-phenylhydrazineylidene)methyl)styryl)-1H-benzo[d]imidazole

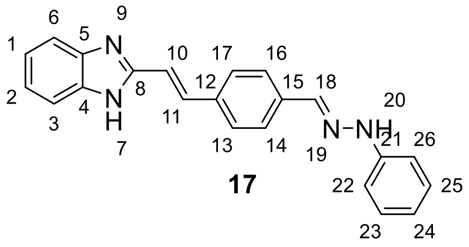

17

Isolated as orange solid (13.6 mg, 40% yield, starting from compound 5 (25 mg, 100.69 µmol)

M.p.: 217-220 ºC

^{1}H NMR (300 MHz, DMSO-*d_6*) δ (ppm) 7.88 (s, 1H, H18), 7.69 (s, 5H, H3,13,14,16,17), 7.58 – 7.48 (m, 2H, H6,11), 7.34 – 7.14 (m, 5H, H22,23,24,25,26), 7.10 (d, *J* = 8.0 Hz, 2H, H1,2), 6.77 (t, *J* = 7.3 Hz, 1H, H10).

^{13}C NMR (75 MHz, DMSO) δ (ppm) 150.98 (C8), 145.09 (C18), 136.30 (C4), 135.84 (C21), 135.19 (C5), 133.91 (C12), 132.26 (C15), 131.63 (C11), 129.14 (C23,25), 127.38 (C14,16), 126.06 (C13,17), 122.07 (C24), 118.97 (C3), 117.36 (C10), 112.10 (C22,26), 99.03 (C6).

IR (ATR) ν (cm^{-1}): 2964.68, 2918.85, 2853.52, 1599.29, 1257.84, 1209.47, 1101.21, 1015.68, 967.53, 803.84, 740.63, 690.88

***(E)*-4-(*(E)*-2-(1H-benzo[d]imidazol-2-yl)vinyl)benzaldehyde O-benzyl oxime**

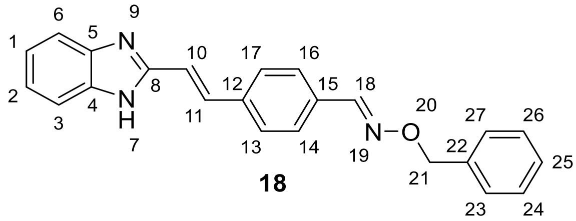

18

Isolated as dark yellow solid (25.5 mg, 72% yield, starting from compound **5** (25 mg, 100.69 µmol).

M.p.: 188-190 ºC

^{1}H NMR (300 MHz, DMSO-d_6) δ (ppm) 8.33 (s, 1H, H18), 7.69 (d, *J* = 7.2 Hz, 4H, H13,14,16,17), 7.55 (dd, *J* = 6.0, 3.3 Hz, 2H, H3,6), 7.50 – 7.31 (m, 5H, H23,24,25,26,27), 7.27 (d, *J* = 16.5 Hz, 1H, H10), 7.19 (dd, *J* = 6.1, 3.0 Hz, 2H, H1,2), 5.19 (s, 2H, H21).

^{13}C NMR (75 MHz, DMSO) δ (ppm) 150.70 (C8), 148.82 (C18), 137.57 (C22), 137.30, 133.46 (C11), 132.05, 128.35 (C24,26), 128.26 (C23,27), 127.85 (C25), 127.42 (C13,17), 127.41 (C14,16), 122.18 (C1,2), 118.66 (C10), 75.58 (C21).

IR (ATR) ν (cm^{-1}): 3061.42, 3026.76, 2981.18, 1429.50, 1411.93, 1206.65, 1010.41, 981.92, 967.64, 950,66, 915.78, 816.00, 733.72, 694.42

5.2.8. General procedure for catalytic hydrogenation attempts

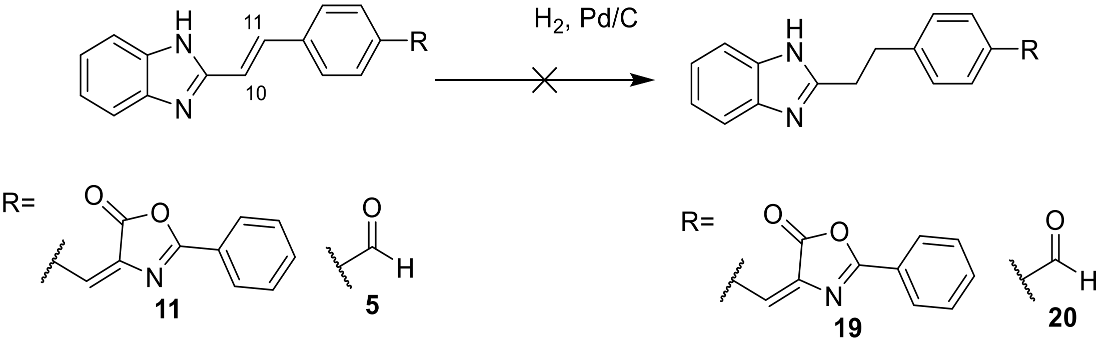

11 **5** **19** **20**

Method A

Pd/C (10 %, 2.5 mg)) was added to a solution of compound **11** or **5** in methanol (0.1 M). The reaction was purged with nitrogen and then filled with hydrogen balloon and the mixture was vigorous stirred overnight. The balloon was removed, the reaction mixture was filled with nitrogen, the catalyst was removed by filtration and solvent was evaporated.

The compounds desired was not obtained after hydrogenation. In the case of compound **11** was degraded, already in the case of the hydrogenation using compound **5** as starting material, no reaction occurred, verified the presence only starting material.

Method B

Pd/C (10 %, 2.5 mg) was added to a solution of compound **11** or **5** in methanol (0.1 M) inside a steal reactor. The reactor was filled with nitrogen 3 times, then purged with hydrogen, filled with hydrogen (9.87 atm) and the mixture was vigorous stirred overnight. The reactor was purged with nitrogen, the catalyst was removed by filtration and solvent was evaporated.

Hydrogenation of compound **11** or **5** did not occur, having verified the occurrence in method A.

5.2.9. Preparation of hippuric acid derivates

5.2.9.1. *N*-acetylglycine[50]

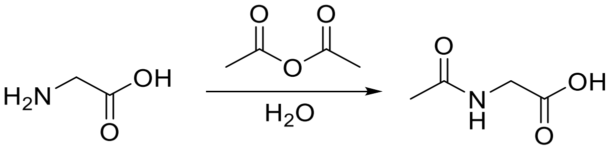

21

Glycine (303 mg, 4.0 mmol, 1 equiv.) was added to water. The mixture was stirred vigorously until glycine dissolved completely. Then, acetic anhydride (755.54 µmL, 2 equiv.) was added and vigorous stirring was continued for 30 minutes. The solution was kept overnight in a refrigerator to complete crystallization. The solid was collected by filtration and dried in vacuum.[56]

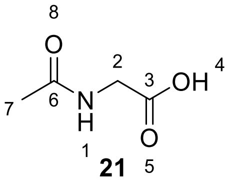

21

Isolated as white solid (199.9 mg, 49% yield)

M.p.: 200-206ºC

^{1}H NMR (300 MHz, Deuterium Oxide) δ (ppm) 3.90 (s, 2H, H2), 1.97 (s, 3H, H7).

^{13}C NMR (75 MHz, D_2O) δ (ppm) 174.64 (C3), 173.47(C6), 41.01 (C2), 21.46 (C7).

IR (ATR) ν (cm^{-1}): 3349.85 (N-H), 1717.20 (C=O), 1582.10 (C=O), 1541.54, 1438.72, 1379.62, 1351.63, 1275.51, 1231.26, 1033.12, 993.86, 684.53, 626.06, 599.56

The analytical data consistent with literature values.[50,57]

5.2.9.2. General procedure for the preparation hippuric acid derivates

Method 1

a)

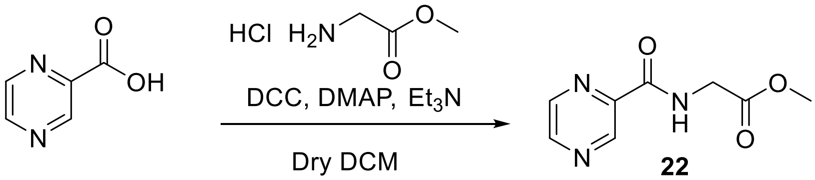

22

To a mixture of pyrazine-2-carboxylic acid (0.101 mg, 806 µmol, 1 equiv.) under inert atmosphere and in dried DCM (2.3 mL, 0.1 M) was added DCC (190 mg, 886.39 µmol 1.2 equiv.) and DMAP (19.69 mg, 161 µmol, 0.15 equiv.). The mixture was stirred overnight. Then, was added glycine methyl ester hydrochloride (111.3 mg, 886.39 µmol, 1.1 equiv.) and triethylamine (123.55 µL, 3 equiv.), monitoring the reaction by TLC. The solvent was evaporated and the crude was purified through chromatographic column using AcOEt:Hex (1:1) as eluent.

Methyl (pyrazine-2-carbonyl)glycinate

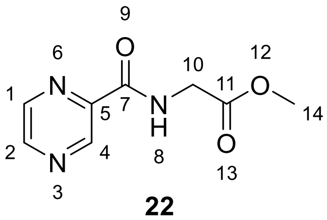

22

Isolated as yellow solid in (86.2 mg, 55% yield)

M.p.: 107-109ºC

^{1}H NMR (300 MHz, Chloroform-*d*) δ (ppm) 9.38 (d, *J* = 1.5 Hz, 1H, H4), 8.76 (d, *J* = 2.4 Hz, 1H, H1), 8.55 (dd, *J* = 2.5, 1.5 Hz, 1H, H2), 8.25 (s, 1H, H8), 4.27 (d, *J* = 5.6 Hz, 2H, H10), 3.79 (s, 3H, H14).

^{13}C NMR (75 MHz, CDCl$_3$) δ (ppm) 169.92 (C11), 163.32 (C7), 147.61 (C1), 144.40 (C4), 143.92 (C2), 52.55 (C10), 41.17 (C14).

IR (ATR) ν (cm^{-1}): 3317.73 (N-H), 2955.18, 2921.58, 2851.78, 1738.23 (C=O), 1658.65 (C=O), 1526.54, 1443.21, 1371.51, 1219.24, 1160.09, 1046.93, 1025.14, 973.81, 866.36, 774.81, 7707.12, 625.01, 579.52

The analytical data were consistent with literature values.[58]

b)

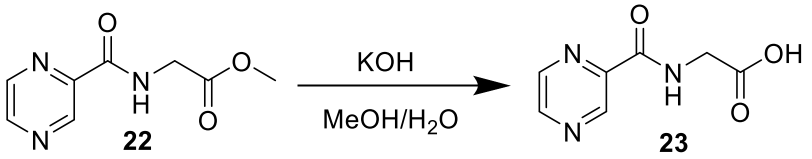

To a solution of KOH (130 mg, 2.31 µmol , 3 equiv.) in water (1.15 mL, 2 M) was added dropwise to a solution of methyl (pyrazine-2-carbonyl)glycinate (142 mg, 768.53 µmol, 1 equiv.) in methanol (2.33 mL, 0.33 M). The mixture was reflux for 3h, monitored by performing TLC. After cooling down to the room temperature, HCl 1M was slowly added until solid precipitate. The solid was filtrate and dried under vacuum.

(Pyrazine-2-carbonyl)glycine

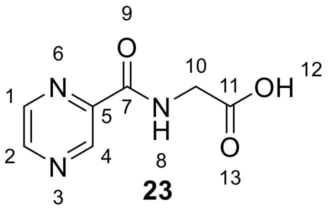

23

Isolated as a white solid (91.3 mg, 69% yield).

M.p.: 224-226ºC (decomposition)

^{1}H NMR (300 MHz, Deuterium Oxide) δ (ppm) 9.13 (d, *J* = 1.4 Hz, 1H, H4), 8.76 (d, *J* = 2.5 Hz, 1H, H1), 8.71 (dd, *J* = 2.6, 1.4 Hz, 1H, H2), 4.20 (s, 2H, H10).

^{13}C NMR (75 MHz, D$_2$O) δ (ppm)173.28 (C11), 165.74 (C7), 147.23 (C2), 147.18 (C5), 144.19 (C4), 142.87 (C1), 41.18 (C10).

IR (ATR) ν (cm^{-1}): 3348.88, 3074.68, 2928.57, 2360.13, 2340.21, 1722.50 (C=O), 1657.24 (C=O), 1588.58, 1530.28, 1391.22, 1356.64, 1236.37, 1163.38, 1151.30, 1050.89, 1019.77, 876.06, 780.86, 647.34

The analytical data were consistent with literature values.[58]

Method 2

a) Formation of acid chloride with oxalyl chloride

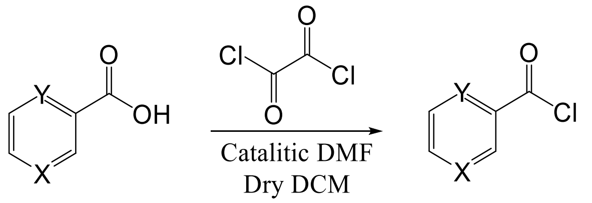

24 X = N, Y = H
25 X = Y = N

Oxalyl chloride (1.2 equiv.) was dropwise added to a solution of carboxylic acid (1.6 mmol scale, 1 equiv.) and 3 drops of DMF in DCM (0.3 M). The mixture was stirred in room temperature for 2 hours. Then, the mixture was used in the next reaction without any work-up.

b) Reaction with glycine with compound 24

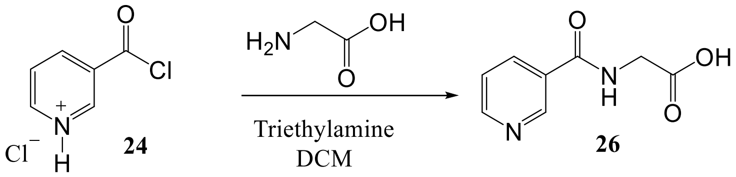

Glycine (1.5 equiv.) and triethylamine (3.5 equiv.) was added to the mixture of acid chloride synthesized with oxalyl chloride and the mixture was stirred at room temperature. The solvent was evaporated under vacuum, obtained the desired compound containing triethylamine.

Nicotinoylglycine

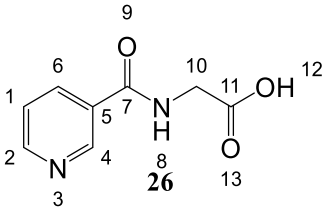

26

Isolated as a white solid (6.2 mg, 22% yield, starting from nicotinic acid (25 mg, 203.07 mmol)

M.P. 259-261 ºC

^{1}H NMR (300 MHz, Deuterium Oxide) δ (ppm) 9.14 (s, 1H, H4), 9.05 – 8.79 (m, 2H, H2,6), 8.07 (dd, *J* = 8.1, 5.8 Hz, 1H, H1), 3.60 (s, 3H, H10).

^{13}C NMR (75 MHz, D$_2$O) δ (ppm) 172.37 (C11), 168.90 (C7), 145.19 (C2), 143.75 (C4), 143.15 (C6), 135.46 (C5), 126.73 (C1), 41.48 (C10)

c) **Reaction with glycine methyl ester with compound 25**

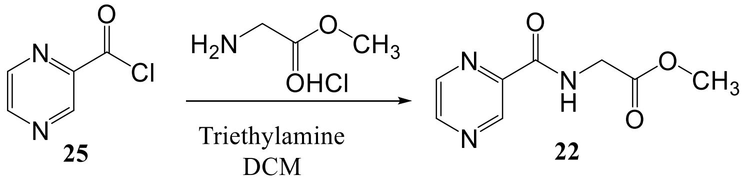

Glycine methyl ester hydrochloride (1.5 equiv.) and triethylamine (3.5 equiv.) was added to the solution of compound **25** (prepared with oxalyl chloride) in atmosphere of argon and the mixture was stirred at room temperature. The solvent was evaporated and the crude was purified through chromatographic column using AcOEt:Hex (1:1) as eluent, obtaining the desired compound.

Method 3

a) **Formation of acid chloride with thionyl chloride**

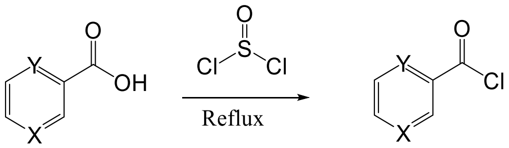

24 X = N, Y = H
25 X = Y = N

Thionyl chloride (15 equiv.) was added to carboxylic acid (1 equiv.) in argon atmosphere. The mixture was reflux overnight. Then, the solvent was removed to under reduce pressure and the crude was used in the next reaction without any purification.

a) **Attempted reaction of glycine with compound 24**

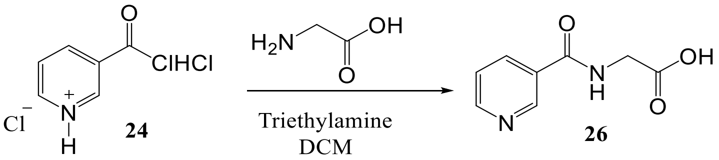

To the mixture from the previous step was added dropwise a solution containing glycine (1.5 equiv.) and triethylamine (3.5 equiv.) in dry DCM (0.1 M). The mixture was stirred at room temperature. The solvent was evaporated under vacuum. However, the desired compound was not obtained.

b) Reaction with glycine methyl ester with compound 25

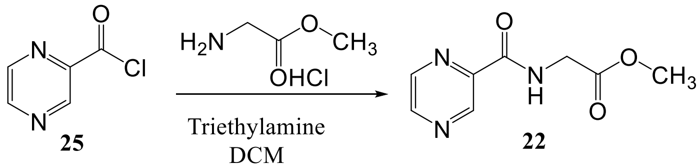

In atmosphere of argon, to a mixture of pyrazine-2-carbonyl chloride (1 equiv.) in dry DCM (0.1 M) was dropwise added to solution of methyl glycinate (2 equiv.) and triethylamine (3.5 equiv.) in DCM (0.1 M). The mixture was stirred for 3 hours. Then, the solvent was evaporated and the crude was purified through chromatographic column using ethyl acetate: hexane (1:1) as eluent.

5.3. Metabolic Stability Assays

A stock solution in the range of 10^{-3} M was prepared by dissolving the **OXA 12** in ACN (compound not fully solubilized).

5.3.1. UV spectra

In a thermostated UV (37 °C) and using a quartz cuvette of 3 mL of solvent (methanol, acetonitrile and phosphate buffer), 20 µL of stock solution (concentration in the 10^{-5} M range) was injected. Then, the absorption of the compound was read between 200-500 nm. The maximum absorption of **OXA 12** was identified (λ_{max}= 414 nm).

5.3.2. Method for detecting OXA 12

The **OXA 12** detection method was created using a HPLC Elite LaChrom (VWR Hitachi) system comprised of an L-2130 pump, an L-2400 UV detector and a Rheodyne® manual sample injector with a 20 µL sample loop. Chromatography separation was achieved on a LichroCART® 125-4-Lichrospher® 100 RP-18 (5 µm) using as mobile phase, flow rate 1.0 mL/min of a mixture H_2O/MeOH. UV detector was set at 400 nm, after identification of the UV maximum absorption by UV spectroscopy.

Gradient Mode

This run was performed in order to obtain information on the suitable mobile phase for the detection of compound and lasted for 30 minutes. The mobile phase used was a mixture of H_2O/MeOH (8:2 to 0.5:9.5). The compound was detected with a R_T = 26 min

Isocratic Mode

Using the same equipment and column, a run in isocratic mode was performed using the H_2O/MeOH (0.5:9.5) mixture as mobile phase, at a flow rate of 1 mL/min^{-1}. The compound was detected with R_T= 1.82 min.

Repeated run using as the mobile phase the H_2O/MeOH (1:9) mixture, since the compound was detected with a very small R_T and can be influenced by the solvent. In this run the compound was detected with a R_T = 2.42, slightly larger, and this method can be used for detection of **OXA 12**

All runs performed above were repeated under the same conditions to confirm the results obtained.

5.3.3. Metabolic Stability Assays

5.3.3.1. PBS and 20% Acetonitrile

Preparation of solution:

To a solution containing 2940 µL of PBS and 60 µL of acetonitrile was added 30 µL of the stock solution of **OXA 12** and the solution which was maintained at 37 ° C

Stability assay:

Using the method created for the detection of **OXA 12**, a run was performed shortly after the introduction of the **OXA 12** stock solution into the PBS to obtain the starting spectrum. For each run, 20 µL were withdrawn from the solution and injected into the HPLC to quantify the amount of remaining compound. From there several spectra were made along 26 h to verify the decrease of the area of the peak, but this did not occur as shown in the discussion.

The assay should be repeated three times to confirm the results obtained, however due to poor solubility of the compound and to the results obtained in the first assay, no repetitions were performed.

5.3.3.2. Human plasma

Preparation of solution:

To a tube containing 2 mL human plasma and 0.5 mL of PBS (pH= 7.4) was added 30 µL of **OXA 12** stock solution (10^{-2} M). The solution which was maintained at 37 °C

Stability assay:

200 µL aliquots were removed over time which were then diluted into eppendorfs containing 400 µL of ACN to precipitate the plasma proteins. The sample is immediately vortexed and centrifuged at 10,000 rpm. For each injection, 20 µL of supernatant were removed which were analyzed by HPLC, quantifying the amount of compound remaining over time. There were runs for 26h to check the behavior of the compound.

The assay should have been repeated three times, however with the results obtained, no repetition was required.

5.4. Biological assays

The biological assays were realized in the laboratory of the Cellular Function and Therapeutic Targeting research group, at the iMed.ULisboa, Faculty of Pharmacy, Universidade de Lisboa by Ph student, Sara Oliveira accordingly to a reported method.[59]

5.4.1. Cell culture and reagents

BV2 murine microglia cells (kindly provided by Elsa Rodrigues, University of Lisbon) were cultured in RPMI 1640 medium (GIBCO® Life Technologies, Inc. Grand Island, USA), supplemented with 10% heat inactivated fetal bovine serum (FBS), 1% antibiotic/antimycotic solution and 1% GlutaMAXTM 363 (GIBCO). Throughout experiments, the culture media was replaced by RPMI supplemented with 1% antibiotic/antimycotic solution, 1% insulin-transferrin-selenium (RPMI/ITS) and 1 mg/mL bovine serum albumin (BSA; GIBCO). The L929 murine fibrosarcoma cell line (kindly provided by Junying Yuan, Harvard Medical School) was cultured in DMEM (GIBCO) supplemented with 10% FBS and 1% GlutaMAXTM. Cells were maintained at 37°C in a humidified atmosphere of 5% CO2. Other chemicals used were as follows: LPS from Escherichia coli 055:B5 (#437625; Calbiochem, San Diego, CA, USA), Nec-1 (Sigma-Aldrich, St. Louis, MO, USA), dimethyl sulfoxide (DMSO; Sigma-Aldrich), Z-Val-Ala-Asp fluoromethylketone (zVAD-fmk) pan caspase inhibitor (Enzo Life Sciences, Farmingdale, NY, USA), and recombinant murine TNF-α (PeproTech EC Ltd., London, UK). A small in-house library of potential inhibitors of necroptosis was tested, including **OXA 12** ((Z)-4-(4-(*(E)*-2-(1H-benzo[d]imidazol-2-yl)vinyl) benzylidene)-2-phenyloxazol-5(4H)-one) that was synthetized accordingly to a reported method.[43,44]

5.4.2. Viability assay

BV2 cells were plated in 96-well plates at $5x10^3$ cells/well. Twenty-four hours after cell plating, media was replaced by fresh RPMI/ITS containing 100 ng/mL LPS, or no addition, and cell were incubated for additional 24 h. Then, BV2 cells were exposed to 25 µM zVAD-fmk for additional 24 h. Nec-1 (30 µM) was added 1 h before zVAD-fmk. Cellular metabolic activity was measured using the CellTiter 96® Aqueous Non384 Radioactive Cell Proliferation (MTS) Assay (Promega, Madison, WI, USA). Changes in absorbance were measured at 490 nm using GloMax® Multi Detection System 386 (Sunnyvale, CA, USA).

5.4.3. General cell death assays

Cell membrane integrity was evaluated using the lactate dehydrogenase (LDH) Cytotoxicity KitPLUS (Roche Diagnostics GmbH, Mannheim, Germany). Briefly, 50 µL of cell supernatants were incubated with 50 µL of assay substrate for 10–30 minutes, at room temperature, protected from light. Absorbance readings were measured at 490 nm, with 620 nm reference wavelengths using a Bio-Rad Model 680 microplate reader. Further, cell death was also determined using the ToxiLight^{TM} BioAssay Kit (Lonza 395 Walkersville Inc., Walkersville, MD, USA), according to the manufacturer's instructions. The release of adenylate kinase enzyme from damaged cells was determined using 10 µL each of cell supernatants and bioluminescent cytolysis assay in the microplate reader.

5.4.4. Drug screening

Drug screening was performed using BV2 and L929 cell lines. BV2 cells were seeded in 96-well plates at $7x10^3$ cells/well; necroptosis was induced using 25 µM zVAD-fmk and compounds were incubated at a final concentration of 30 µM. Cell viability and death were assessed 24 h later by MTS and LDH assays. For the L929 cell line, cells were seeded in 384-well plates at $1x10^3$ cells/well, necroptosis was induced using 30 µM TNF-α, and compounds were incubated at a final concentration of 30 µM. Cell death was assessed 8 h later using the ToxiLight™ BioAssay Kit (Lonza Walkersville Inc., 408 Walkersville, MD, USA). All measurements were performed in duplicate. A percentage of control was calculated to normalise for variability across different plates. Half maximum effective concentration (EC50) at inhibiting necroptosis and half maximal inhibitory concentration (IC50) were calculated for the selected hits in both cell lines, using the GraphPad Prism Software version 5.00 (GraphPad Software, Inc., San Diego, CA, USA) with the log (inhibitor) versus response (variable slope) function.

5.4.5. Total and soluble/insoluble protein extraction

For total protein extraction, BV2 cells were plated in 60 mm culture dishes at $4x10^5$ cells/dish, and L929 cells were plated in 6-well plates at $2.5x10^5$ cells/well. Floating and adherent cells were collected directly in nonyl phenoxypolyethoxylethanol (NP-40) lysis buffer (1% NP-40, 20 mM Tris-HCl pH 7.4, 150 mM NaCl, 5 mM EDTA, 10% glycerol, 1 mM dithiothreitol, and 1x Halt Protease and Phosphatase Inhibitor Cocktail EDTA-free (Pierce, Thermo Fisher Scientific, Rockford, IL, USA)), followed by sonication and centrifugation at 3 200 g during 10 minutes at 4°C. Total protein extracts were recovered and stored at -80ºC. Protein concentration was determined by the colorimetric Bradford method (Bio-Rad). BSA (Sigma-Aldrich) was used as standard, and absorbance measurements were performed at 595 nm using the microplate reader (Bio-Rad). To isolate the soluble and detergent-insoluble proteome of BV2 cells, floating and adherent cells were collected in phosphate-buffered saline (PBS)/EDTA, centrifuged at 600 g for 5 minutes at 4°C, and the pellet homogenized in NP-40 lysis buffer. Then, cell lysates were rotated for 30 minutes at 4°C and centrifuged at 16 000 g for 20 minutes at 4°C. Supernatants were recovered and used as the soluble fractions. To remove carryovers, the pellet was washed with NP-40 lysis buffer and 452 centrifuged again at 16 000 g for 10 minutes at 4°C. Urea-sodium dodecyl sulfate (SDS) 22 buffer composed by 8 M urea and 3% SDS in NP-40 lysis buffer was used to resuspend the pellet and followed by sonication. Lysates were then spun at 16 000 g for 20 minutes at 4°C, and the supernatants recovered and used as the detergent-insoluble fractions.

To determine protein concentration, the bicinchoninic acid (BCA) assay (Thermo Fisher Scientific) was used, according to the manufacturer's recommendations.

5.4.6. Immunoblot analysis

Equal amounts of total, insoluble or soluble protein extracts were electrophoretically resolved on 8% SDS-polyacrylamide gels and transferred onto nitrocellulose membranes. Then, transient staining with 0.2% Ponceau S (Merck, Darmstadt, Germany) was used to confirm protein loading and transfer. Following blocking with 5% milk solution in Tris-buffered saline (TBS), blots were incubated overnight at 4°C with primary rabbit polyclonal antibodies reactive to RIP1, RIP3, Akt, p-Akt (Ser473), NF-κB p65 and IκBα (#7881, #135170, #8312, #7985, #372 and #371; Santa Cruz Biotechnology, Santa Cruz, CA, USA), MLKL (#M6697; Sigma Aldrich), p-MLKL (Ser358) and p-NF-κB p65 (Ser536) (#196436, #131109; Abcam, Cambridge, UK), p-p38 (Thr180/Tyr182) (#9211; Cell Signalling, Danvers, MA, USA); and with primary mouse monoclonal antibodies reactive to JNK, p-JNK (Thr183/Tyr185),and p38α/β (#7345, #6254, #7972; Santa Cruz Biotechnology) and p-IκBα (Ser32/36) (#9246; Cell Signalling), and finally with secondary goat anti-mouse or anti-rabbit IgG antibody conjugated with horseradish peroxidase (Bio-Rad Laboratories) diluted 1:5000 in blocking solution for 1 hour at room temperature. Membranes were processed for protein detection using Immobilon TM Western (Merck Millipore, Burlington, MA, USA) or 23 SuperSignal substrate (Pierce, Thermo Fisher Scientific). β-actin (AC-15; Sigma Aldrich) was used as endogenous control. Densitometric analysis was performed with the Image Lab Software version 5.1 Beta (Bio-Rad).

5.4.7. Quantitative RT-PCR

BV2 cells were plated in 12-well plates at 8x10^5 cells/well for real-time RT-PCR analysis. Briefly, total RNA was extracted using TRIzol™ reagent (Invitrogen, Grand Island, USA). RNA was quantified using a Qubit™ 2.0 fluorometer (Invitrogen) and then converted into cDNA using NZY Reverse Transcriptase (NZYTech, Lisbon, Portugal). RT-PCR was performed in an Applied Biosystems 7300 System (Thermo Fisher Scientific). The following primer sequences were used: COX2 gene, 5'- CAGCCAGGCAGCAAATCCTT (forward) and 5'-AGTCCGGGTACAGTCACACT 489 (reverse); IL-6 gene, 5'-GACGATACCACTCCCAACAGACC (forward) and 5'-AAGTGCATCATCGTTGTTCATACA (reverse); NRLP3 gene, 5'-AGAGCCTACAGTTGGGTGAAATG (forward) and 5'-CCACGCCTACCAGGAAATCTC (reverse); and TNF-α gene, 5'-AGGCACTCCCCCAAAAGATG (forward) and 5'-TGAGGGTCTGGGCCATAGAA (reverse). Two independent reactions for each primer set were performed in a total volume of 12.5 µl containing 2x Power SYBR Green PCR master mix (Thermo Fisher Scientific) and 0.3 µM of each primer. The relative amounts of each gene transcript were calculated based on the standard curve normalized to the level of hypoxanthine-guanine phosphoribosyltransferase (HPRT) and expressed as fold-change from control cells.

5.4.8. Enzyme-Linked Immunosorbent Assay (ELISA)

Sandwich ELISA kits (PeproTech) were used to determine TNF-α concentration in culture media. Firstly, the plates were covered with a capture antibody specific for TNF-α overnight at room temperature, followed by removal of the liquid and washing 4x with washing buffer (0.05% Tween-20 in PBS). Then, blocking buffer (1% BSA in PBS) was added for 1 h at room temperature to block non-specific binding, followed by the same cycle of washes. Afterwards, 100 µL of BV2 cell supernatants were added to each well and incubated for 2 h at room temperature, followed by additional four washes. The detection antibody was then added to each well and incubated for 2 h at room temperature, followed by 4 washes as before. Avidin peroxidase was finally incubated during 30 minutes at room temperature, followed by 4 washes as before. Addition of a peroxidase substrate solution then allows the colourless substrate to convert into a soluble blue coloured product. Colour intensity is proportional to the quantity of TNF-α contained in each sandwich structure. Samples were then incubated at room temperature until green colour was visually detectable (± 30 minutes), followed by absorbance reading at 450 nm, with 590 nm reference wavelengths using a Bio-Rad Model 680 microplate reader. TNF-α concentration (pg/mL) was calculated from standard curves.

5.4.9. Image analysis

BV2 and L929 cells morphology was evaluated by phase-contrast microscopy using a Primo Vert microscope and fluorescence images were captured using an Axio ScopeA.1 fluorescent microscope (Carl Zeiss MicroImaging GmbH, Gottingen, Germany). At least 8 images per condition were acquired using an AxioCam 105 Color camera with the Zen lite 2012 (both from Carl Zeiss MicroImaging GmbH). Quantification of p65 NF-κB signal was performed using ImageJ v3.91 software, by selecting a region of interest according to the localization of the nucleus and measurement of fluorescence intensity in the same region.

5.4.10. Statistical analysis

All data are presented as mean ± standard error the mean (SEM) of at least three independent experiments. Comparison between groups was made by one-way analysis of variance (ANOVA) followed by post hoc Bonferroni's test. Analysis and graphical presentation were performed with the GraphPad Prism Software version 5.00. The statistical significances were achieved when $p < 0.05$.

6. Bibliography

(1) Alberts, B.; Johnson, A.; Lewis, J.; Raff, M.; Roberts, K.; Walter, P. *Molecular Biology of the Cell, 4th Edition*; 2002.

(2) Cooper, G. M.; Hausman, R. E. *The Cell: A Molecular Approach 2nd Edition*; 2007.

(3) Scienceset - Eukaryotic Cell Cycle http://www.scienceset.co.uk/portfolio-6.html (accessed Sep 19, 2018).

(4) Pasparakis, M.; Vandenabeele, P. Necroptosis and Its Role in Inflammation. *Nature* **2015**, *517* (7534), 311–320.

(5) Elmore, S. Apoptosis: A Review of Programmed Cell Death. *Toxicol. Pathol.* **2007**, *35* (4), 495–516.

(6) Zheng, W.; Degterev, A.; Hsu, E.; Yuan, J.; Yuan, C. Structure–activity Relationship Study of a Novel Necroptosis Inhibitor, Necrostatin-7. *Bioorg. Med. Chem. Lett.* **2008**, *18* (18), 4932–4935.

(7) Zhou, W.; Yuan, J. Necroptosis in Health and Diseases. *Semin. Cell Dev. Biol.* **2014**, *35*, 14–23.

(8) Sun, L.; Wang, X. A New Kind of Cell Suicide: Mechanisms and Functions of Programmed Necrosis. *Trends Biochem. Sci.* **2014**, *39* (12), 587–593.

(9) Degterev, A.; Huang, Z.; Boyce, M.; Li, Y.; Jagtap, P.; Mizushima, N.; Cuny, G. D.; Mitchison, T. J.; Moskowitz, M. A.; Yuan, J. Chemical Inhibitor of Nonapoptotic Cell Death with Therapeutic Potential for Ischemic Brain Injury. *Nat. Chem. Biol.* **2005**, *1* (2), 112–119.

(10) Jouan-Lanhouet, S.; Riquet, F.; Duprez, L.; Vanden Berghe, T.; Takahashi, N.; Vandenabeele, P. Necroptosis, in Vivo Detection in Experimental Disease Models. *Semin. Cell Dev. Biol.* **2014**, *35*, 2–13.

(11) Wang, Z.; Guo, L.-M.; Zhou, H.-K.; Qu, H.-K.; Wang, S.-C.; Liu, F.-X.; Chen, D.; Huang, J.-F.; Xiong, K. Using Drugs to Target Necroptosis: Dual Roles in Disease Therapy. *Histol. Histopathol.* **2018**, *33* (8), 773–789.

(12) Oerlemans, M. I. F. J.; Liu, J.; Arslan, F.; Ouden, K.; Middelaar, B. J.; Doevendans, P. A.; Sluijter, J. P. G. Inhibition of RIP1-Dependent Necrosis Prevents Adverse Cardiac Remodeling after Myocardial Ischemia–reperfusion in Vivo. *Basic Res. Cardiol.* **2012**, *107* (4), 270.

(13) Xu, X.; Chua, K.-W.; Chua, C. C.; Liu, C.-F.; Hamdy, R. C.; Chua, B. H. L. Synergistic Protective Effects of Humanin and Necrostatin-1 on Hypoxia and Ischemia/Reperfusion Injury. *Brain Res.* **2010**, *1355*, 189–194.

(14) Coornaert, Isabelle1. Coornaert, I. et al. Novel drug discovery strategies for atherosclerosis that target necrosis and necroptosis. Expert Opin. Drug Discov. 13, 477–488 (2018).; Hofmans, S.; Devisscher, L.; Augustyns, K.; Van Der Veken, P.; De Meyer, G. R. Y.; Martinet, W. Novel Drug Discovery Strategies for Atherosclerosis That Target Necrosis and Necroptosis. *Expert Opin. Drug Discov.* **2018**, *13* (6), 477–488.

(15) Günther, C.; Martini, E.; Wittkopf, N.; Amann, K.; Weigmann, B.; Neumann, H.; Waldner, M. J.; Hedrick, S. M.; Tenzer, S.; Neurath, M. F.; et al. Caspase-8 Regulates TNF-α-Induced Epithelial Necroptosis and Terminal Ileitis. *Nature* **2011**, *477* (7364), 335–339.

(16) Najafov, A.; Chen, H.; Yuan, J. Necroptosis and Cancer. *Trends in Cancer* **2017**, *3* (4),

294–301.

(17) Halestrap, A. P. Calcium, Mitochondria and Reperfusion Injury: A Pore Way to Die. *Biochem. Soc. Trans.* **2006**, *34* (2), 232.

(18) You, Z.; Savitz, S. I.; Yang, J.; Degterev, A.; Yuan, J.; Cuny, G. D.; Moskowitz, M. A.; Whalen, M. J. Necrostatin-1 Reduces Histopathology and Improves Functional Outcome after Controlled Cortical Impact in Mice. *J. Cereb. Blood Flow Metab.* **2008**, *28* (9), 1564–1573.

(19) Walker, F. O. Huntington's Disease. *Lancet* **2007**, *369* (9557), 218–228.

(20) Teng, X.; Degterev, A.; Jagtap, P.; Xing, X.; Choi, S.; Denu, R.; Yuan, J.; Cuny, G. D. Structure–activity Relationship Study of Novel Necroptosis Inhibitors. *Bioorg. Med. Chem. Lett.* **2005**, *15* (22), 5039–5044.

(21) Qinli, Z.; Meiqing, L.; Xia, J.; Li, X.; Weili, G.; Xiuliang, J.; Junwei, J.; Hailan, Y.; Ce, Z.; Qiao, N. Necrostatin-1 Inhibits the Degeneration of Neural Cells Induced by Aluminum Exposure. *Restor. Neurol. Neurosci.* **2013**, *31* (5), 543–555.

(22) Mareninova, O. A.; Sung, K.; Hong, P.; Lugea, A.; Pandol, S. J.; Gukovsky, I.; Gukovskaya, A. S. Cell Death in Pancreatitis. *J. Biol. Chem.* **2006**, *281* (6), 3370–3381.

(23) He, S.; Wang, L.; Miao, L.; Wang, T.; Du, F.; Zhao, L.; Wang, X. Receptor Interacting Protein Kinase-3 Determines Cellular Necrotic Response to TNF-α. *Cell* **2009**, *137* (6), 1100–1111.

(24) Linkermann, A.; Brasen, J. Dichotomy between RIP1- and RIP3-Mediated Necroptosis in Tumor Necrosis Factor-α-Induced Shock. *Mol. Med.* **2012**, *18* (4), 1.

(25) Roychowdhury, S.; Chiang, D. J.; Mandal, P.; McMullen, M. R.; Liu, X.; Cohen, J. I.; Pollard, J.; Feldstein, A. E.; Nagy, L. E. Inhibition of Apoptosis Protects Mice from Ethanol-Mediated Acceleration of Early Markers of CCl4-Induced Fibrosis but Not Steatosis or Inflammation. *Alcohol. Clin. Exp. Res.* **2012**, *36* (7), 1139–1147.

(26) Roychowdhury, S.; McMullen, M. R.; Pisano, S. G.; Liu, X.; Nagy, L. E. Absence of Receptor Interacting Protein Kinase 3 Prevents Ethanol-Induced Liver Injury. *Hepatology* **2013**, *57* (5), 1773–1783.

(27) Bonnet, M. C.; Preukschat, D.; Welz, P.; van Loo, G.; Ermolaeva, M. A.; Bloch, W.; Haase, I.; Pasparakis, M. The Adaptor Protein FADD Protects Epidermal Keratinocytes from Necroptosis In Vivo and Prevents Skin Inflammation. *Immunity* **2011**, *35* (4), 572–582.

(28) Kovalenko, A.; Kim, J.; Kang, T.; Rajput, A.; Bogdanov, K.; Dittrich-Breiholz, O.; Kracht, M.; Brenner, O.; Wallach, D. Caspase-8 Deficiency in Epidermal Keratinocytes Triggers an Inflammatory Skin Disease. *J. Exp. Med.* **2009**, *206* (10), 2161–2177.

(29) Wang, Z.; Guo, L.-M.; Zhou, H.-K.; Qu, H.-K.; Wang, S.-C.; Liu, F.-X.; Chen, D.; Huang, J.-F.; Xiong, K. Using Drugs to Target Necroptosis: Dual Roles in Disease Therapy. *Histol. Histopathol.* **2018**, *33* (8), 773–789.

(30) Degterev, A.; Linkermann, A. Generation of Small Molecules to Interfere with Regulated Necrosis. *Cell. Mol. Life Sci.* **2016**, *73* (11–12), 2251–2267.

(31) Najjar, M.; Suebsuwong, C.; Ray, S. S.; Thapa, R. J.; Maki, J. L.; Nogusa, S.; Shah, S.; Saleh, D.; Gough, P. J.; Bertin, J.; et al. Structure Guided Design of Potent and Selective Ponatinib-Based Hybrid Inhibitors for RIPK1. *Cell Rep.* **2015**, *10* (11), 1850–1860.

(32) Harris, P. A.; Bandyopadhyay, D.; Berger, S. B.; Campobasso, N.; Capriotti, C. A.; Cox, J. A.; Dare, L.; Finger, J. N.; Hoffman, S. J.; Kahler, K. M.; et al. Discovery of Small Molecule RIP1 Kinase Inhibitors for the Treatment of Pathologies Associated with Necroptosis. *ACS Med. Chem. Lett.* **2013**, *4* (12), 1238–1243.

(33) Fauster, A.; Rebsamen, M.; Huber, K. V. M.; Bigenzahn, J. W.; Stukalov, A.; Lardeau, C. H.; Scorzoni, S.; Bruckner, M.; Gridling, M.; Parapatics, K.; et al. A Cellular Screen Identifies Ponatinib and Pazopanib as Inhibitors of Necroptosis. *Cell Death Dis.* **2015**, *6* (5), e1767-10.

(34) Mandal, P.; Berger, S. B.; Pillay, S.; Moriwaki, K.; Huang, C.; Guo, H.; Lich, J. D.; Finger, J.; Kasparcova, V.; Votta, B.; et al. RIP3 Induces Apoptosis Independent of Pronecrotic Kinase Activity. *Mol. Cell* **2014**, *56* (4), 481–495.

(35) Rodrigues, C. A. B.; Martinho, J. M. G.; Afonso, C. A. M. Synthesis of a Biologically Active Oxazol-5-(4H)-One via an Erlenmeyer–Plöchl Reaction. *J. Chem. Educ.* **2015**, *92* (9), 1543–1546.

(36) Fisk, J. S.; Mosey, R. A.; Tepe, J. J. The Diverse Chemistry of Oxazol-5-(4H)-Ones. *Chem. Soc. Rev.* **2007**, *36* (9), 1432.

(37) Sharada, L. N.; Aparna, Y.; Saba, M.; Sunitha, S. N. T.; Viveka, L. A Review on Reactions and Applications of Oxazolones. *Int. J. Sci. Res. Publ.* **2014**, *5* (6), 2250–3153.

(38) Zerong Wang. *Erlenmeyer-Plochl Azlactone Synthesis*; JohnWiley & Sons, I., Ed.; 2010, 2010.

(39) Alexandra, C.; Rodrigues, B.; Em, D. Synthesis and Photochemical Characterization of Multiphoton Absorbing Chromophores, 2013.

(40) Chavez, F.; Kennedy, N.; Rawalpally, T.; Williamson, R. T.; Cleary, T. Substituents Effect on the Erlenmeyer-Plöchl Reaction: Understanding an Observed Process Reaction Time. *Org. Process Res. Dev.* **2010**, *14* (3), 579–584.

(41) Ikeda, G. K.; Jang, K.; Mundle, S. O. C.; Dicks, A. P. The Hammett Equation: Probing the Mechanism of Aromatic Semicarbazone Formation. *J. Chem. Educ.* **2006**, *83* (9), 1341.

(42) Blanco-Lomas, M.; Funes-Ardoiz, I.; Campos, P. J.; Sampedro, D. Oxazolone-Based Photoswitches: Synthesis and Properties. *European J. Org. Chem.* **2013**, No. 29, 6611–6618.

(43) Rodrigues, C. A. B.; Mariz, I. F. A.; Maçôas, E. M. S.; Afonso, C. A. M.; Martinho, J. M. G. Unsaturated Oxazolones as Nonlinear Fluorophores. *Dye. Pigment.* **2013**, *99* (3), 642–652.

(44) Rodrigues, C. A. B.; Mariz, I. F. A.; Maçôas, E. M. S.; Afonso, C. A. M.; Martinho, J. M. G. Two-Photon Absorption Properties of Push–pull Oxazolones Derivatives. *Dye. Pigment.* **2012**, *95* (3), 713–722.

(45) Ertekin, K.; Karapire, C.; Alp, S.; Yenigül, B.; Içli, S. Photophysical and Photochemical Characteristics of an Azlactone Dye in Sol-Gel Matrix; a New Fluorescent PH Indicator. *Dye. Pigment.* **2003**, *56* (2), 125–133.

(46) Ozturk, G.; Alp, S.; Ertekin, K. Fluorescence Emission Studies of 4-(2-Furylmethylene)-2-Phenyl-5-Oxazolone Embedded in Polymer Thin Film and Detection of Fe3+ion. *Dye. Pigment.* **2007**, *72* (2), 150–156.

(47) Ozturk, G.; Timur, S.; Alp, S. Optical Determination of Glucose with Glucose Oxidase Immobilized in PVC Together with Fluorescent Oxazol-5-One Derivatives. *Anal. Lett.* **2008**, *41* (4), 608–618.

(48) Gazit, A.; Yee, K.; Uecker, A.; Böhmer, F.-D.; Sjöblom, T.; Östman, A.; Waltenberger, J.; Golomb, G.; Banai, S.; Heinrich, M. C.; et al. Tricyclic Quinoxalines as Potent Kinase Inhibitors of PDGFR Kinase, Flt3 and Kit. *Bioorg. Med. Chem.* **2003**, *11* (9), 2007–2018.

(49) A. Shafiee, N. Rastkary, A. F. Syntheses of 2-(2-Arylrthyl)Imidazoles. *J. Heterocycl. Chem.* **1998**, *35*, 607–609.

(50) Taylor, N. J.; Emer, E.; Preshlock, S.; Schedler, M.; Tredwell, M.; Verhoog, S.; Mercier, J.; Genicot, C.; Gouverneur, V. Derisking the Cu-Mediated 18 F-Fluorination of Heterocyclic Positron Emission Tomography Radioligands. *J. Am. Chem. Soc.* **2017**, *139* (24), 8267–8276.

(51) Clayden, J. P.; Greeves, N.; Warren, S. *Organic Chemistry*; Oxford University Press, 2001.

(52) Wager, T. T.; Hou, X.; Verhoest, P. R.; Villalobos, A. Moving beyond Rules: The Development of a Central Nervous System Multiparameter Optimization (CNS MPO) Approach to Enable Alignment of Druglike Properties. *ACS Chem. Neurosci.* **2010**, *1* (6), 435–449.

(53) Armarego, W. L. F.; Chai, C. L. L. Purification of Organic Chemicals. In *Purification of Laboratory Chemicals*; Elsevier, 2009.

(54) Fortenberry, C.; Nammalwar, B.; Bunce, R. A. Ammonium Chloride-Catalyzed Synthesis of Benzo-Fused Heterocycles from o -Substituted Anilines and Orthoesters. *Org. Prep. Proced. Int.* **2013**, *45* (1), 57–65.

(55) Jędrzejewska, B.; Krawczyk, P.; Pietrzak, M.; Gordel, M.; Matczyszyn, K.; Samoć, M.; Cysewski, P. Styryl Dye Possessing Donor-π-Acceptor Structure – Synthesis, Spectroscopic and Computational Studies. *Dye. Pigment.* **2013**, *99* (3), 673–685.

(56) Holla, B. S.; Malini, K. V.; Sarojini, B. K.; Poojary, B. A Novel Three-Component Synthesis of Triazinothiazolones. *Synth. Commun.* **2005**, *35* (3), 333–340.

(57) Hancker, S.; Kreft, S.; Neumann, H.; Beller, M. Synthesis of N -Lauroyl Sarcosine by Amidocarbonylation: Comparing Homogeneous and Heterogeneous Palladium Catalysts. *Org. Process Res. Dev.* **2017**, *21* (12), 2045–2051.

(58) Kotevar, M.; Polanc, S.; Vereek, B.; Tisler, M. Syntheses of Some N-(Pyrazinecarbonyl) Amino Acids and Peptides. **1988**, *369*, 366–369.

(59) Oliveira, S. R.; Dionísio, P. A.; Brito, H.; Franco, L.; Rodrigues, C. A. B.; Guedes, R. C.; Afonso, C. A. M.; Amaral, J. D.; Rodrigues, C. M. P. Phenotypic Screening Identifies a New Oxazolone Inhibitor of Necroptosis and Neuroinflammation. *Cell Death Discov.* **2018**, *5* (1), 10.

7. Attachments

7.1. Appendix 1 - 5-fluoro-2-methyl-1H-benzo[d]imidazole (1)

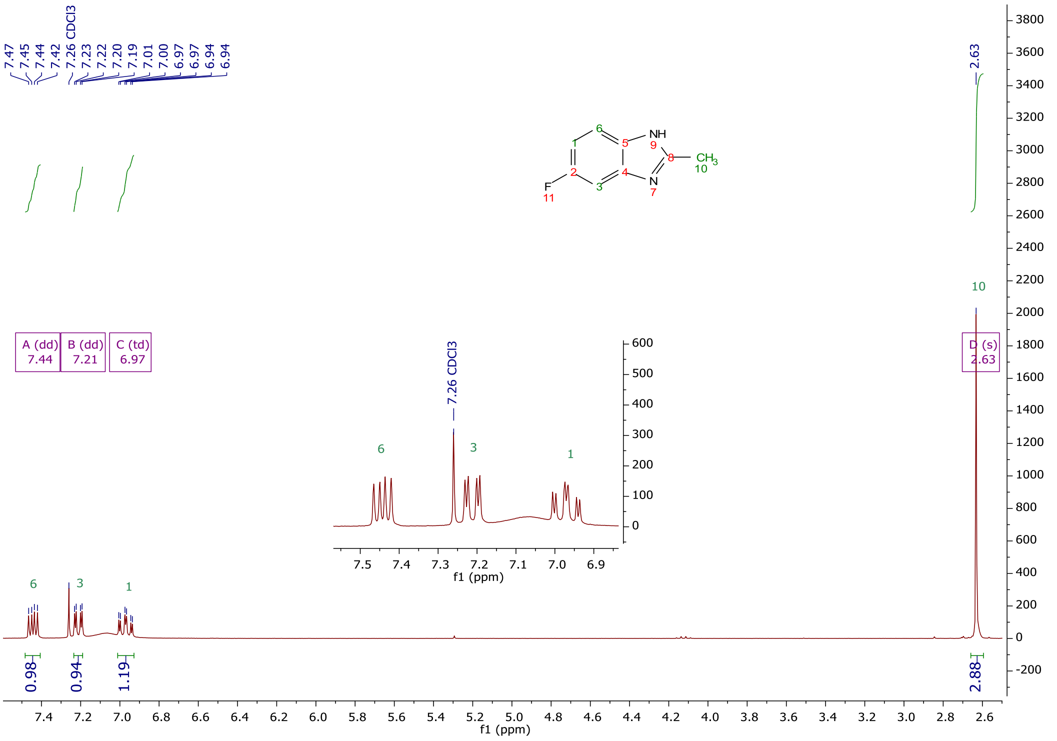

Figure7.1. ^{1}H-NMR spectra of compound **1**, in CDCl$_3$

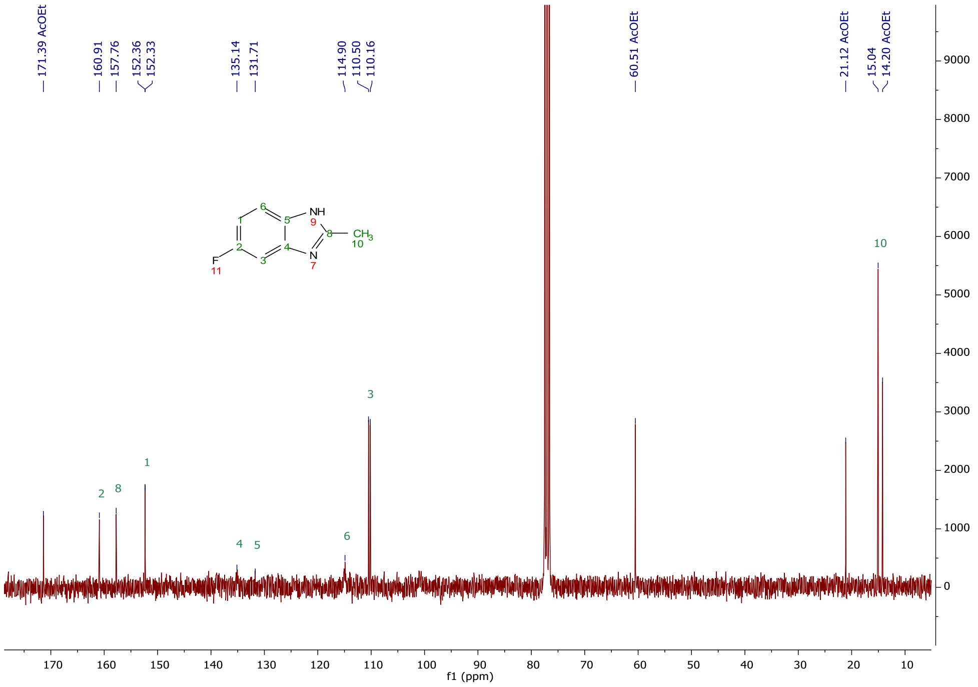

Figure 7.2. ^{13}C-NMR of compound **1**, in CDCl$_3$

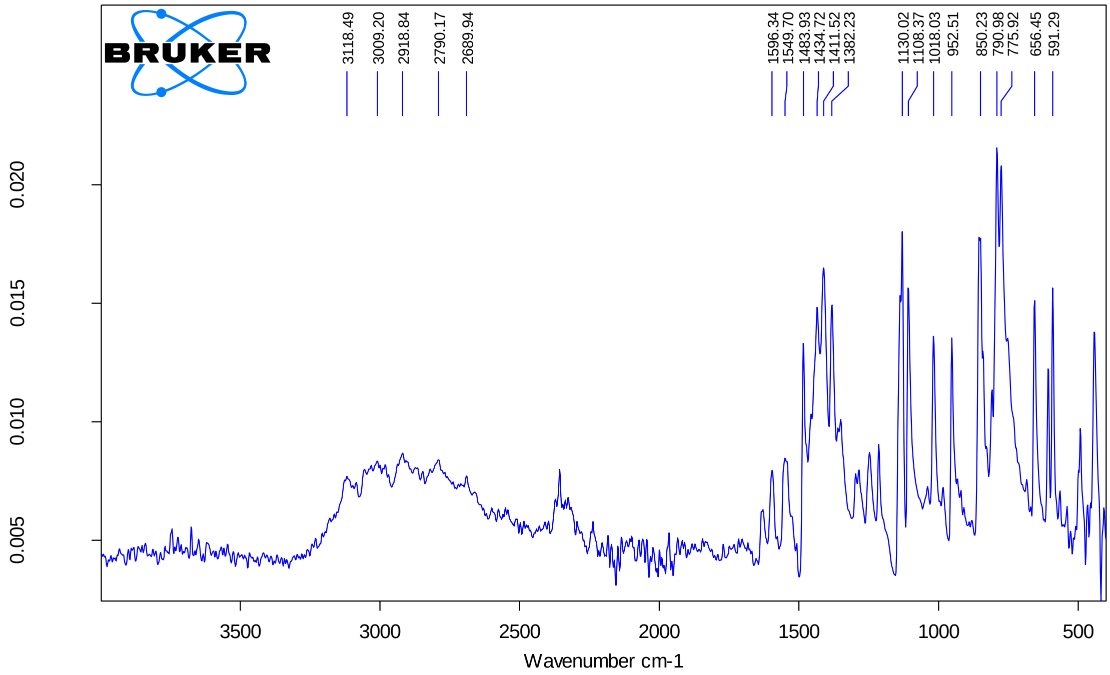

Figure 7.3. IR spectrum of compound **1**, in ATR

7.2. Appendix 2 – *5-(tert-butyl)-2-methyl-1H-benzo[d]imidazole (2)*

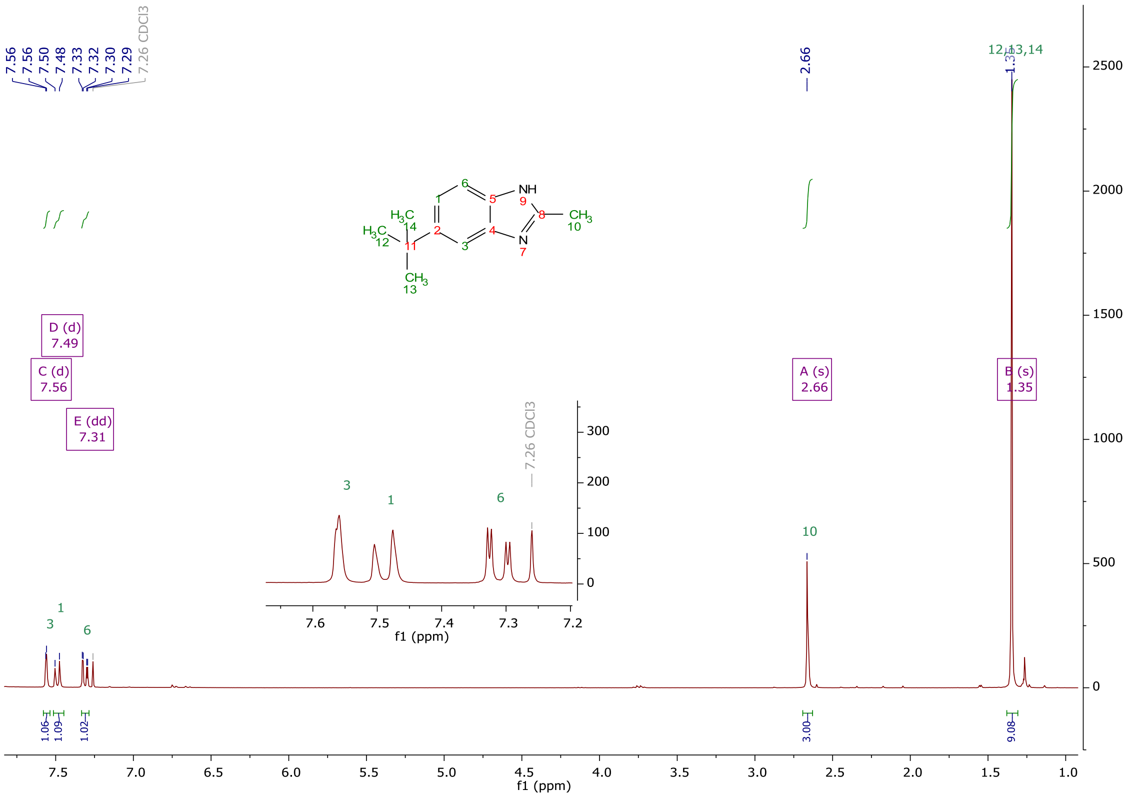

Figure 7.4. ^{1}H-NMR spectra of compound **2**, in CDCl$_3$

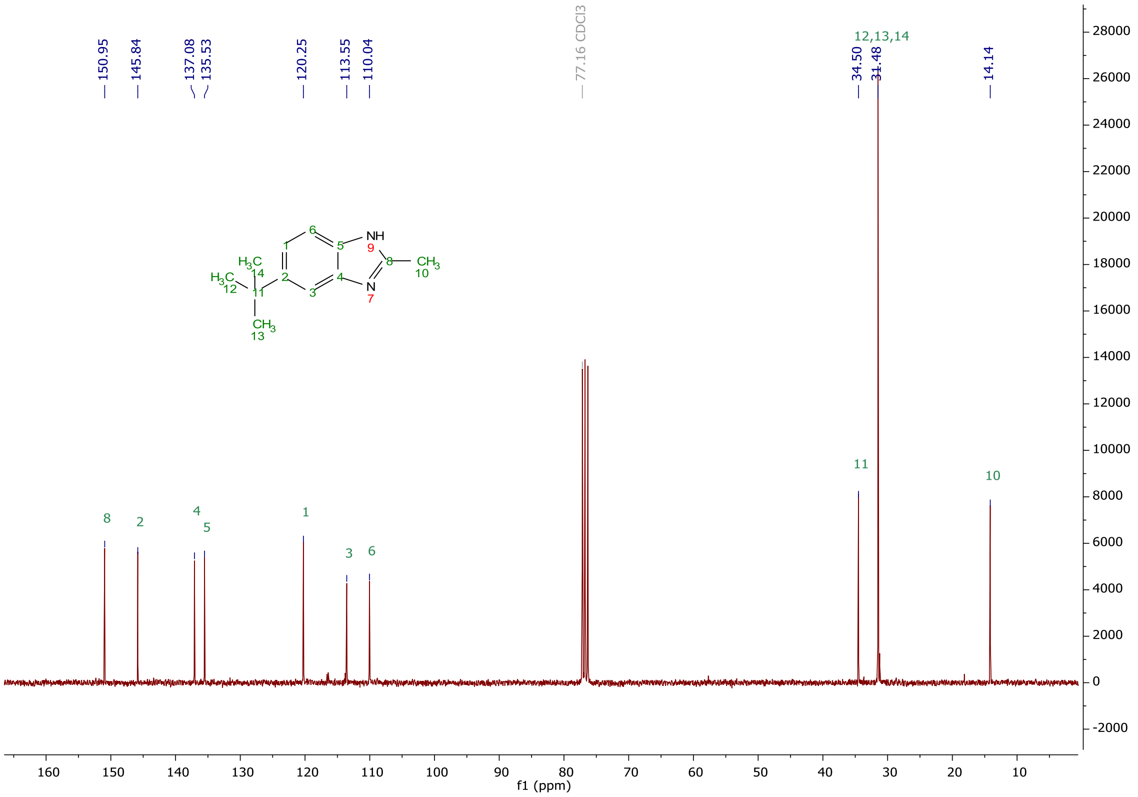

Figure 7.5. ^{13}C-NMR spectra of compound **2**, in CDCl$_3$

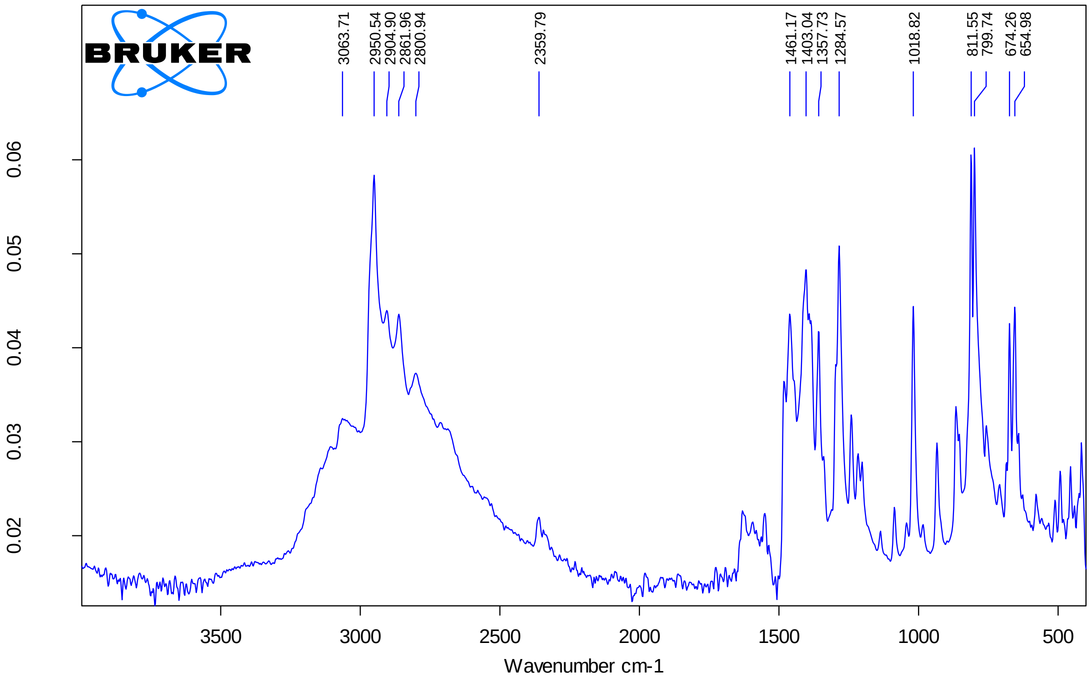

Figure 7.6. IR spectrum of compound **2**, in ATR

7.3. Appendix 3 - *2,4-dimethyl-1H-benzo[d]imidazole (3)*

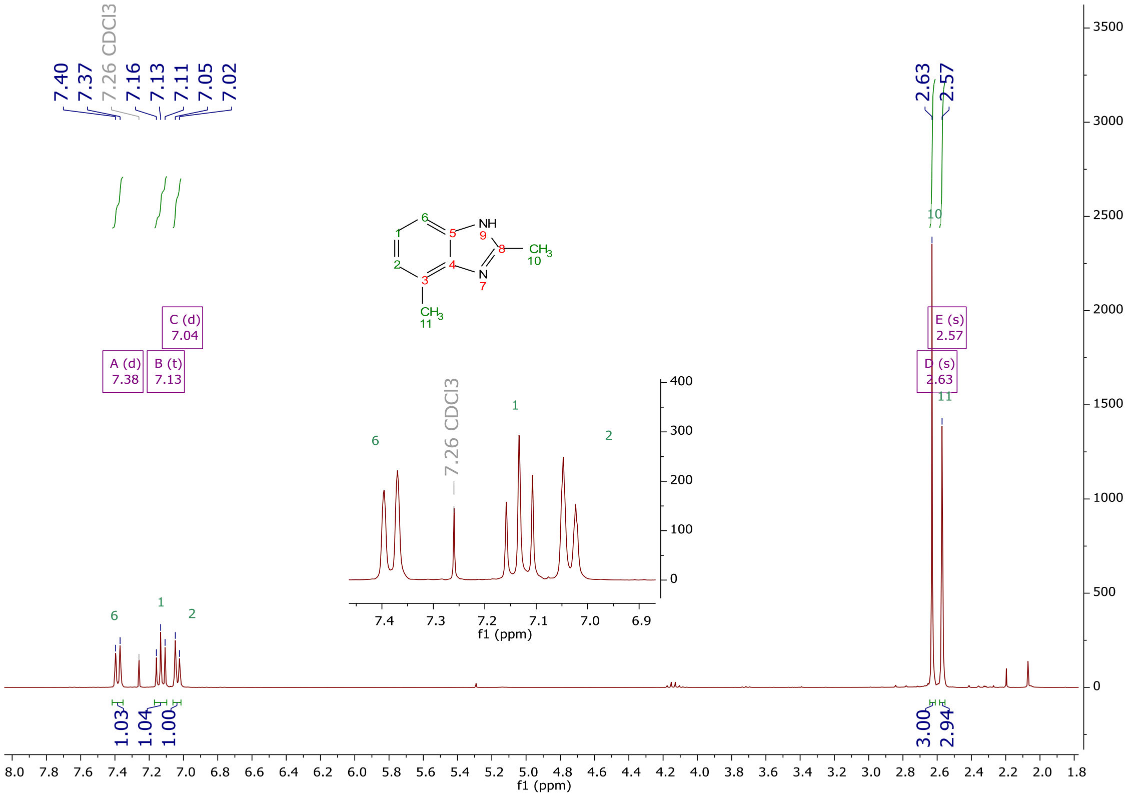

Figure 7.7. ^{1}H-NMR spectra of compound **3**, in CDCl$_3$

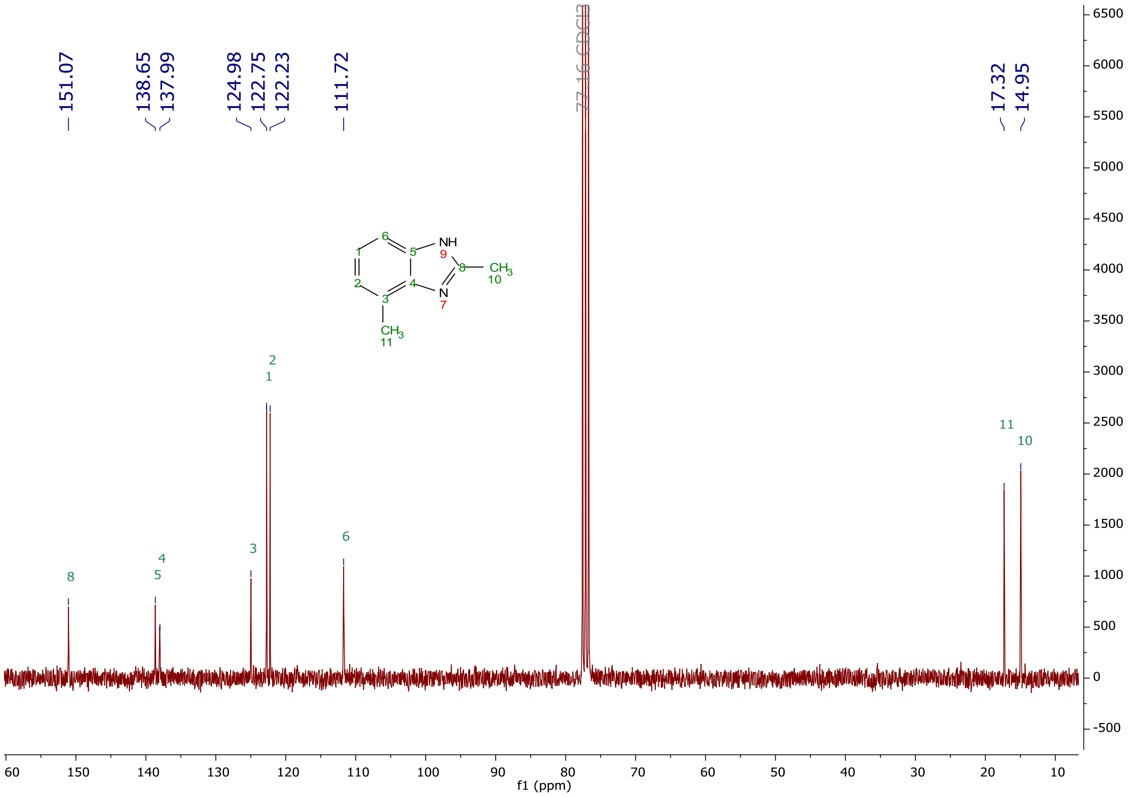

Figure 7.8. ^{13}C-NMR spectra of compound **3**, in CDCl$_3$

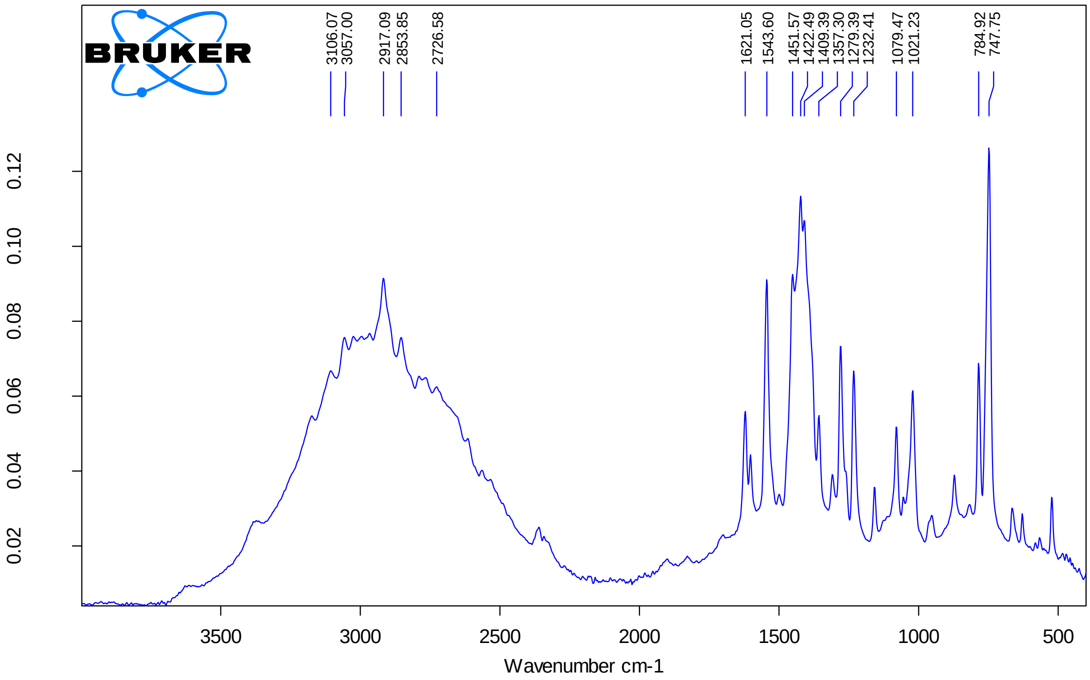

Figure 7.9. IR spectrum of compound **3**, in ATR

7.4. Appendix 4 - 1,2-dimethyl-1H-benzo[d]imidazole (4)

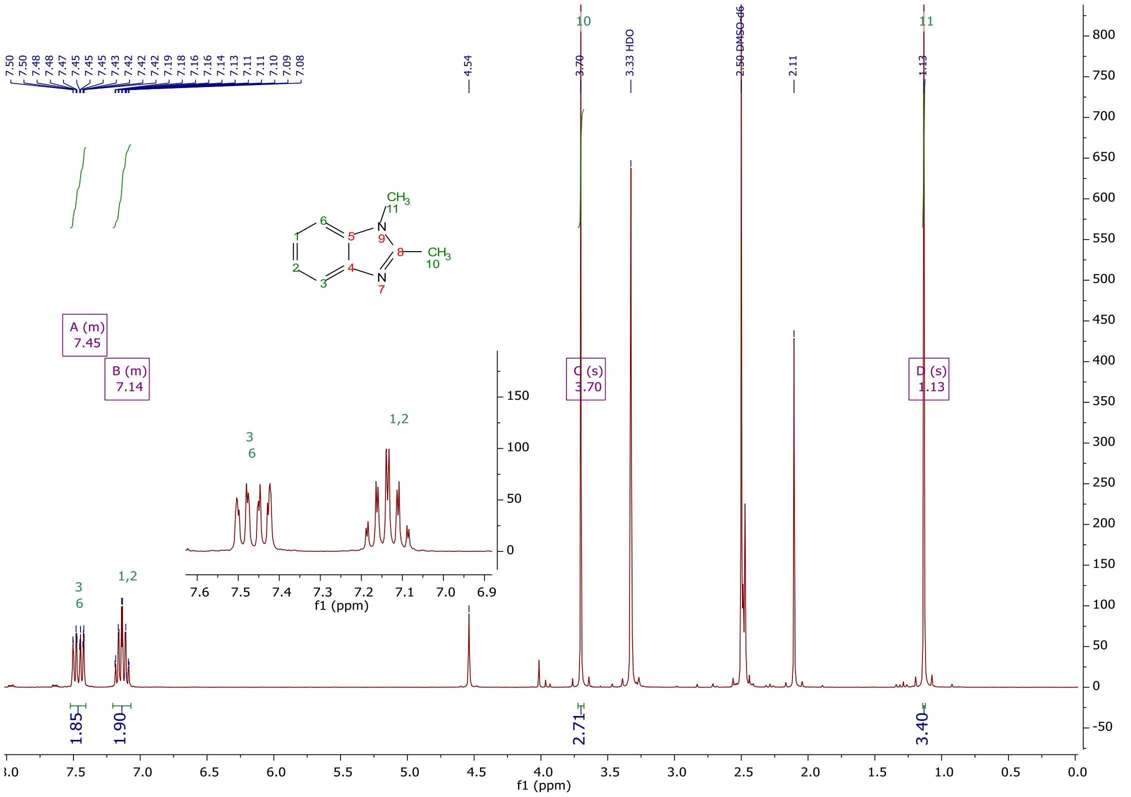

Figure 7.10. ^{1}H-NMR spectra of compound **4**, in DMSO

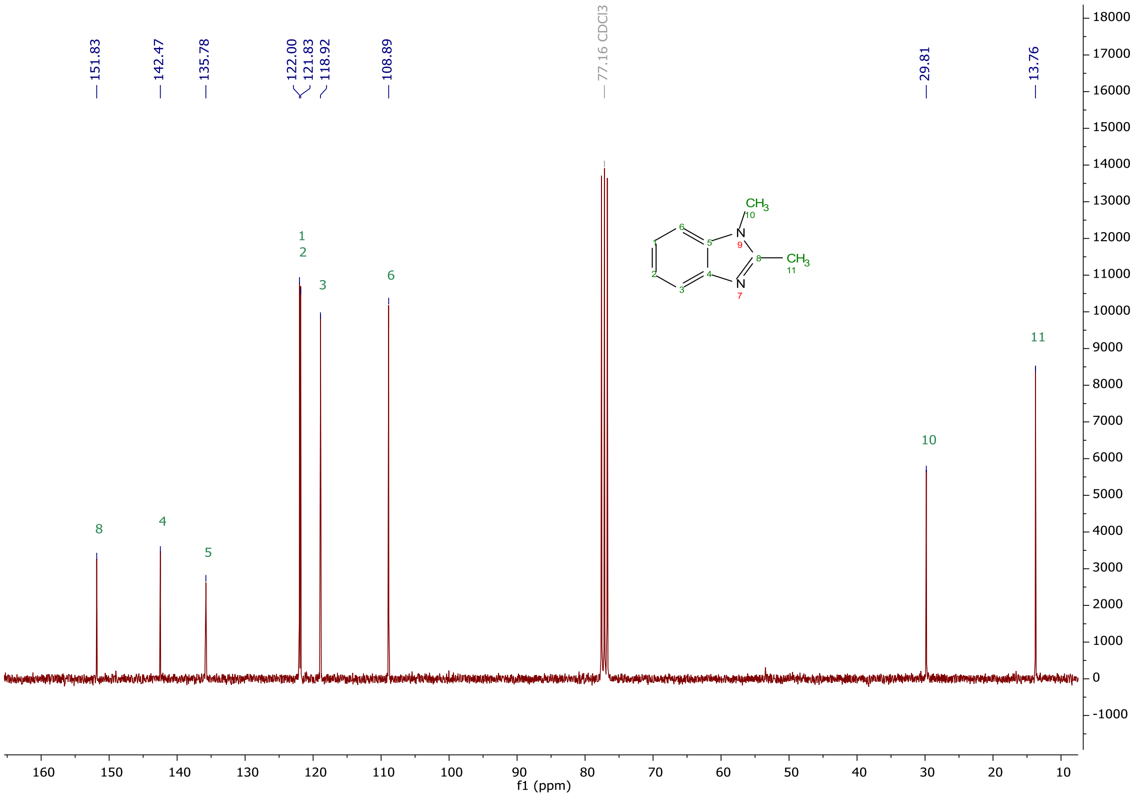

Figure 7.11. ^{13}C-NMR spectra of compound **4**, in $CDCl_3$

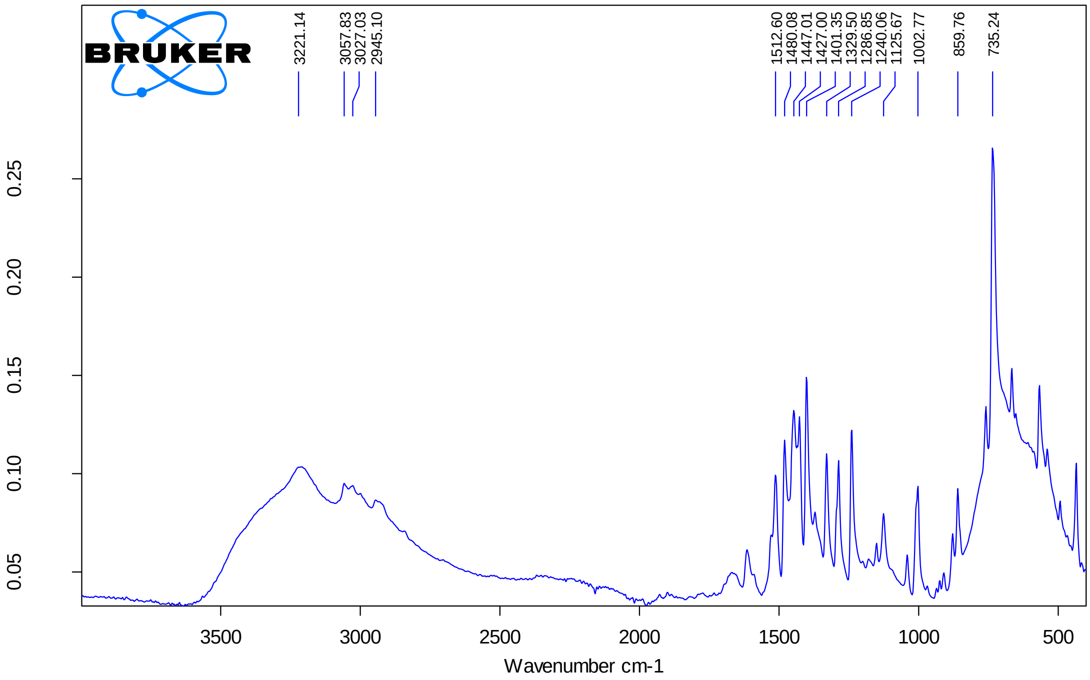

Figure 7.12. IR spectrum of compound **4**, in ATR

7.5. Appendix 5 - *(E)-4-(2-(1H-benzo[d]imidazol-2-yl)vinyl)benzaldehyde (5)*

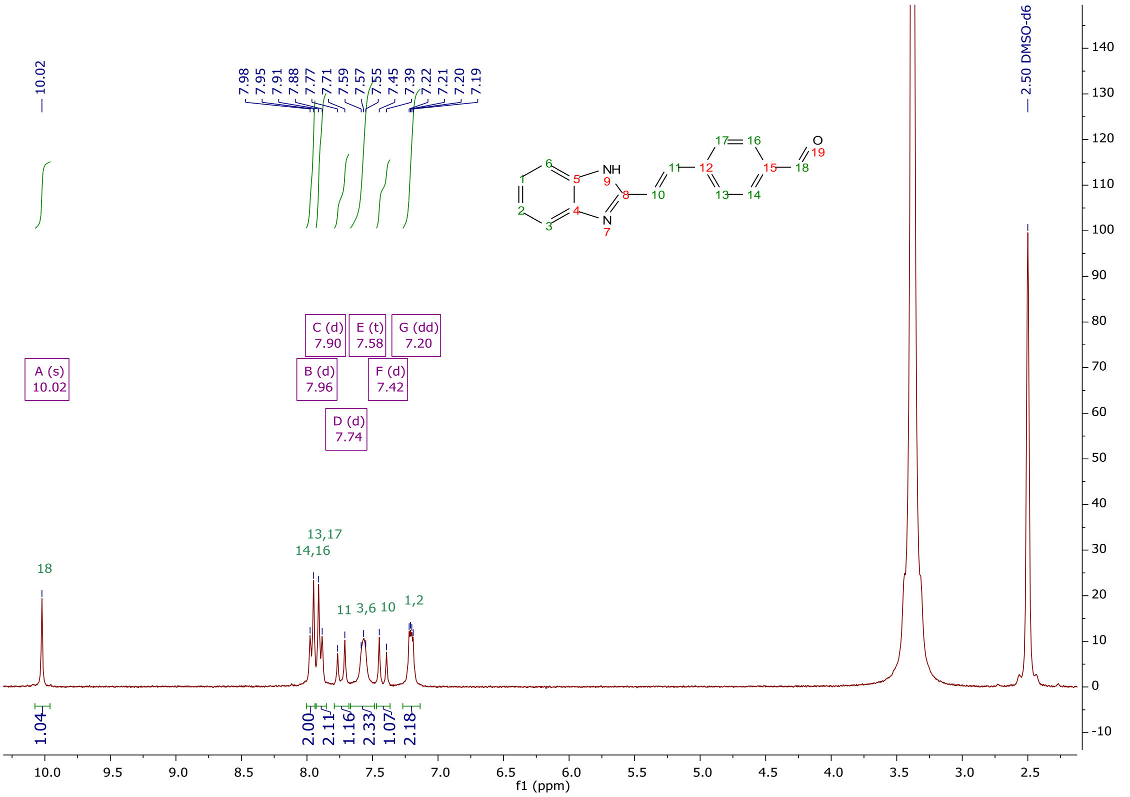

Figure 7.13. ^{1}H-NMR spectra of compound **5**, in DMSO

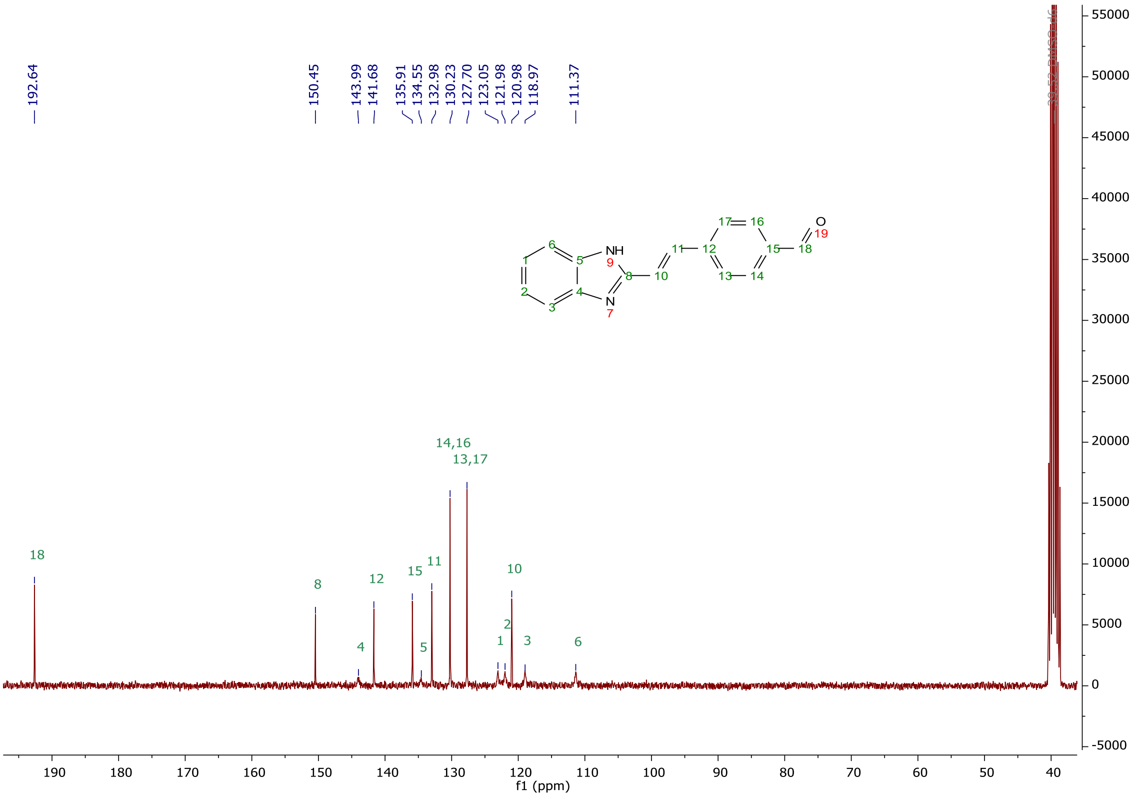

Figure 7.14. ^{13}*C*-NMR spectra of compound **5**, in DMSO

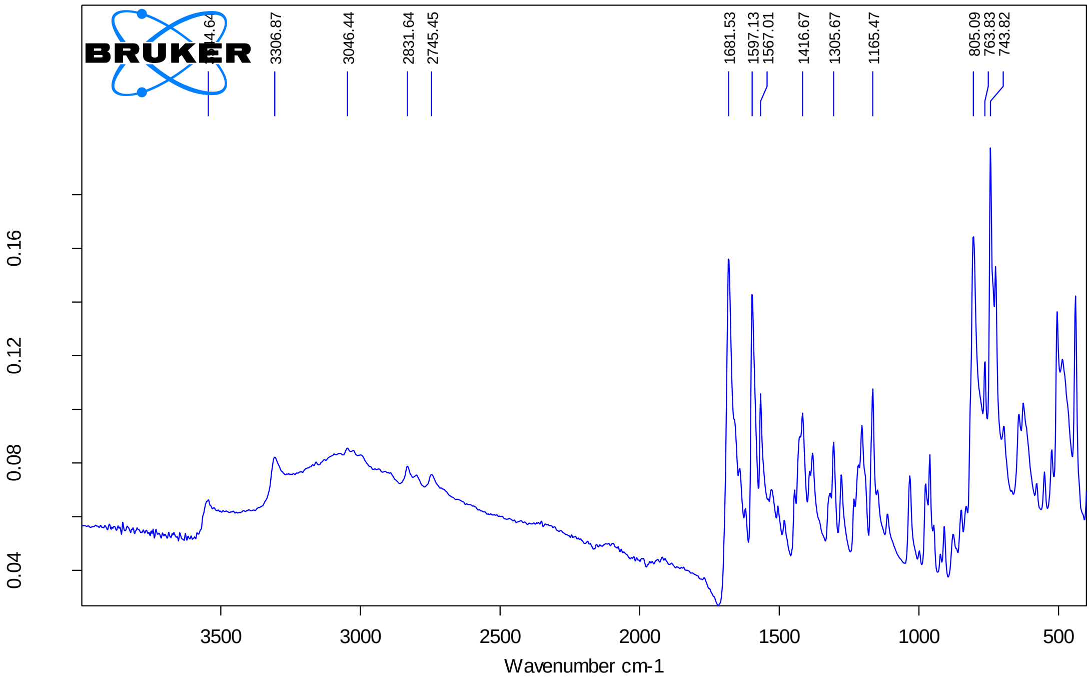

Figure 7.15. IR spectrum of compound **5**, in ATR

7.6. Appendix 6 - *(E)*-4-(2-(5-fluoro-1H-benzo[d]imidazol-2-yl)vinyl)benzaldehyde (6)

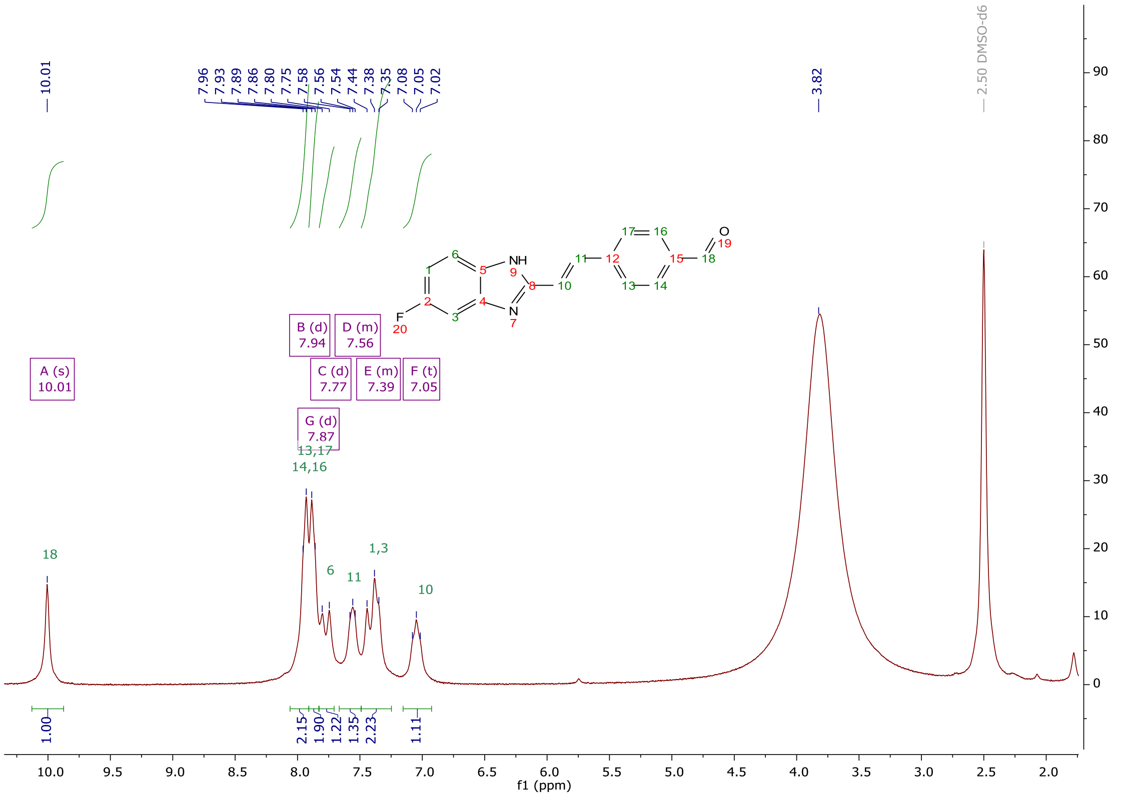

Figure 7.16. ^{1}H-NMR spectra of compound **6**, in DMSO

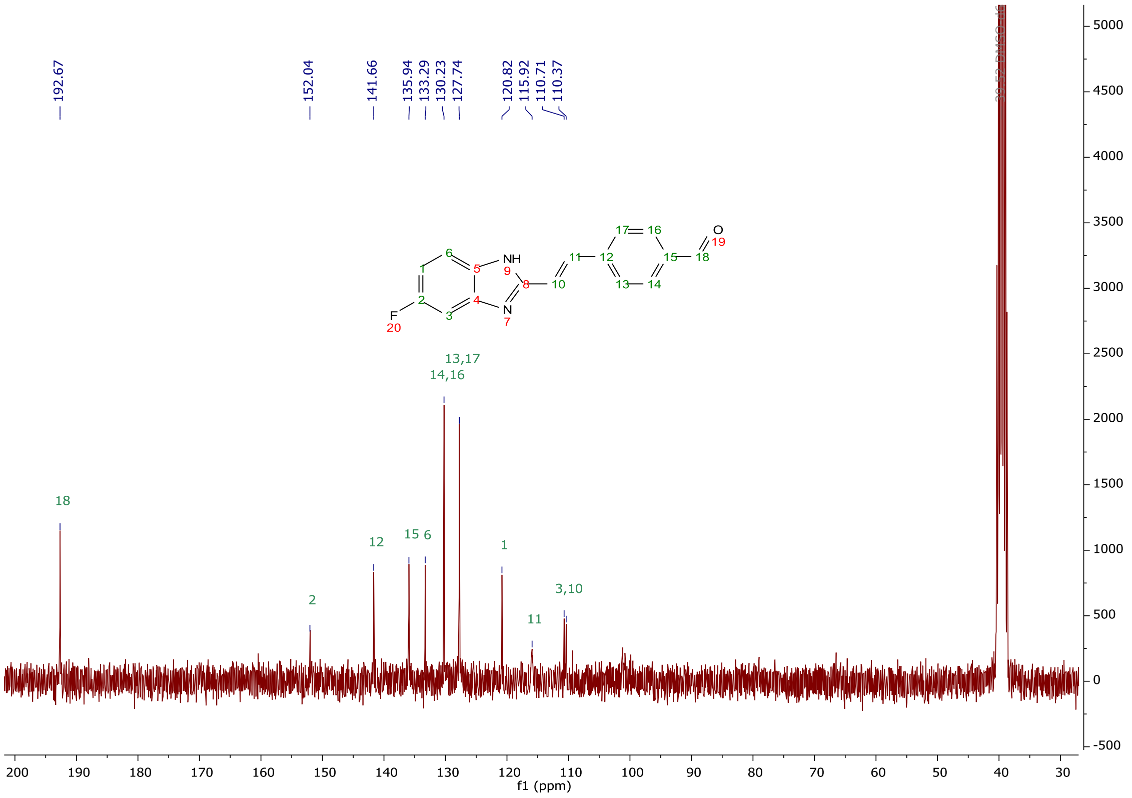

Figure 7.17. *^{13}C*-NMR spectra of compound **6**, in DMSO

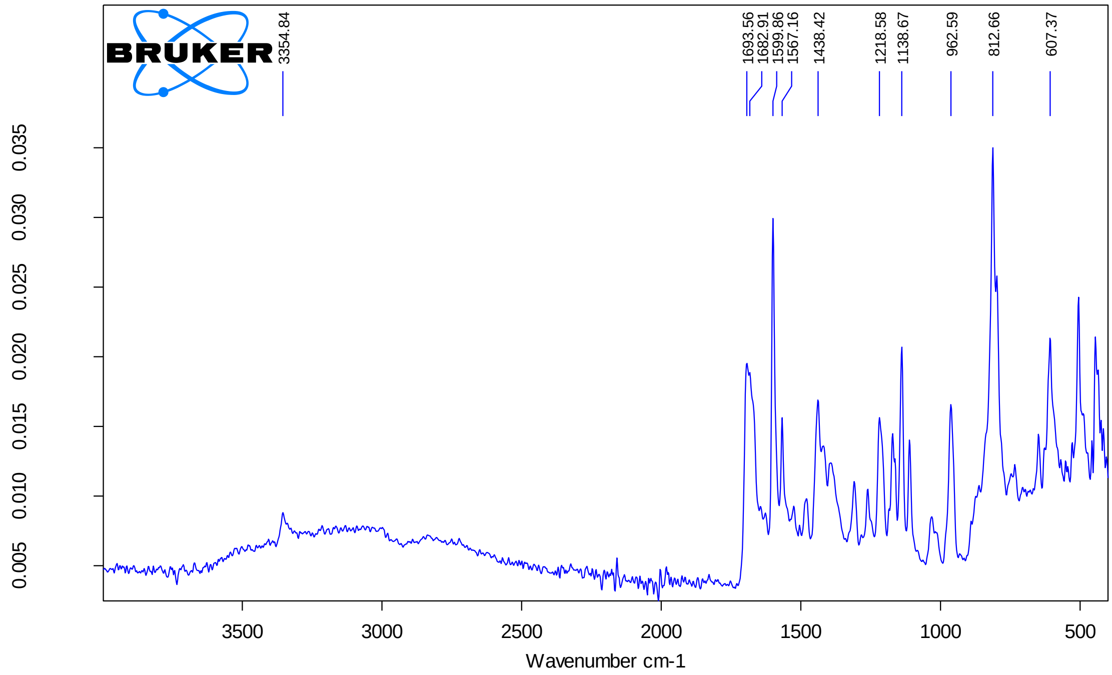

Figure 7.18. IR spectrum of compound **6**, in ATR

7.7. Appendix 7 - *(E)*-4-(2-(5-(tert-butyl)-1H-benzo[d]imidazol-2-yl)vinyl)benzaldehyde (7*)*

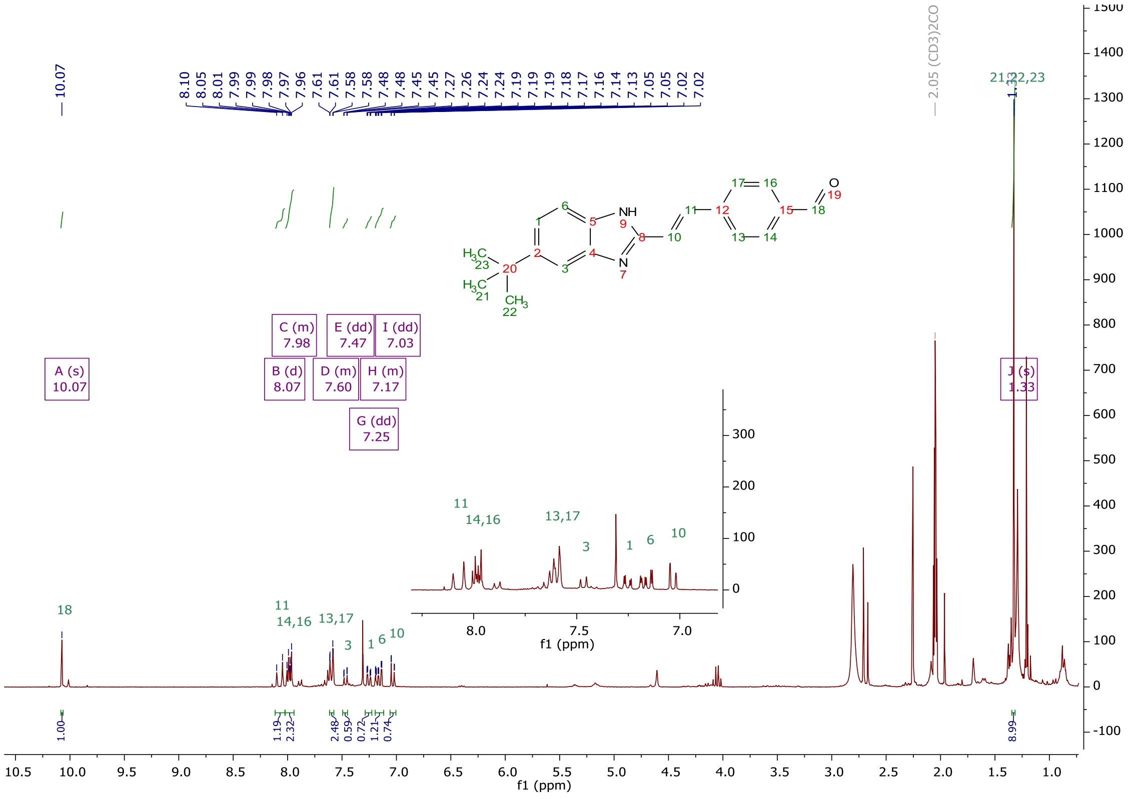

Figure 7.19. ^{1}H-NMR spectra of compound **7**, in DMSO

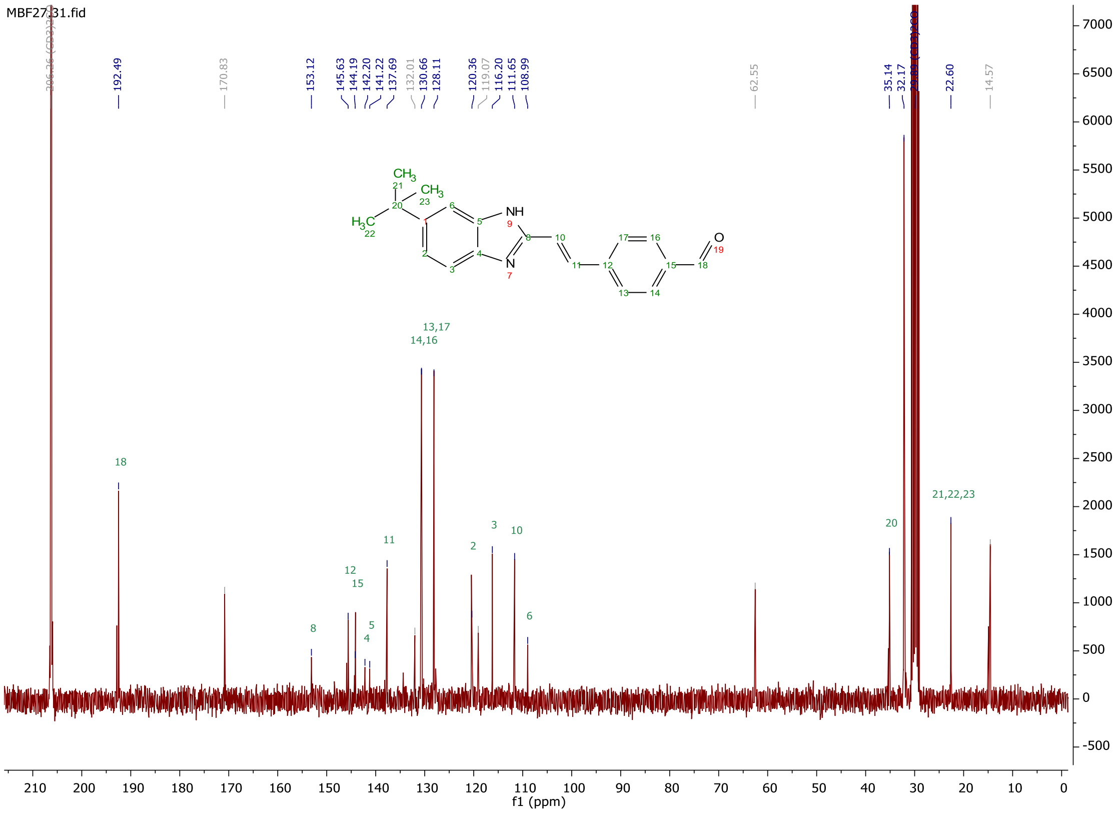

Figure 7.20. ^{13}*C*-NMR spectra of compound 7, in DMSO

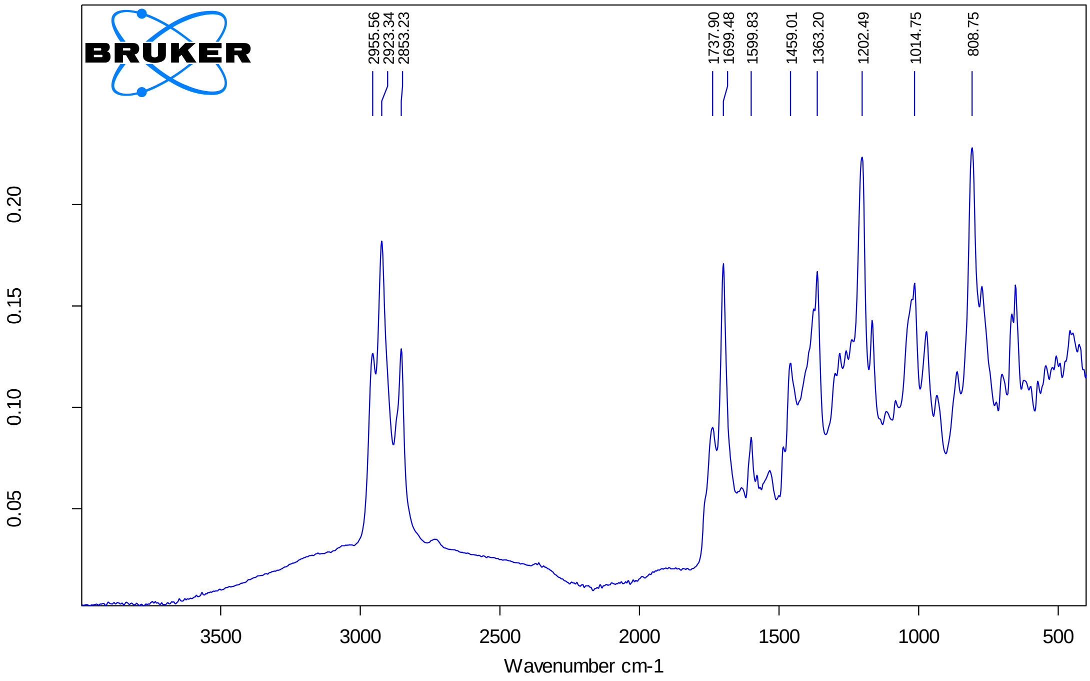

Figure 7.21. IR spectrum of compound **7**, in ATR

7.8. Appendix 8 - *(E)*-4-(2-(4-methyl-1H-benzo[d]imidazol-2-yl)vinyl)benzaldehyde (8)

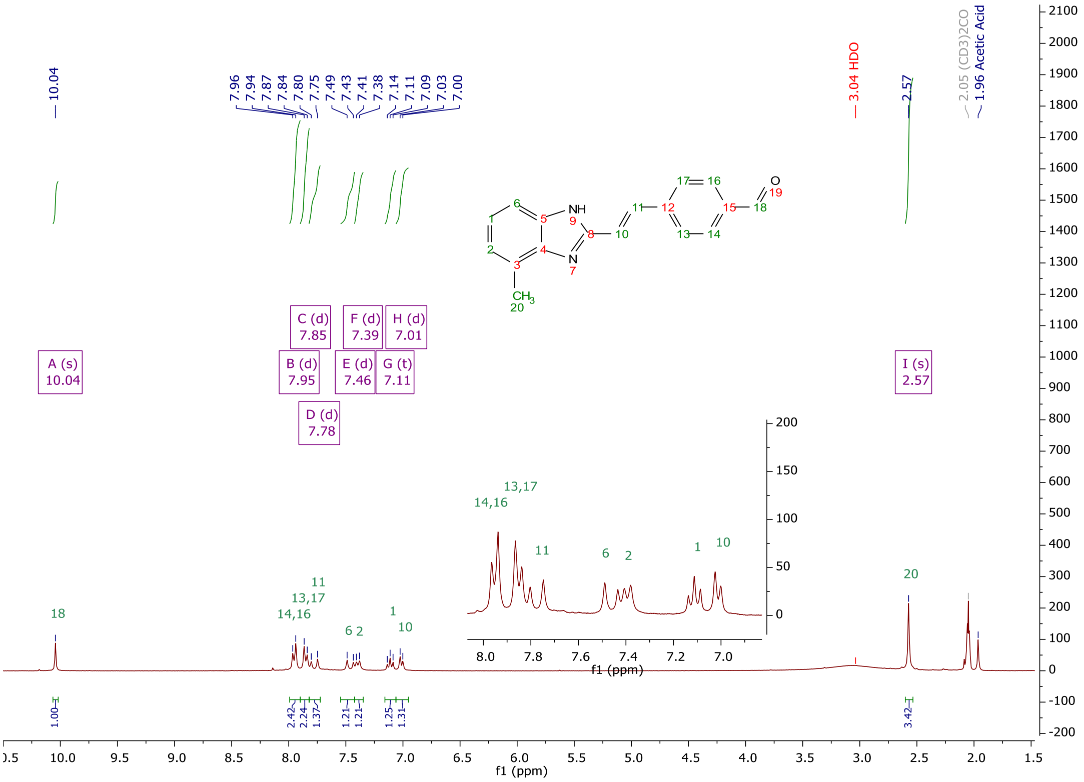

Figure 7.22. ^{1}H-NMR spectra of compound **8**, in DMSO

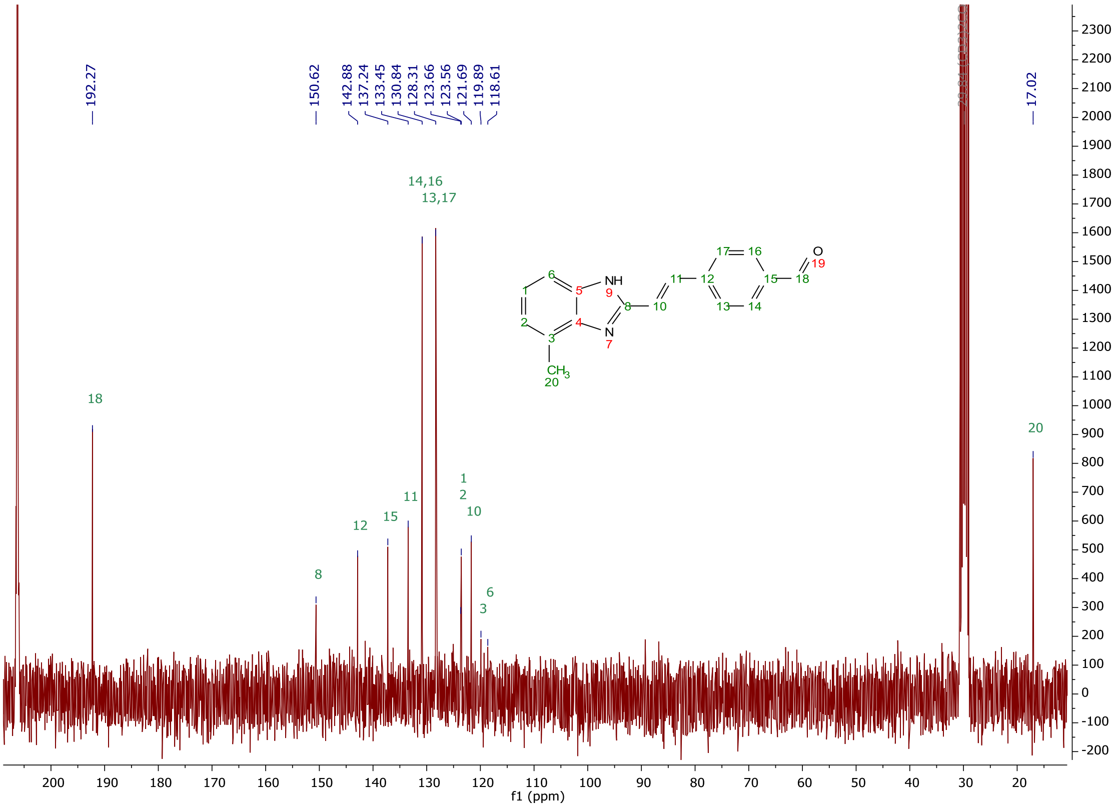

Figure 7.23. ^{13}*C*-NMR spectra of compound **8**, in DMSO

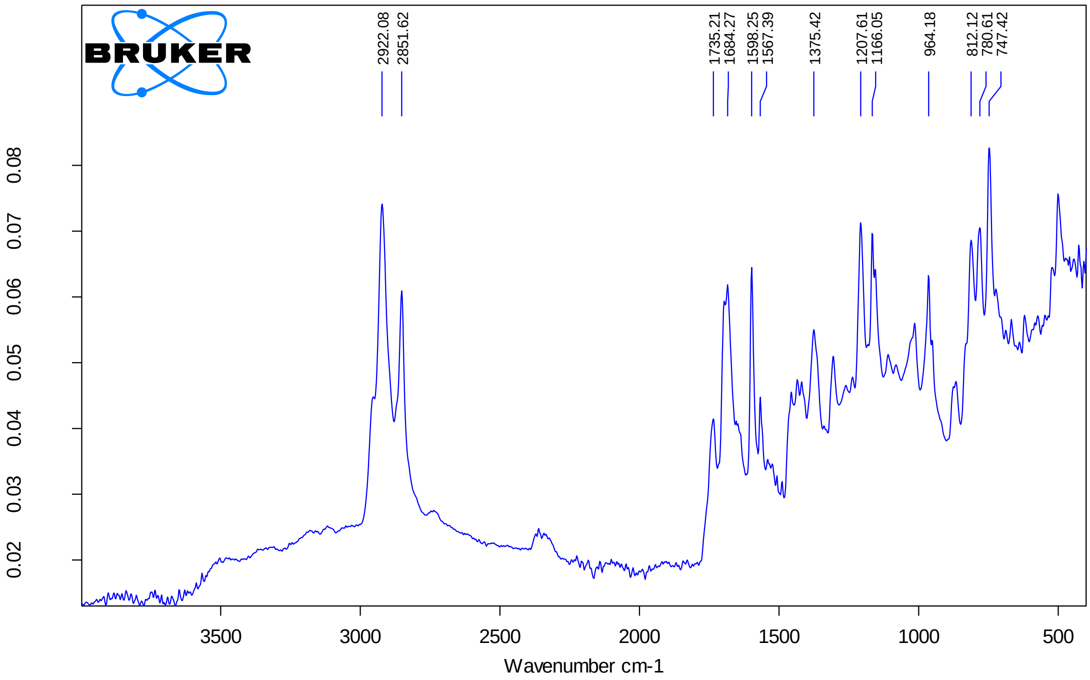

Figure 7.24. IR spectrum of compound **8**, in ATR

7.9. Appendix 9 - *(E)*-4-(2-(1-methyl-1H-benzo[d]imidazol-2-yl)vinyl)benzaldehyde (9)

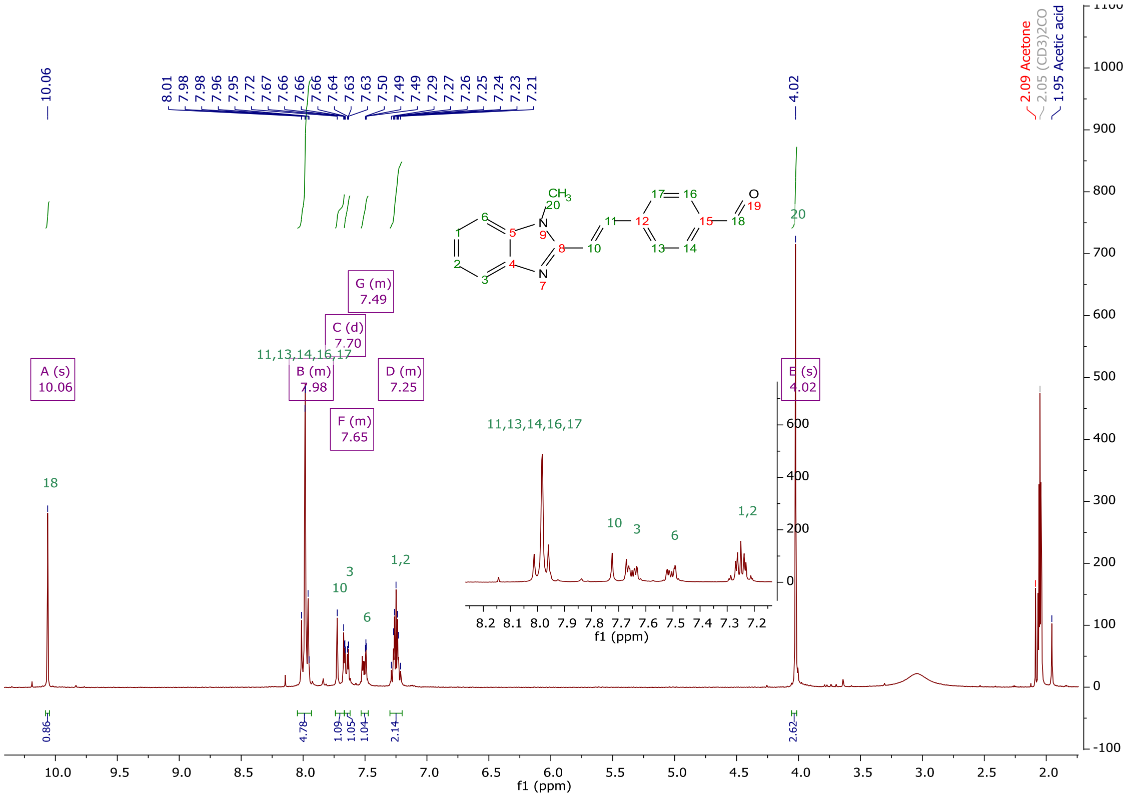

Figure 7.25. ^{1}H-NMR spectra of compound **9**, in Acetone

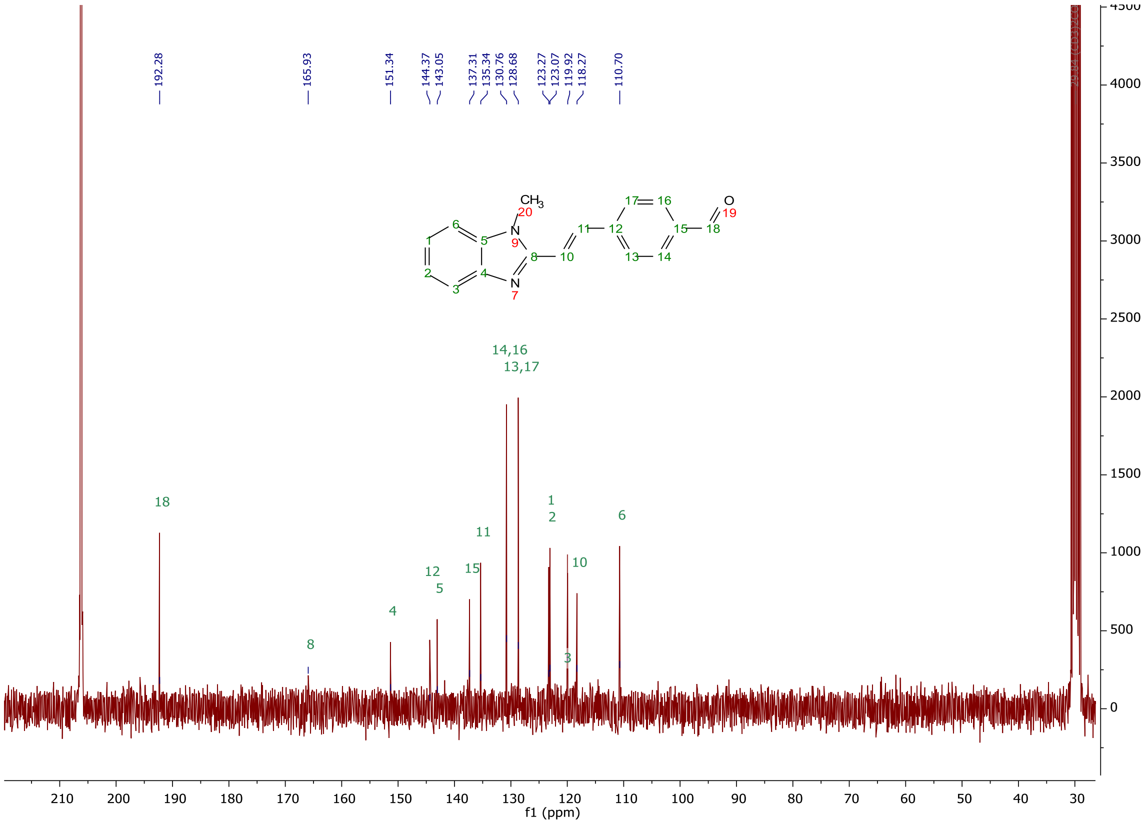

Figure 7.26. *^{13}C*-NMR spectra of compound **9**, in Acetone

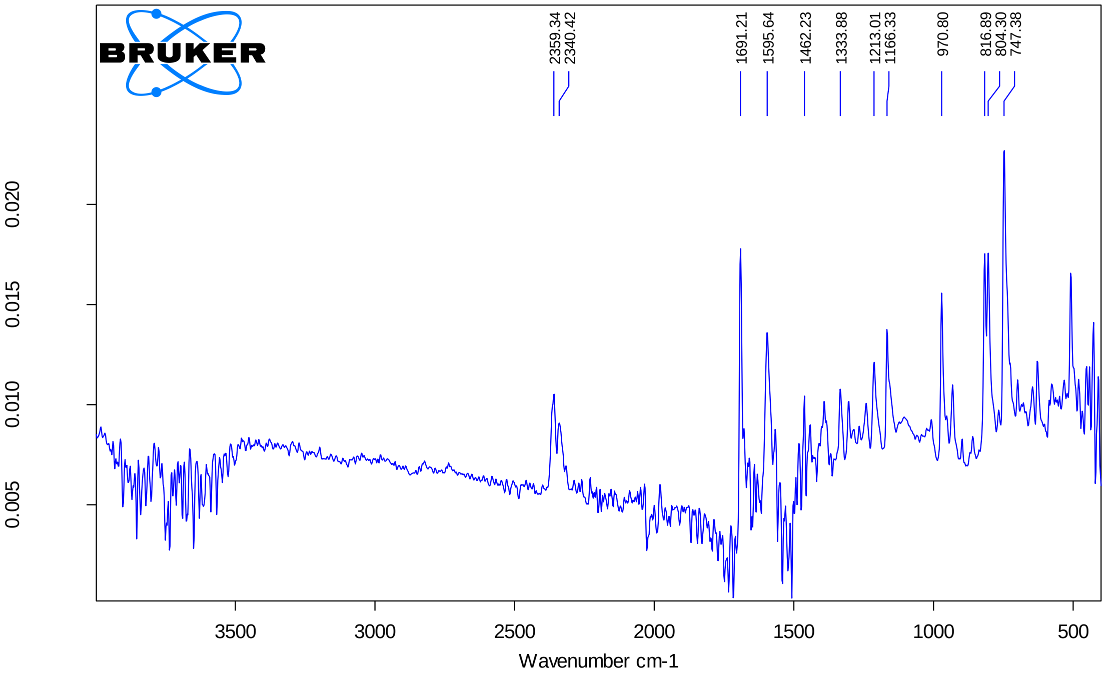

Figure 7.27. IR spectrum of compound **9**, in ATR

7.10. Appendix 10 -Attempt synthesis of *(E)*-4-(2-(1H-imidazol-2-yl)vinyl)benzaldehyde (10)

Method A

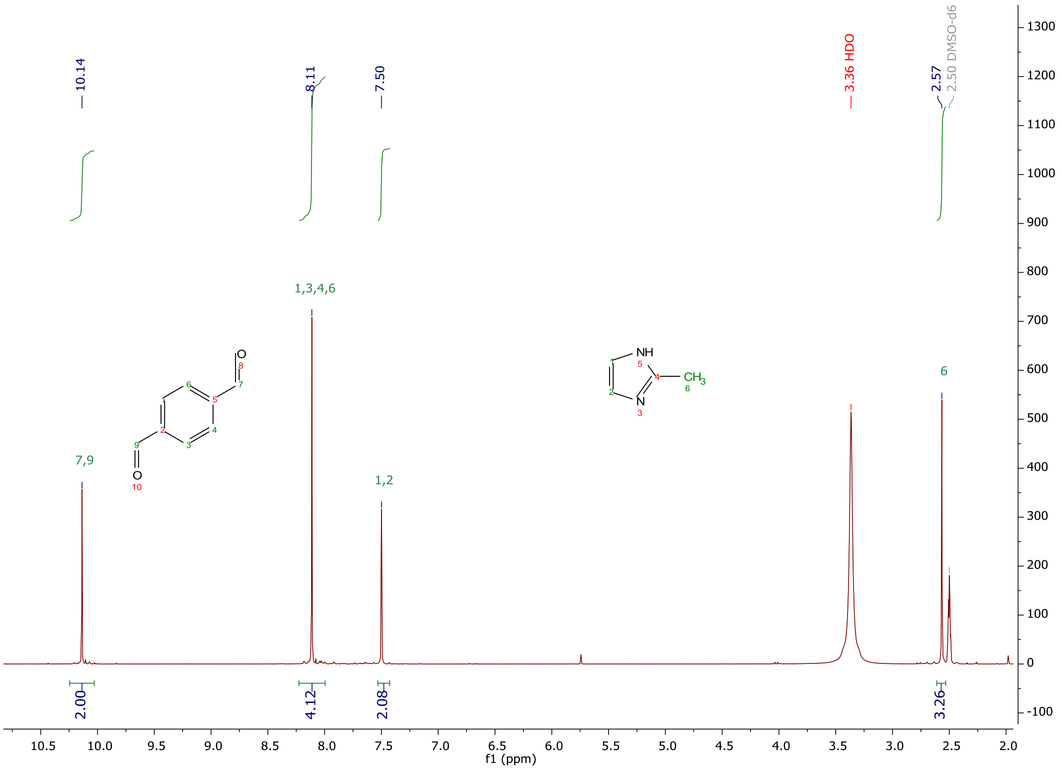

Figure 7.28. ¹H-NMR spectra of the attempt to synthetize compound **10**, in DMSO

Method B

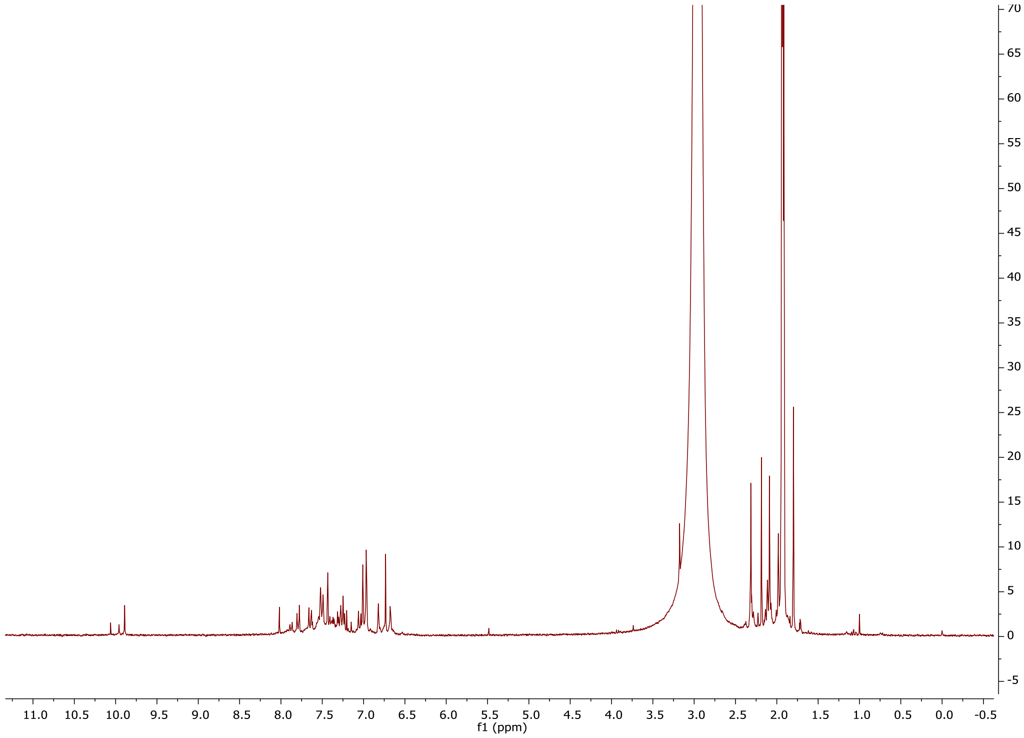

Figure 7.29. ¹H-NMR spectra of the attempt to synthetize compound **10**, in DMSO

7.11. Appendix 11 - 4-((Z)-4-((E)-2-(1H-benzo[d]imidazol-2-yl)vinyl)benzylidene)-2-phenyloxazol-5(4H)-one (11)

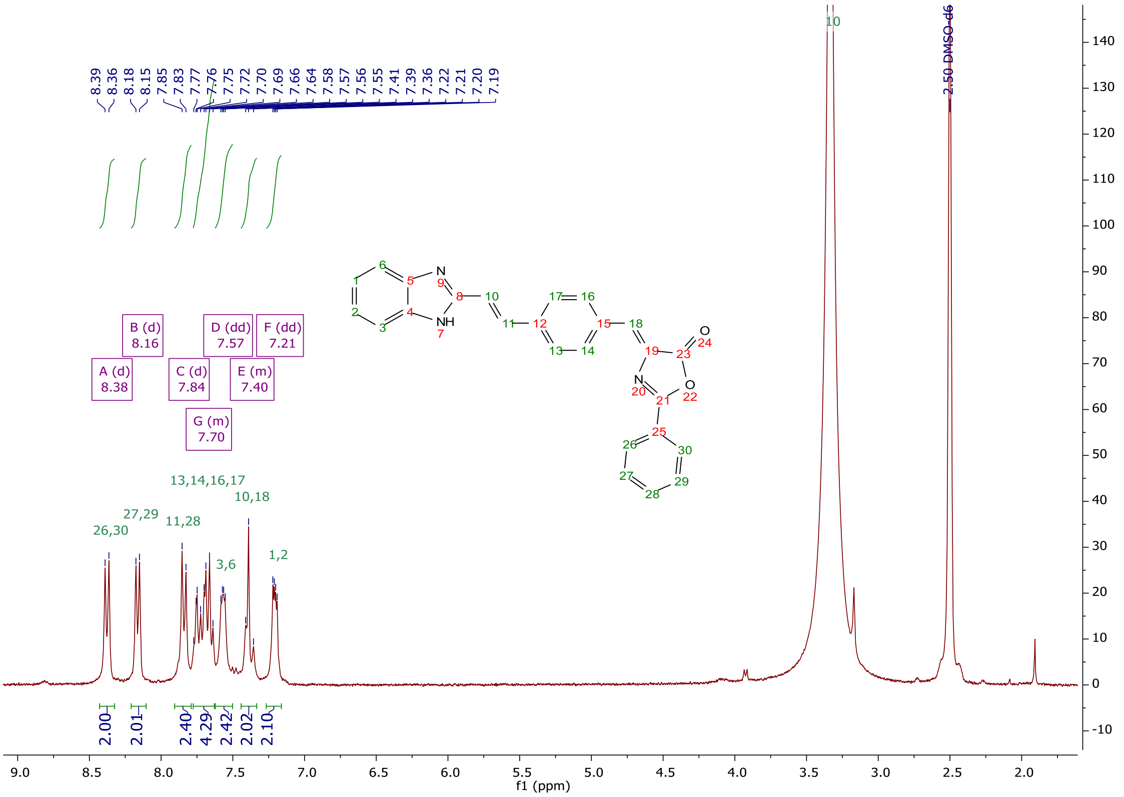

Figure 7.30. ^{1}H-NMR spectra of compound **11**, in DMSO

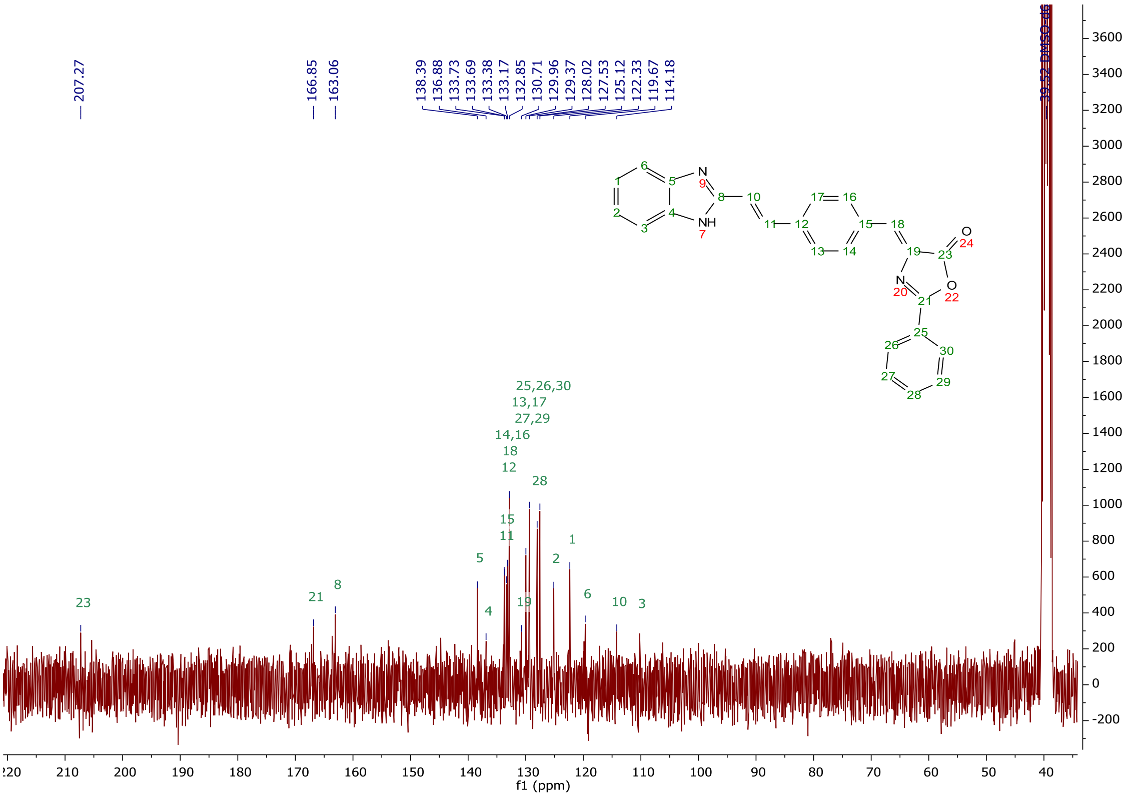

Figure 7.31. ^{13}C-NMR spectra of compound **11**, in DMSO

7.12. Appendix 12 - 4-((E)-4-((E)-2-(4-methyl-1H-benzo[d]imidazol-2-yl)vinyl)benzylidene)-2-phenyloxazol-5(4H)-one (12)

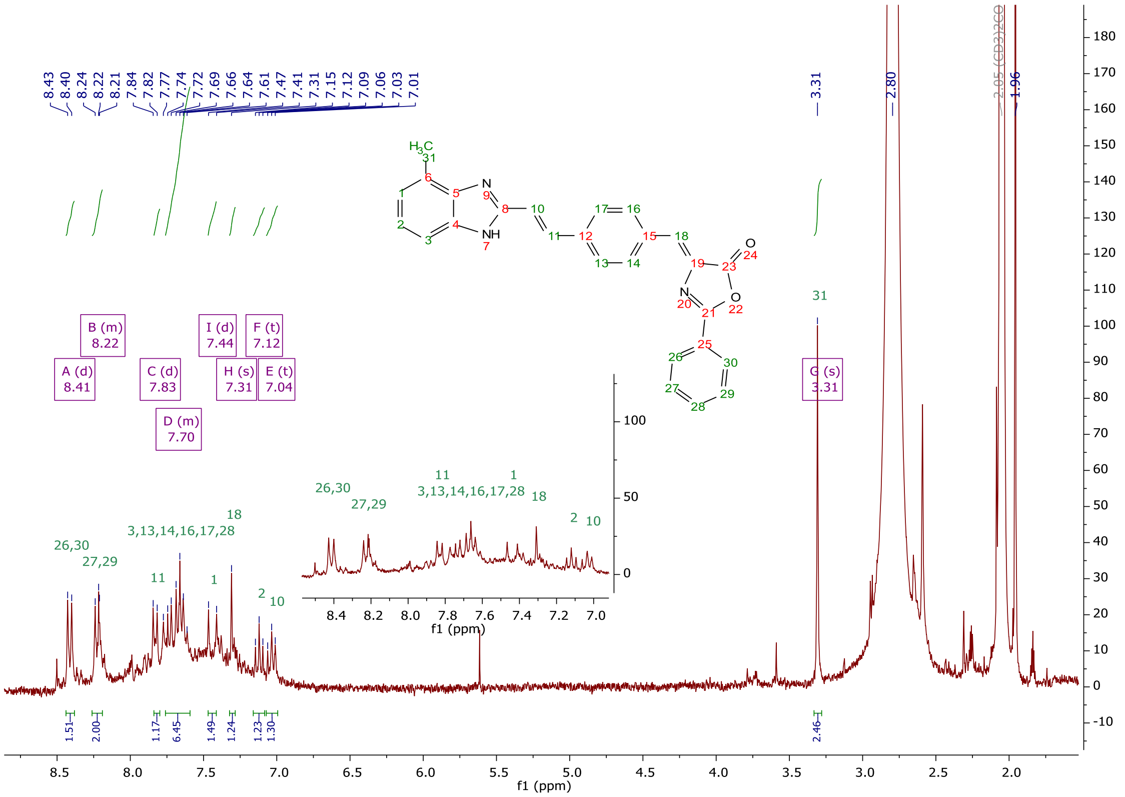

Figure 7.32. ^{1}H-NMR spectra of compound **12**, in Acetone

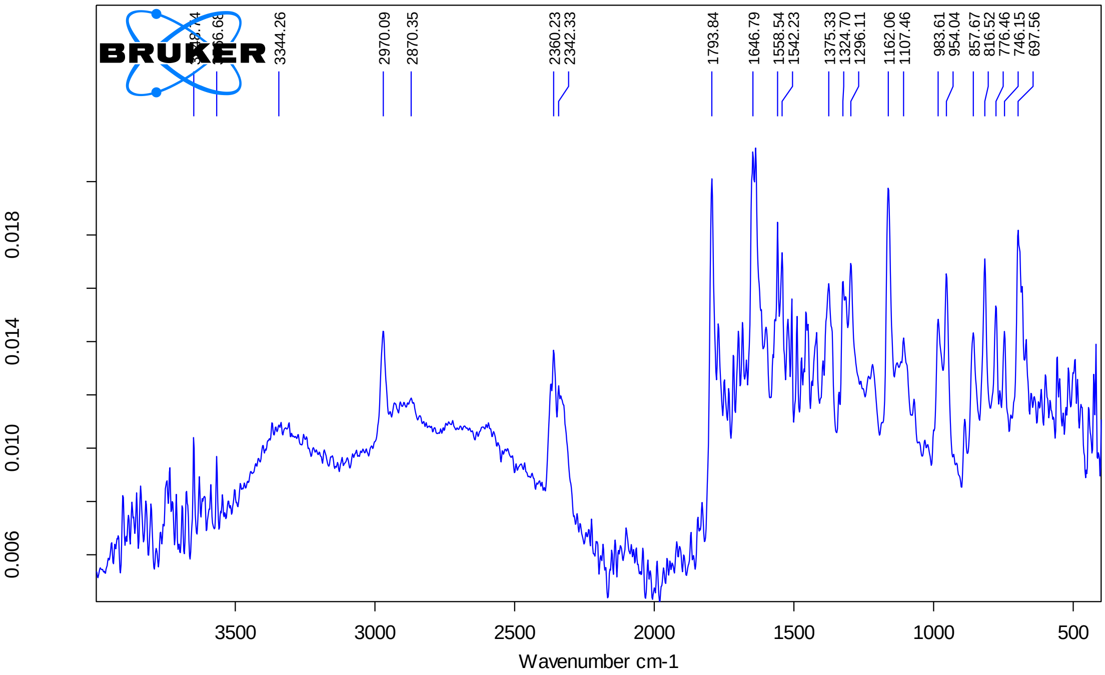

Figure 7.33. IR spectrum of compound **12**, in ATR

7.13. Appendix 13 - 4-((Z)-4-((E)-2-(1-methyl-1H-benzo[d]imidazol-2-yl)vinyl)benzylidene)-2-phenyloxazol-5(4H)-one (13)

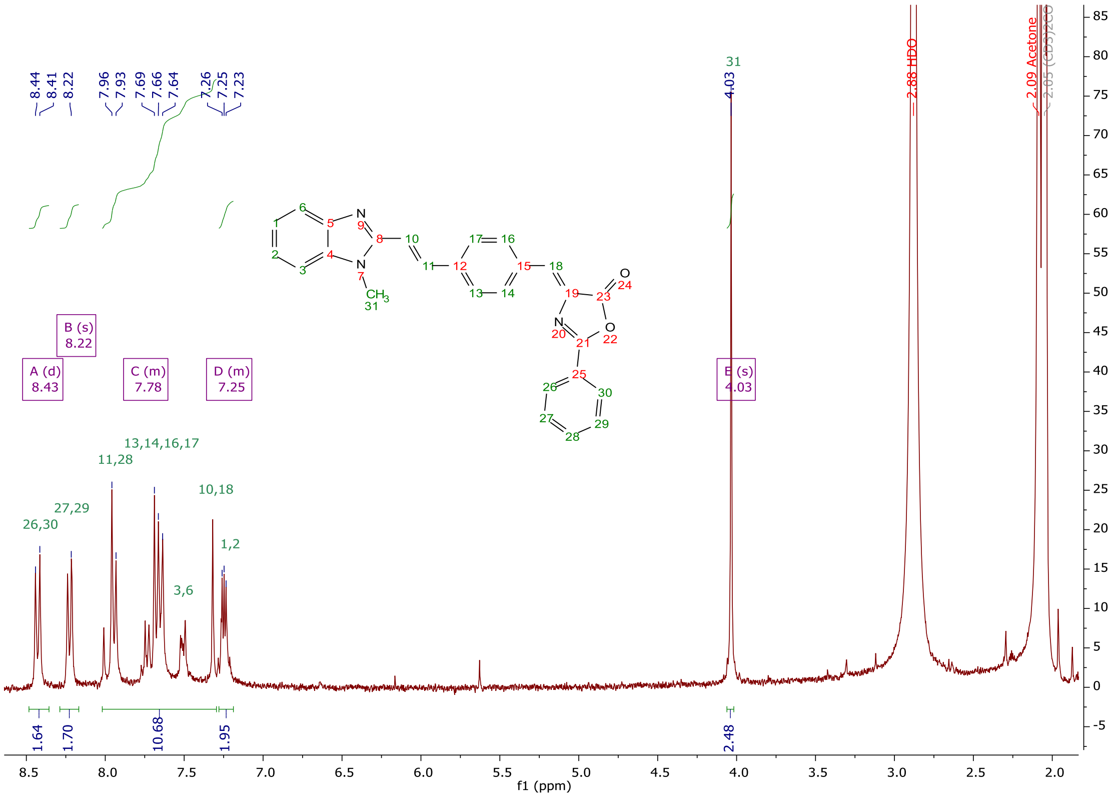

Figure 7.34. -^{1}H-NMR spectra of compound **13**, in Acetone

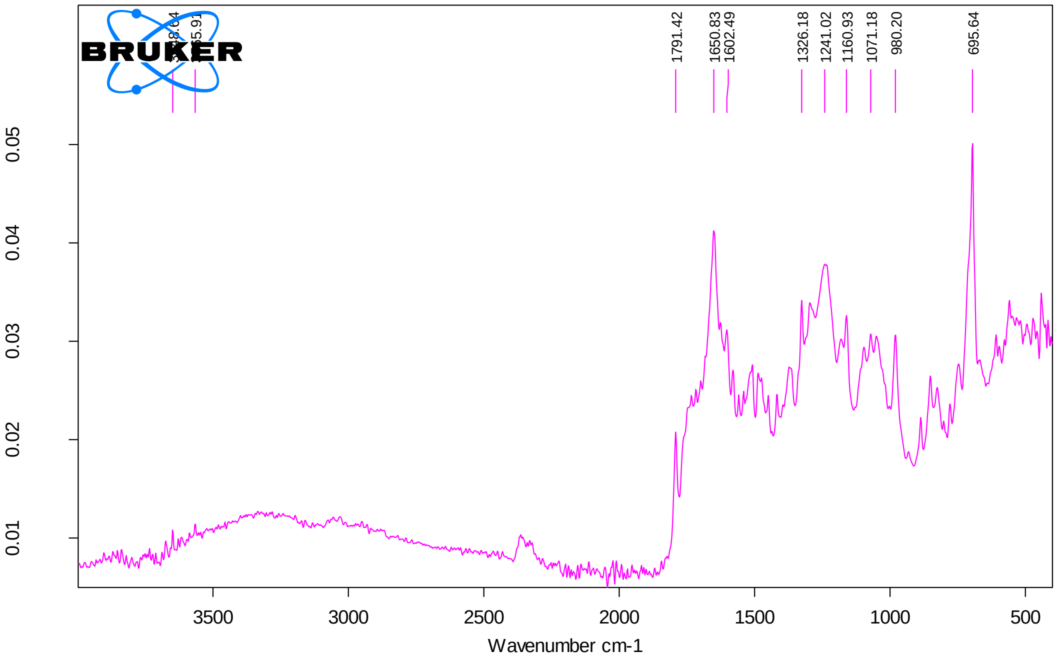

Figure 7.35. IR spectrum of compound **13**, in ATR

7.14. Appendix 14 - 4-((E)-4-((E)-2-(1H-benzo[d]imidazol-2-yl)vinyl)benzylidene)-2-methyloxazol-5(4H)-one (14)

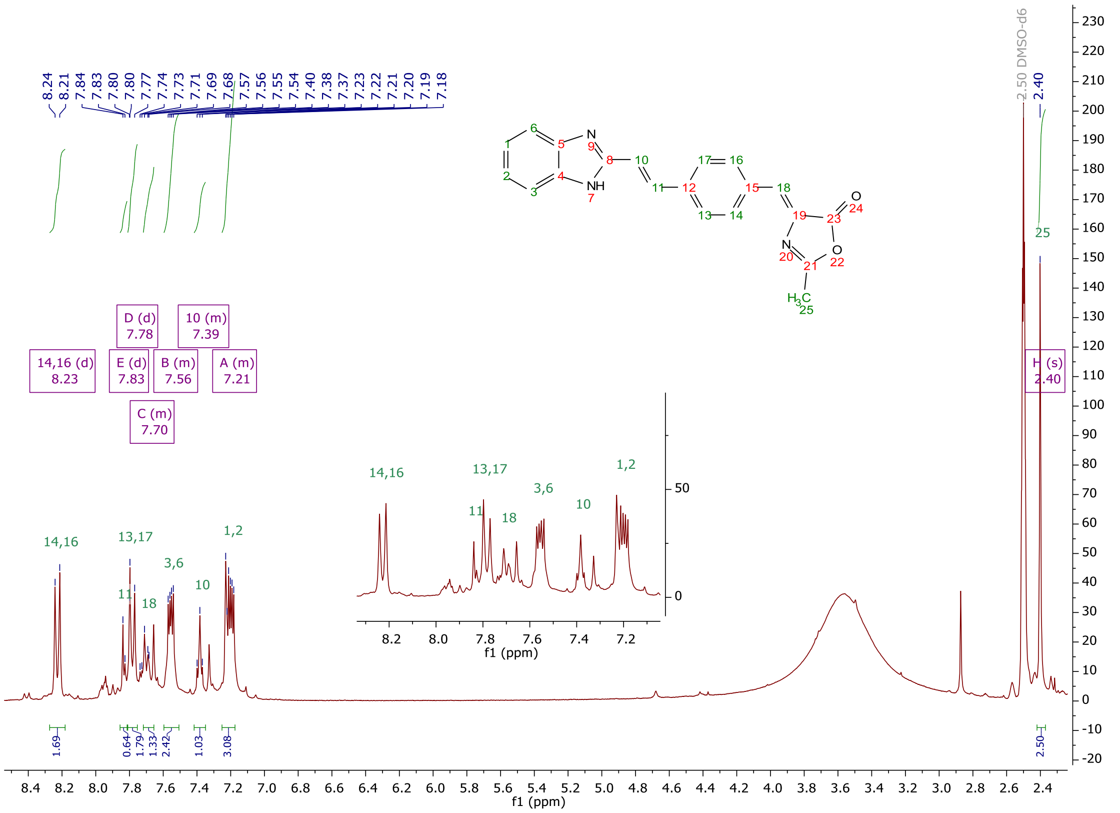

Figure 7.36. ^{1}H-NMR spectra of compound **14**, in DMSO

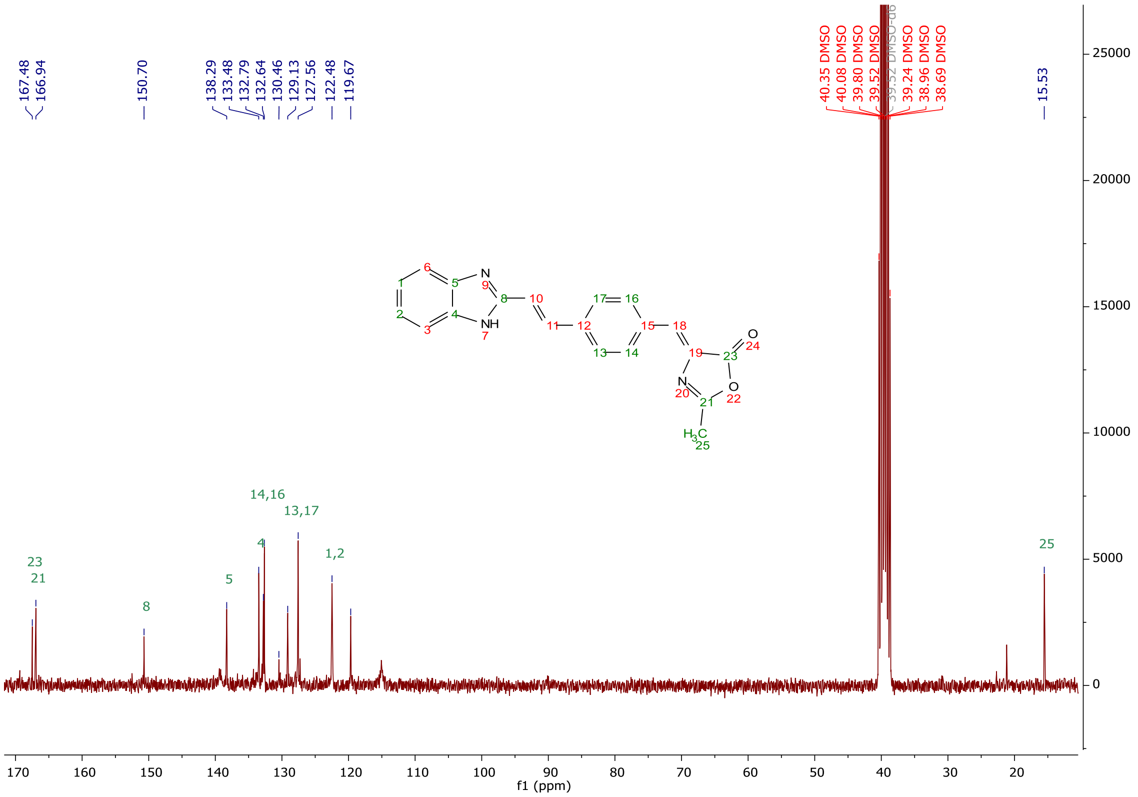

Figure 7.37. ^{13}C-NMR spectra of compound **14**, in DMSO

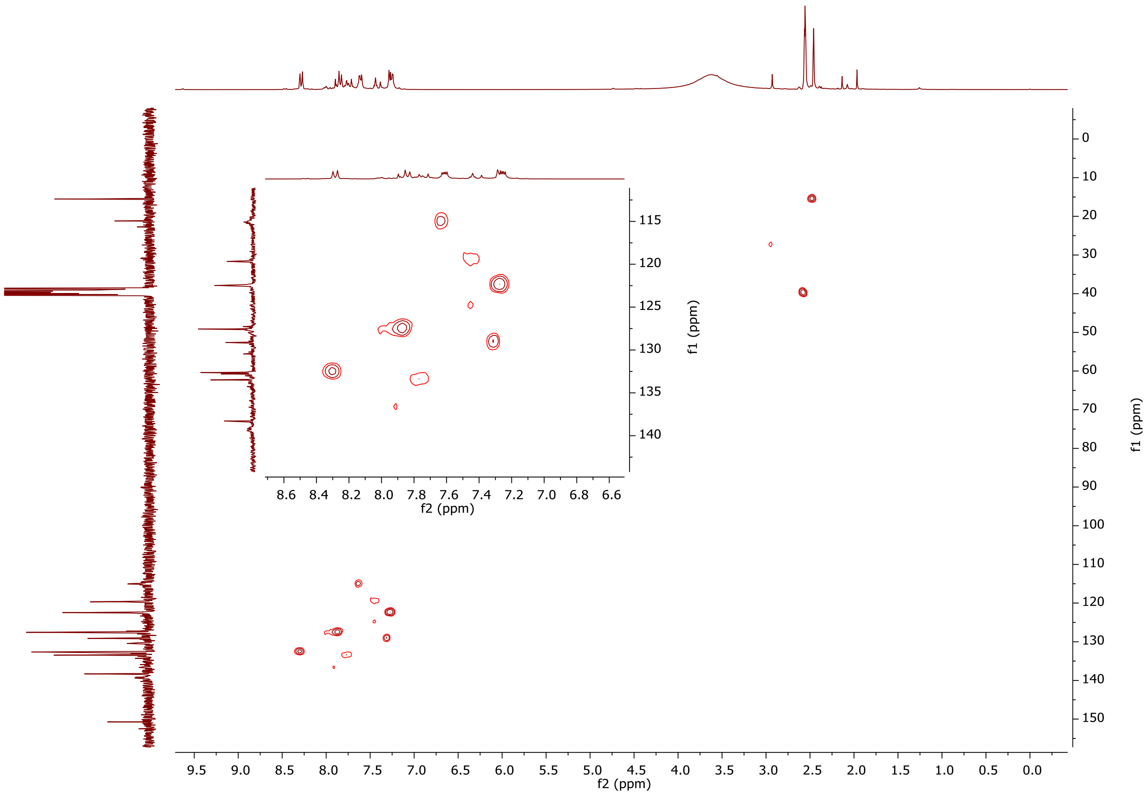

Figure 7.38. HSQC spectra of compound **14**, in DMSO

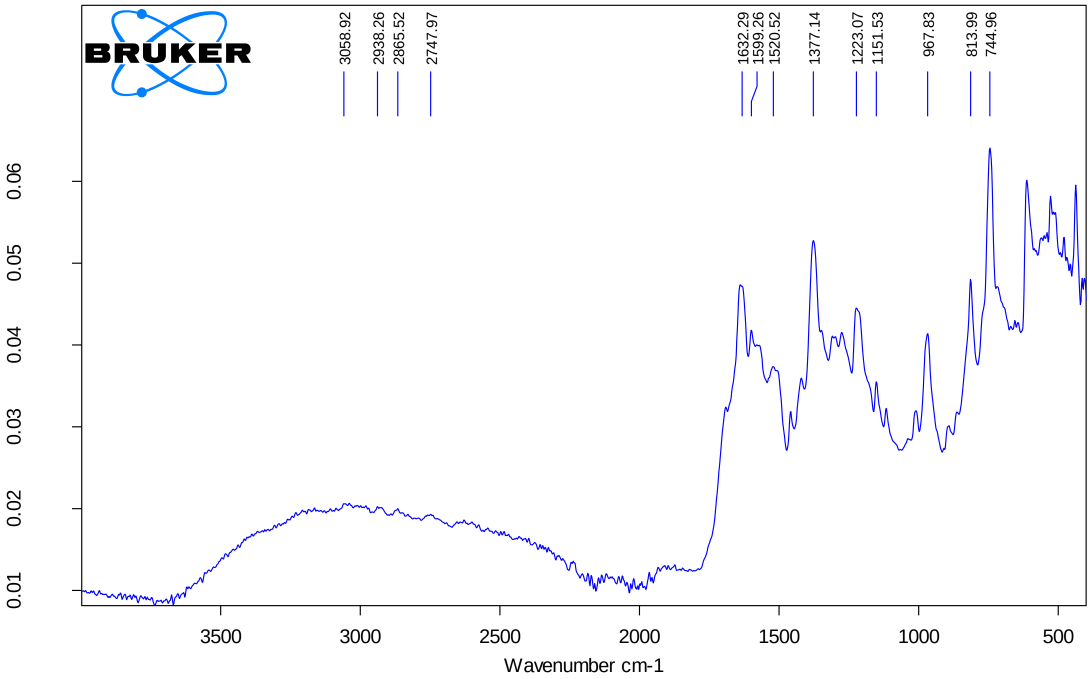

Figure 7.39. IR spectrum of compound **14**, in ATR

7.15. Appendix 15 - (E)-(4-(2-(1H-benzo[d]imidazol-2-yl)vinyl)phenyl)metanol (15)

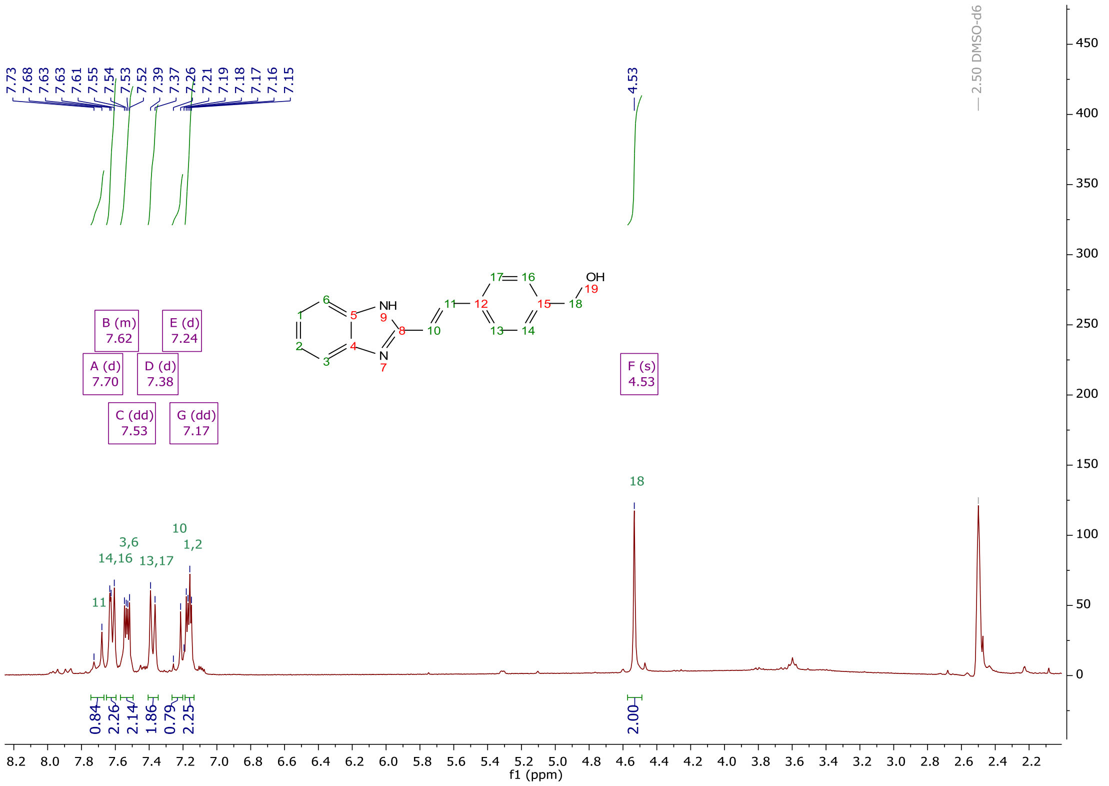

Figure 7.40. ^{1}H-NMR spectra of compound **15**, in DMSO

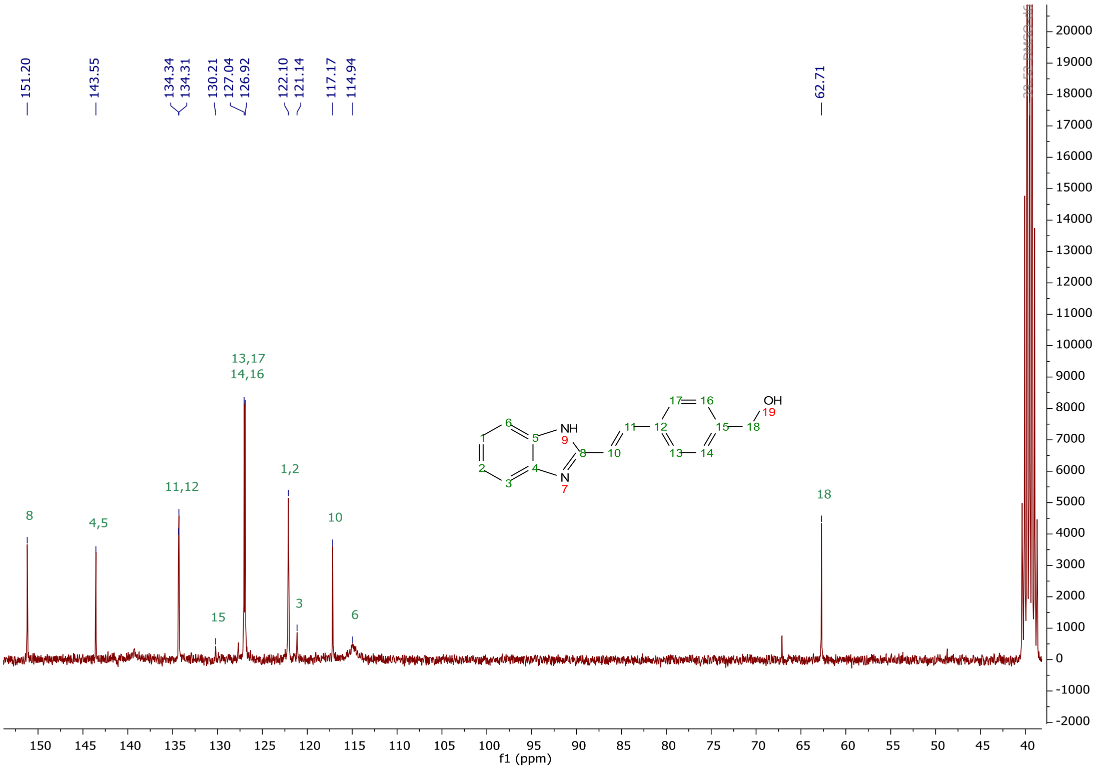

Figure 7.41*.* *^{13}C*-NMR spectra of compound **15**, in DMSO

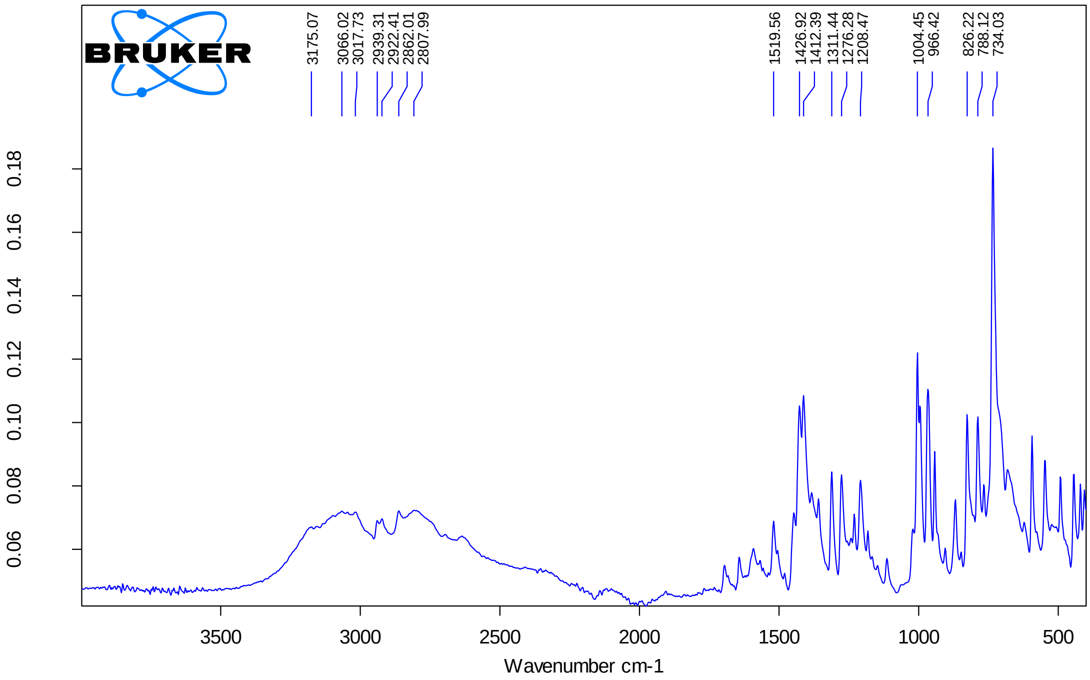

Figure 7.42. IR spectrum of compound **15**, in ATR

7.16. Appendix 16 - 2-((E)-4-((E)-(2-benzylhydrazineylidene)methyl)styryl)-1H-benzo[d]imidazole (16)

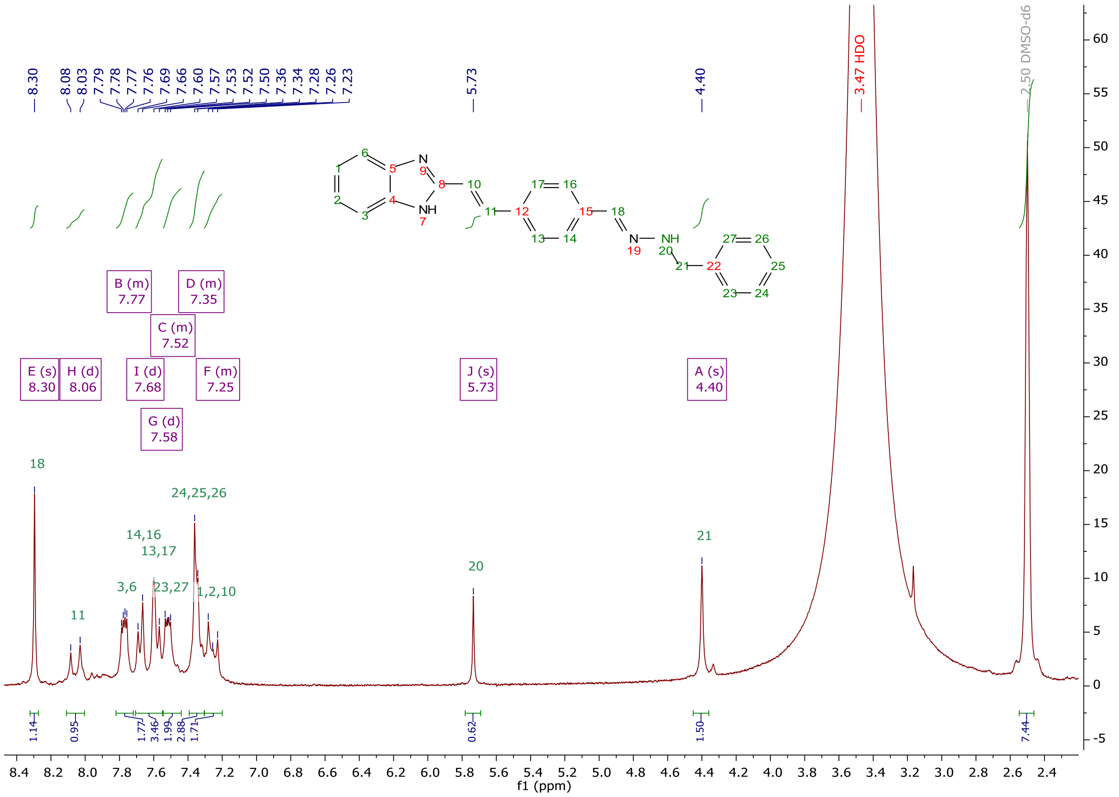

Figure 7.43.^{1}H-NMR spectra of compound **16**, in DMSO

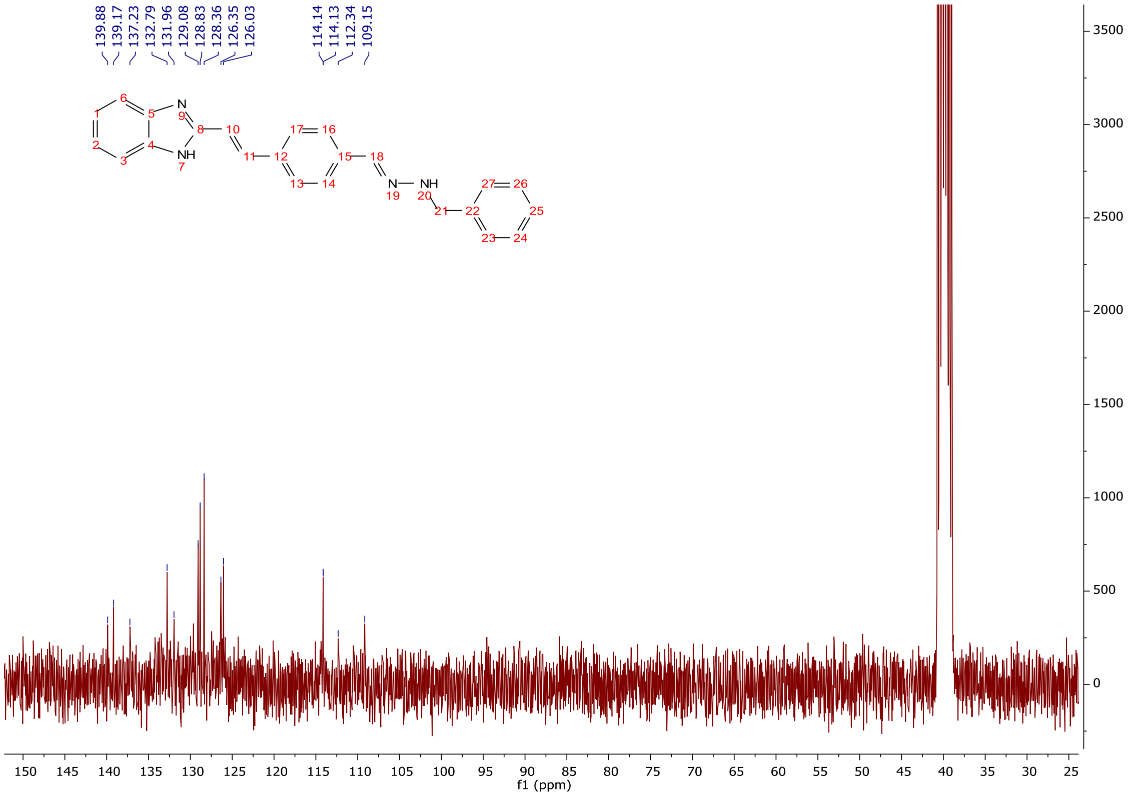

Figure 7.44. ^{13}C-NMR spectra of compound **16**, in DMSO

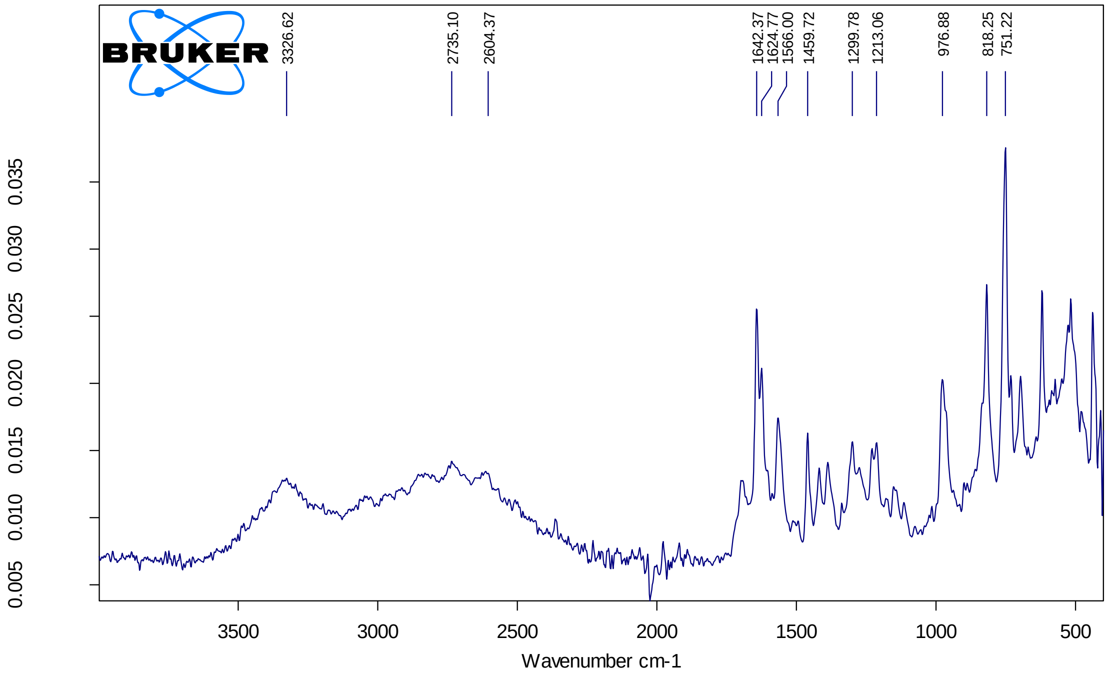

Figure 7.45. IR spectrum of compound **16**, in ATR

7.17. Appendix 17 - 2-((E)-4-((E)-(2-phenylhydrazineylidene)methyl)styryl)-1H benzo[d]imidazole (17*)*

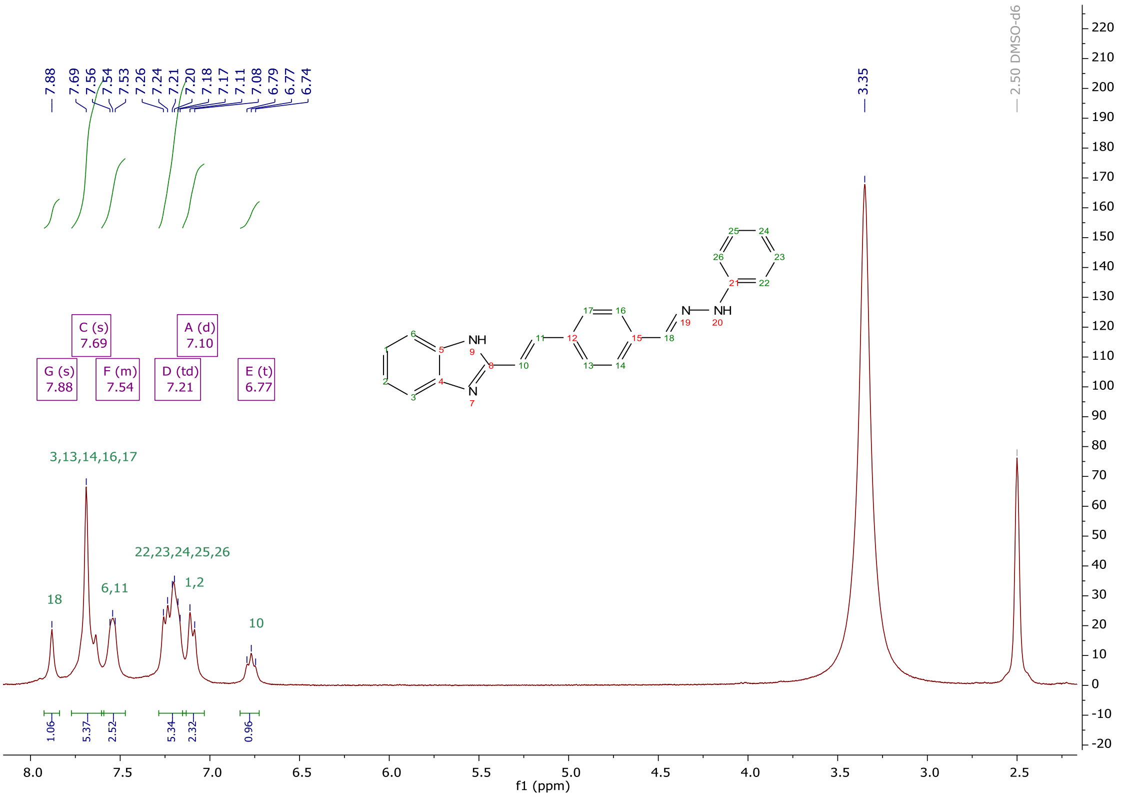

Figure 7.46. ^{1}HNMR spectra of compound **17**, in DMSO

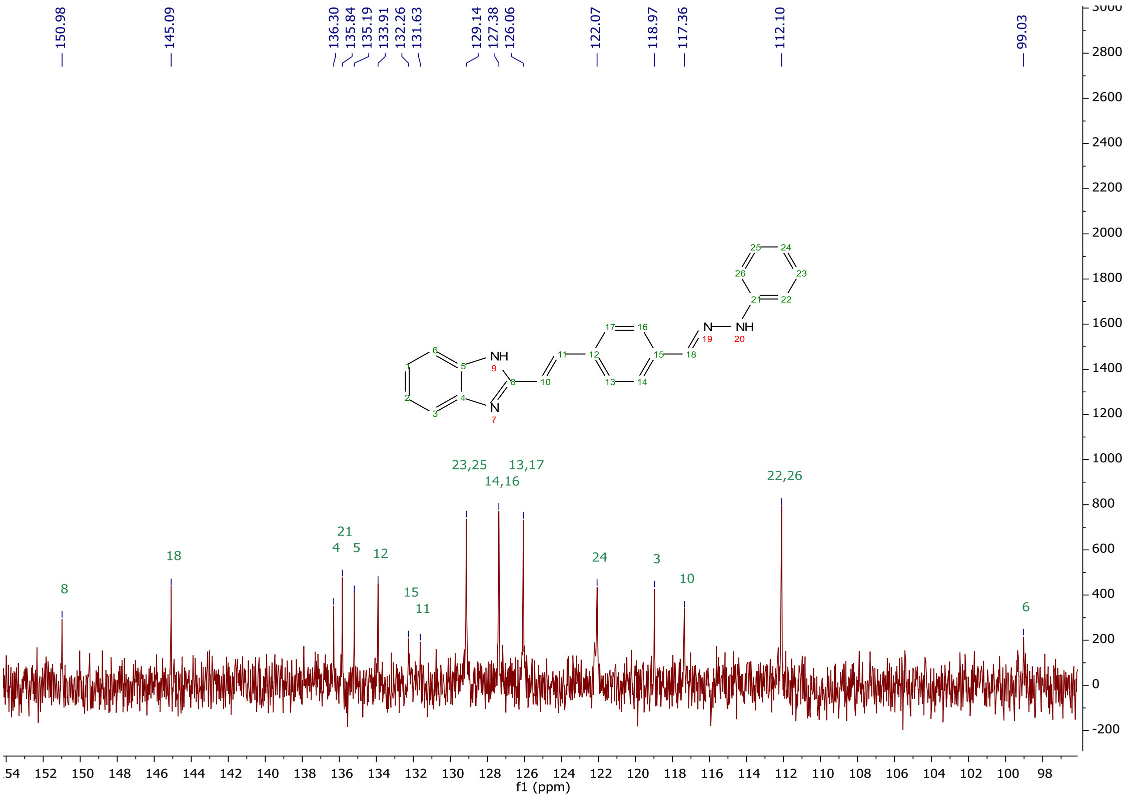

Figure 7.47. ^{1}H-NMR spectra of compound **17**, in DMSO

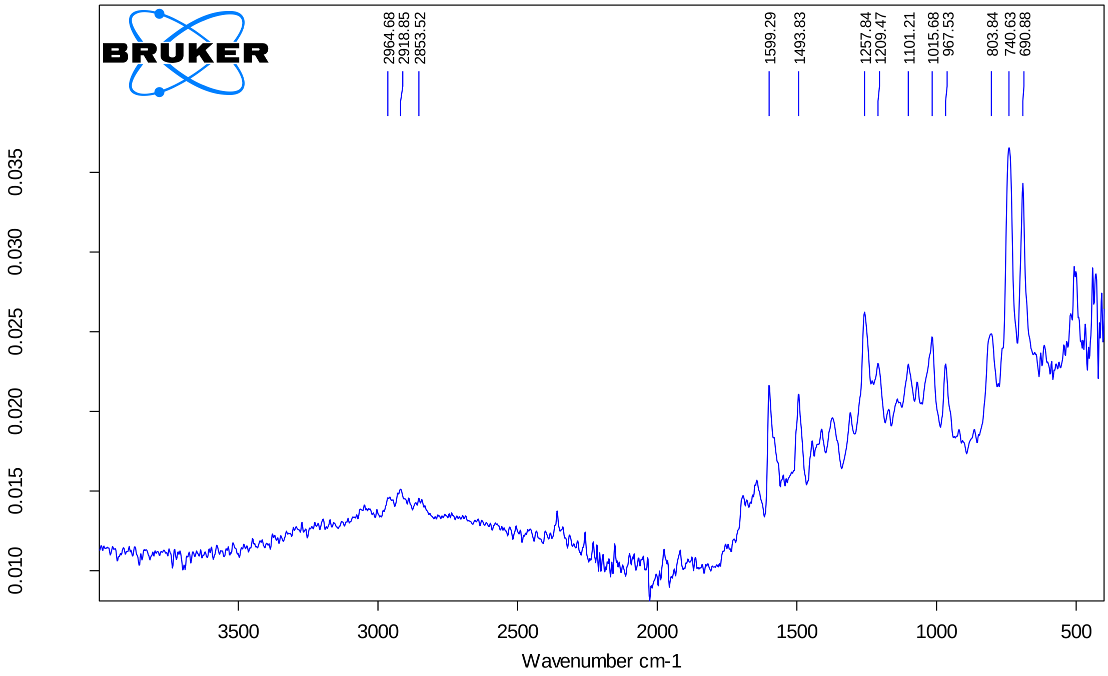

Figure 7.48. IR spectrum of compound **17**, in ATR

7.18. Appendix 18 - (E)-4-((E)-2-(1H-benzo[d]imidazol-2-yl)vinyl)benzaldehyde O-benzyl oxime (18)

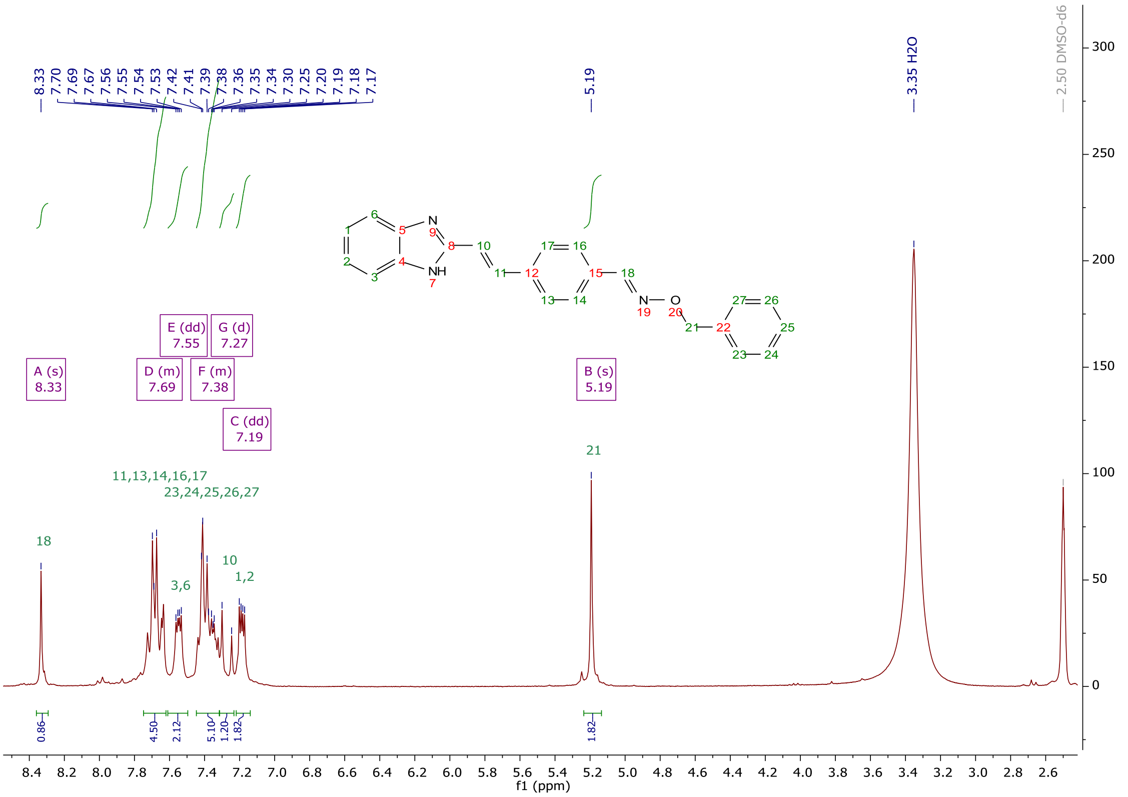

Figure 7.49. ^{1}H-NMR spectra of compound **18**, in DMSO

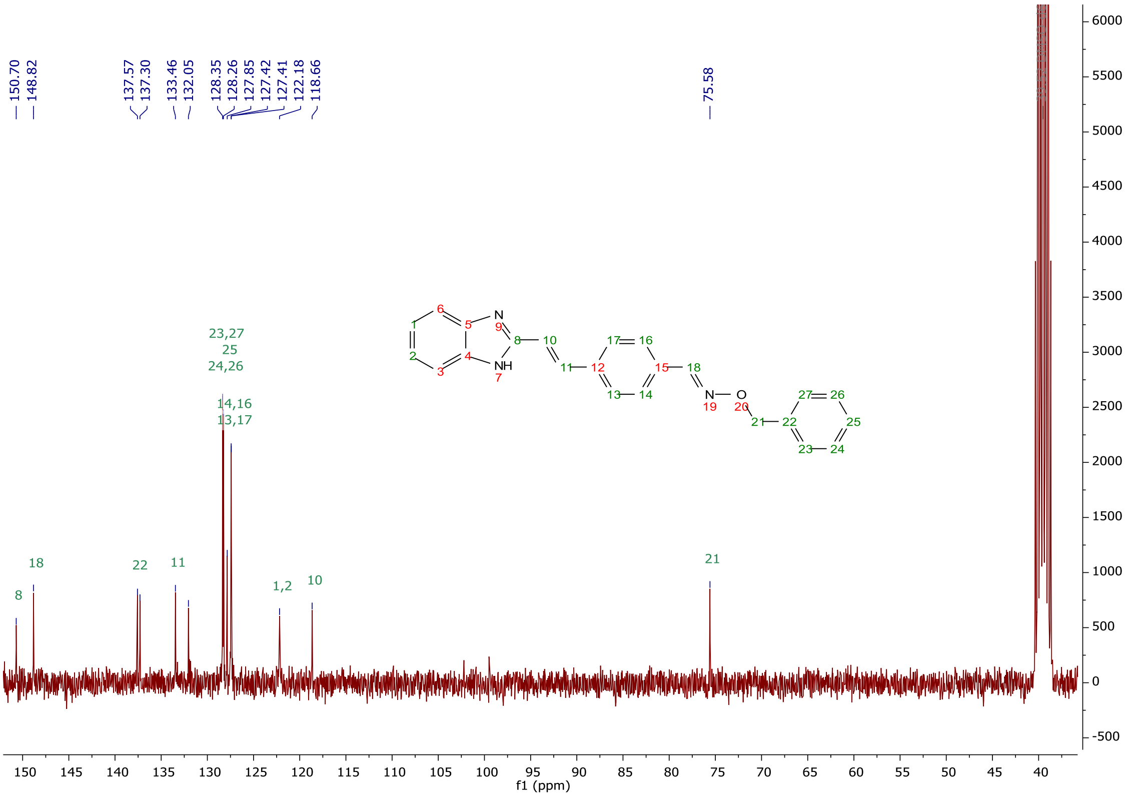

Figure 7.50.^{1}H-NMR spectra of compound **18**, in DMSO

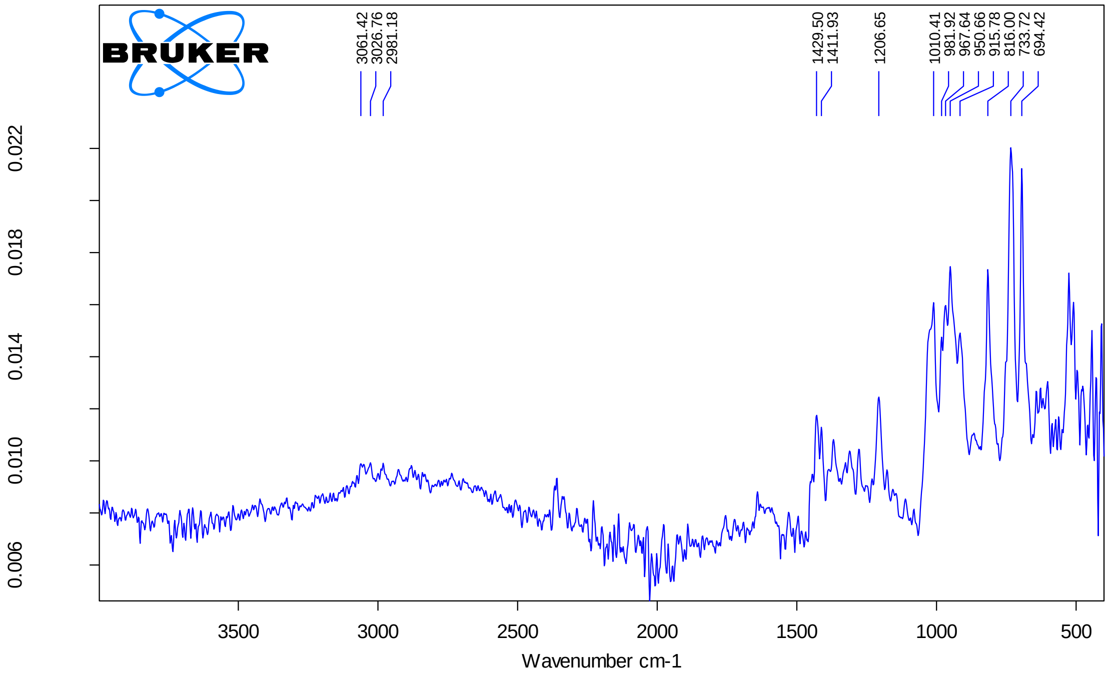

Figure 7.51. IR spectrum of compound **18**, in ATR

7.19. Appendix 19 – Attempt to synthetized (E)-4-(4-(2-(1H-benzo[d]imidazol-2-yl)ethyl)benzylidene)-2-phenyloxazol-5(4H)-one

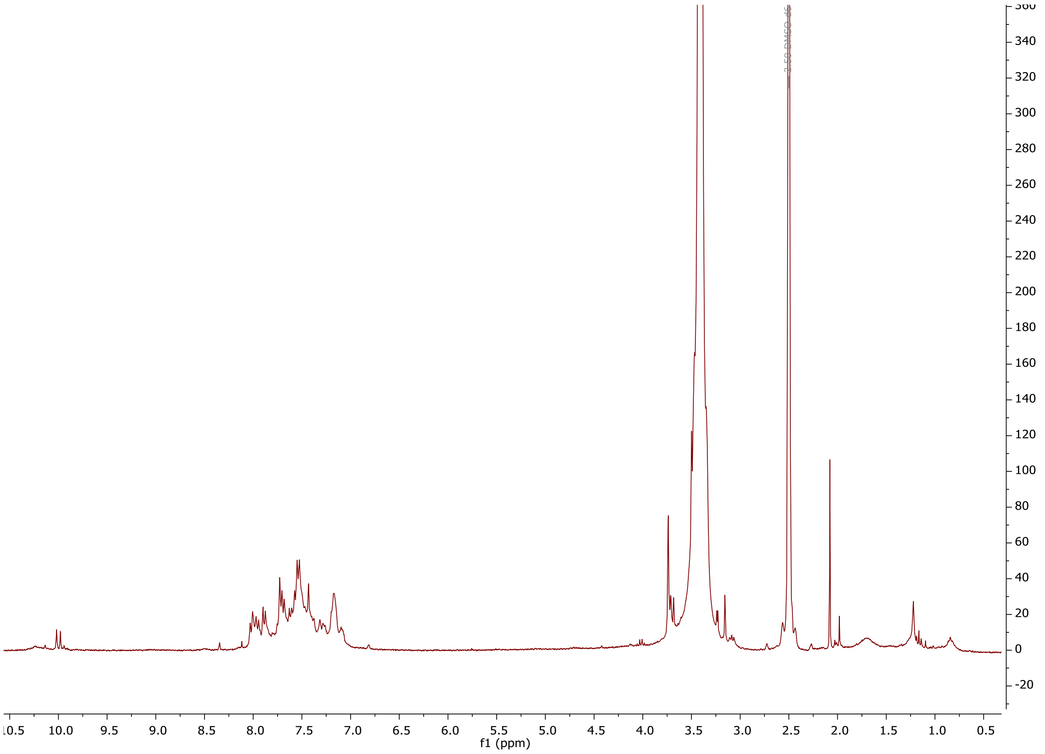

Figure 7.52. ^{1}H-NMR spectra of the attempt to synthetize compound **19**, in DMSO

7.20. Appendix 20 - 4-(2-(1H-benzo[d]imidazol-2-yl)ethyl)benzaldehyde

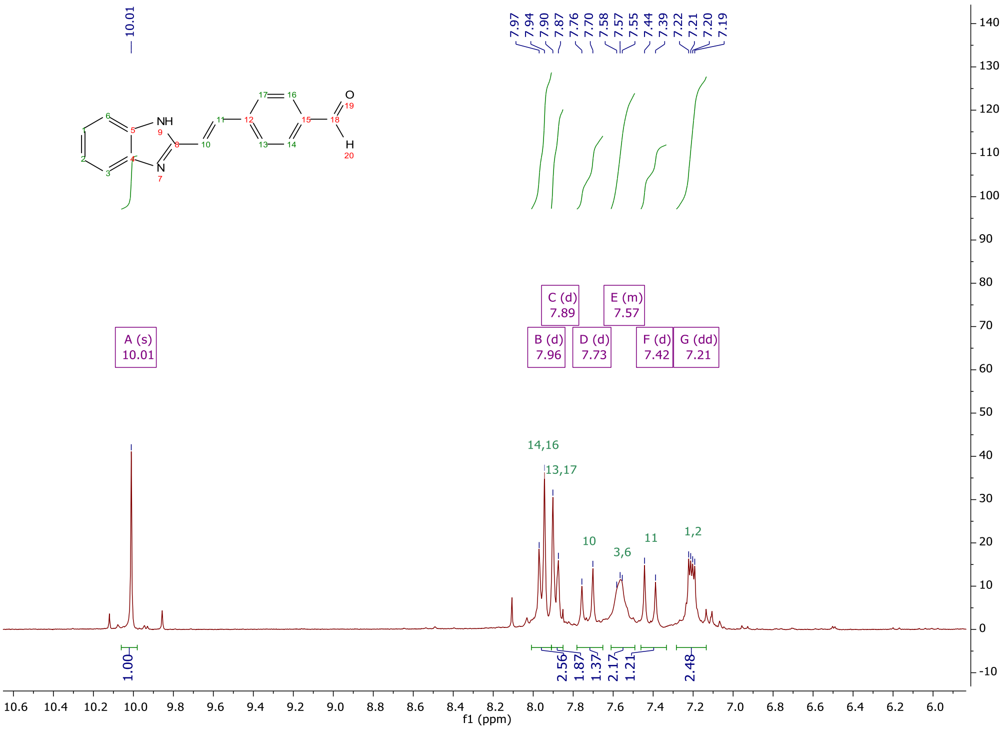

Figure 7.53. ^{1}H-NMR spectra of the attempt to synthetize compound **20**, in DMSO

7.21. Appendix 21 - *N*-acetylglycine (21)

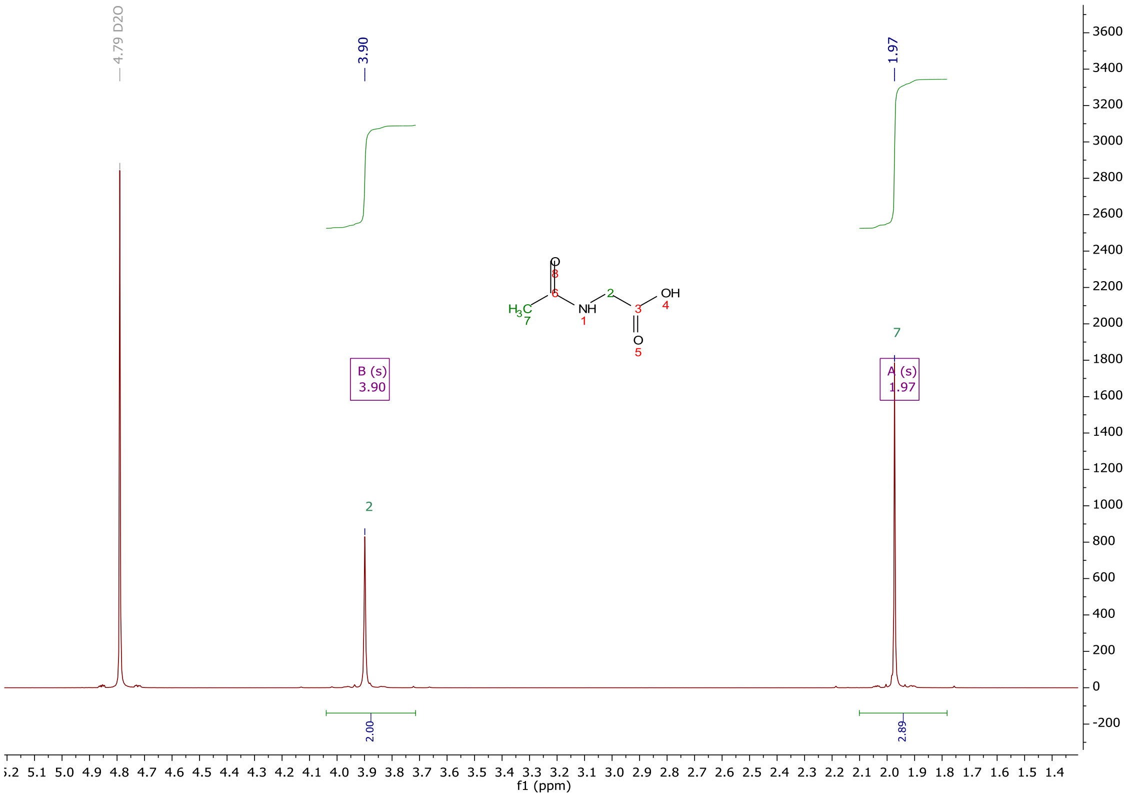

Figure 7.54. ^{1}**H-** NMR spectra of compound **21**, in D_2O

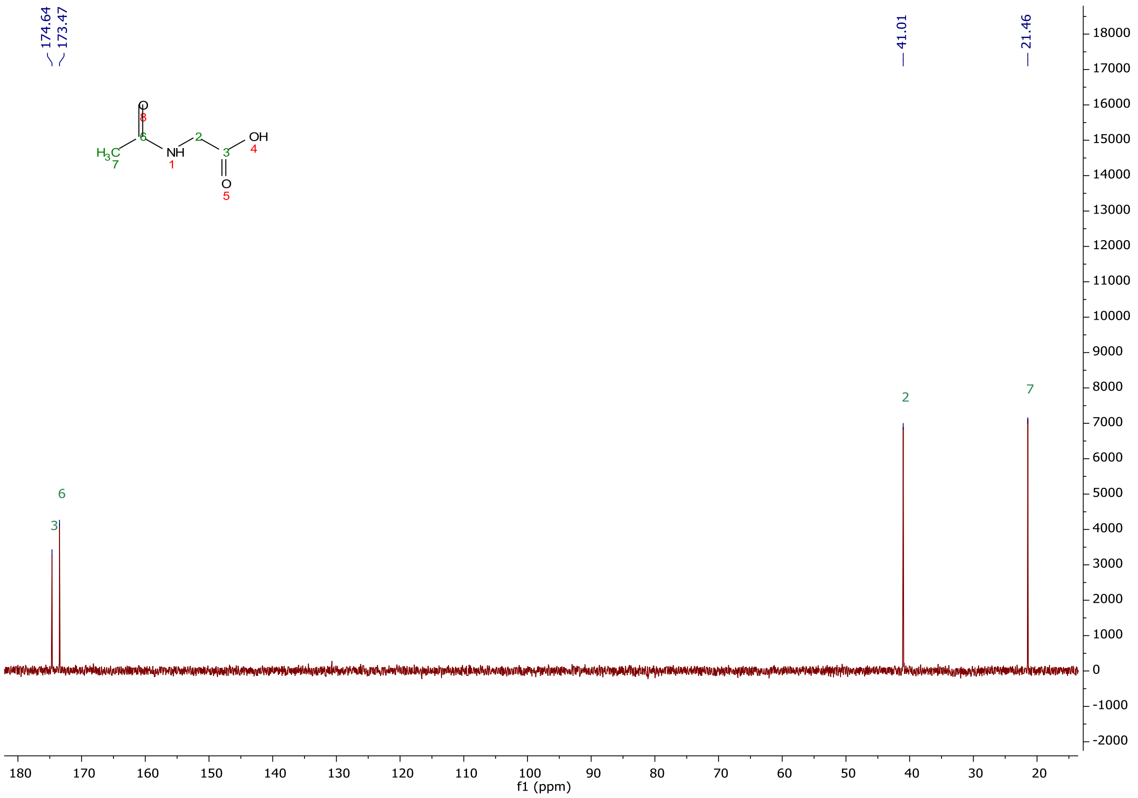

Figure 7.55. ^{13}C-NMR spectra of compound **21**, in D_2O

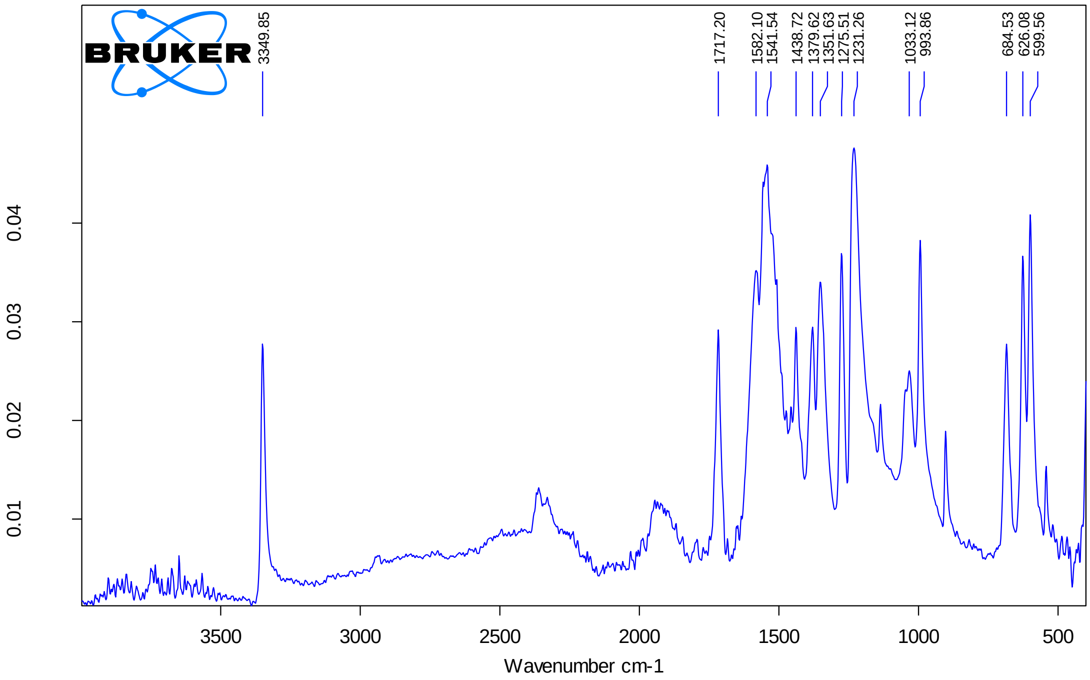

Figure 7.56. IR spectrum of compound **21**, in ATR

7.22. Appendix 22 - Methyl (pyrazine-2-carbonyl)glycinate (22)

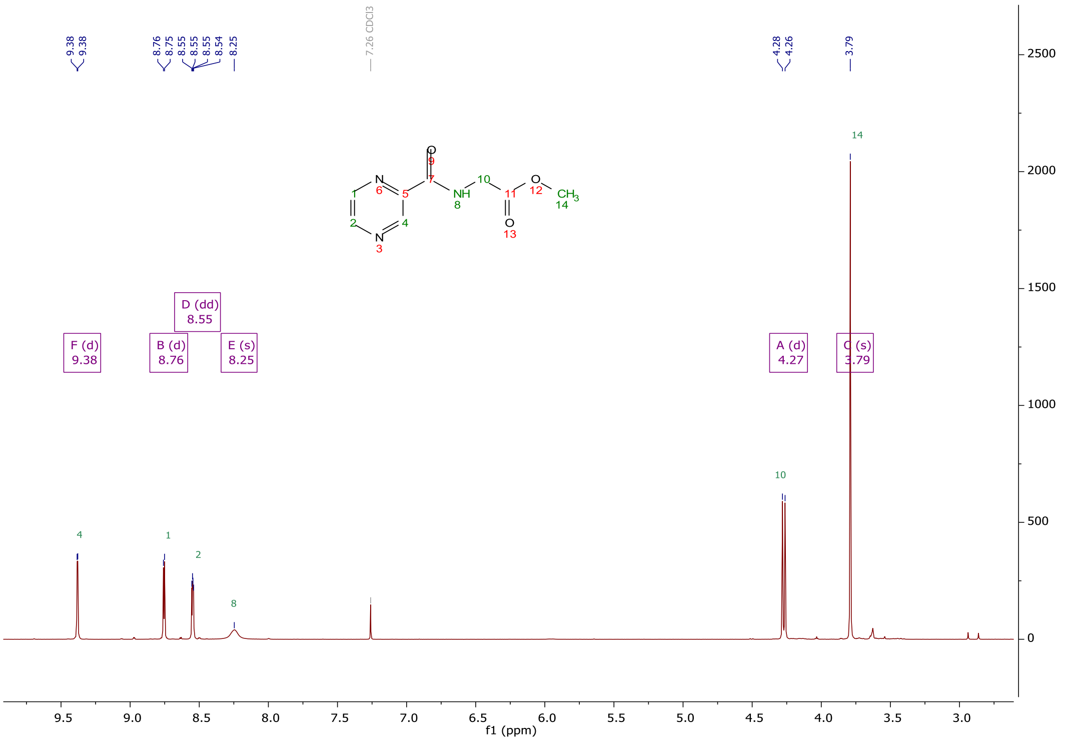

Figure 7.57. ^{1}H-NMR spectra of compound **22**, in CDCl$_3$

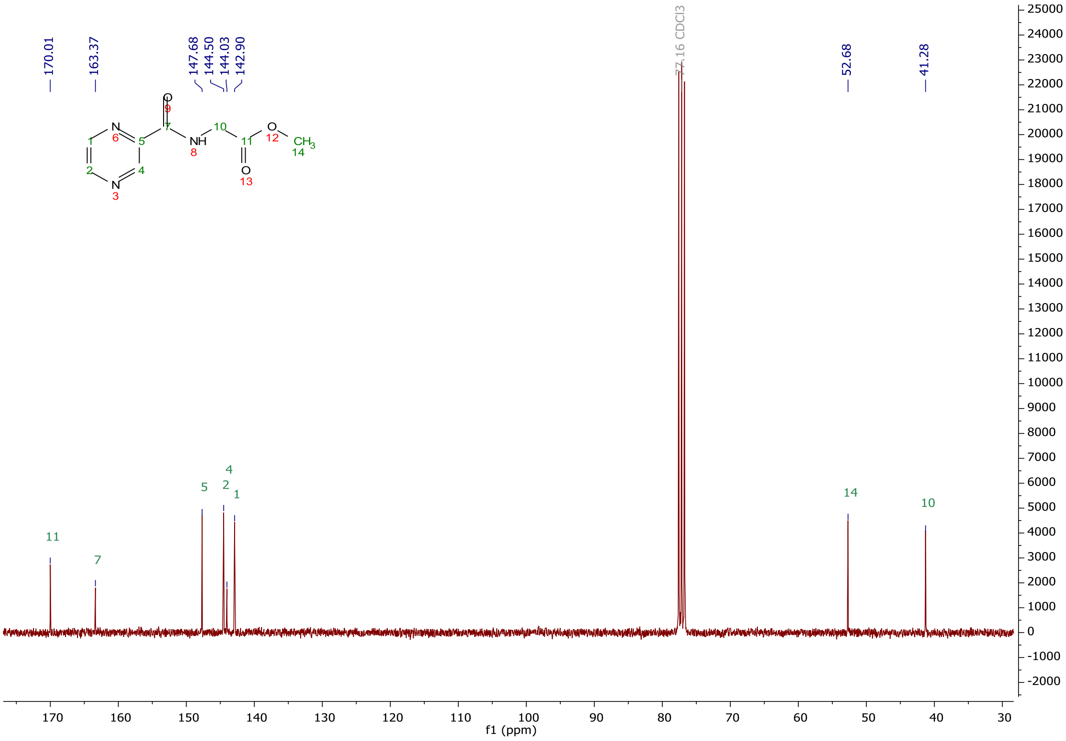

Figure 7.58. ^{13}C-NMR spectra of compound **22**, in CDCl$_3$

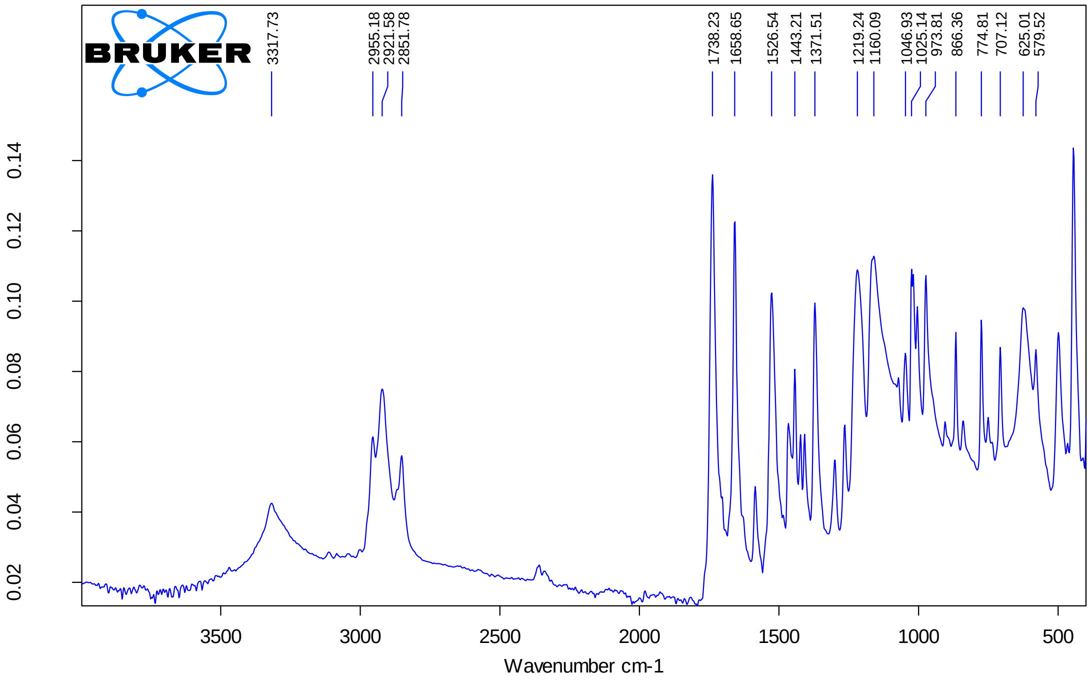

Figure 7.59. IR spectrum of compound **22**, in ATR

7.23. Appendix 23 - (Pyrazine-2-carbonyl)glycine (23)

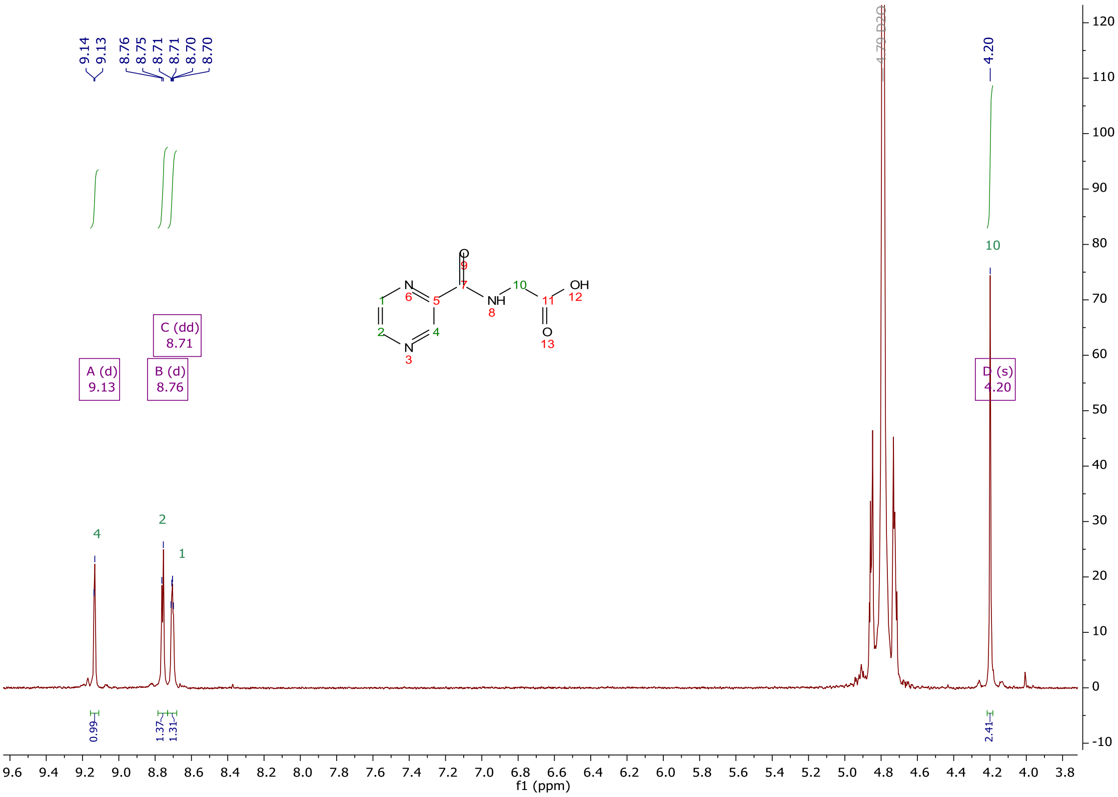

Figure 7.60. ^{1}H-NMR spectra of compound **23**, in D$_2$O

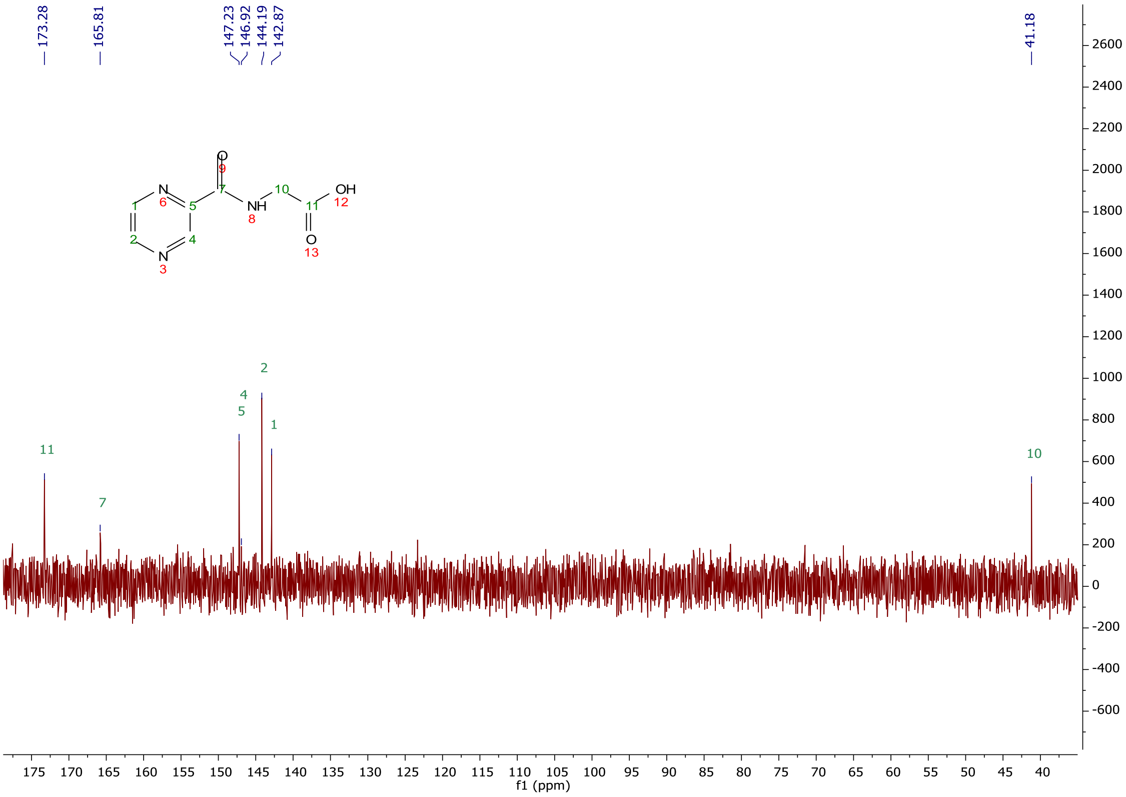

Figure 7.61. ^{13}C-NMR spectra of compound **23**, in D$_2$O

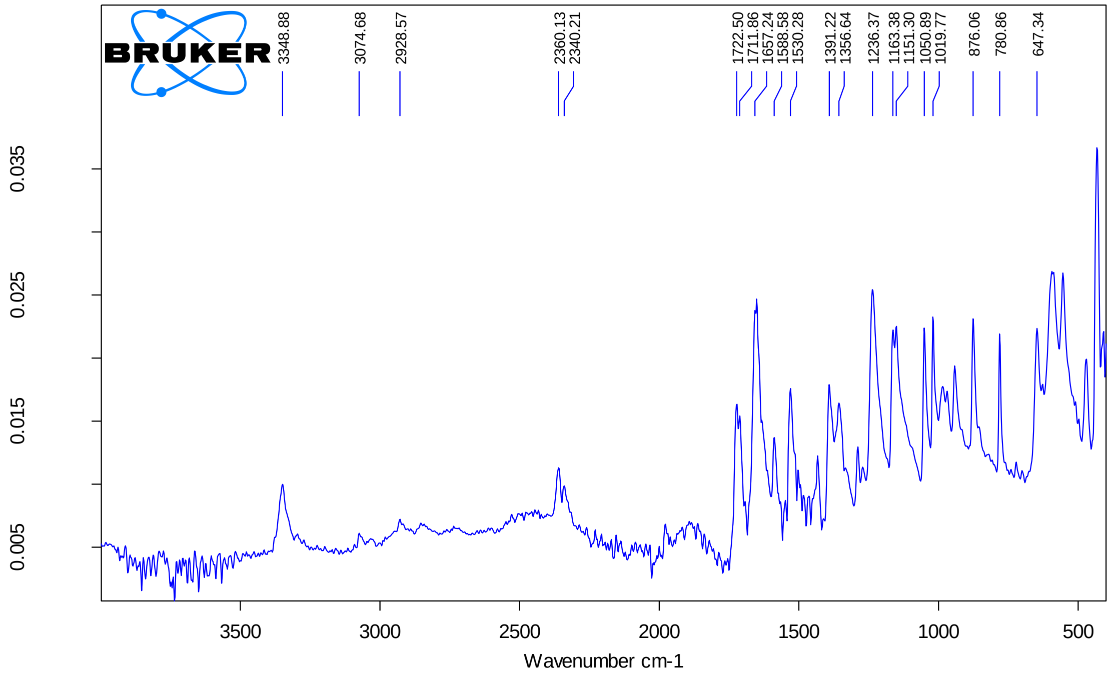

Figure 7.62. IR spectrum of compound **23**, in ATR

7.24. Appendix 24 – Nicotinoylglycine (26)

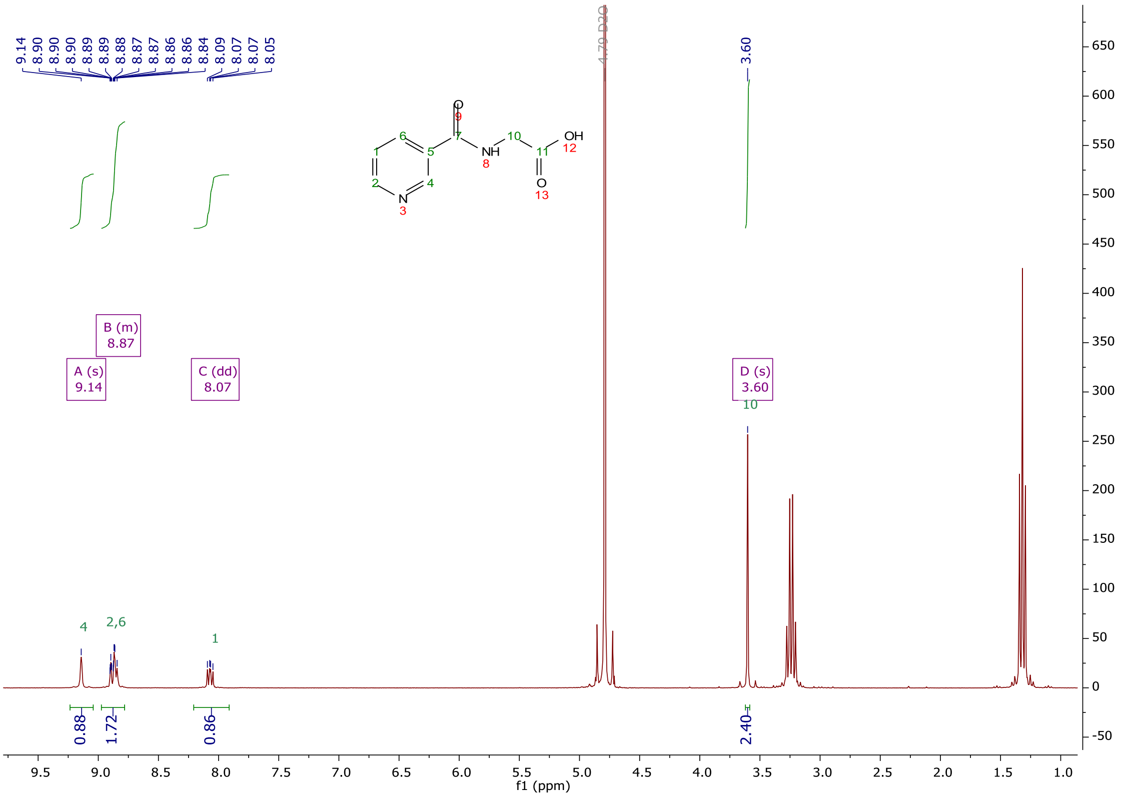

Figure 7.63. ^{1}H-NMR spectra of compound **26**, in D_2O

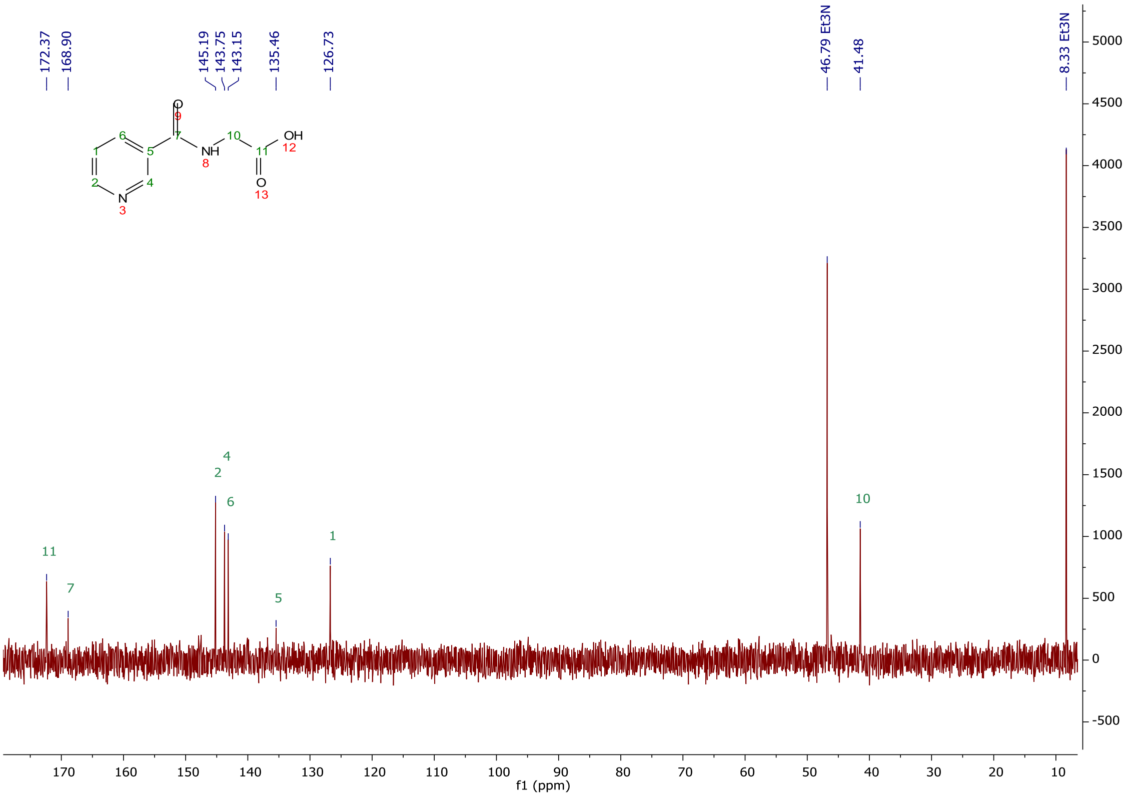

Figure 7.64. ^{13}C-NMR spectra of compound **26**, in D_2O